TALUS SLOPES AND PROTALUS ROCK GLACIERS IN CENTRAL YUKON

James T. Gray, Ph.D.

Department of Geography

"Processes and rates of development of talus slopes and protalus rock glaciers in the Ogilvie and Wernecke Mountains, Yukon Territory".

ABSTRACT

Erosion rates on ten rock walls in central Yukon over a 10,000-14,000 year postglacial period range from 5 to 388 mm/1,000 years, with a median of 50 mm/1,000 years. They are lower in igneous intrusives than in metasediments.

Of observed debris accretion processes, rock-falls are most important, followed by spring snow avalanches, torrent avalanches and slow debris shift. Medium and large scale events, of infrequent and unobserved occurrence, are quantitatively more important, however.

Fall sorting on talus slopes occurs due to surface roughness effects. Several factors, including erosion by other processes, reduce correlations between particle size and distance downslope. Avalanches redistribute debris and reduce upper talus slopes without affecting basal zones.

Some talus cones feed into valley-wall and cirque-floor rock glaciers. The latter appear to contain massive ice, and the former interstitial ice. The majority developed between the culmination of the last glaciation and 1,000 years B.P., and exhibit maximum advance of only 0.1-0.4 m/year during the last few centuries.

"Processes and rates of development of talus slopes and protalus rock glaciers in the Ogilvie and Wernecke Mountains, central Yukon Territory".

by

James T. Gray

Department of Geography
McGill University
Montreal

A thesis submitted to the Faculty of Graduate Studies and Research in partial fulfillment of the requirements for the degree of Doctor of Philosophy.

July 1971

ACKNOWLEDGMENTS

I would like to thank a number of organisations and individuals for their contributions to my thesis research.

The Arctic Institute of North America provided a grant in aid of the field-work in 1966. The Geological Survey of Canada undertook sponsorship of the project for the summers of 1967, 1968 and 1969, and the financial and logistical support given by the Survey were principal factors in the success of the field-work. I am grateful to Geological Survey personnel Dr. O.L.Hughes, Dr.J.G. Fyles and Dr. B.G.Craig for their support and advice.

The McConnell Foundation supported the writer's office work at McGill University through a McConnell Fellowship. Professor J.B.Bird supervised the project and I would like to record my appreciation of his help in gaining financial support for both office and field-work and for his comments on interim reports and on the final thesis manuscript.

Messrs. W.Gray, R.Holt, I.Gray, D.Reimer, A.Gray and T.Crow assisted ably in the field. Mr. J.Tibert assisted with data processing and with the building of a laboratory model at McGill.

The field-work was greatly aided by logistical help received from helicopter pilot Mr. C.Ford, Dr. R.Harington of the National Museum of Canada, Mr. G.Leverman of Whitehorse, and from the Territorial Government of the Yukon Territory. Equipment loans were made by the

Meteorological Branch in Toronto, the Glaciology Division of Inland Waters Branch in Ottawa and Mr. R.Wall, Airport Weather Office, Whitehorse.

Mr. and Mrs. A. Nordling and family are thanked for their kindness. They afforded hospitality and assistance to the field party whenever it was in Dawson City.

I have had frequent valuable discussions on various topics in the thesis with Mr. B.Luckman of the University of Western Ontario, and with Mr. A.Pearce of McGill University. The latter is thanked for reading and commenting on the final manuscript.

I am grateful to Mr. W.Evershed and Mr. R. Labbé for drafting the maps and diagrams. Finally I would like to thank my wife Nicole for typing several drafts, including the final one, and for assistance in editing the thesis.

TABLE OF CONTENTS

CHAPTER 1

INTRODUCTION

1. SCOPE OF THE INVESTIGATION

The present study evaluates the effectiveness of mass wasting processes on steep bedrock slopes in the Ogilvie and Wernecke Mountains, central Yukon Territory, in the Holocene period. These processes have transported weathered debris down the steep upper slopes and have deposited it in the form of talus accumulations and rock glaciers on the more gently inclined basal slopes.

Mean rates of postglacial rock wall recession were established from ten mountain slopes and are important in adding to the limited information available, mainly from Scandinavia, on rates of rock wall erosion in periglacial regions.

The nature and relative role of individual mass wasting processes of rock-fall, snow avalanches, torrent avalanches, debris flows and slow debris shift, and of fluvial processes, are assessed through direct observations and measurements and through indirect studies of talus slope form and surficial debris characteristics.

Rock glaciers beyond some of the talus slopes are the end products of postglacial debris transport down the steep rock walls. The variability in the distribution of these forms, their age, their probable ice content, their current rates of advance, and the information they provide on postglacial rock wall recession are evaluated.

2. OUTLINE OF THESIS

In the remainder of chapter 1, the location of the field areas, their bedrock geology and topography, their glacial history and their present climate are assessed.

In chapter 2 the postglacial rates of transfer of debris from rock walls to talus slopes are determined for ten slopes in the field areas.

Chapter 3 assesses the relative importance of rock-falls, avalanches, debris flows and debris shift in transporting debris from the rock walls to the talus slopes over recent short time periods of a few weeks to a few years.

In chapters 4, 5, 6 and 7 the long term erosional modification of the talus slopes is indirectly assessed from the characteristics of the surficial sediments and from the slope form itself. Since these slopes are obviously a response to a group of sub-aerial processes acting together in a somewhat complex manner, a series of models was introduced to aid understanding of the real world situation. The discussion progresses through a series of stages, from relatively simple hypothetical and artificial debris slopes developed under the influence of rock-fall alone, to the complex talus slopes of the Ogilvie and Wernecke Mountains developed by multiple processes. In chapter 4 a theoretical model of debris build-up by rock-fall, on a basally concave rock wall, is constructed. In chapter 5 the form and surficial characteristics of artificially built slopes are analysed. The latter are small scale slopes built by rock-fall in the laboratory and medium scale mine dump slopes.

In chapter 6 the slope form and characteristics of the surficial debris are analysed for talus slopes in the Ogilvie and Wernecke Mountains. The results are then compared with the theoretical and artificial models and explanations suggested for the major differences. Processes other than rock-fall are responsible for some of the differences and these processes are discussed in chapter 7.

Discussion of the protalus rock glaciers in chapter 8 completes the picture of postglacial debris transport on the rock walls of the Ogilvie and Wernecke Mountains.

In chapter 9 the conclusions on all aspects of the research are presented in summary form.

The terms used for forms and processes in this thesis are discussed in Appendix I.

Appendices II, III, IV and V are referred to at appropriate places in the text.

3. LOCATION OF FIELD AREAS (Fig. 1.1)

The Tombstone field area lies within the Ogilvie Mountains, 56 km (35 mi) north east of Dawson City. It was selected for detailed

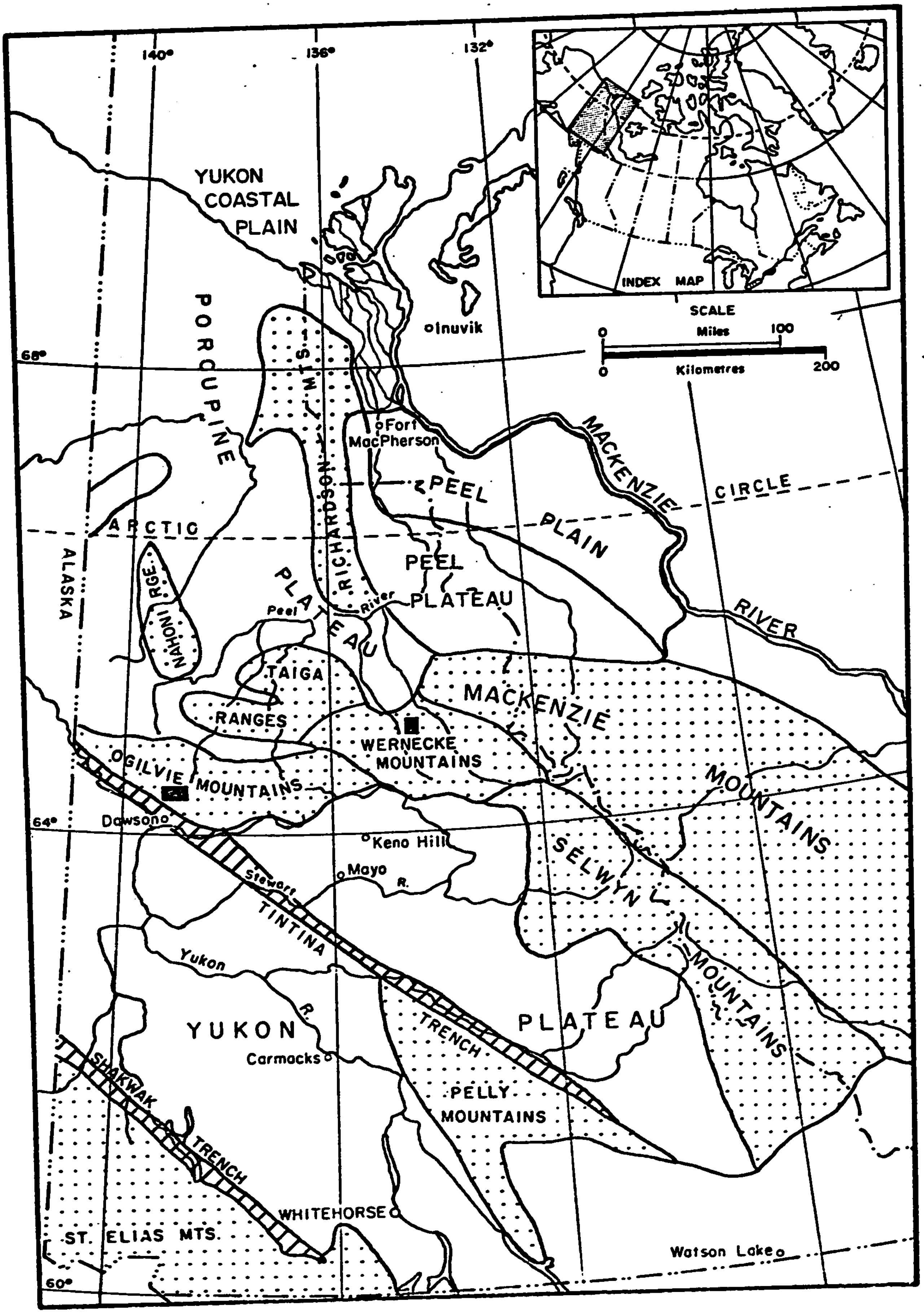

FIG. 1.1 LOCATION OF FIELD AREAS

study on account of its high elevation 1,400-2,300 m (4,500-7,500 ft) above sea level, its high steep rock walls, varying from 450-775 m (1,500-2,500 ft) in elevation, and its marked contrasts in rock wall morphology.

Reconnaissance work was carried out in this area over a ten day period in the summer of 1966, and was followed by detailed research in the summers of 1967, 1968 and 1969. Several modes of access to the area were used during the research. Game trails up the North Klondike valley allowed access on foot from the Dempster Highway 16 km (10 mi) to the east. The party was able to land on several occasions by float plane and ski plane on Divide Lake (Plate 5) and a helicopter was also used to get into the area.

The Bear River area lies within the Wernecke Mountains, 160 km (100 mi) north east of Mayo. The Wernecke Mountains display an abundance of protalus rock glaciers in contrast to the Tombstone area. Therefore, in order to obtain a balanced picture of debris transport on and below mountain walls in the central Yukon Territory, the field-work was extended to the Bear River area for the summers of 1967, 1968 and 1969. The scale of the rock walls and the elevations of the peaks within the field area are similar to those of the Tombstone area.

An airstrip in the Bear River valley, built in 1966 by a mineral exploration company Pacific Giant Steel, was used for access in the summer of 1967 and 1968. After 1968 the airstrip was no longer maintained, and in the summer of 1969 the field party was taken in by helicopter after landing equipment by float plane on Gillespie Lake, 22 km (14 mi) to the east.

The research sites in the Tombstone area mentioned in the text are located in Plate 5; those in the Bear River area are located in Plate 6. Tables 1.1 and 1.2 summarise the work done on talus slopes in the two areas.

4. BEDROCK GEOLOGY AND PHYSIOGRAPHY

a) Tombstone area (Map in end pocket)

The lithology and structure of the area has been described in detail by Tempelman-Kluit (1970). It consists essentially of a large elliptical stock of igneous intrusives of mid-Cretaceous age forcefully emplaced into a zone of folded and thrust faulted Lower Cretaceous orthoquartzites with minor slate and limestone. A previously intruded diabase sill is present in the basal zone of the orthoquartzites.

The thrust faults in the metasediments dip in a southerly or south easterly direction. The strata between these faults have been folded asymmetrically, the anticlines having steeply dipping northerly and north westerly limbs and gently dipping southerly and south easterly limbs. Subsequent erosion has removed the tops of the anticlinal structures and the predominant dip of the exposed strata is to the south and south west. Consequently the high angle rock walls and talus slopes are mostly located on slopes with a northerly or

TABLE 1.1

FIELD-WORK ON TALUS CONES IN TOMBSTONE AREA.

Cone no.	Lithology	Cone volumes	Debris Accretion	Surface sediment analysis	Slope angles & profiles	Slow debris shift
6821	diabase	x			x	
6822	"				x	
6823	quartzite (slate)				x	
6824	"	x	x	x	x	x
6825	"	x		x	x	
6826	slate (diabase)				x	x
6827	"				x	x
6828	"		x		x	
6829	"				x	
6830	syenite	x	x	x	x	x
6831	""			x	x	x
6832	"				x	
6833	"				x	
6834	"				x	
6835	"				x	
6836	quartzite (slate)				x	
6837	"				x	
6838	syenite				x	
6839	"				x	

TABLE 1.2

FIELD-WORK ON TALUS CONES IN BEAR RIVER VALLEY.

Cone no.	Lithology	Cone volumes	Debris accretion	Surface sediment analysis	Slope angles & profiles	Slow debris shift
6801	quartzite (slate)	x	x		x	
6802	dolomite				x	
6803	slate				x	
6804	dolomite	x			x	
6805	slate (quartzite)			x	x	
6806	"				x	x
6807	quartzite (slate)				x	
6808	dolomite	x		x	x	
6809	quartzite (slate)			x	x	x
6810	dolomite			x	x	x
6811	"			x	x	x
6812	"			x	x	x
6813	quartzite (slate)				x	
6814	"	x			x	
6815	"	x			x	
6816	"	x			x	
6817	quartzite (slate)	x				x
6818	"					x
6819	dolomite					x
6820	"		x		x	

north westerly component, i.e. on the scarp slopes. The southerly and south westerly facing dip slopes generally have gradients of 15^{o}-30^{o}, and are mantled with weathered debris and frequently with skeletal soils and a vegetation mat.

The contact between the intrusives and the metasediments is very abrupt, dipping at angles greater than 60^{o} (Tempelman-Kluit, 1970, p. 40). This gives rise to a striking contrast in rock wall morphology (Plate 8). The smooth walls of the Tombstone intrusion are only occasionally interrupted by narrow joint controlled gullies and chimneys. They slope upwards at 60^{o}-70^{o} and culminate in sharp pinnacles and towers joined together by narrow arêtes (Plate 7). By contrast the rock walls in the metasediments are seamed at frequent intervals by large dendritic gully networks. They are of high rugosity and slope upwards at 35^{o}-45^{o} to culminate in broad wedge shaped or pyramidal peaks. Local steepening of the basal sections of the rock walls in the metasedimentary zone sometimes occurs, however, where the diabase sill outcrops over vertical ranges of 15-60 m (50-200 ft).

In the reconnaissance in 1966 it was noted that the debris cones developed below the gully networks on the metasedimentary rock walls are much larger than the debris aprons developed below the rock walls in the igneous intrusive zone. In the latter case, individual talus cones occur, but only at infrequent intervals below joint controlled chimneys on the rock walls. Much of the subsequent research was devoted to examination of this observed contrast.

b) Bear River area (Map 2 in end pocket)

Geologically the Bear River area consists of a Precambrian series of slates, argillites and quartzites which grade by interbedding into an overlying orange weathering dolomite unit (Green and Roddick, 1962, p. 2-3). Both units have been fractured and folded considerably and therefore the structure is rather complex. Scarp and dip slopes are not so consistent in direction as in the Tombstone area but the rock walls and talus slopes studied are nearly all on east, west and north facing slopes as they are mainly associated with the steep cirque walls incised in the mountain ranges.

5. GLACIAL HISTORY OF THE FIELD AREAS

Assessment of the late glacial events for the Ogilvie and Wernecke Mountains enables a probable time span to be placed on the postglacial interval during which the present talus slopes have been developed. This allows calculation of the rates of talus build-up and rock wall erosion.

Vernon and Hughes (1966, p. 6) note a contrast in the general character of glaciation between the Ogilvie Mountains in the western part of their field area, and the Wernecke Mountains, in the eastern part of their field area. The former includes the

Tombstone area and the latter the Bear River area.

> "In the western region, glaciation was characterised by successive advances of valley glaciers originating in cirques along the axis of the southern Ogilvie Ranges. For the most part the ice flowed outward in the direction of modern drainage and extended only short distances beyond the mountains, thus leaving much of the western part of Dawson map area and Taiga Valley unglaciated. The valleys of the eastern region were filled by ice of a vast transection glacier system that flowed generally northwesterly and westerly from sources southeast of the three map areas. This ice was augmented by local ice from cirques within the region".

a) Ogilvie Mountains (Map 3 in end pocket)

Evidence for three glaciations originating in the southern Ogilvie Ranges has been found in the drainage basin of the East Blackstone River.

There are no well defined moraines left to indicate the limits of the earliest of these glaciation but the upper limit of rounded glacial erratics in the Blackstone valley at Windy Pass near Mile 96 of the Dempster Highway lies at 1,070 m (3,500 ft) above sea level and 230 m (750 ft) above the present river level. These erratics, consisting of syenite and monzonite, were readily recognised among the frost weathered limestone which forms the country rock. Their source areas are the Tombstone and Brenner intrusive stocks and this indicates movement of ice northwards from sources in the southern Ogilvie Ranges, across the low relief zone, described physiographically by Bostock (1948) as the Taiga valley, and into the central Ogilvie Ranges. Judging by their abundance, the erratics at Windy Pass represent a degraded lateral moraine of the ice sheet. The considerable elevation of the ice sheet above the Blackstone River at this point suggests that the terminus was several miles further north down the Blackstone valley.

The limit of this glaciation to the south of the Ogilvie Mountains has not been demarcated yet but both the Tombstone and North Klondike valleys must have been glaciated. The ice which flowed down the latter may have reached the confluence of the North and South Klondike Rivers in the Tintina Trench. No evidence of glaciation has been found in the Tintina Trench north west of this point, nor in the entire area of the Klondike Plateau stretching westwards into central Alaska. Dawson City and the Klondike gold fields are part of the unglaciated terrain.

No date has been assigned to this glaciation but the poorly preserved lateral moraines and the lack of terminal moraines suggest that it dates from at least as far back as Early Wisconsin.

A large end moraine at Chapman Lake, near Mile 74 of the Dempster Highway, indicates a later less extensive glaciation in the Blackstone valley. The minimum date for ice recession from the Chapman Lake moraine, determined from a radiocarbon date on organic material above till is 13,870 years B.P. (Dyck et al., 1966; GSC 296).

The North Fork moraine, between mile 48 and mile 54, Dempster Highway, forms the evidence for a still younger advance of a glacier in the upper East Blackstone valley (Plate 9). A minimum date of 11,250 $\pm$ 160 years B.P. was obtained for this moraine (Lowdon and Blake, 1968; GSC 470, p. 231). The neighbouring valley of Foxy Creek has a terminal moraine with a minimum age of 13,740 years B.P. (Hughes in Ricker, 1968; GSC 515, p. 25A). No evidence of later glacial advances beyond the cirque zone were found in the upper East Blackstone valley, or in its tributary valleys.

During the intermediate and youngest glacial advances in the Blackstone valley, ice passed in a westerly direction down Tombstone valley and in an easterly direction down the North Klondike valley.

The Chapman Lake moraine in the Blackstone valley is not matched by well defined moraines in the Klondike valley. A weakly developed terminal moraine (Plate 9 in end pocket) is developed at the big bend in the North Klondike River 16 km (10 mi) from its source. This moraine may mark the limit of an advance of the North Klondike Glacier contemporaneous with the North Fork advance or the Chapman Lake advance of the Blackstone Glacier a few miles to the north. Notable features in the vicinity are a series of sub-marginal meltwater channels cut in debrock on the north side of the valley just above the level of the valley floor, which suggest a prolonged ice stand at that level with the front nearby (Hughes, pers. comm.). Above the big bend the lower slopes on both sides of the Klondike valley are plastered with ground moraine. This merges indistincly into the weathered mantle of the upper slopes.

The large number of cirques at the head of Tombstone valley and the current existence of debris covered glaciers in some of these cirques, indicate that this valley has undoubtedly been glaciated as recently as the North Klondike valley. Moraine evidence is scarce, however. A lateral moraine has been noted 13 km (8 mi) down Tombstone valley on the south slope at 1,070-1,200 m (3,500-4,000 ft), and this feature may be contemporaneous with the moraine at the big bend in the North Klondike valley.

The evidence from the North Klondike and Tombstone valleys suggests that the last valley glaciers extended at least 13 km (8 mi) and 16 km (10 mi) down the Tombstone valley and the North Klondike valley respectively. A radiocarbon date of 9,650 $\pm$ 200 years B.P. (Gray, 1970; GSC 1172) was obtained for the organic material at a depth of 5 m (16.5 ft), above inorganic silts in a palsa bog 3 km (2 mi) below the cirque zone in the upper North Klondike valley, (Locality TL1, Plate 5) and may be considered the minimum age for this valley glaciation. If the glacial advance in the North Klondike valley was contemporaneous with that producing the North Fork moraine in the Blackstone valley it must have taken place prior to 11,250 years B.P., and if contemporaneous with that producing the Chapman Lake moraine it may have occurred a little prior to 13,870 years B.P. The dates 9,650 years B.P. and 13,870 years B.P. may therefore be taken as reasonable outside limits for the period of retreat of the last valley glaciers in the upper North Klondike and Tombstone valleys.

In these two valleys the details of the glacial history assume great relevance to the present study, for volumes of talus accumulation and rates of erosion of the rock wall supply area have been assessed for three talus cones (cones 6821, 6824 and 6825) in the North Klondike valley between the cirque zone and the palsa bog from which the dated sample was obtained. The period of non-disturbance by glacier ice dates back to the recession of the valley glaciers in the upper North Klondike valley. i.e. between 9,650 and 13,870 years B.P. To simplify the calculations the assumed postglacial period of the sites of the cones will be taken as 12,000 $\pm$ 2,000 years.

Small well formed moraines are located at the lips of many of the cirques in the Tombstone area. They possess a better developed vegetation and soil cover than appears to be the case on the outer neoglacial moraines of the Natazhat and Klutlan Glaciers in the southern Yukon, which are between 3,500 and 500 years old (Rampton, 1969, p. 79). The cirque moraines in the Tombstone area probably represent either a recessional phase of the last valley glaciation between 10,000 and 14,000 years B.P., or a subsequent minor readvance between 10,000 and 3,500 years B.P. In either case they have not affected the rock walls for which talus volumes and erosion rates have been calculated.

Several ice cored rock glaciers, described as <u>debris-covered glaciers</u> by Vernon and Hughes (1966) and termed <u>cirque-floor rock glaciers</u> by the writer, may be found inside these moraine limits.

They probably represent a readvance subsequent to the deposition of the cirque moraines. A minimum age of 1,000 years for the advance of one of these rock glaciers is suggested from the present state of its lichen cover[1].

The ice core in the cirque-floor rock glaciers may be progressively melting today. This is deduced from the occurrence of large hollows along the backs of several of these forms, where talus is not being actively supplied to their surfaces.

Only three small debris free glaciers exist in the Tombstone region today. A detailed examination of one glacier located in an east facing cirque below Mount Monolith, (Plate 10), indicates a presently negative glacial regimen. It has retreated half a mile from a terminal moraine of very fresh appearance. Crustose lichens of Rhizocarpon geographicum spp attain maximum thalli diameters of 10 mm on the moraine, suggesting glacial recession from this moraine limit within the last 50-100 years.

b) Wernecke Mountains (Map 4 in end pocket)

In the eastern region evidence for the oldest of three glaciations exists only in the form of high level erratics found in widely scattered localities (Camsell, 1905, p. 187-188; Vernon and Hughes, 1966, p. 12). Two subsequent glacial advances have

---

1. For discussion of minimum ages based on lichen cover, see chapter 3, p. 45 and chapter 8, p. 185.

been deduced from terminal and lateral moraine limits in the Hart and Wind valleys. During these advances, large glaciers emanated from ice sheets in the Selwyn Mountains and the Backbone Ranges to the south east of the Wernecke Mountains, and pushed north west down tributaries in the upper part of the Bonnet Plume and Stewart basins. Distributary lobes of ice then moved west from the Bonnet Plume valley, across a low divide into the Wind valley; and north from the Stewart basin up the Beaver valley and across another low divide into the Hart valley. During the earlier of these two advances the transection glaciers were joined by tributary glaciers from valleys heading in cirques in the Wernecke Mountains, and moved northwards onto the Peel Plateau well beyond the northern limit of the Wernecke Mountains. A locally nourished glacier in the Bear River valley probably coalesced with the Wind valley transection glacier during this advance.

During the last major glacial advance, the transection glaciers in the Wernecke Mountains did not extend so far to the northwest. The glacier in the Wind River valley terminated about 13 km (8 mi) north of the confluence of the Bear River and the Wind River. Lateral moraines of the Wind River glacier deposited during this advance curve continuously around into the re-entrant created by the lower Bear River valley, in one case blocking off a tributary of the Bear River and impounding a lake. It is therefore suggested that the Bear Glacier was not coalescent with the Wind Glacier, but that a lobe from the latter moved into the ice free lower Bear River valley.

The locally considerable thickness of outwash deposits 7 km (4 mi) above the mouth of the Bear River marks the probable terminus of the Bear Glacier at the time of this advance, although morainal deposits were not noted. There is no evidence between this point and the cirque zone at the head of the Bear River valley of any subsequent valley glacier readvance.

A minimum date of 12,120 ± 140 years B.P. (Dyck and Fyles, 1963; GSC 67-2, p. 8) has been established for the culmination of the last major advances of the Hart transection glacier at Hart Lake (64°35' N, 138°17' W). The Bear River valley is about 80 km (50 mi) to the east of Hart Lake and so correlation of the Hart Lake advance with the last major advance of the Wind and Bear Glaciers is somewhat tentative. 12,000 ± 2,000 years B.P. is taken to be a reasonable interval for the deglaciation of these valleys, however. Knowledge of this interval enables calculations of the rate of talus accumulation and rock wall erosion to be made for the upper Bear River valley.

Vigourous glaciation in the upper Bear River valley during the last regional glacial advance is attested by striae observed in two localities on the metasediments of the region, (Plate 6). One group occurs on quartzite 155 m (500 ft) above the floor of the valley of the South Fork of the Bear River (Locality BL1, Plate 6), and has a trend parallel to the valley. The second group occurs on a dolomite rock bar crossing the floor of a tributary valley 1.5 km (1 mi) from the headwall, (Locality BL2, Plate 6). The scarcity of striae evidence is due to the rapid destruction of the outcrop surfaces on the metasediments especially in the dolomites. The latter rapidly acquire a rough, orange weathering crust upon exposure to the atmosphere.

6. PRESENT CLIMATE

The Ogilvie and Wernecke Mountains have a Polar tundra climate according to Köppen's classification (Haurwitz and Austin, 1944, p. 153-155). They are characterised by very cold winters, cool short summers and low annual precipitation. Dawson City and Mayo, two stations on the southern periphery of this mountain area at elevations of 340 m (1,100 ft) and 490 m (1,600 ft) respectively, have mean temperatures of -5°C and -3°C and mean annual precipitation values of 29.5 cm (11.8 in) and 28 cm (11.2 in). The mountain zone is 950-1,900 m (3,000-6,000 ft) higher than these stations and probably has a mean annual temperature of about -10°C. The mean annual precipitation in the mountain zone probably ranges between 50-75 cm (15-30 in). The relative aridity is the principal reason for the presently insignificant glacier cover in this cold climate region.

In response to the cold climate most of the Ogilvie and Wernecke mountain region lies within the tundra zone, the treeline being located at 750-1,050 m (2,500-3,500 ft). Permafrost is widespread and is at least 120 m (400 ft) thick at comparable elevations in the Keno Hill area about 160 km (100 mi) to the south of the field areas (Brown, 1970, p. 153).

Morphogenetically the region may be classed as periglacial because it is characterised by the presence of permafrost and by a tundra vegetation cover and, above all, because it displays in its landforms evidence of the importance of cryogenic processes, (Bird, 1967, p. 159).

CHAPTER 2

POSTGLACIAL ROCK WALL EROSION

1. INTRODUCTION

Several local rates of erosion by scarp recession have been calculated in recent years (Freise, 1933; Poser, in Rapp, 1960a, p. 88; King, 1956; Rapp, 1960a; Wahrhaftig and Cox, 1959; Pearce, 1970). Denudation on a larger scale has been assessed by measuring the suspended, dissolved and bed load carried by rivers from their drainage basins (Langbein and Schumm, 1958; Corbel, 1959; Judson and Ritter, 1964).

Scarp retreat has usually been given in terms of the mean retreat, in linear measure, of a vertical projection of the scarp. Rapp's method entailed estimation of the volume of talus cones and the area of the vertical projection of the rock wall source. Division of the former by the latter gave the total retreat normal to a vertical projection of the wall.

A discrepancy between the present rates of scarp retreat and the rates of general down wasting of complete river basins within glaciated mountain regions in alpine and arctic areas was noted by Rapp (1960a, p. 86-89). His rates of postglacial scarp retreat in Spitsbergen are in the order of either 120-370 mm/1,000 yr, depending on whether the postglacial is taken as 30,000 years or 10,000 years. He quotes values of 400 to 2,000 mm/1,000 yr for basins in continental

Europe which were wholly or partially glaciated. Rapp suggests that the latter figures represent erosion of glacially derived overburden rather than underlying bedrock. Comparisons between rates of erosion established for such diverse geomorphological systems as river basins and scarps is therefore not a very fruitful enterprise. Indeed it is obvious that study of variation in effectiveness of erosive processes on bedrock of different lithologies and in different climatic environments will have to be based on the study of limited and well bounded areas of bedrock and not on large river basins which oontain varying thicknesses and sizes of unconsolidated material.

The present study of the rate of postglacial scarp retreat in the Ogilvie and Wernecke Mountains was undertaken partly to augment the limited evidence of erosion rates in periglacial regions and partly to test the superficial observation that the rate of erosion of the igneous intrusives in the Ogilvie Mountains is slower than that of the metasedimentaries. An advantage of the study regions in the Yukon as compared with Rapp's escarpment in Spitsbergen is that the postglacial interval can be estimated more precisely from the available evidence.

2. BASIC ASSUMPTIONS

The system must be clearly divisible into the zone of erosion, viz. the bedrock wall, and the zone of deposition, viz. the talus slope. The former supplies debris through processes of weathering and removal to the latter. Plate 1 illustrates the zone of bedrock erosion and the zone of talus accumulation in such a system. The talus accumulations and their rock wall source areas were usually very easy to delimit, and they are also of dimensions small enough to be amenable to measurement by means of field traverses.

Erosion of the rock wall is considered to include both weathering of the bedrock and transportation of the weathered products to the major zone of accumulation within the postglacial period, i.e. to the talus slope below the rock-wall. Thus temporary accumulations of debris in the gullies on the rock walls are not included in the calculations of talus volumes.

The method necessitates that the bi-zonal system be considered closed both in space and time. The talus accumulation is assumed to represent all products of erosion from the same wall area throughout the postglacial period. It is therefore implied that the wall area has not changed, that all pre-existing products of erosion were removed by the last glaciation, and that there has been no postglacial removal of debris from the talus slope. The calculation and comparative assessment of rates of erosion, also supposes that the postglacial time interval is known and that it is the same for all examples considered. These assumptions are now discussed in turn.

a) <u>Assumption of unchanging rock wall area</u>.

The only way the areal bounds of the rock walls in the Ogilvie and Wernecke Mountains could have appreciably changed postglacially is by the operation of erosional processes on the rock walls themselves. The measured volumes of talus accumulated below the rock walls (Appendix II, Table II.5) indicate that change in the rock wall areas postglacially is negligible, however.

b) <u>Assumption of removal of all pre-existing talus debris during last glaciation.</u>

The complete absence of boulder trains down valley from the talus slopes suggests removal of all or nearly all pre-existing talus by the last valley glaciers. The talus cones presently observed are fairly symmetrical in form and are clearly undisturbed by the passage of glacial ice. They must have been formed during and since the disappearance of the valley glaciers from the two field areas.

c) <u>Assumption of zero loss of debris from the toe of the talus slope.</u>

Little debris appears to have been removed from the toes of the talus slopes during the postglacial period. Streams issue from the talus only during the period of the spring snow melt and during occasional heavy summer rain storms. Even at these times, however, they are remarkably clear, and obviously transport little debris in suspension. No debris aprons were observed in the protalus footslope which would indicate the washing out of fines during heavy precipitation, and in any case the fines appear to constitute a minor fraction of the debris in the talus cones. (Table 2.1 and Figs. 2.1 and 2.2).

TABLE 2.1

PROPORTION OF FINES ON THE SURFACE OF TALUS CONES.

	% of cone area covered by particles with 'b' axis < 12.5 mm
Cone 6805	3.7
Cone 6808	6.0
Cone 6809	5.9
Cone 6810	18.3
Cone 6811	5.5
Cone 6812	4.6
Cone 6824	0.9
Cone 6825	0.3
Cone 6830	6.7
Average for all cones	5.8

Tables 2.1 reveals that an average of only 5.8% of the surface area of nine talus cones is covered by debris whose 'b' axis is less than 12.5 mm. Mechanical analyses of fines sampled on cones 6808, 6809 and 6830 in Figure 2.1 and fines sampled on cone 6811 in Figure 2.2 reveal that only 5 to 45% of the fines by weight are less than gravel sized, and only 0 to 5% are less than sand sized according to the Wentworth classification of particle sizes (Wentworth, 1922).

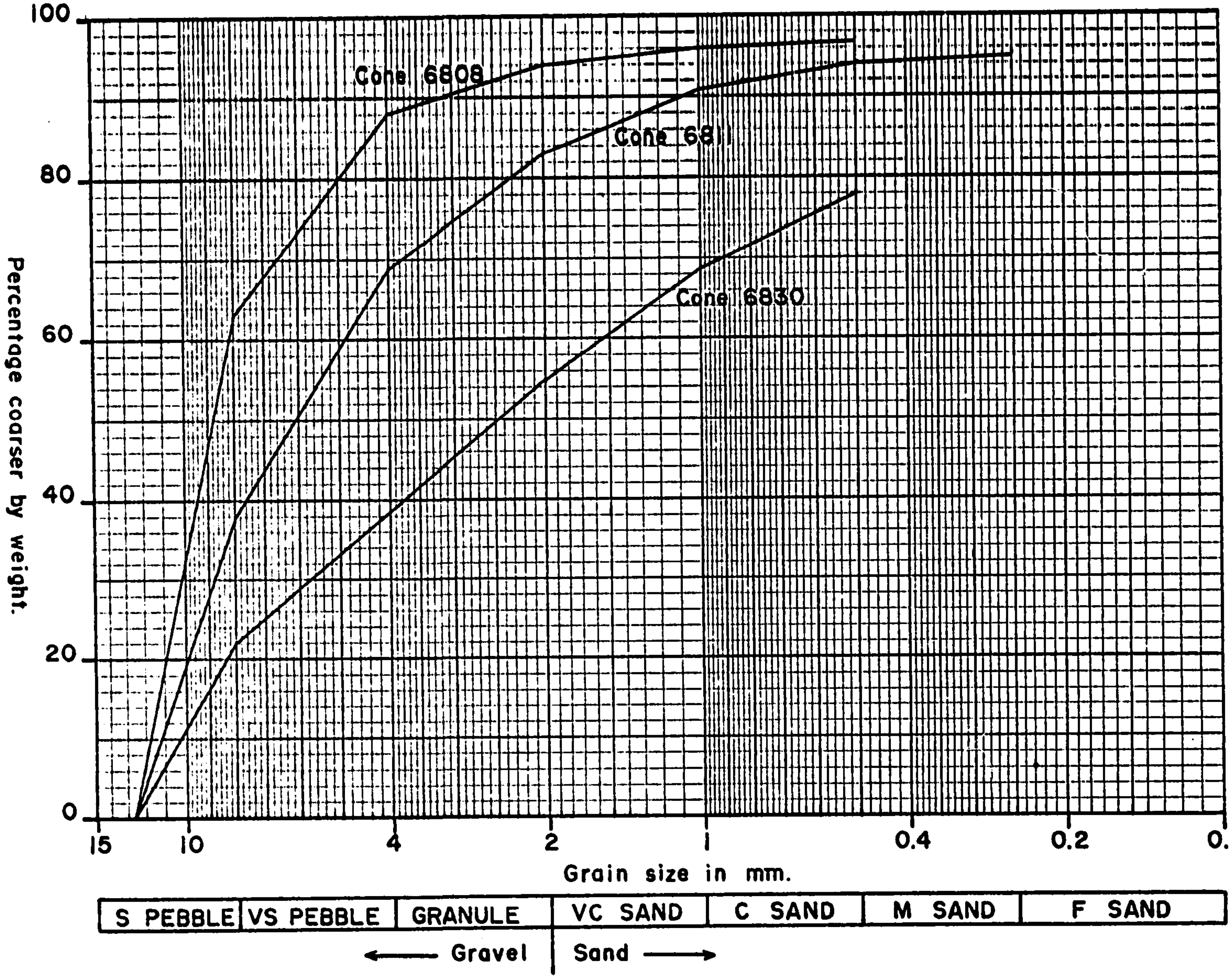

FIG. 2.1 CUMULATIVE GRAIN SIZE CURVES ON THREE CONES

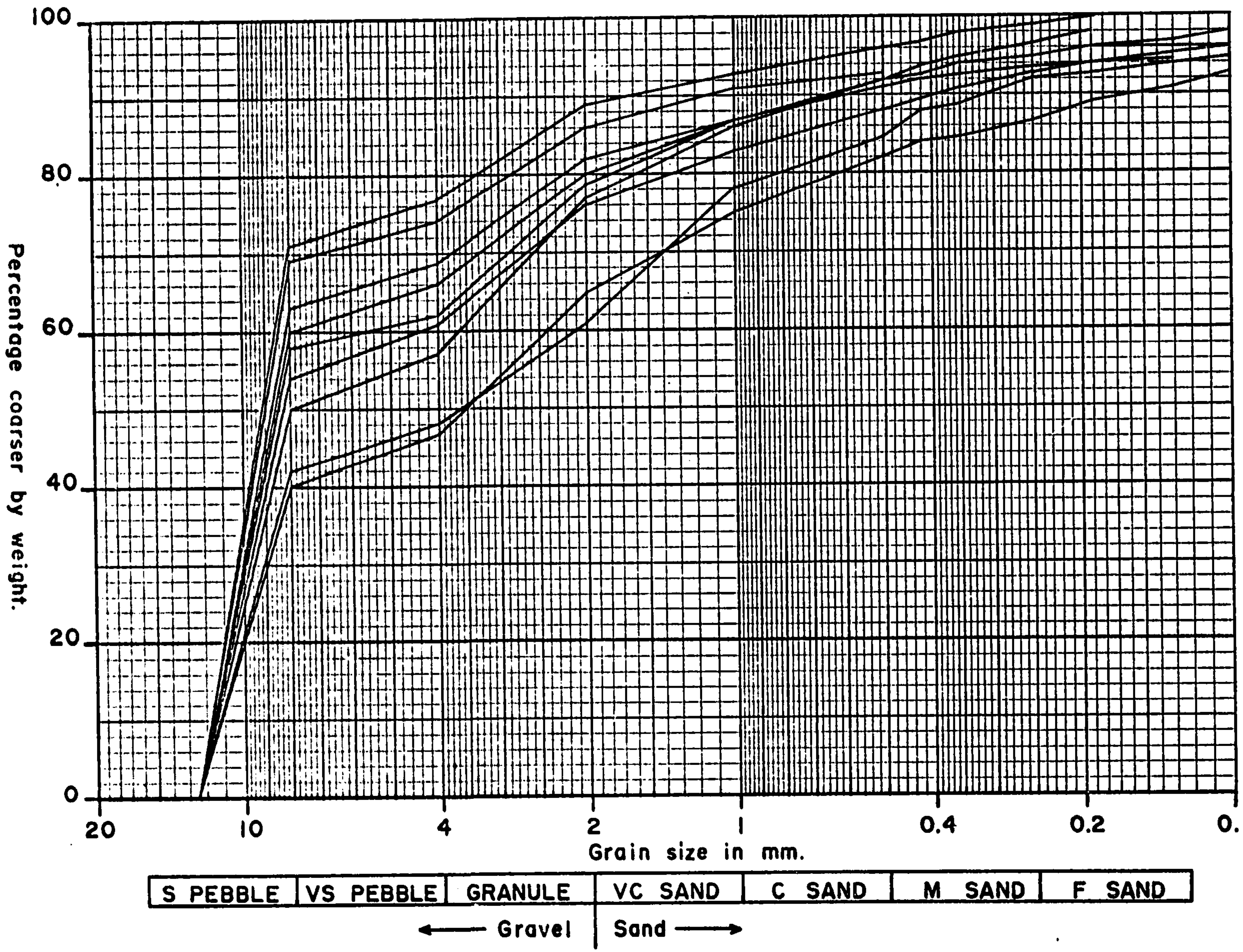

FIG. 2.2 CUMULATIVE GRAIN SIZE CURVES ON CONE 6811

If the supply of fines had exceeded that of coarse material during the build-up of the surficial layer of talus, a much larger percentage of fines would be expected, near the surface. Penetration of fines into the frozen talus 1-2 m (3.25-6.5 ft) below the surface is unlikely since ice lenses, interstitial ice and previously deposited fines fill the void spaces in the debris mass. Thus the recently deposited fines can at the most only fill the voids between the coarse particles in the surficial layer. Similar conditions could be applied to the accumulation of former surficial layers throughout the postglacial period and hence to the entire debris mass. Loss of all fines which could be present in the talus mass would give a potential porosity increase of about 20% (Fraser, 1935, p. 992), and so the net loss of solids from the cone could theoretically reach 20%. The actual loss of solids in fluid suspension is probably much less than this, however.

Solutional loss is insignificant since the rock surfaces are wetted only emphemerally, since there is no percolation in the frozen zone, and since the rock types are not susceptible to rapid solutional loss with the possible exception of the dolomite which forms the talus particles in two of the cones for which volumes have been calculated, (cones 6804 and 6808).

d) <u>Assumption concerning postglacial interval</u>

The evidence given in chapter 1 suggests that deglaciation in the Bear River valley and Tombstone areas occurred 12,000 ± 2,000 years B.P. It is practically certain in the Bear River valley that all the sites for which erosion rates were calculated were deglaciated within a few hundred years of each other, as they are only spread along a four mile stretch of the valley. Three of the four critical sites in the Tombstone area, are within 3 km (2 mi) of each other in the North Klondike valley and have also been deglaciated within an interval of a few hundred years. The fourth site, in the Tombstone area, is in Tombstone valley but in a topographically similar position to the other sites, inside limits of the last regional glaciation and outside the zone of the later cirque glacier advance.

Although good reasons have been forwarded for considering the uncontrollable errors introduced by these assumptions as small, it is valid to indicate which of the errors would increase the amount and rate of erosion, and which of the errors would decrease these values, (Table 2.2).

TABLE 2.2

EFFECT OF UNCONTROLLABLE ERRORS IN EROSION MEASUREMENTS

Assumption	Direction of possible change in values			
	Talus vol.	Rock wall area	Erosion amount	Erosion rate
a	0	0	0	0
b	-ve	0	-ve	-ve
c	+ve	0	+ve	+ve
d	0	0	0	-ve

Assumption a gives negligible error; assumptions c and d give errors believed to be of slight significance as compared with assumption b which probably gives the most important residual error. Thus the volume of talus accumulated postglacially and the amount of erosion are probably overestimated, due to the fact that the glaciers may not have removed all the pre-existing talus debris.

3. EQUATION FOR ROCK WALL EROSION

Mean recession of present rock wall surface in m[1]

$$E1 = \frac{\text{Net vol. in cu.m of debris on talus slope (VN) divided by}}{\text{Source area in sq.m of rock-wall (RK)}}$$

Mean postglacial rate of recession of present rock wall surface (mm/1,000 yrs)

$$= \frac{E1 \times 10^6}{12{,}000}$$

The details of the method, the calculation of VN and RK and an assessment of the empirical errors introduced are presented in Appendix II. The maximum possible errors are accumulated through all the steps of the calculation, and the mean, maximum and minimum values for VN, RK and the postglacial interval are finally fitted into the above equations. The mean values for the amount and rate of postglacial erosion are therefore bounded on either side by maximum and minimum values.

---

1. The units used in calculation of erosion rates in this thesis are metric.

4. RESULTS OF CALCULATIONS AND COMPARISON WITH OTHER ARCTIC AND ALPINE ENVIRONMENTS.

The results of the analysis of amounts and rates of postglacial rock wall recession are presented in Table 2.3. These values are for recession on the sloping wall, and not the vertical projection of the rock wall.

TABLE 2.3

AMOUNTS AND RATES OF POSTGLACIAL RECESSION OF ROCK WALLS

Cone	Amount of recession			Mean annual rate of recession		
	Mean (m)	Max. (m)	Min. (m)	Mean mm/1000 yr	Max. mm/1000 yr	Min. mm/1000 yr
6801	0.636	1.170	0.388	053	117	028
6804	0.863	1.865	0.450	072	187	032
6808	0.510	1.161	0.270	043	116	019
6813	2.060	3.880	1.235	173	388	088
6814	1.025	1.925	0.615	086	193	044
6816	0.271	0.620	0.144	023	062	010
6821	0.085	0.160	0.051	007	016	004
6824	1.245	2.340	0.748	104	234	054
6825	0.345	0.650	0.207	029	065	015
6830	0.358	0.674	0.215	030	067	015

The median value for amount of erosion in the postglacial period is between 0.636 and 0.510 m. The values range from a maximum possible amount of 3.88 m above one cone to a minimum of 0.051 above another cone.

The median rate of erosion is between 53 and 43 mm/1,000 yr. The values range from a maximum of 388 mm/1,000 yr to a minimum of 4 mm/1,000 yr.

The two igneous rock walls for which values were derived, a syenite rock wall, and a diabase rock wall, have lower values than six of the eight metasedimentary walls. The substantive evidence from the zone of syenites, in the form of the low ratio of talus height to rock wall height and the frequently thin talus mantle, through which bedrock can be observed in places, indicates in association with the quantitative evidence that the rate of weathering in the intrusives is much slower than in the metasediments.

Table 2.4 compares the figures derived above for mean amount and rate of rock wall retreat under postglacial conditions with those derived by other workers for rock walls in periglacial, alpine and temperate environments.

In order to achieve comparability with some of the results of other workers, the values for the amount and rate of erosion of the sloping rock walls in the field areas had to be converted approximately to their vertical and horizontal equivalents. The latter were calculated by multiplication of the values for the sloping wall by the secant and cosecant respectively of the mean rock wall angle.

The erosion rates derived from the Ogilvie and Wernecke Mountains are lowest of four detailed analyses in mountain areas of Europe and north west North America. They are also very much lower than the rates established by King, (1956) and Freise, (in Rapp, 1960 a,

TABLE 2.4

LONG TERM RATES OF ROCK WALL EROSION IN ARCTIC, ALPINE AND TEMPERATE ENVIRONMENTS WITHIN THE HOLOCENE PERIOD

Author	Locality	Period of erosion	Rock type	Nature of accumulation	No. of cases	Erosion normal to wall surface: Amount m	Erosion normal to wall surface: Rate mm/1,000 yrs.	Vert. recession equivalent: Amount m yrs	Vert. recession equivalent: Rate mm/1,000 yrs.	Horiz. recession equivalent: Amount m	Horiz. recession equivalent: Rate mm/1,000 yrs
Poser, 1954	Austrian Alps	10,000 yrs	gneiss schist serpentine		3					7-10	700-1,000
Rapp, 1959	Mt. Templet, Spitsbergen	10,000 yrs	limestone chert sandstone	talus cones	4	2.3-2.7	230-270 80-90*			3.4-4	340-400
Wahrhaftig & Cox, 1959	Alaska Range	1,000-3,000 yrs		rock glaciers	40			9.4	3,000-9,000		
Pearce, 1970	St. Hilaire, Quebec.	13,000 yrs	igneous breccia	talus debris	1	0.52	40				
			gabbro	talus cone	1	0.24	18				
Gray, 1971	Ogilvie & Wernecke Mts. Yukon Terr.	12,000 yrs	quartzites dolomites & slates	talus cones	8	0.27-2.06	20-170	0.35-2.70	20-230	0.42-3.19	30-260
		12,000 yrs	syenite diabase		2	0.08-0.36	7-30	0.24-1.05	20-90	0.08-0.38	7-320

* Erosion rate if postglacial interval in Tempelfjord, Spitsbergen is 30,000 yrs.

p. 88) for scarp recession in tropical regions, and emphatically indicate that rock wall recession in periglacial zones is relatively slow.

The rates quoted by Wahrhaftig and Cox (1959, p. 430) for central Alaska are in the order of sixty times that of the median value for the central Yukon. The regions are climatically not dissimilar and so other reasons must be sought for the disparity in the rates. One of the reasons may be that although the postglacial period was 10,000 years in length in the central Alaska Range, (Wahrhaftig and Cox, 1959), these authors calculated rock wall erosion rates on the basis of a maximum erosion interval of only 3,000 years, i.e. the maximum interval allowed by them for postglacial rock glacier development. This is thought to be erroneous since it is likely that debris was being accumulated in considerable volumes prior to being involved in the activation of rock glaciers. If the rates were derived for a 10,000 year period the values would be ten times that of the median value in the central Yukon. A second reason for the discrepancy in rates may be that several of the rock glaciers used by Wahrhaftig and Cox in their calculations headed in cirques, and an ice core, rather than simply interstitial ice, may have been present. If the ice content were higher the figure for the volume of debris and hence the rate of erosion would be correspondingly reduced. A third possible reason for the very high rate of erosion quoted by Wahrhaftig and Cox is the possibility that many of the larger blocks eroded from the rock walls were not removed far from the source areas by the last glaciation and were re-incorporated by subsequent rock glacier movement. Despite these considerations erosion rates on rock walls above rock glaciers are probably an order of magnitude greater than the erosion rates of rock walls above talus slopes. This topic is discussed further in chapter 8.

Recent work by Pearce on postglacial rock wall recession at a low altitude site near Montreal, Quebec, indicates a rate of erosion of 40 mm/1,000 yr for a cliff composed of igneous breccia and 18 mm/ 1,000 yr for a cliff composed of gabbro. These values are near the low end of the range of values found for ten rock walls in the Yukon. They are in fact remarkably close to the mean values for the two rock walls composed of igneous intrusives.

CHAPTER 3

PRESENT DEBRIS ACCRETION ON THE TALUS SLOPES

1. INTRODUCTION

There is a general difficulty common to most of the previous studies of mass wasting on steep mountain slopes, e.g. by Rapp, (1960a, 1960b); Gardner, (1968); Stock, (1969); Luckman, (1971). This is the difficulty in distinguishing between the effect of processes in removing debris from the rock walls onto the talus slopes, and their effect in transporting already deposited debris further down the talus slopes. In this study the two distinct effects are isolated, removal of debris from rock walls to the talus slopes is discussed in this chapter whereas the present transport role of processes on the talus slopes and within the protalus rock glaciers is examined in subsequent chapters.

Short term rates of erosion can be calculated from recent debris accretion measurements and compared with mean postglacial erosion rates. The problem of assessing the frequency of erosional events of different magnitudes (Wolman and Miller, 1960) is a serious drawback to such a comparison and plagues even relatively long term studies such as Rapp's seven year study in northern Sweden (Rapp, 1960b).

For this reason the emphasis has been placed on the evaluation of the probable role of different processes, viz rock-falls snow avalanches, torrent avalanches, ephemeral run-off and slow debris shift, in transporting debris from the rock wall zone to the talus zone.

2. MEASUREMENT PROBLEMS

The chief problems encountered in the measurement of debris volumes transported onto talus slopes are the large size of these slopes, the frequent disturbance of the surfaces, and the potential hazards from rock-fall during the measurement process.

Freshly accreted debris must be adequately differentiated from old talus. A lichen cover exists on the little disturbed debris near the base of the talus slopes and so, freshly accreted debris can be measured if it reaches the basal zone of the talus slopes. But this method is useless for measurement of debris accretion over the frequently disturbed upper zones of the talus slopes.

Mats on nets placed on the talus surface have been used to differentiate freshly fallen debris from old debris (Rapp, 1960b, Gardner, 1968; Caine, 1969; Stock, 1968; Luckman, 1971). Limitations of this method have been the negligible fractions of the talus surfaces covered, the derivation of some of the debris on the mats from higher on the talus slopes, rather than from the rock walls, and their susceptibility to natural destruction.

The most valuable measurements of short term debris accretion have probably been obtained by measurements of debris on continuously snow covered talus surfaces (Caine, 1969) and on large elevated boulders (Luckman, 1971), although the limitations of these methods are that only winter and spring debris accretion can be measured.

Debris accretion due to the following processes or groups of processes was measured at suitable sites on talus slopes in the Ogilvie and Wernecke Mountains, using techniques designed to minimise these previously encountered difficulties.

1. Rock-falls
2. Snow avalanches
3. Torrent avalanches and ephemeral storm run-off
4. Combination of rock-falls, snow avalanches and slow debris shift.

3. ROCK-FALL ACCRETION

a) Rock-fall accretion on a continuous snow surface

In his work on talus slopes in the southern Alps, New Zealand, Caine, (1969, p. 94) measured debris accumulation on a continuous surface of undisturbed snow below a rock wall. He found a regular increase in debris accretion from the base to the top of the slope, with successive values of 0, 6, 48 and 61 cc/m^2 for four 100 m^2 quadrats. Gardner, (1970) also made measurements of debris on snow surfaces but his results are difficult to assess as the snow cover was not continuous and much of the debris is probably derived from a higher point on the talus itself.

On June 18th, 1969, recently fallen debris was measured on the snow covered basal slopes of a high steep syenite wall, at the head of the cirque above Moraine Lake in the Tombstone area (Plate 5, Locality TL4). At the time of measurement the snow on the basal slopes was deep and well packed. The rock wall averages 70° in inclination and is too steep to sustain the build-up of a thick snow cover. Avalanching is therefore of insignificant importance, and the debris on the snow slope was entirely derived by rock-fall.

Figure 3.1 is a diagrammatic view, from the north, of the main features of the rock wall and sampled snow slope. The snow slope was divided into zone A, situated below a steep chimney on the north wall and zone B, situated between this chimney and a deep cleft on the west wall at the head of the cirque.

In zone A the slope was divided into vertical segments so that the vertical distribution of the rock-fall debris on the slope could be ascertained and compared with the results obtained by Caine, (1969) in New Zealand. In zone B the total rock-fall accumulation was directly measured for the whole zone.

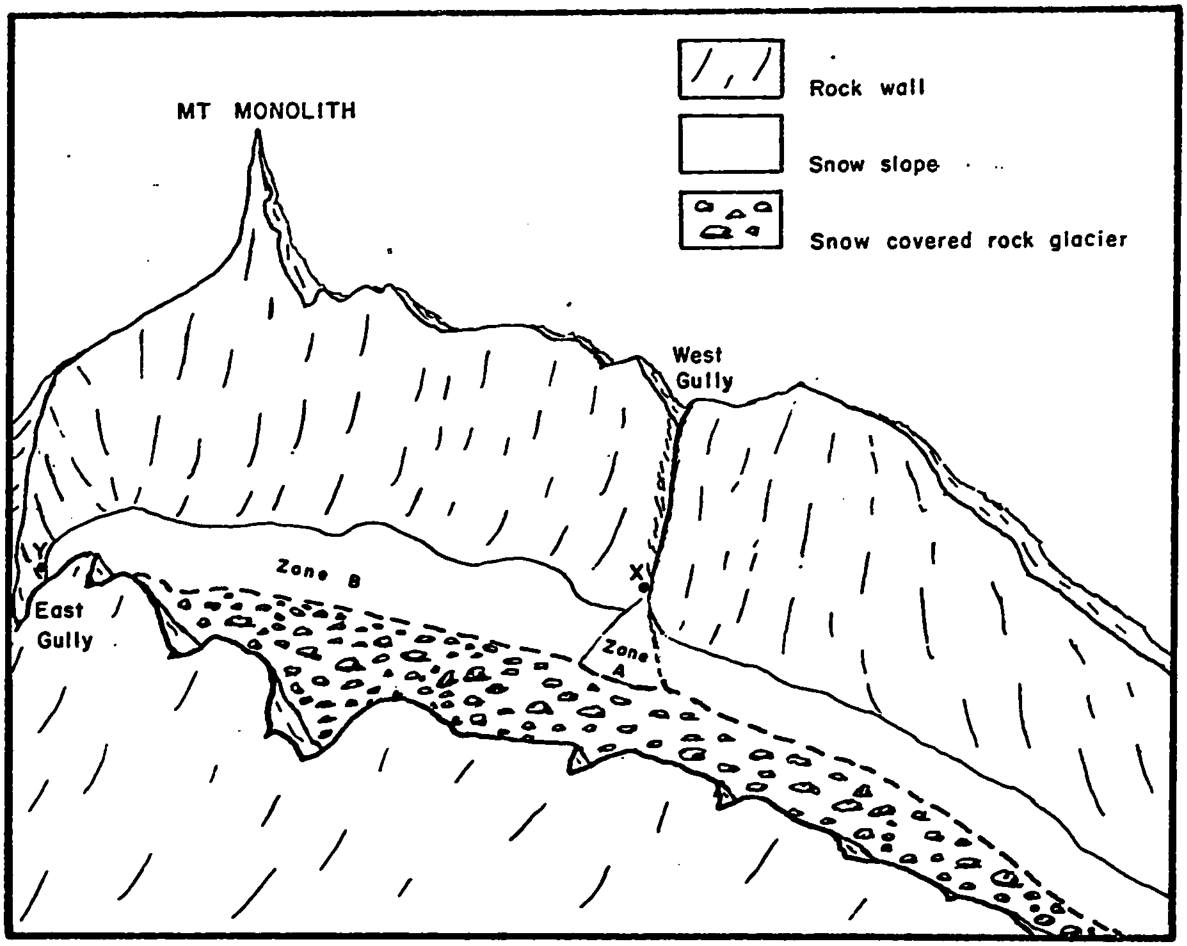

Mean wall height 430 m

Length XY along base of wall 475 m

Mean rock wall angle 70°

FIG. 3.1 ROCK WALL AND SNOW SLOPE AT LOCALITY TL4, TOMBSTONE AREA

In detail the method involved measurement of the 'a', 'b' and 'c' axes of fallen particles and conversion to volumes using empirical equations relating particle volume to the product of the three axes. Derivation of these equations for syenite, dolomite and orthoquartzite particle in Appendix III suggests that, in the aggregate, the volume of particles is approximately 0.5 to 0.6 times the product of the three axes. The weight of the particles is then calculated as the product of the volume and the assumed density of 2.7 gm/cc. Table 3.1 shows the total volume and weight of accreted debris for both zones.

TABLE 3.1

ROCK-FALL ACCRETION BELOW SYENITE WALL IN LOCALITY TL4, TOMBSTONE AREA, SPRING, 1969.[1]

	Total weight (kgm)	Total volume (m^3)	Rock wall area above zone (m^2)	Rock wall erosion (mm)
Zone A	3,205	1.188	48,600	.0240
Zone B	950	0.352	534,500	.0007
Total	4,155	1.540	583,100	.0026

[1] Only slight errors in total volume result from a subjective decision not to measure particles with 'a' axis <30 cm for top half of Zone A and all of Zone B, and 'a' axis <5 cm for lower half of Zone A. Haste was paramount in a zone of potential rock-fall danger.

It is clear from this table that erosion has been thirty times more vigorous in the zone below the narrow gully at the west end of the wall section than in the large zone below the smooth walls. This is a clear indication of the strongly localised erosion of the rock walls by small rock-falls over a short term period.

The 'b' axis of the largest fallen particle was 0.64 m. The total volume of particles finer than 5 cm in 'a' axis was slight. Therefore the rock-falls may be classified, after Rapp, (1960b, p. 97) as small boulder and pebble falls, which occurred as falls of individual or small groups of particles.

In Table 3.2 the rock-fall in Zone A is classified according to its vertical distribution on the slope. Each section covers an area of 40 m (130 ft) in a horizontal direction by 5 m (16 ft) in a vertical direction, viz. 200 m^2 (2,100 ft^2). Figure 3.2 is a graphical illustration of the vertical distribution of rock-fall volumes per unit area.

The density of debris measured on the Tombstone slope is about ten times greater than that measured by Caine, (1969) in New Zealand. The strong negative correlation of debris volumes with distance downslope observed by the latter is not noted in the Tombstone example. Apart from the possibility that this contrast is random, only one slope having been considered in each study, several systematic factors could be of importance, e.g. varying hardness of snow surfaces which retard particle movement to a varying degree (Gardner, 1970)

TABLE 3.2

VERTICAL DISTRIBUTION OF ROCK-FALL ON SNOW IN ZONE A.

Section	Distance from top of slope (m)	Slope angle	Volume (m^3)	Vol. in cc/m^2	Comments
1	0-25	43°	0	0	Measurements on boulders with 'a' axis > 30 cm
2	25-50	40°	.003	3	"
3	50-55		0	0	"
4	55-60		.034	170	"
5	60-65	31°	.175	880	"
6	65-70		.219	1100	Measurements on particles with 'a' axis > 5 cm
7	70-75		.146	730	"
8	75-80		.174	870	"
9	80-85		.116	580	"
10	85-90	24.5°	.242	1210	"
11	90-95		.026	130	"
12	95-100		.053	270	"

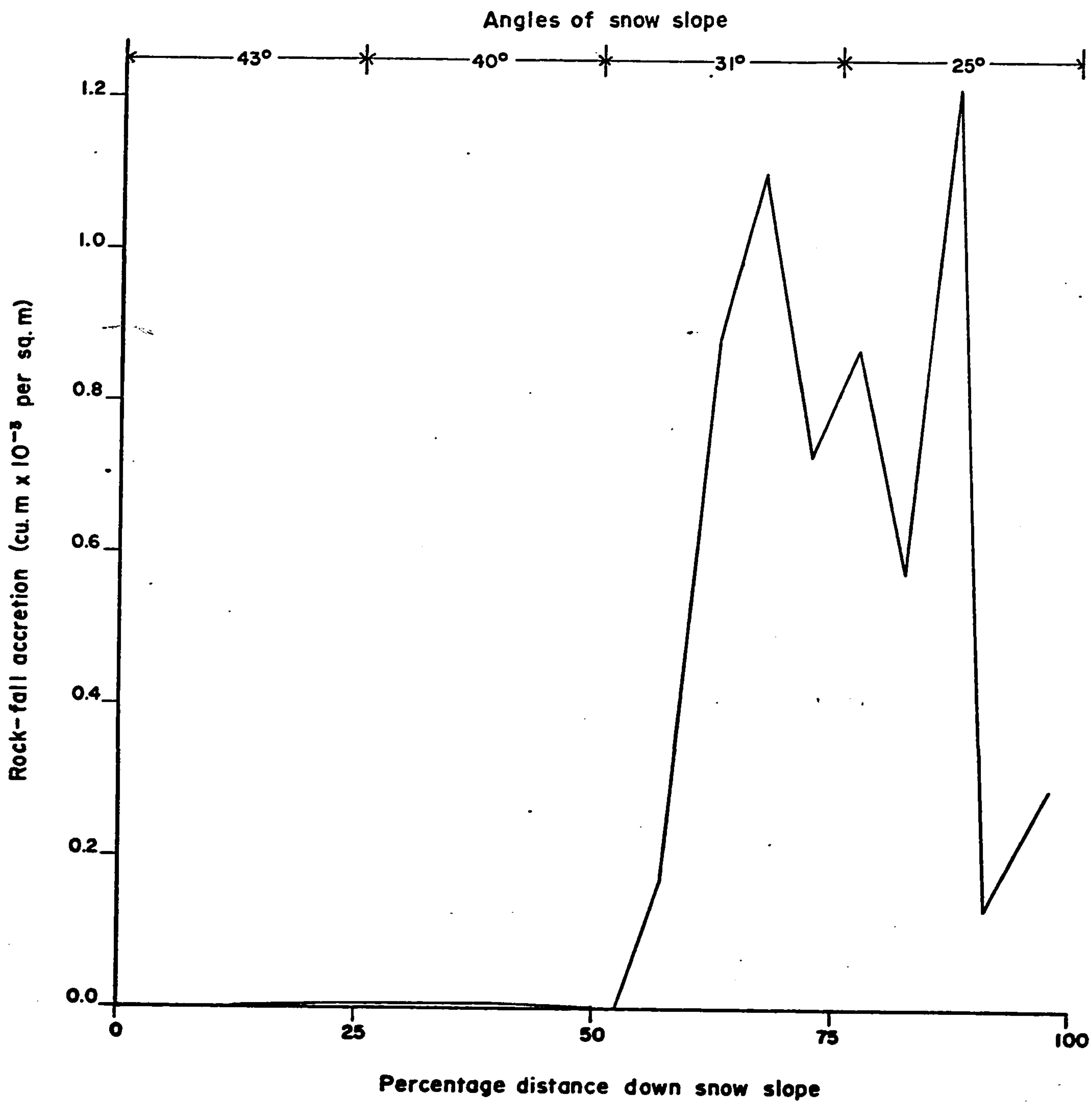

FIG. 3.2 DISTRIBUTION OF ROCK-FALL ACCRETION ON SNOW SLOPE AT LOCALITY TL4

and differences in frequency distribution of particle size which mean that particles have varying initial momentum on otherwise similar slopes. The particles contributing the greater part of the debris to the slope in the southern Alps appear to have been smaller in size than those in the Tombstone example (Caine, 1969, p. 93). Many more measurements of debris accretion on snow surfaces are necessary before Caine's hypothesis concerning vertical distribution of rock-fall debris on talus surfaces can be widely validated.

From Figure 3.2 the angle of 20° appears to be an approximate lower limit for debris accretion as a result of small boulder and pebble falls on snow surface. Debris accretion does not occur on the Tombstone snow slope above but does occur on snow at an angle of 37° in the New Zealand example discussed by Caine, (1969). Therefore there seems to be a general limit of 37°-40° for debris accretion on snow slopes.

b) <u>Rock-fall accretion on lichenous surfaces</u>

Below several syenite walls the talus zone consists merely of a narrow fringe of large boulders and cobbles interspersed with vegetated patches of fine gravel. Because of the steep walls and lack of gullies there are no avalanche processes to redistribute this coarse talus, and lichen cover has a chance to become established. Occasionally there are fresh rock-falls onto these slopes and if rock-fall has occurred within the last few decades the large particles involved can be identified by their sparse or non-existent lichen cover. By measuring the 'a', 'b' and 'c' axes of such debris below a known rock wall area, and converting them to volumes using the appropriate empirical relationship in Appendix III, a reasonable estimate can be made of the volume of debris which has fallen during a certain time interval prior to establishment of an extensive lichen cover on the fallen particles.

This estimate, however, is predicated on the fact that an average lichen free period and an early rate of lichen growth can be established in this environment. Lichen growth rates were studied in the central Yukon for several lichen species by measuring the largest lichen diameters on sample plots on the gold tailings in the lower Klondike valley and its southern tributary valleys.

Dredging operations on the gravels commenced in 1906 and continued until 1966. Maps showing the localities dredged on the Klondike tailings at different periods between 1906 and 1966 were made available by C.R. McLeod of the Geological Survey of Canada. They were used in the selection of seven sample plots, each 200 m^2 in area, on tailings dredged in 1907-1910, 1918, 1919, 1930-1933, 1932, 1940, 1952.

Crustose lichens of Rhizocarpon geographicum spp were the most easily recognised, and are useful age indicators for a longer period than the foliose lichens observed on the tailings. Therefore particular attention was given to finding sufficient numbers of examples of Rhizocarpon geographicum spp to calculate a mean value for the diameter of the largest five examples for each sample plot in addition to the diameter of the largest single example. This approach avoids the possible danger of a sampling a single large lichen which has accidentally survived on a fresh surface (Stork, 1963). The results are compiled in Table 3.3 in which the measurements made on other lichen species have also been indicated. Growth curves for Rhizocarpon geographicum ssp have been plotted in Figure 3.3 by linearly regressing the series of mean values and maximum values against the age in years since the surface was exposed to the colonisation process.

TABLE 3.3

LICHEN DIAMETERS (IN MM) ON KLONDIKE GOLD TAILINGS

SPECIES		1907-10	1918	1919	1930-33	1932	1940	1952
Rhizocarpon geographicum spp	mean of 5	18	14	13	10	8.5	7.5	2
	max.	22	16	14	10	9	8	3
Xanthoria elegans spp	mean of 5	25	16.5		12			
	max.	35	20		15			1
Umbilicaria spp	mean of 5	37	21		19			
	max.	43	25		22			
Parmelia spp	mean of 5				31			6
	max.				55			8

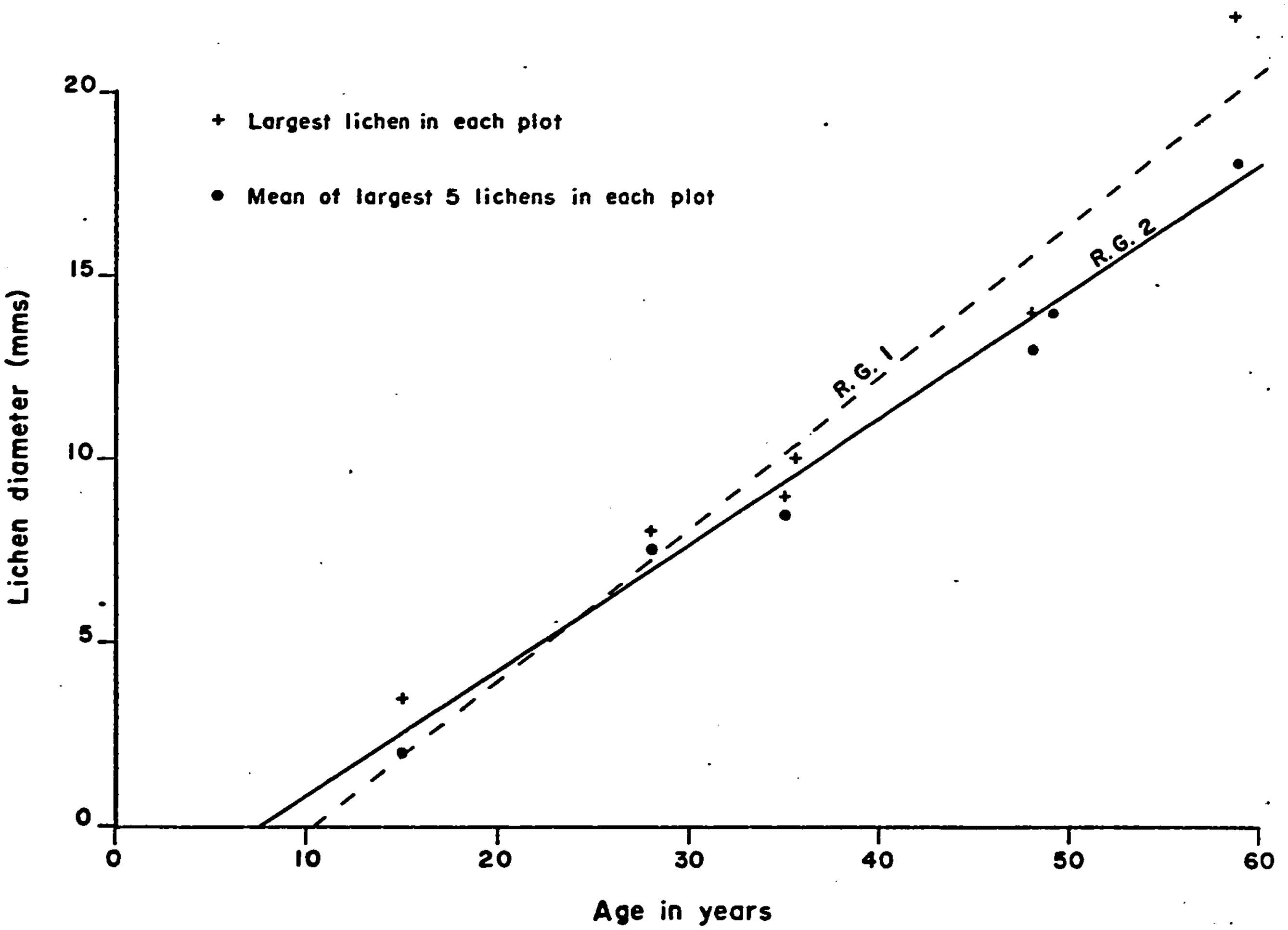

R.G. 1 = Regression line for means of largest 5 thalli of *Rhizocarpon geographicum spp* against age.

$y = 0.35x - 2.86, \quad r = 0.99, \quad S_{XY} = 0.77$

Rate 1 = 41 mm/century with 10 year colonisation period.

R.G. 2 = Regression line for means of largest single thallus of *Rhizocarpon geographicum spp* against age.

$y = 0.41x - 3.96, \quad r = 0.98, \quad S_{XY} = 1.46$

Rate 2 = 35 mm/century with 10 year colonisation period.

FIG. 3.3 LICHEN GROWTH CURVES FOR KLONDIKE GOLD TAILINGS

The mean and maximum rates of 35 mm/century and 41 mm/century are much greater than the rates quoted for most of the studies in arctic and alpine environments. (Beschel, 1958, 1965; Andrews and Webber, 1964; Benedict, 1967; Rampton, 1969). They are in reasonable accord, however, with Reger's long term growth rate of about 45 mm/century from the Gulkana Glacier moraines in the central Alaska Range (Reger, 1968).

Benedict (1967) and Andrews (1969) have discussed some of the objections to lichenometry based on the problems of variability of lichen growth due to differences in substrates and microclimates. (Jochimsen, 1966). The reliance on indirect dating of exposure of fresh substrates in many cases and the fact that lichens may occasionaly survive burial by ice (Goldthwait, 1966) can lead to gross errors in lichen factors. The present study was done on the surfaces of pebbles that have been dredged from beneath frozen muck, however, and definitely possessed no initial lichen cover. Furthermore the large area of the sample stations and the precise dates placed on them give a high degree of confidence in the growth curves. Beschel (1961) has suggested a rapid early growth phase for _Rhizocarpon geographicum spp_ before the lichen assumes a lower more uniform long term rate of growth up to its maximum size of several hundred millimetres. Therefore the rates of 35 mm and 41 mm per century may become somewhat lower as growth continues.

Examination of tailings surfaces exposed for less than fifteen years, did not reveal distinguishable thalli of _Rhizocarpon geogra-_

phicum spp. The lichen growth curve in Figure 3.3 indicates that colonisation may have commenced as recently as ten years after exposure of the surfaces, but if so, the lichens are too small to be identified positively in the field.

The lichen growth curve may be applied to the talus cones below the rock walls in the Tombstone area with certain reservations. The increase in altitude of 1,075 m (3,500 ft) means an average reduction in temperature of 10°F and a longer annual snow cover. The former may not significantly diminish the rate of lichen growth (Benedict, 1967), but the latter certainly reduces the growth season by about two months. Although the more frequent wetting of the talus surface due to summer showers in the mountains may compensate somewhat for this, it is valid to regard the growth rate established for the gold tailings as a maximum for the talus environment.

A second problem in the utilisation of the technique to calculate the age of recent rock-falls is the limited surface area of the fallen blocks examined for lichen cover. Thus random factors may dictate the presence or absence of lichens on individual rocks. Since many blocks were examined, chance error, which can give an overestimate or underestimate of age, was ignored.

Recently fallen debris below two rock walls in the Tombstone intrusion was measured. The results from the base of talus cone 6830 are presented in Table 3.4 which includes only the proportion of large rock-falls which have extended beyond the present talus base onto old debris. Thus it represents only very large rock-falls, not the smaller scale events which lead to accumulation of debris within the bounds of the talus cone itself. The corrected volume of the debris fragments are calculated and the volume totals placed into groups according to the lichen cover. Minimum ages are assigned to each group on the basis of the lichen growth curve.

TABLE 3.4

ROCK-FALL DEBRIS ACCUMULATION BEYOND THE BASE OF CONE 6830

Lichen cover	Lichens absent	Foliose spp only	*Rhizocarpon geographicum* ssp size range (mm)					
			2-7	8-12	13-17	18-23	24-35	0-35
Min. age of debris (yrs)	0-15		15-30	30-45	45-60	60-75	75-100	0-100
Vol. of debris (m^3)	$\underbrace{4.36 \quad 5.24}_{9.60}$		3.94	3.63	5.40	13.47	1.48	37.52
No. of particles	24	18	9	8	7	3	1	70

A low total accumulation of 37.52 m^3 over a minimum period of 100 years is noted. The rock wall from which the debris is derived has an approximate area of 48,000 m^2 (see Appendix II, Table II.7). The maximum rate of rock wall erosion resulting from very large rock-falls, over a minimum period of 100 years before the present, is therefore 8 mm/1,000 years. This represents .078 m of erosion if extrapolated through the postglacial period. Extreme rock-fall variability is indicated throughout the 100 year minimum period in Table 3.4.

The inherent weakness in the data from below talus cone 6830 is that no account can be taken of large recently fallen fragments which did not reach the base of the slope, a problem especially serious if they fell on a soft snow surface and became arrested in their progress down the slope.

In the second basal slope examined in the syenite zone this problem is eliminated. The site is represented by Locality TL5, in Plate 5. The rock wall from which the debris fell is illustrated in Plate 15. Gullies and associated talus cones are absent along a wall length of 750 m (2,450 ft). The basal slope is covered with large lichenous blocks, interspersed with vegetated zones of fines indicative of the lack of regular disturbance by spring avalanches or frequent pebble falls. Several recently fallen blocks, distinguished by their lack of a lichen cover, lie scattered among the older lichenous debris. Volumetric measurements were made on blocks, of 'a' axis >30 cm, on which lichens were absent.

A total volume of 37.56 m^3 was calculated over a basal fringe 400 m (1,300 ft) long by 100 m (325 ft) wide. This is the rock-fall accretion over a period of at least fifteen years before the present from a rock wall area of approximately 130,000 m^2 (calculated photogrammetrically). This represents a rate of erosion of 19 mm/1,000 yrs and would represent 0.19 m of recession if extrapolated through the postglacial period.

A very large rock-fall occurred near the top of a diagonally sloping crack in this rock wall on Sept. 2nd, 1968. The operative process was frost bursting and thawing, as indicated by below freezing shade temperatures in the vicinity, and by the fact that the rock-fall occurred at 19:00 hours, shortly after early evening insolation had commenced to raise the rock surface temperature at the source.

This was the only major rock-fall occurrence on this wall in sixty days spent in the vicinity over parts of three summers. The magnitude of the event was estimated by measuring the fragments. They could be readily identified by the texture and colour of the mineral assemblage, by their abrasions and powdered surfaces and by fresh bump-holes on the slopes. The total volume of the recovered debris was 0.318 m^3. At least half the fragments from the fall must have been recovered and so the volume is not believed to have exceeded 0.6 m^3. These figures are only 0.8-1.6% of the rock-fall during a minimum period of fifteen years before the present. This suggests that the observed rock-fall is not as infrequent an event as three summers' observations indicate, that the non lichenous rock-fall debris on the slope accumulated over a much longer period than fifteen years, or else that one or a few rock-falls of very much greater magnitude have taken place within this time interval. The latter is likely in any case, since there are many non lichenous blocks whose size exceeds that of the largest fragment derived from the rock-fall observed on Sept. 2nd, 1968.

4. DEBRIS ACCRETION DUE TO SNOW AVALANCHES

The slopes below several rock walls in the metasedimentary ang igneous intrusive zones in the Tombstone area were observed from May 9th until June 23rd, 1967. Spring avalanches commenced on May 20th, shortly after the mean diurnal air temperature in the area had risen above 0°C. The areal distribution of avalanches and their geomorphic significance were subsequently noted. In the metasedimentary zone, the northerly and north westerly facing rock walls of Quartzite Peak (Localities TL2 and TL3) and the northerly facing rock wall of Landslide valley were observed most closely. In the igneous intrusive zone, the rock walls between Divide Lake and Moraine Lake received the greatest attention.

Most of the early spring avalanches which occurred on the north facing metasedimentary rock walls were debris free (Plate 11). This is accounted for by the fact that, when conditions were favourable for release of avalanches from the exposed parts of the rock walls, the gullies, in shadow for most of the day, possessed a basal layer of hard snow which protected the underlying debris from removal. This basal layer of snow would often remain after the passage of three or four avalanches down the same gully from different tributary gullies. A number of the later spring avalanches were ground avalanches, and did erode some debris from the rock walls, but by this time the snow cover on the talus slopes was disappearing and the avalanches picked up most of their debris load from the talus slope itself. (Plate 12).

A much smaller number of avalanche occurrences were observed on the rock walls in the Tombstone intrusion. These that did occur were usually localised falls of fresh fallen powder snow. Debris was not observed in the avalanche deposits.

Debris content of sample areas in some of the most debris laden avalanche deposits in the metasedimentary zone was assessed (Table 3.5). The information was collected from two of the slopes studied in the Tombstone area in 1967 and from two slopes studied in the Bear River area in 1968. The debris volumes in the table were calculated from the 'a', 'b' and 'c' axes of the individual particles using the appropriate equation in Appendix III.

TABLE 3.5

AVALANCHE DEBRIS CONTENT ON FOUR SLOPES IN METASEDIMENTARY ZONE

Locality	Date	Area of avalanche (m^2)	Area sampled (m^2)	Vol. debris for sampled area (m^3)	Vol. estimate for avalanche (m^3)
Loc. TL2 Tombstone	6/67	36,000	420 1,890 2,310	0.031 0.084 0.115	1.79
Loc. TL3 Tombstone	6/67		400	0.013	
Loc. BL3 cone 6801 Bear River	6/68	600	80 10 90	0.057 0.033 0.090	0.60
Loc. BL4 Bear River	6/68	5-10,000	44	0.0017	0.17-0.34

All measurements were necessarily made on surficial debris. The estimated volumes of debris are therefore subject to possible error from neglect of buried debris. Three pits were dug at points where the surface was fairly debris laden, but debris was not observed at depth.

From Table 3.5 a mean range of 0.25 to 1.79 m^3 is evident for debris content in the sampled avalanches. An extreme range of 0.17 to 2.66 m^3 is evident for all individual sample areas within the avalanche deposits. In northern Sweden, for the year 1953, Rapp (1960 b, p. 133) estimated from a study of seventy-five examples that the average dirty avalanche contained 0.3 m^3 of debris, although one unusually dirty avalanche contained 10.3 m^3. Table 3.5 shows that the volumes of debris brought down from the rock walls by the most debris laden avalanches in the field areas are close to Rapp's average figure. This is a good indication of the minor erosive importance of the avalanches on the rock walls of the Ogilvie and Wernecke Mountains.

5. ACCRETION BY TORRENT AVALANCHES AND EPHEMERAL RUN-OFF

The south facing slope of Tombstone valley has a general inclination of 36°. It is not strictly a free face but a slope covered with deeply weathered coarse detritus judged to be in situ or creeping slowly downslope, because of conformity of the general angle of inclination with the structural dip. It has been subject to gullying, however, with associated removal of large volumes of weathered debris. At intervals the slope is marked by long straight gashes where incision has taken place down to the unweathered bedrock. These are very conspicuous by their lack of a lichen cover compared with the intervening expanses (Plate 16). From the bed of these gullies the weathered mantle can be seen to reach a depth of up to 6 m (20 ft).

At the base of one of these gullies (Plate 5, Locality TL6) a large fresh debris tongue was examined in detail (Plate 17). It is formed at the lower end of a large channel in debris, laterally bounded by almost vertical levées 1.5 m (5 ft) high and 4.5 m (15 ft) wide. The channel continues for 100 m (325 ft) upslope before grading into the bedrock gully. The minimum bulk volume of this tongue was estimated as 225 m^3. If 30% is assumed for the porosity, the minimum volume of debris moved from higher up the slope, by the associated debris flow, was 158 m^3.

The debris tongue was formed at least 17 years prior to 1968 since it is visible on the 1951 air photographs of the region, and yet its surface is completely bare of moss or lichens. It therefore appears that subsequent to an initial debris flow the associated erosional channel has been used probably several times by snow or torrent avalanches or by ephemeral run-off. Indeed the presence of some fine gravel and sand on exposed surfaces indicates that sufficient time has not elapsed since the last erosional event for the fines to be washed into the crevices.

The mechanism associated with the debris flow may simply have been very heavy summer rainfall, but is more likely to have been a torrent avalanche on the steep slope. In spring under special conditions, a snow and ice dam in a previously existing gully probably dammed up a considerable volume of melting snow which saturated the surrounding area of weathered detritus. Upon release of the dam under pressure a debris flow occurred.

Several torrent avalanches without associated debris flows were observed during the spring of 1967 on the metasedimentary slopes but they are small in scale and were associated with slopes not deeply mantled with weathered debris. If torrent avalanches have caused debris flows onto the talus cones below the rock walls in the past, the evidence, in the form of tongues and large levées, has been destroyed by subsequent snow avalanches. Small levées are present among gravel sized slate particles near the apices of cones 6826 and 6827 in the Tombstone area but are believed to be caused merely by sporadic surficial run-off in the early spring when the frost line is near the talus surface. Tongue-like termini and distributary lobes characteristic of saturated debris flows, are found on a number of talus slopes below low angle rock walls, but are associated with only two of the high steep rock walls and talus slopes examined in the field areas.

6. ACCRETION BY ROCK-FALLS, SNOW AVALANCHES AND SLOW DEBRIS SHIFT ON NETS ANCHORED TO TWO TALUS SLOPES

Measurement of debris accretion on snow surface and in avalanche deposits does not give information concerning the effective morphological activity on the rock wall during the late spring or summer after the talus slope has lost its snow cover, and lichenometry could only be used to measure maximum volumes produced by large rock-falls on certain slopes in the Tombstone intrusion. Therefore in the summer of 1968, nets were installed on two slopes to examine debris accretion resulting from most processes during the fall to spring period and during the summer period. The following procedures were used in installation of the nets on the slopes.

a) Installation of nets

Cone 6820 in a zone of thin bedded dolomites in the Bear River area and cone 6830 in a zone of syenites in the Tombstone area were selected for sample coverage as they were accessible enough for nets to be air-dropped near the cone apices and as they were small enough for a reasonable proportion of their surface area to be covered by the nets. Cone 6820 is located at the south west corner of a cirque 3 km (2 mi) from the airstrip in the Bear River area. It has an east north easterly aspect. Cone 6830 is located on the south side of Tombstone valley and has a northerly aspect. Insolation received in the spring by both cones is of short diurnal duration and it was predicted that a late snow cover would protect the netting from disturbance by avalanches from the rock walls.

The netting itself was made of cotton, heavily creosoted to resist rotting in damp conditions. When stretched out on the slope, the mean mesh size in a downslope direction is 2.5 cm and in a direction across the slope 0.7 cm. Since only a small proportion of particles finer than the mesh size are present on the talus cone surfaces the debris filtered through the net mesh may be neglected.

The nets were anchored firmly to bedrock at the apices of the cones by means of rock bolts and cables, and to several points on the talus surface by attachment to large embedded boulders. The weight of the net, itself, tended to hold it in place in any case. When stretched out, the nets covered a rectangular strip extended down the talus cones from their apices. The areal coverage by the netting is illustrated in plan view for the two cones in Figure 3.4. The debris near the base of cone 6830 is of such large calibre that it was easier to spray paint the talus surface than to stretch the net across the large voids between the blocks. In the case of cone 6820 sufficient netting was not available to have an even width along the full length of the cone. The narrow zone covers the steep sections in the lower middle part of the cone. These sections trapped such a tiny proportion of debris that the smaller area of net was considered to be of slight significance when vertical distribution of the debris accretion was examined. The total sample area for cone 6820 is 222.5 m^2 i.e. 12.4% of the cone area; for cone 6830 it is 1,435 m^2 i.e. 12.8% of the cone area. The nets and associated painted zones therefore provide channel samples running from the apex to the base of each of the cones.

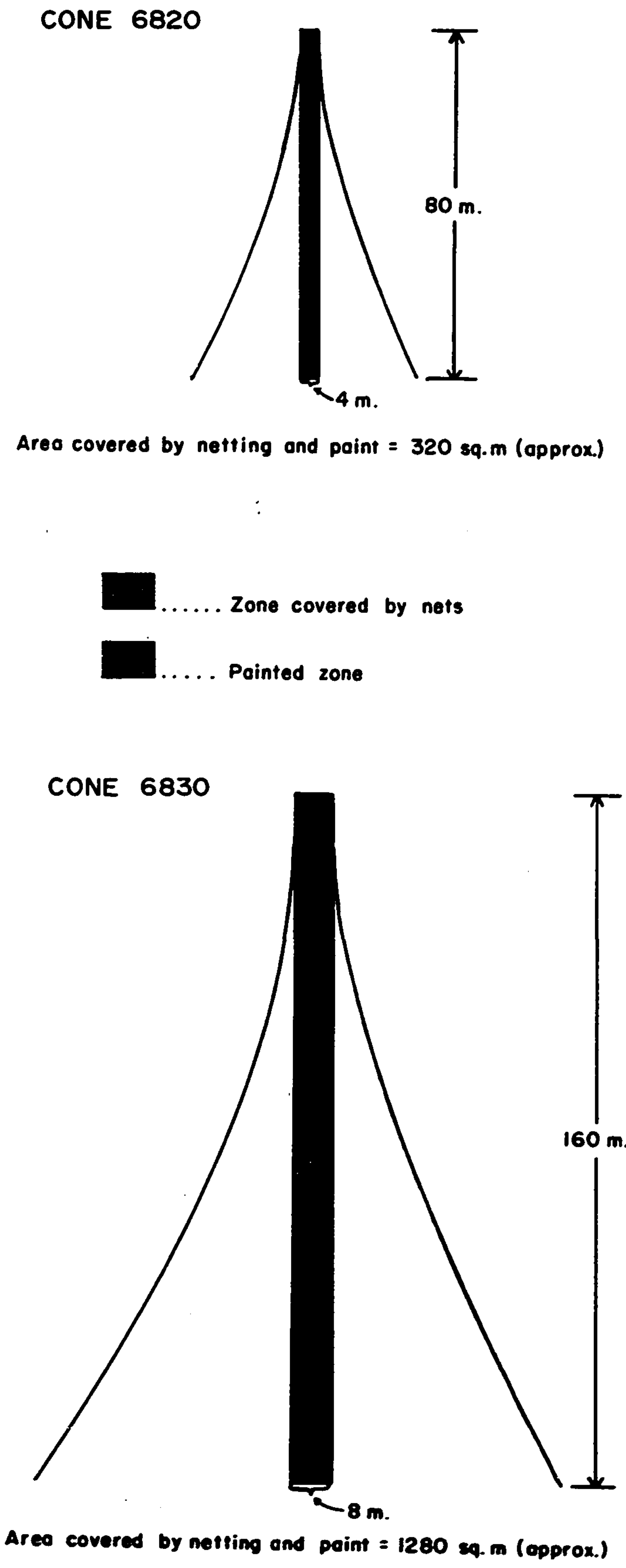

FIG. 3.4 DEBRIS ACCRETION NETS ON TALUS CONES

The principal assumption of the method, invalid for small isolated squares of sacking and plastic, is that the debris on the nets has been derived from the rock wall zone. The nets had to be of sufficient width to preclude avalanches from acquiring debris from the talus surface and depositing it on the net at a lower point. Thus, the nets were designed to fill the narrow sections of the cones betwen the buttresses guarding the entrances to the rock wall gullies. The net on cone 6820 has a width of 3 m (10 ft); that on cone 6830 has a width of 8 m (26 ft). It is still possible for avalanches to move downslope at a slight angle from the fall line, strip debris from the uncovered talus on one side of the net and deposit it on the net itself. Then the debris on the net would give a false indication of debris accretion on the cone. In order to establish whether or not this happened over the period 1968-69, 25 cm wide bands of talus were painted down the edge of the netting on cone 6830 in 1968, with the aim of assessing upon re-examination of the slope, if any disturbance of debris at the edge of the net by avalanches had occurred. These lines remained undisturbed and indicate that none of the debris was derived in this manner. In the summer of 1969 lines were painted along the edges of the netting on cone 6820 for future reference.

b) Results

The net on cone 6830 which was installed on August 22nd, 1968 was re-examined for debris accretion after the winter of 1968-69, on June 20th, 1969. The net was sub-divided along its length into sixteen 10 m (38 ft) sections and the weight distribution of the fallen debris measured and tabulated (Table 3.6). The net was then cleared of debris and left until August 14th, 1969 when it was re-examined. The weight distribution of debris accumulated as a result of rock-fall over the two month period in the summer of 1969 was measured and is also shown in Table 3.6. Most of the debris in sections 15 and 16, may be regarded, however, as a residue from the 1968-69 fall, winter and spring period, which could not be measured in June 1969 due to a deep cover of snow.

A total weight of 336 km (0.124 m^3) of debris was added to the net in the annual period August 1968-August 1969, of which between 152 and 275 kgm (0.056 and 0.102 m^3) was derived in the fall, winter and spring periods, and between 61 and 183 kgm (0.022 and 0.068 m^3) was derived during the summer of 1969.

If the debris accretion on the area of the cone covered by the net can be regarded as representative of debris accretion on the whole cone, then the debris transported from the rock wall above cone 6830 over the annual period is 2,620 kgm (0.97 m^3). But this is almost certainly an overestimate because the net covers the whole of the talus cone apex, which receives the bulk of the debris reaching the cone. A corrected estimate of 0.43 m^3 for debris accretion on cone 6830 takes this bias into account.

The corrected estimate of 0.43 and the maximum estimate of 0.97 m^3 are relatively low figures when compared with that for the average annual accumulation of talus from the same rock wall

TABLE 3.6

DEBRIS ACCRETION ON NET INSTALLED ON CONE 6830.

Section	Weight of debris (kgm)		Total
	August 22/68-June 19/69	June 20/69-August 13/69	
1			
2			
3			
4	10.450	2.490	12.94
5	1.009	0.933	1.94
6	17.860	0.054	17.91
7	0.749	0.263	1.01
8	0.010	0.271	0.28
9	0.007	0.045	0.25
10	0.013	0.019	0.03
11	44.130	2.155	46.29
12	30.010	25.080	5.09
13	16.200	4.330	20.53
14	35.340	25.710	61.05
15	10.220	63.090*	73.31
16	4.150	59.270*	63.42
Total	152.250	183.440	335.69

* Most of the debris is 15 and 16 on August 14th, 1969 may be regarded as a residue from the 1968-69 period as it could not be measured in the spring due to a deep cover of snow. As a result the maximum debris accretion for winter period August 1968-June 1969 may have been 274.61 kgm and the maximum debris accretion for the summer period June-August 1969 may have been 61.08 kgm.

throughout the postglacial period. The latter value is between 1.18 and 2.74 m^3 (Appendix II, Table II.5).

The net on cone 6820 was installed on July 20th, 1968 and was re-examined on June 26th and again on July 20th, 1969. The net was divided into eight 10 m (33ft) sections along its length and the weight distribution of the accreted debris assessed (Table 3.7). Totals of 309 kgm (0.115 m^3) and 12 kgm (0.005 m^3) were calculated for the 11 month period, July 21st, 1968-June 26th, 1969 and the 23 day period, June 27th, 1969-July 20th, 1969, respectively. These figures represent a total accretion of 320 kgm (0.119 m^3) for the one year period July 1968-July 1969. A notable feature for cone 6820 is the small amount of debris derived during a period of one month in the summer of 1969 relative to that derived during the preceeding fall, winter and spring. If the net covers a fraction of the cone representative of the whole cone with regard to its debris accretion then the maximum value for a year's debris accretion is 0.96 m^3. But due to the complete coverage of the top quarter of the talus cone it was necessary to prepare a corrected estimate as for cone 6830. The revised estimate for debris accretion on cone 6820 is 1.15 m^3, only a little different from the uncorrected estimate.

The vertical distribution of debris on the nets is plotted on Figure 3.5 for talus cones 6820 and 6830. The graphs indicate accumulation concentrations at the apex and base of both cones, with hardly any debris located in the middle sections.

TABLE 3.7

DEBRIS ACCRETION ON NET PLACED ON CONE 6820, BEAR RIVER.

Summary of rock-fall data for cone 6820
for a period of 1 year

	July 20/68-June 27/69	June 27/69-July 20/69	Total
Section	Weight kgm	Weight kgm	Weight kgm
A	B	C	D
1	110.0	0.905	110.9
2	28.2	0.059	28.26
3	19.95	0.116	20.07
4	4.55	0	4.55
5	3.62	0.43	4.05
6	0.95	2.58	3.53
7	13.95	7.06	21.0
8	28.65	0.79	29.44
TOTAL	210.0	11.9	221.9*

* A 2 m wide section at top of net showed an accumulation of 98.5 kgm by slow debris shift from the gully zone during the period July 1968-June 1969. This gives a grand total of debris accumulation on the net on cone 6820, for the period July 1968 to July 1969, of 320.4 kgm.

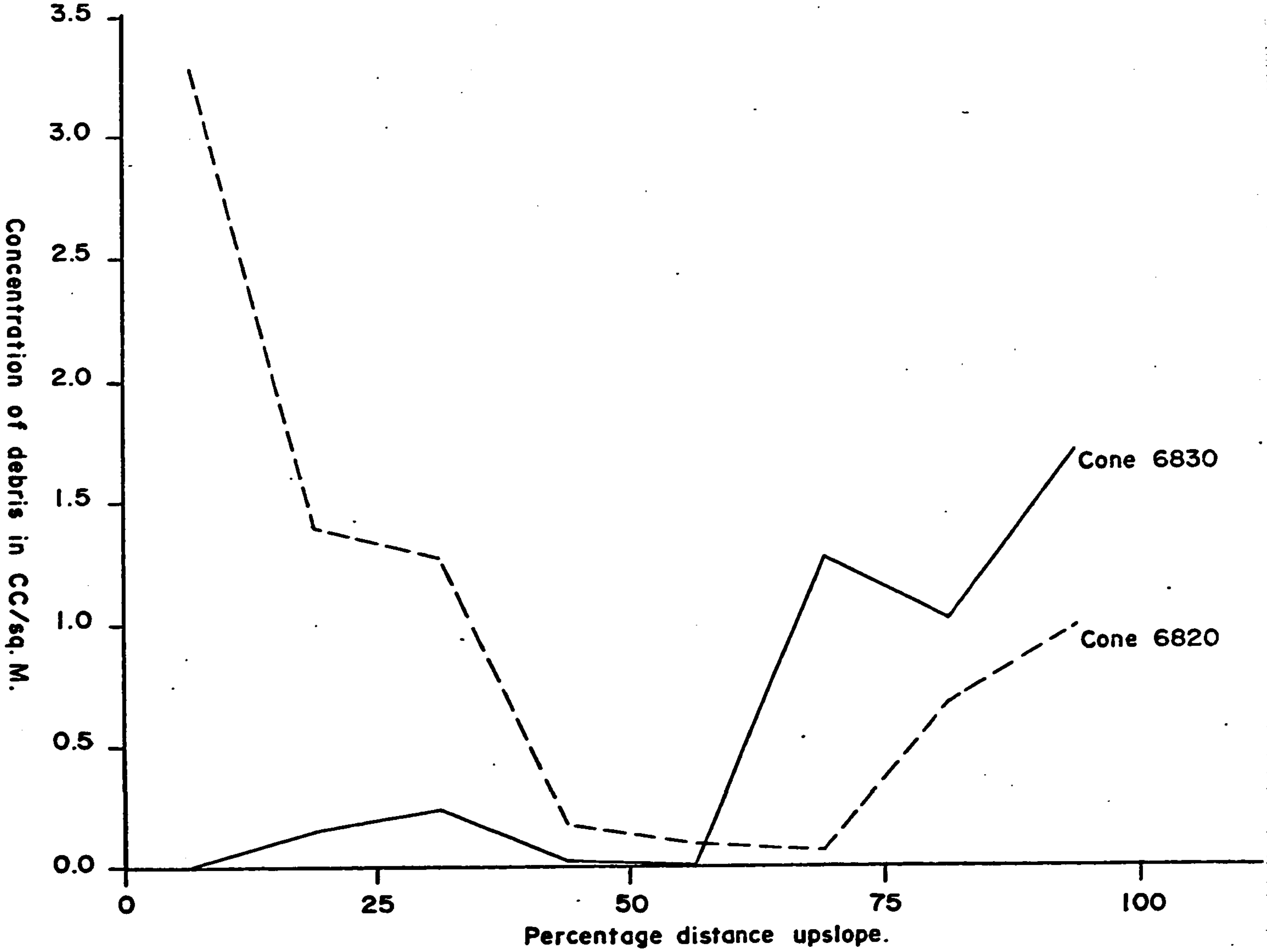

FIG. 3.5 DEBRIS ACCRETION ON NETS FOR 1968-1969

The debris accretion peak at the apices of both of the talus cones results from the rapid reduction of velocity of falling particles when they arrive on the rough talus surface, during the late spring, summer and fall. The mean angles on the upper parts of cones 6820 and 6830 are 35.8° and 32.3° respectively. Therefore the reduction in velocity due to a lessening of the slope angle would tend to be more appreciable on cone 6830 than on cone 6820, and this may explain why the debris accretion peak at the top of cone 6820 is less pronounced than on cone 6830.

At the base of cone 6820 there is a second and more important debris accretion peak not exhibited by cone 6830. It may be partially the result of avalanche erosion, which is of some importance on the well dissected dolomite rock wall above the cone. It may also be partially the result of spring rock-fall debris sliding on a hard snow surface at an angle of about 36° to the base of the slope.

Cone 6830, on the other hand, is little affected by avalanche activity and, unlike cone 6820, snow does not linger on the slope till late in the spring to form a smooth surface for the sliding or rolling of spring rock-falls.

7. DISCUSSION OF RESULTS

The principal results of the debris accretion measurements are collated in Table 3.8. Rates of rock wall erosion are derived by dividing the volumes of debris accretion by the respective rock wall areas. Although it is difficult to compare the rates of erosion, represented by short term accretion, with the rates derived over the entire postglacial period, there is some indication that the currently observed level of operation of geomorphic processes is insufficient to account for the postglacial talus accumulations. Large scale events, of more infrequent occurrence than those for which observations or measurements have been made in the field areas, are probably responsible for an increase in the mean rate of postglacial rock wall erosion of talus development.

This view is supported by evidence contained in rock glacier T1 in the Tombstone area. The rock glacier surface is covered with boulders, which have been entirely derived from the rock wall on the south side of the cirque. A traverse, from the largest tributary talus cones to the front of the rock glacier, revealed a zone in the middle of the rock glacier, where the boulders are of unusually large size ($>$10 m in length) as compared with the boulders around it (Plate 18). These blocks are clearly the product of one or several unusually large scale rock-falls in the postglacial period. The distance of the boulders from the base of the source wall and the sizes of lichen thalli of Rhizocarpon geographicum spp on the surfaces

TABLE 3.8

RECENT DEBRIS ACCRETION ON THE BASAL PARTS OF ROCK WALLS IN THE OGILVIE AND WERNECKE MOUNTAINS, YUKON TERRITORY

Process	Technique	Locality	Rock wall lithology	Date measured	Accretion period	Debris volume estimate	Erosion rate mm/1000 yrs	Precision of erosion rate mm/1000 yrs	Comments
Rock-falls									
1	measurement on snow surface	loc. TL4 Tombstone	syenite & monzonite	18/6/69	1-6 mths	1.54	3	1-6	Complete slope sampled
2	lichenometry	loc. TL5 Tombstone	"	8/8/69	>10 yrs	37.56	<19	<19	" "
3	lichenometry	cone 6830 Tombstone	"	24/8/68	>10 yrs	37.56	<8	<8	Very large rock-falls only
Snow avalanches									
1	debris in avalanche deposits	loc. TL2 Tombstone	quartzite minor slate	21/6/67	1-4 wks	1.79	57	20-200	
2	"	loc. BL4 Bear River	" "	12/6/68	1-4 wks	0.17-0.34	9-17	3-30	
3	"	loc. BL3 cone 6801 Bear River	" "	4/6/68	1-4 wks	0.60	3	?	
Slow debris shift									
1	measurement on net	cone 6820 Bear River	dolomite	20/7/69	1 yr	0.36	1	0-2	
Debris flow									
1	vol. measurement of debris tongue	loc. TL6 Tombstone	syenite & monzonite	9/6/67	18 yrs	158	-	-	Special localities only
All processes									
1	measurement on net	cone 6820 Bear River	dolomite	20/7/69	1 yr	1.148	44.3	10-100	12.5% of cone area sampled
2	"	cone 6830 Tombstone		14/8/69	1 yr	0.428	8.8	3-30	" "

suggests that these very large scale rock-falls occurred at least 400 years B.P. The distribution of debris sizes on the rock glacier surface indicates that there was a long time span before and since the deposition of this very large debris, during which lesser rock-falls occurred.

The data in Table 3.8 indicate the much greater geomorphic significance of a single debris flow as compared with more frequent events such as avalanches and rock-falls. Rapp (1960b, p. 185) concluded for a mountain zone in northern Sweden that slush avalanches on gentle slopes and torrent avalanches on steep slopes are far more effective as agents of transport than all rock-falls and dirty avalanches. But in the Ogilvie and Wernecke Mountains evidence of debris flows on the slopes was limited only to moderately inclined slopes on the north side of Tombstone valley, covered with deeply frost weathered bedrock, and to well dissected rock walls of relatively low inclination in the Bear River area. The processes leading to debris flow, viz. torrent avalanches and ephemeral run-off are not considered to be significant on the steep rock walls when compared with rock-falls and snow avalanches.

In the igneous intrusives of the Tombstone area, avalanching is considered to be of minor importance as compared with rock-falls. Avalanche deposits were not noted on the snow covered syenite talus slopes in this zone. Indeed the rock walls are too steep to permit the build-up of a snow pack which could release spring avalanches, or to permit the accumulation of a potential debris load for such avalanches as do occur.

Even in the metasedimentary zone, where they are of frequent occurrence in the spring, most of the observed avalanches were debris free. The dirtiest avalanches contained between 0.17 and 1.79 m^3 of debris, which corresponds to mean erosion rates two to ten times slower than the mean postglacial rate of erosion by all processes for metasediments (see chapter 2, Table 2.3).

Frequent small rock-falls have been observed in the gullies above the talus cones after summer rain showers and these certainly augment debris accretion on the talus slopes. On the basis of one year's measurements on cones 6820 and 6830, the summer of 1969 has been of less importance than the previous fall, winter and spring for debris accretion resulting from small scale events.

Slow shift of debris from the gully zone, amounting to 0.036 m^3 in one year, has been observed at the top of cone 6820. This total is about 1/30th of the total estimated accretion for the talus cone for that year, which suggests that debris shift may be a process of only slight importance to debris accretion.

CHAPTER 4

THEORETICAL MODEL OF TALUS DEVELOPMENT BY ROCK-FALL

1. INTRODUCTION

The purpose of this chapter is to predict the effect of all possible variables on the velocity and distance of travel of particles falling down a rock wall. The probable theoretical pattern of distribution of surficial debris on the talus slopes and the general form of the latter are then predicted. Particular attention is paid to theoretical evaluation of the phenomenon of fall sorting on the talus slopes. Fall sorting is the term used to describe downslope increase in size of rock-fall derived particles, and has been documented from many mountain regions (e.g. Rapp, 1960a; Gardner, 1968).

2. DYNAMICS OF A FALLING PARTICLE ON A ROCK WALL

The velocity acquired by a particle falling down a rock wall depends on the nature of its motion, and on various characteristics of the particle and the surface over which it travels. The nature of motion of the particles with which the model is concerned is translational and may be in the form of free-fall, bounding, rolling or sliding. The basic force acting on the particles and tending to cause their downslope acceleration is a component of the gravitional force. It is counteracted by air resistance when the particle is falling through the air medium and by friction when the particle is in contact with the slope itself. Velocities acquired by a particle under the different forms of motion may now be considered.

a) Free fall

The general Newtonian equation describing the velocity (v) of free fall of a particle from rest, after a given distance (s) has been travelled, momentarily neglecting air resistance, is:-

$$v^2 = \sqrt{2gs}$$

Thus, the velocity acquired by the free falling particle is a function of the distance it falls.

Air resistance cannot be neglected, however. Its precise effect on any individual particle cannot be readily determined for many reasons. Among these are variation in the size of the component of angular motion (spinning) which is largely a function of shape, the different types of motion by which a particle can travel down a rock wall, and the variation in the coefficient of drag for particles of different sizes and shapes falling through the air at different velocities.

Nonetheless, its approximate effect on an aggregate of falling particles can be determined for several hypothetical free fall situations.

The velocity achieved by a spherical particle at the end of its free fall from a rock wall is calculated from the knowledge that a particle can only accelerate until the gravitational force is balanced by the force of air resistance which is increasing all the time by some power of the velocity. When this balance is achieved the particle moves with a constant limiting or terminal velocity.

Loney (1960, p.114) suggested that for projectiles falling through air at velocities up to about 250 m/sec (800 ft/sec), the retarding force R is approximately proportional to the second power of the velocity. The resistance R is then given by the following expression (Timoshenko and Young, 1948, p. 25-26).

$$R = \tfrac{1}{2} C d_f a v^2 \qquad \text{...... equation 1}$$

where d_f = mass density of the fluid medium (in this case air)

a = maximum horizontal projection plane of the falling particle

v = velocity of the particle

C = coefficient of resistance

Timoshenko and Young suggest that C be taken as an approximate constant of 1.12 for motion of short, blunt, sharp edged bodies or rough elongated blunt nosed bodies below the speed of sound. Talus particles approximate this slope description and this figure was applied to the equation for air resistance and to subsequent equations used to calculate the velocity of particles.

If the particles were relatively smooth spheres C values of as low as 0.5-0.2 are indicated for high Reynolds Number dynamic situations such as exist for particles falling down rock walls (Wieselsberger in Prandtl and Tietjens, 1936, p. 100). In order to note the effect of reducing the coefficient of resistance to its probable minimum of 0.2, the latter value was applied to the equation for resistance and to subsequent equations used to determine the velocities achieved by falling particles.

Now the gravitational force F causing downward motion in a particle of mass m can be expressed in the following terms

$$F = mg$$

When the particle has reached its terminal velocity the force of resistance is equal to the gravitational force

i.e. $F = R$

$\therefore$ $mg = \frac{1}{2}Cd_f a v^2$

$\therefore$ v (the terminal velocity) $= \sqrt{\frac{2mg}{Cd_f a}}$ ..... equation 2

if the falling particle is assumed to be approximately spherical, although angular at the corners and rough surfaced, then the equation can be simplified as follows:

$$v = \sqrt{\frac{8/3\,\pi\, r^3 d_s g}{1.12\, d_f \pi r^2}}$$

where d_s is density of the sphere

$$= \sqrt{\frac{8rd_s g}{1.12 \times d_f}}$$ .... equation 3

Now the velocity w at any point between the starting point of the falling sphere and the point at which it achieves its terminal velocity can be calculated from the following equation (Norris and Legge, 1950, p. 253).

$$w^2 = v^2 (1 - e^{-2gx/v^2}) \quad \text{.... equation 4}$$

where $e = 2.718$

x = distance particle moves from its starting point before it achieves velocity w

v = terminal velocity previously calculated

These equations were applied to approximately spherical particles, of 1 cm, 5 cm, 10 cm, 50 cm and 250 cm radius falling through distances of 100 m (325 ft), 500 m (1,625 ft) and 1,000 (3,250 ft) respectively, in order to determine the possible magnitude of variation in velocity achieved under natural rock-fall conditions. The values chosen for the size of falling particle and their height of fall are quite realistic. The rock walls of the Ogilvie and Wernecke Mountains are usually between 500 m (1,625 ft) and 1,000 m (3,250 ft) in height, and nearly all the particles on the talus slopes lie within the range of 1 cm to 250 cm radius. The following approximate values were inserted into equation 3

Particle density $d_s = 2.6$ gm/cc

Air density $d_f = 1.3 \times 10^{-3}$ gm/cc

The results of the calculations for C = 1.12 and C = 0.2 are presented in Tables 4.1 and 4.2 respectively. Figure 4.1 expresses the data in Table 4.1 in a visual form.

TABLE 4.1

VELOCITIES OF FREE FALLING PARTICLES
WITH HIGH AIR RESISTANCE COEFFICIENTS.

C = 1.12

Particle size (radius in cm)	Terminal Velocity m/sec	Velocities of falling particles m/sec		
		At 100 m	At 500 m	At 1,000 m
1	36.8	32.1	36.8	36.8
5	82.2	41.3	71.8	80.0
10	116.3	42.7	83.5	101.7
50	260.0	42.7	95.6	130.5
250	581.4	44.3	97.3	137.5

TABLE 4.2

VELOCITIES OF FREE FALLING PARTICLES
WITH LOW AIR RESISTANCE COEFFICIENTS.

C = 0.2

Particle size (radius in cm)	Terminal velocity m/sec	Velocities of falling particles m/sec.		
		At 100 m	At 500 m	At 1,000 m
5	197	44.0	93.0	124.4
10	279	44.1	96.2	131.4
50	625	44.1	100.7	142.5

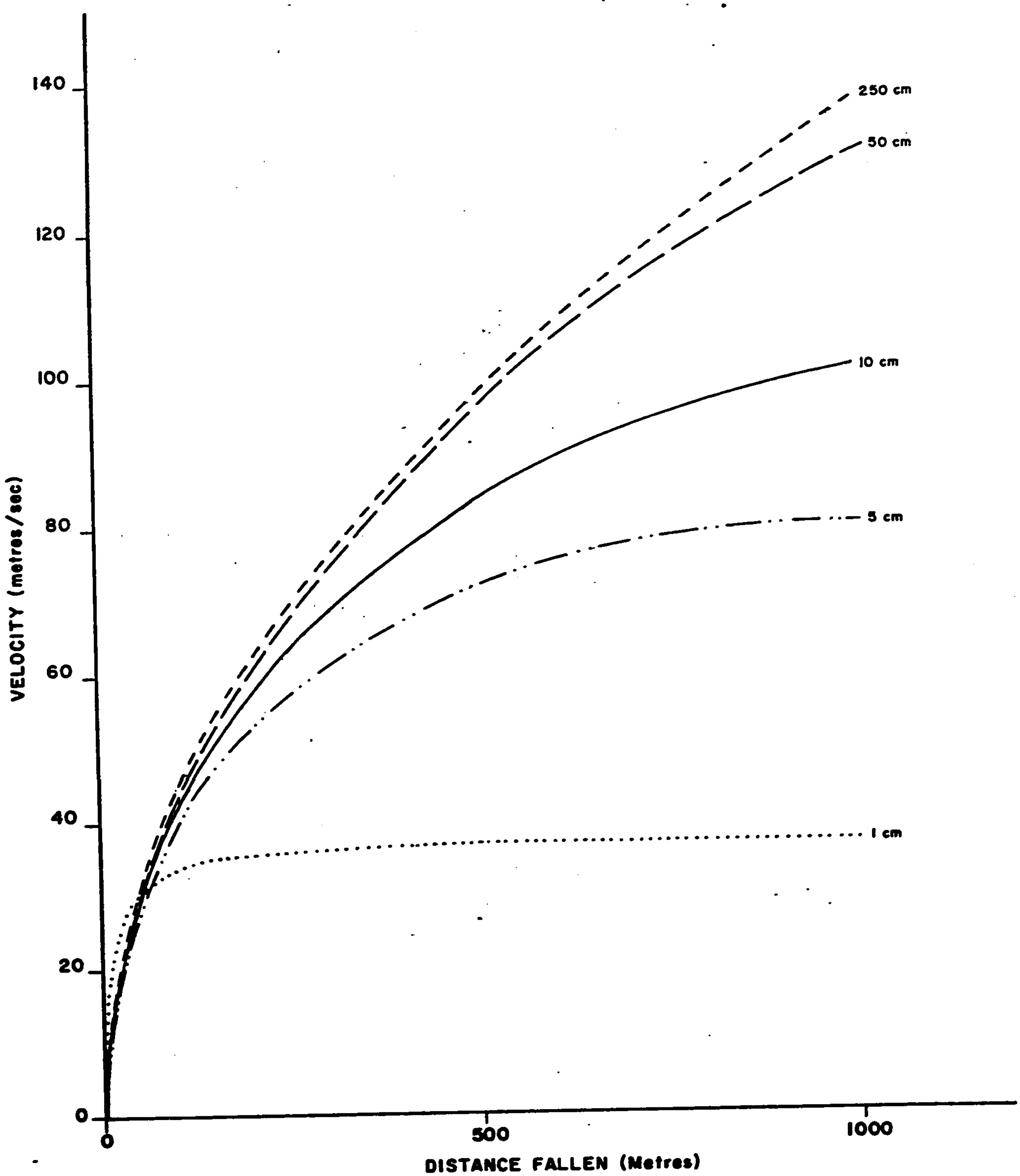

FIG. 4.1 RELATIONSHIP BETWEEN PARTICLE RADIUS, DISTANCE FALLEN AND VELOCITY FOR FREE FALLING PARTICLES SUBJECT TO AIR RESISTANCE

In Table 4.1 and Figure 4.1 an increase in velocity with height of fall is conspicuous for all particle sizes but particularly for the larger ones. For spherical particles of 1 cm or less there is only a very slight increase in velocity after a particle has fallen 100 m (325 ft).

An increase in velocity as particle size increases is also evident but for drops of 100 m or less the differences for particle sizes ranging from 5 cm to 250 cm are hardly measurable. Greater differences are evident for bigger falls, but even after a fall of 500 m a particle of radius 10 cm has almost 90% of the velocity of a particle of radius 50 cm. In weight terms the former is 1/125th of the weight of the latter.

Reduction of the coefficient of resistance to its probable minimum value does not alter the direct relationship between velocity and distance of fall (Table 4.2). It does reduce the effect of particle size differences on velocity differences, however. It can be seen that at a distance of 100 m and 500 m from the source there are velocity differences of only 0% and 3% for particles of radius 5 cm and these of radius 50 cm. For rock-falls from very high rock walls, e.g. rock walls in excess of 1,000 m velocity differences for particles of different sizes may become significant. But for rock-falls of the magnitude noted on rock walls in most mountain areas the notion that the large particles fall much faster than the small particles does not appear to be correct. The former acquire greater momentum because of their great mass, but not appreciably greater velocities than the latter.

b) Bounding motion

Motion of particles on the rock walls is rarely by free fall for long distances since the rock walls are seldom vertical. Bounding with a strongly developed rotational component replaces free fall. The velocity model developed above is still valid for bounding motion, however, with some modification.

Figure 4.2 is a diagrammatic representation of a rock-fall down a steeply sloping wall after an initial free fall.

When the particle strikes the slope surface at B it rebounds with a new velocity and new direction. The velocity after impact is calculated from the following Newtonian equation (Loney, 1906, p. 146), assuming negligible frictional retardation at the time of impact.

$$V_2 = V_1 \sqrt{\sin^2\alpha + e^2 \cos^2\alpha}$$

where V_2 = velocity of particle on rebound after impact

V_1 = velocity of particle prior to impact

α = angle made by incoming particle with normal to the plane

e = the coefficient of restitution of the bodies upon impact. It is dependent on their elastic properties and lies between 0 and 1.

If the two bodies are perfectly elastic, $e = 1$

then $V_2 = V_1 \sqrt{\sin^2\alpha + \cos^2\alpha} = V_1$

i.e. there is no overall velocity loss

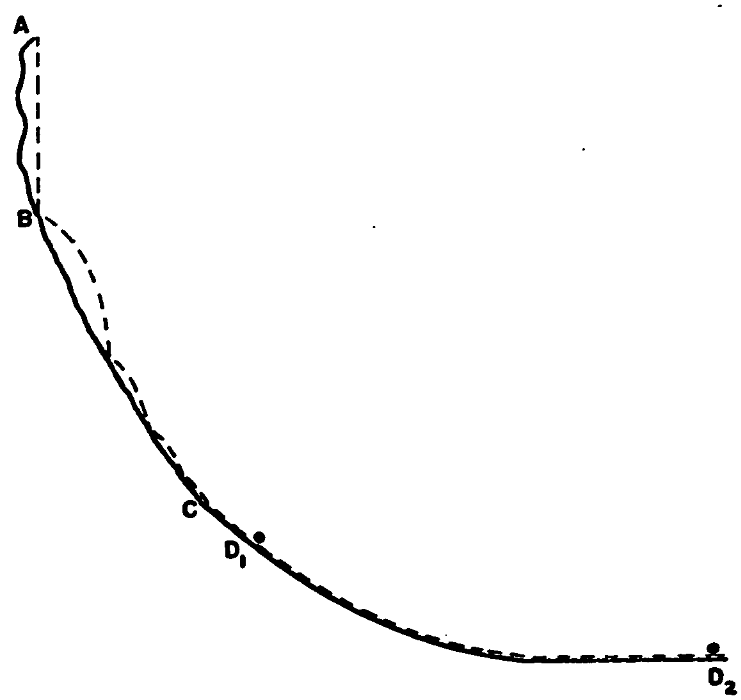

FIG. 4.2 PARTICLE TRAJECTORY DOWN A ROCK WALL

The direction of the particle after impact is calculated from the equation

$$\cot \theta = e \cot \alpha$$

where θ = angle made by rebounding particle with the normal to the plane.

For perfectly elastic impact $e = 1$

then, $\cot \theta = \cot \alpha$

Thus the angle made by the moving particle with the normal to the plane prior to impact equals the angle made by the particle with the normal to the plane after impact.

The velocity and the direction of motion of a particle after impact at B can be obtained by these equations for a number of inclined plane angles, for a number of incoming velocities which would depend on the height of free fall prior to bounding, and for a number of different values of the coefficient of restitution e. This coefficient is likely to be quite low, and therefore the angle made by the particle with the normal to the plane is greater than the angle between the path of the incoming particle and the normal to the plane. After each bounce on a uniformly sloping rock surface the particle trajectory tends to become more nearly parallel to the rock surface.

After leaving B the particle moves with a known initial trajectory and a known velocity V_2. The point C at which it again hits the plane, the velocity at impact and the angle of the particle with the plane at impact are all readily calculated using the Newtonian equations of motion and the parallellogram of velocities, with appropriate modifications for air resistance.

After several bounces the particle has such a low trajectory relative to the slope that the roughness of both the particle and the slope surface cause frictional retardation of the particle. The bounding motion then changes to rolling or sliding motion and the acceleration of the particle is governed by different equations which take account of friction. In Figure 4.2 this stage is reached at C.

The velocity which a particle has achieved at the point C where the bounding motion ends, is a direct function of the height of initial free fall, length of slope over which bounding occurs, slope angle and elasticity of impact. The relationship between particle size and velocity achieved at C is considered insignificant for the range of particle sizes and heights of fall normal for rock walls.

c) Rolling motion

The more spherical a particle is, the greater is the chance that bounding motion will be succeeded by rolling motion on the rock surface. If a particle is perfectly translated downslope by rotation i.e. undergoes perfect rolling motion, a very slight, but significant, frictional retarding force is actually induced at the point of contact of the particle with the surface. This force, in conjunction with a gravitational force, imparts an angular acceleration to the particle and it rolls downslope gaining speed as it travels. In Figure 4.2 a rolling particle theoretically continues to accelerate from C until it reaches D_2 where the angle of slope is zero and the gravitational force ceases to affect its motion. Then the small retarding force of friction causes the particles to come to rest.

The acceleration in a downslope direction for a rolling solid sphere = $5/7 g\sin\theta$, where θ = slope angle and g = gravitational constant, (Mendenhall, Eve, Keys and Sutton, 1956, p. 84). From this it is clear that the velocity achieved by a rolling particle varies directly with the slope angle.

But the velocity also varies with the degree of sphericity of a particle. As sphericity decreases, the acceleration in a downslope direction of a rolling particle decreases (e.g. for a rolling solid cylinder this acceleration is $2/3\ g\sin\theta$). Indeed the particle sphericity may even be too low for rolling to take place after bounding has ceased and sliding motion would then occur instead. If particles are of low sphericity but are disc shaped, rolling can occur after bounding has ceased provided the 'c' axis of the particles hits the slope first and is oriented at right angles to the downslope direction (Fig. 4.3).

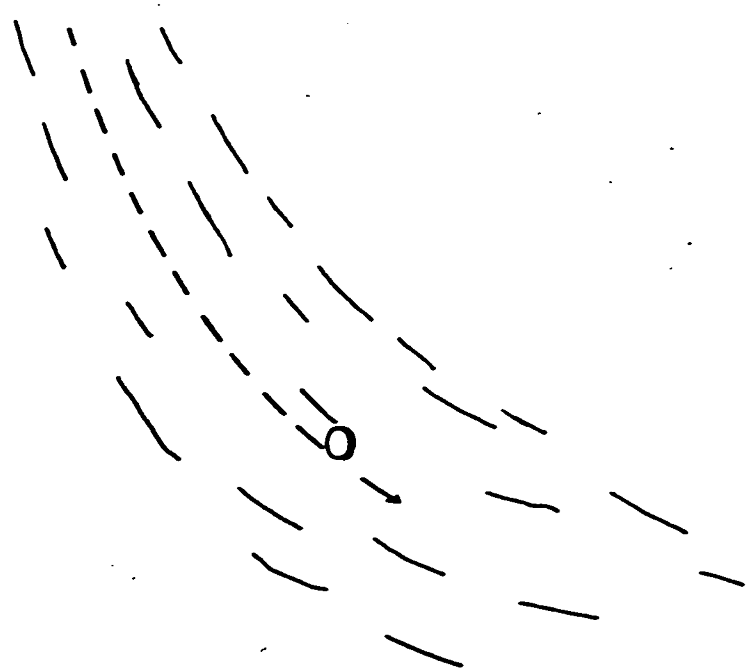

FIG. 4.3

d) Sliding motion

For angular particles, sliding is the principal means of translation downslope after bounding has ceased. If friction between the particle and the surface is completely absent, acceleration of the particle in a downslope direction is $g\sin\theta$, which is greater than for a rolling sphere or cylinder. But friction is called into play due to the lack of perfect smoothness of the area of contact between the particle and the slope, and this reduces the downslope acceleration of the sliding particle. The forces acting on a particle sliding on a bedrock slope are illustrated in Figure 4.4.

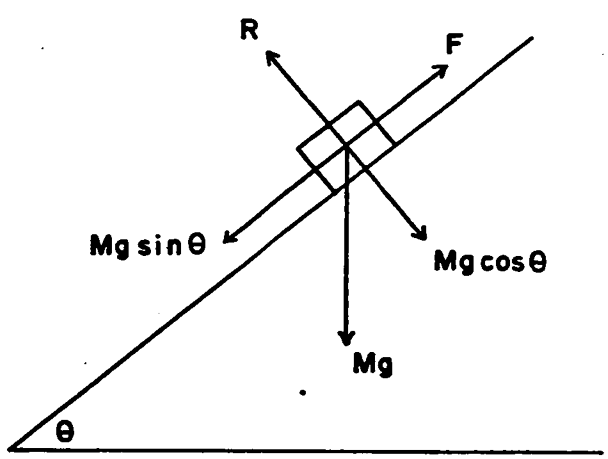

FIG. 4.4

i) Force caused by downslope component of gravitational acceleration $= mg\sin\Theta$

ii) Force of friction $= F$

$= \tan\lambda R$ (where λ = angle of kinetic friction)

$= \tan\lambda\, mg\cos\Theta$

These two forces oppose one another

The resultant force acting downslope $= mg\sin\Theta - \tan\lambda\, mg\cos\Theta)$

$= mg\,(\sin\Theta - \tan\lambda\cos\Theta)$

$\therefore$ Acceleration downslope $= g(\sin\Theta - \tan\lambda\cos\Theta)$

From this equation it is evident that if the slope angle Θ exceeds the angle of kinetic friction λ , the particle moves downslope with positive acceleration (i.e. its velocity increases). If $\Theta = \lambda$, the acceleration of the particle is zero (i.e. its velocity remains constant). If Θ is less than λ, the particle moves downslope with negative acceleration (i.e. its velocity becomes less and it tends to come to rest).

If it is assumed that there are no major irregularities in the surface topography, other than normal roughness of particle and bedrock surfaces then the angle of kinetic friction and the slope angle determine the acceleration of a sliding particle and the distance travelled by the latter.

3. EFFECT OF SURFACE ROUGHNESS

So far in the dynamic model it has been assumed that there are no major topographic irregularities on the rock walls other than the general surface roughness which calls friction into play. It is clear, however, that rock walls in all mountain areas possess topographic irregularities such as low angle rock ledges and small reverse slopes. The degree of rugosity varies from one mountain wall to another depending on such factors as lithology, structure and degree of gullying by various subaerial processes. On an individual mountain wall surface roughness becomes particularly significant near the base of the slope as a debris cover builds up. The resultant irregular surface has a marked effect on the velocity of the particles arriving at the top of the slope. A model is developed in Appendix III to establish the retardational effect of surface roughness on a particle arriving on the debris slope and travelling subsequently by sliding, rolling or bounding motion on the latter. The model demonstrates that the retardation of the particle is proportional to the ratio of size of the debris already on the slope to the size of the particle. This relationship is exemplified in Figure 4.5.

A B

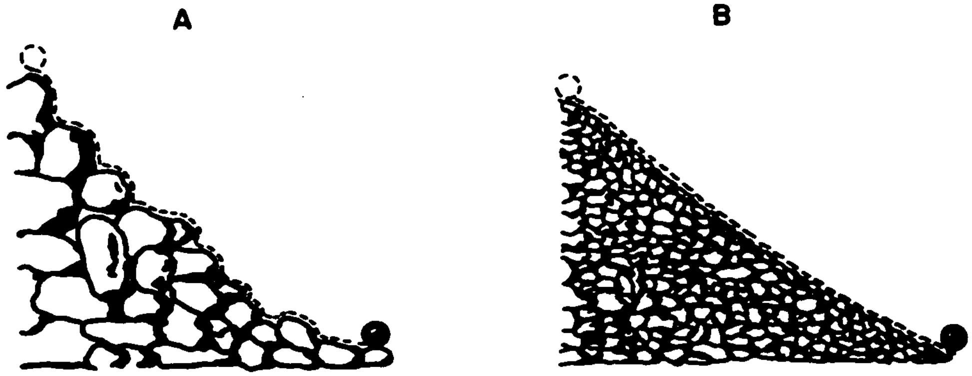

FIG. 4.5

In case A the sliding or rolling particle travels by a more irregular path and is retarded more than in case B.

Theoretically particles will move down the debris slope until they reach particles of their own size or larger and then they will be quickly brought to a halt. In other words a selective checking mechanism operates which encourages the development and maintenance of fall sorting on the debris slopes. A particular effect of irregularities on the rock walls above the debris slopes is the component of horizontal velocity which they impart to falling particles. If sufficiently large, this horizontal velocity component enables particles to avoid impact with the top of the debris slope, and they then travel further downslope.

4. EFFECT OF TRANSFER OF MOMENTUM BETWEEN PARTICLES UPON IMPACT

Apart from the effect on surface roughness, a loose debris cover on the lower slopes causes momentum transfer when a falling particle strikes the slope surface. This momentum transfer upon impact reduces the velocity of the falling particle and causes some movement of the loose debris.

The acquired velocity of the loose debris formerly at rest on the slope is directly dependent on the mass and velocity of the particle causing the impact and inversely dependent on its own mass. Since the momentum transfer is usually distributed among many particles the latter only acquire low velocities and move short distances.

If the particle strikes debris particles whose size is several times smaller than the size of the particle, and if only a partial momentum transfer is affected then small impact craters may be formed and the falling particle continues with a reduced velocity downslope. At points where many impacts occur, viz. the top of the debris slope, many impact craters may be formed and this may lead to flattening of the apex of the debris slope. This effect has been noted by Crompton (1968) on talus slopes in Baffin Island.

5. SUMMARY OF FACTORS AFFECTING VELOCITY OF A PARTICLE FALLING DOWN A ROCK WALL.

a) Type of motion i.e. free fall, bounding, rolling or sliding.

Air resistance reduces the acceleration of free falling and bounding particles, whereas surface friction is the main retardational factor for rolling and sliding particles. Retardation is relatively high for sliding particles and relatively low for rolling, bounding or free falling particles.

b) Distance traversed by particle

For free fall and bounding motion the velocity of particles increases with distance traversed due to gravitational acceleration. For rolling motion the velocity also tends to increase with distance travelled as long as there is a slight angle of slope in order to overcome frictional retardation. For sliding motion the velocity only increases with distance so long as the slope exceeds the angle of kinetic friction for sliding particles.

c) Slope angle

On vertical or overhanging rock walls motion is by free fall. On very steep slopes a particle tends to bound and on gentler slopes it tends to roll or slide. Furthermore, the acceleration downslope of the bounding, rolling or sliding particle varies directly with the slope angle, whether this slope angle is greater than or less than the angle of kinetic friction.

The slope angle of the rock wall may also influence the amount of horizontal velocity imparted to a particle. This factor may be of importance in the distance a particle can move over a debris surface on the lower slopes of the rock wall before being frictionally retarded often impact.

d) Size and weight of particles

For debris in the range of sizes found on talus slopes and for the heights of fall noted on most rock walls the size of the particles has little effect on the velocities of particles arriving at the top of the debris slopes, after free falling and bounding down a relatively smooth rock wall. Correspondingly the weight of the particles do not appreciably affect their velocities. Of course larger and therefore heavier particles have greater momentum when they arrive at the talus slopes than smaller particles but it is an increase only linearly related to particle weight. The greater momentum of larger particles may cause greater disturbance and re-arrangement of particles already on the slope but it does not in itself explain the fall sorting pattern observed on talus slopes.

e) Particle shape

The coefficient of air resistance and hence the velocity achieved by bounding particle is to a large extent determined by its shape. The type of motion induced in a falling particle after bounding has ceased also depends on the shape of the particle. Spherical particles tend to roll downslope whereas tabular particles tend to slide downslope.

f) Slope roughness

Slope roughness results in continuously varying slope angles which on the rock wall have an important effect on the trajectory of particles in bounding motion in that considerable horizontal velocity is imparted to the particles. The most important effect of slope roughness is on the lower slopes of a rock wall once a debris cover has developed. The topographically irregular debris slope surface retards falling particles differentially. Large particles tend to roll or slide over a debris surface until they reach debris of their own size and then they quickly come to rest. This process of differential retardation is the main reason for fall sorting of sliding, rolling, or even, bounding particles.

g) Momentum transfer upon impact

As a result of momentum transfer the velocity of a particle is reduced upon impact and the particles formerly at rest on the slope acquire slight acceleration. The particle either stops dead or continues downslope at a reduced velocity. Impact craters (bump-holes) or slight flattening of the top of the debris slope can result from this momentum transfer.

6. CONCLUSIONS

It is predicted that on a smooth basally concave bedrock slope, a debris cover will initially form at the base of the slope.

As more particles arrive on the basal slope they become fall sorted as a result of the newly acquired surface roughness.

The angle of the debris slope will tend to build up to some undetermined limiting angle below the angle of internal friction of the debris. If falling particles are of low sphericity, e.g. tabular or needle shaped, the slope angle achieved is steeper than for a debris slope where particles are of high sphericity, e.g. cuboid. In the latter case fall sorting is expected to be less well developed than in the former case due to the fact that frictional retardation for rolling particles is less than for sliding particles.

The concavity of the debris slope may remain for some time until a sufficiently thick debris cover eventually eliminates the effect of the underlying bedrock slope. A convexity may exist near the top of the debris slope where frequent rock-fall impacts tend to crease slight flattening of the slope.

CHAPTER 5

FORM AND SURFACE CHARACTERISTICS OF ARTIFICIALLY BUILT SLOPES

1. LABORATORY SIMULATIONS OF ROCK-FALL

Small scale rock-fall experiments were conducted in the laboratory, using crushed gravel and sand separately and in a 1:1 mixture. Figure 5.1 is a three dimensional model of the apparatus used in the experiments.

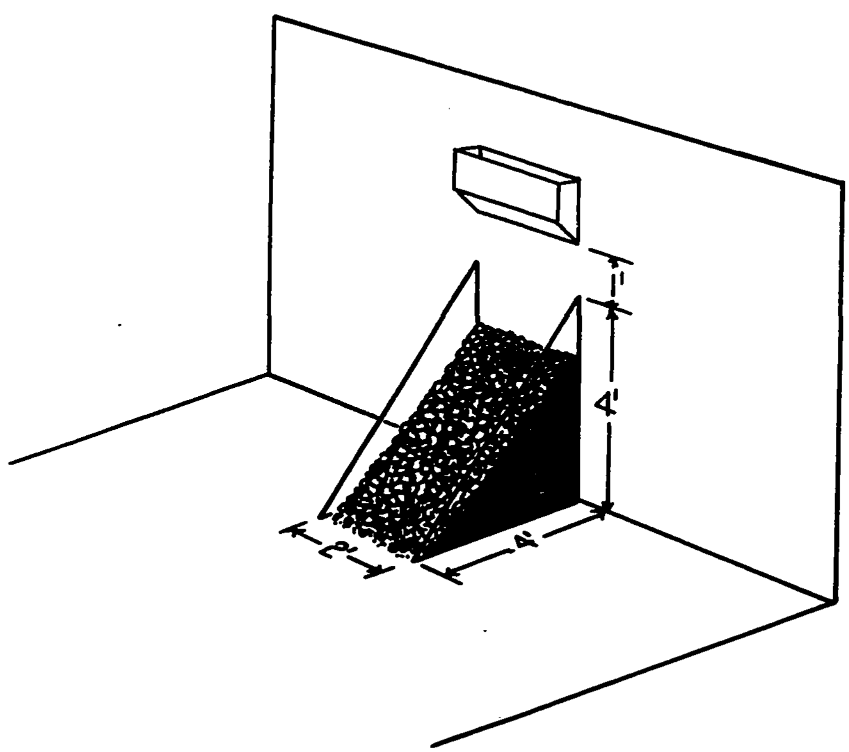

FIG. 5.1

The debris was dropped onto a floor from a height of 1.5 m (5 ft) through a hopper attached to a wall.

The crushed gravel and sand used in the experiments were fairly uniformly sized as indicated by the cumulative size frequency distributions in Figure 5.2. The intermediate diameter of the gravel is about ten times larger than that of the sand.

The main purpose of the experiments was to see whether the fall sorting of debris, suggested in the theoretical model, can be expected to occur in practice, given a simple small scale rock-fall situation. A second purpose was to obtain information on the angles and profiles of debris slopes at varying stages of build-up by the single process of rock-fall.

a) Size sorting

Sand and gravel mixed in a 1:1 ratio was dropped slowly but continuously through the hopper onto the floor. The retaining walls for the resultant debris slope were made of plexiglass so that the distribution of gravel and sand could be observed at the lateral edges throughout the build-up of the slope. Retaining walls may unduly influence the movement of the particles, and therefore a second technique was adopted to examine the sorting pattern on the slope. When the slope had reached a height of 90 cm (36 in), horizontal slices 15 cm (6 in) thick were successively removed from the slope and photographs taken of the truncated surface. The distribution of gravel and sand on each surface was then assessed and the following

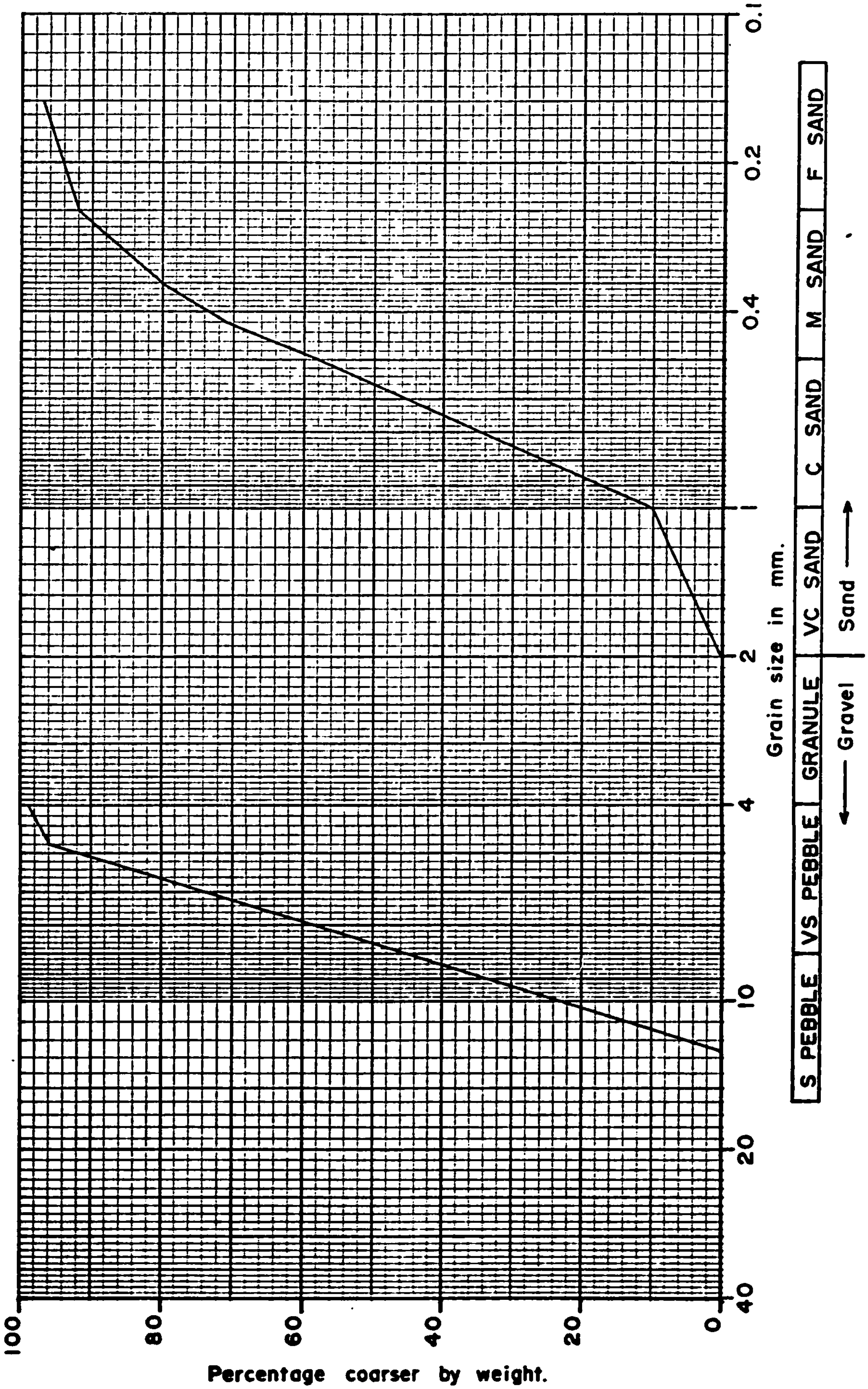

FIG. 5.2 CUMULATIVE GRAIN SIZE CURVES FOR GRAVEL AND SAND IN LABORATORY EXPERIMENTS

pattern established (Fig. 5.3).

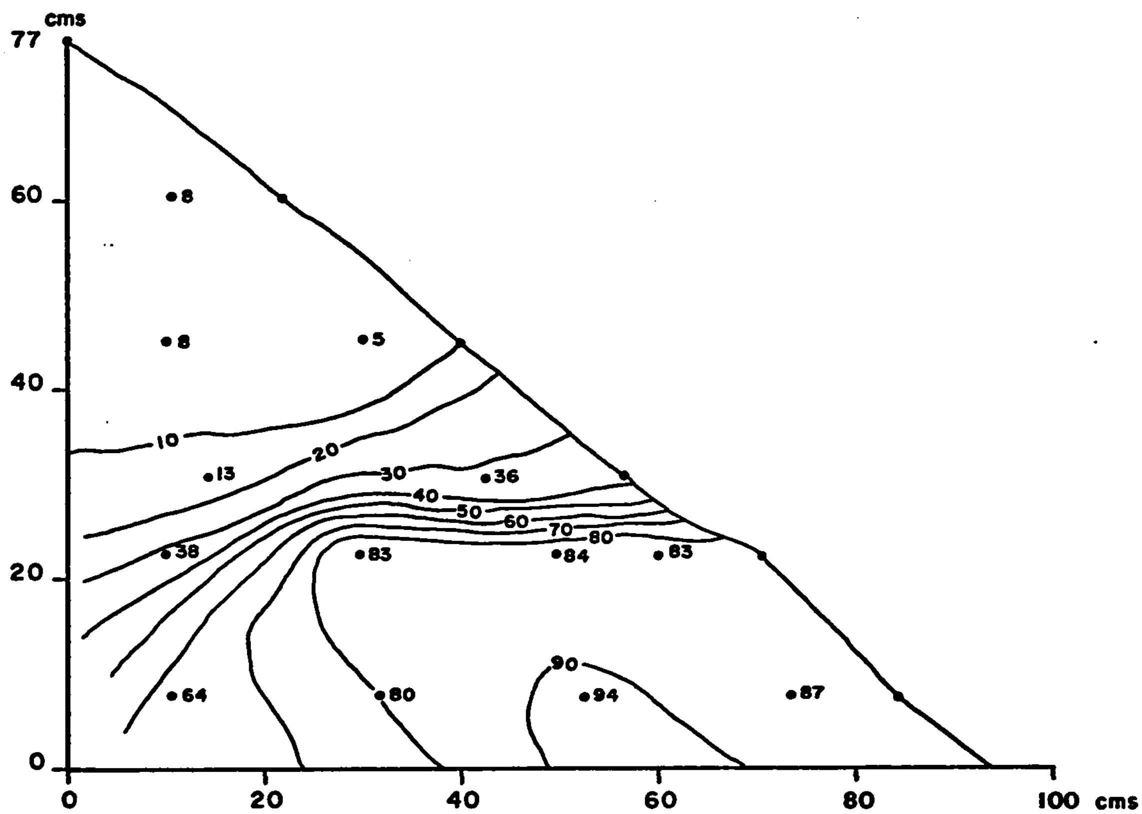

FIG. 5.3 FALL SORTING IN LABORATORY ROCK-FALL MODEL
Figures refer to percentages of gravel

Fall sorting with a rapid transition from sand to gravel in the middle of the slope is evidently a characteristic of the slope throughout the debris build-up. In chapter 4 the effects of original and acquired slope roughness were demonstrated as the reasons for fall sorting in the theoretical model. In the small scale laboratory model the air resistance is even less significant due to the slight distance of fall. Therefore the differential effect of surface roughness is clearly the reason for the creation and maintenance of the fall sorting pattern illustrated in Figure 5.3.

b) Slope angles and profiles

The angle of repose is defined as the slope at which any given deposited material will come to rest under a given set of physical conditions (Glossary of Geology and Related Sciences, 1960, p. 243). Repose angles on sand and gravel slopes have been found to be subject to considerable variation depending on the precise interplay of forces on the falling particles and on characteristics of the particles in aggregate on the developing debris slope. For natural and artifical slopes composed of these relatively cohesionless materials characteristic angles of repose of 30-40^{o} have been noted by many authors e.g. Leblanc, (1842); Piwowar, (in Rapp, 1960a); Poser (in Rapp 1960a); Behre, (1933); van Burkalow (1945); Young, (1956); Rapp, (1960a); Melton, (1965).

Experimental drops were made with gravel, sand and the gravel sand mixture in order to note the effects of the different grades of debris on the angles of repose of debris slopes, under different conditions of accretion. Sand slopes and gravel slopes were first built up by the addition of large discrete quantities of debris through the hopper. In this way rock-fall accretion with maximum disturbance of the developing slope was simulated. Then, the sand slopes, gravel slopes and mixed sand and gravel slopes were built up by the addition of debris slowly and continuously through the hopper, in order to simulate rock-fall accretion with minimum disturbance of the debris slope.

As debris build-up commenced the horizontal floor caused scattering of particles outwards from the point of impact. This effect is gradually eliminated as build-up continues. Eventually the mean slope angle becomes independent of the height of the slope and angles can then be recorded and profiles observed. This stage was reached when the slopes reached a height of about 60 cm (24 in).

The individual angle measurements were made by laying an Abney level gently on the slope. In the case where debris slopes were built up by slow continuous accretion, slumping periodically reduced the mean slope angle 2^{o}-4^{o}. Therefore the slope angles recorded were those reached just prior to a slump. The results of the experiments are summarised in Table 5.1.

A large difference in slope angle under different conditions of accretion is noted in Table 5.1. Using Student's t test this difference was found to be highly significant for both gravel and sand slopes. It is probably associated with the dissipation of kinetic energy. The impact of large discrete drops of debris at the top of the slope necessitates the rapid dissipation of a great quantity of kinetic energy and this is only partially achieved through heat production. The rest is dissipated through destruction of the packing arrangement of particles already present in the debris

TABLE 5.1

ANGLES OF DEBRIS SLOPES BUILD BY LABORATORY ROCK-FALL SIMULATION[1]

Grade of debris	Mean repose angles for large discrete drops (in degrees)			Mean repose angles for small continuous drops (in degrees)		
	Mean	S. Dev.	No. in sample	Mean	S. Dev.	No. in sample
Gravel	36.2	0.2	5	39.9	0.8	10
Sand	30.0	0.5	7	34.8	0.4	9
Gravel and sand				36.5	0.9	21

1 The top 15 cm (6 in) in each profile is not included in the calculation of angles because of the pronounced flattening observed due to impact.

slope. This destruction causes the debris to shift to a lower angle. The smaller quantities of kinetic energy, associated with the small continuous rock-falls, are more readily dissipated through the mass of the debris already on the slope, by slight shifting leading to closer packing rather than by the complete destruction of the mutual arrangement of the particles on the slope.

This suggests that one of the reasons for the considerable variation of repose angles on talus slopes is probably the variation in frequency and intensity of the processes which create impacts on the talus slopes viz. rock-falls and snow and torrent avalanches.

For both maximum and minimum disturbance situations, the sand slopes assume a lower angle than the gravel slopes, the difference being highly significant according to the t test. The mean angles of the mixed gravel and sand slopes for the minimum disturbance accretion lie between the angles observed for sand and those observed for gravel. The overall mean angle for these mixed debris slopes is 36.5°, a figure very close to the average repose angles of debris slopes built almost exclusively by rock-fall processes (Rapp, 1960a, p. 53). It is also close to the values noted later in this chapter for slopes in coarse debris at mine dumps at Sudbury, Ontario and Asbestos, Quebec.

Profiles for different conditions of rock-fall and particle size were rectilinear with one exception. The profile of the fall sorted debris slope built up by the slow continuous addition of mixed sand and gravel displayed a slight convexity which correlated quite well with the transition from sand to gravel (Fig. 5.4) . A highly significant correlation coefficient of 0.50 was computed for the relationship between the slope angle and the percentage of gravel present, and substantiates the previous observations from the separate gravel and sand slopes.

Previous literature on the subject of particle size and the angle of repose for cohesionless debris slopes suggests that the relationship between the two variables has yet to be properly evaluated. Recent experiments with smooth glass spheres suggest that no correlation exists at all between particle size and the angle of repose (Duckworth, 1969). But experiments with natural sands and gravels

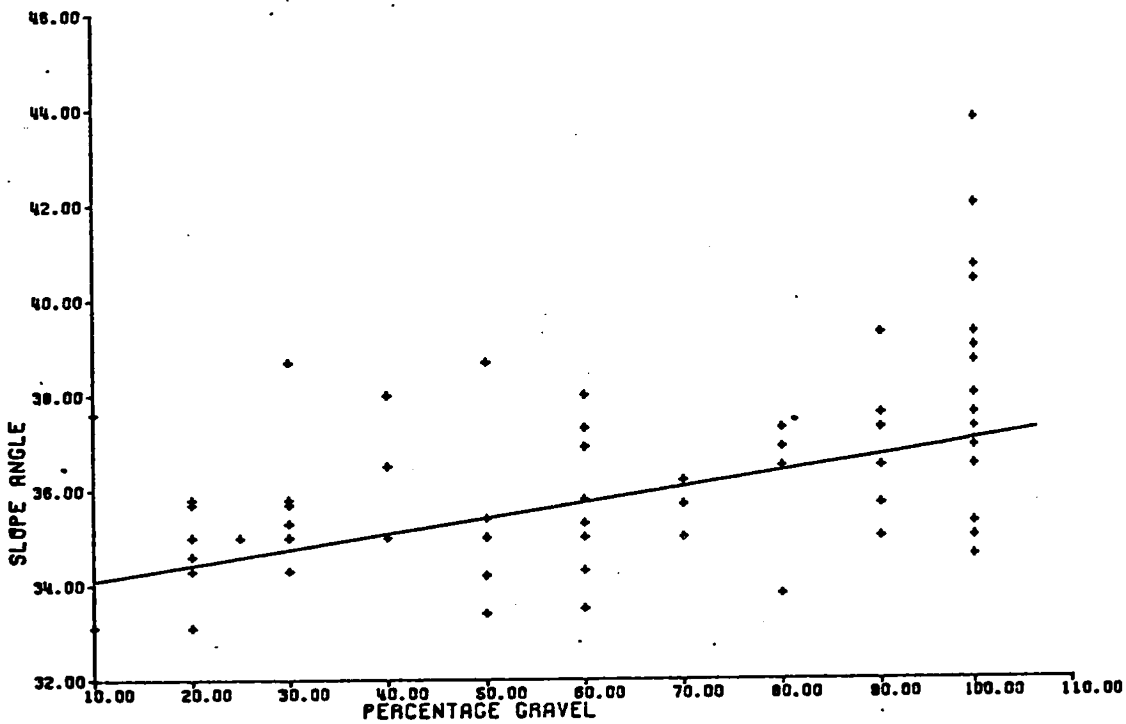

Regression equation: $y = 0.03x + 34.15$

$r = 0.52$

$S_{XY} = 1.77$

FIG. 5.4 CORRELATION BETWEEN SLOPE ANGLE AND PARTICLE SIZE IN LABORATORY ROCK-FALL MODEL over the last fifty years have produced widely divergent opinions concerning this relationship (van Burkalow, 1945 p. 672). This may be because so many external factors are involved e.g. particle shape, size sorting, surface roughness, specific gravity and packing arrangement.

2. MEDIUM SCALE MINE DUMP SLOPES.

Nine sampling traverses were made at one of the Errington mine dumps and one at the Clara Belle in the Sudbury Basin, northern Ontario. The former mine dump is about 40 years old, and is 6-20 m (20-65 ft) in height. Its slope consists mainly of small boulders and coarse gravel, and is a good example of a slope built by minimum velocity rock-falls. Disturbance of the pattern of particle size distribution due to slight gullying, soil creep and soil wash has occurred, but the coarse nature of the debris supplied to the slope, the infrequent spacing of the gullies, and the relatively short time interval since dumping suggest that this effect is minimal. The traverse on the Clara Belle dump was on a slope 25 m (80 ft) high presently being built by the dumping of large and medium size boulders over the edge from trucks. It is therefore influenced only by rockfall processes.

On each sampling traverse the 'a' 'b' and 'c' axes of fifty particles were measured at five equally spaced points downslope. Statistical analysis of the 'b' axis, including an analysis of variance and a logarithmic transformation of the values, indicated that particle size is correlated with distance downslope at a 99% level of significance for nine out of the ten slopes (Table 5.2).

TABLE 5.2

SLOPE ANGLES AND FALL SORTING ON MINE DUMPS IN THE SUDBURY BASIN

Location	Traverse	Height of traverse (m)	Slope angle (degrees)	Correlation coeffts. log 'b' axis and dist. downslope
Errington mine dump	1	15	35.4	0.63
	2	"	34.0	0.35
	3	"	34.5	0.14*
	4	"	34.6	0.52
	5	"	34.4	0.51
	6	"	34.4	0.73
	7	7	33.5	0.53
	8	"	32.0	0.50
	9	"	33.0	0.51
Clara Belle mine dump	10	25	36.5	0.51

* Not significant

From the table it is apparent that distance downslope explains about 20% to 50% of particle size variation. It can be concluded that the fall sorting pattern established in the theoretical and small scale laboratory models is substantiated for medium scale rock-fall built slopes. But the influence of uncontrolled factors, such as variations in particle shape for all traverses, and the washing of fines downslope for the first nine traverses, prevent a very high correlation between particle size and distance downslope.

The mean angles of all ten mine dump slopes are also plotted in Table 5.2. The overall mean is 34.2° with a range of $\pm 2.3^{\circ}$. The most reliable slope angle is from traverse 10, since this is a slope adjusted only to the process of current rock-fall by dumping from its crest. Four profiles were measured on this slope and these were found to be rectilinear or very slightly convex. This suggests that fall sorting has only a slight effect on the profiles of the mine dump slopes.

Information was provided on the slope angles and profiles for three rock dumps at Asbestos, Quebec, by Asbestos Corporation Ltd. These slopes consist of rock waste of talus sized particles, varying in size from 15 cm (6 in) to 180 cm (72 in). The mean angles for the three slopes are 35.5°, 35.5° and 36° quite similar to the angles observed for the recently dumped rock waste near traverse 10 in the Sudbury Basin. All three slopes exhibit fall sorting and are generally rectilinear in profile.

3. SUMMARY OF RESULTS

The study of rock-fall on laboratory and mine dump slopes resulted in the following conclusions that are of potential significance to the study of talus slopes in the Ogilvie and Wernecke Mountains.

Fall sorting was found to be a normal phenomenon at every stage in the build-up of mixed debris slopes in the laboratory. It was also observed on the surfaces of twelve of thirteen mine dump slopes.

The artificial slopes built of sand or gravel were rectilinear, save for impact flattening at the top of the slope. The mixed debris slopes on the mine dumps were rectilinear and those in the laboratory were slightly convex. Statistically, 95% of the repose angles of mixed debris slopes, developed in the laboratory under minimum disturbance accretion, lie between 34.7° and 38.3° with a mean of 36.5°. The thirteen mine dump slopes have mean angles ranging from 32° to 36.5° with an overall mean of 34.7°.

CHAPTER 6

RELATIONSHIP OF TALUS MORPHOLOGY TO ROCK-FALL

1. INTRODUCTION

In order to assess the similarities and differences between the talus slopes and the theoretical and artificial models, certain fundamental characteristics of the former are examined. These include the distribution of particle attributes over the talus surface, and the actual form of the talus slope.

Among the former, particle size variations in the downslope direction were chosen for study and comparison with the model situations, because the phenomenon of fall sorting is an indicator of the importance of rock-fall on talus slopes. Other variables, are introduced into the discussion, however, because they necessarily influence the relationship between particle size and distance downslope.

The characteristics of talus form that receive attention are mean angles, maximum angles and overall slope profiles.

2. PARTICLE SIZE VARIATION

a) Sampling pattern

In previous studies sampling has generally been done in small groups of particles evenly spaced at intervals down the central fall line of the slope. Clearly this does not enable the true population mean of a conical surface to be determined, although it does permit the analysis of population variations with distance from the source of the population (i.e. from the talus apex). Whilst the latter is the main aim of the research a large bias is possible by sampling only on the central fall-line of the slope.

A stratified random sampling pattern was adopted and is illustrated in Figure 6.1. It fulfills the following needs:-

i) A primary stratification in accordance with subjectively observed fall sorting. Variations in debris characteristics other than size were not obvious enough to invite a conflicting pattern of stratification.

ii) The spreading of observations within a stratum to a few randomly chosen stations, to combine randomness and speed of data collection.

iii) Random measurement of a large number of particles at each station.

The cones were divided along the length of their central fall-line into ten horizontal strata, described here as zones. Using this method of proportional division into zones it is easily possible to compare results from cones of different sizes.

Properties of 100 particles were examined for each zone on the talus cones. This is a number calculated from pilot sample data on cones 6824, using methods described by Cochran (1963). It is

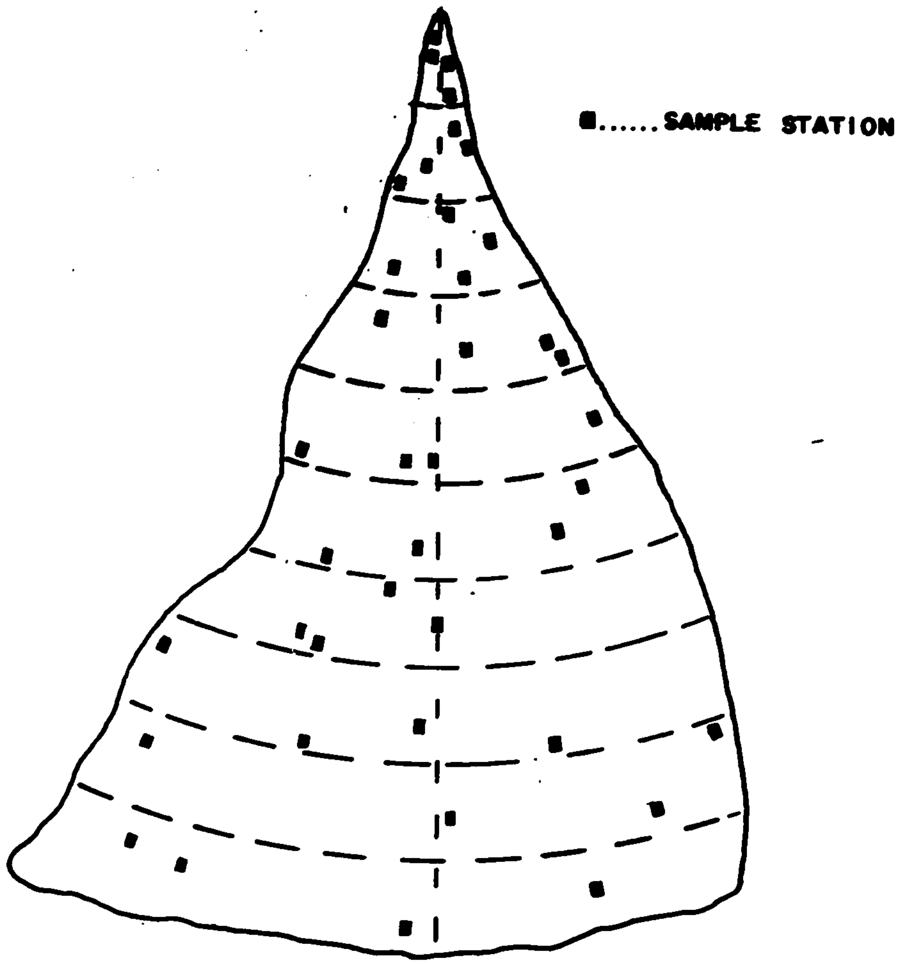

FIG. 6.1 SAMPLING PATTERN ON TALUS SLOPES

sufficiently large so that the true population mean of the particle 'b' axes for each sample zone can be estimated to limits within ± 20% of the true mean with only 5% probability of error. One hundred measurements in each of the ten zones also allows downslope variation of all measured particle variables to be accurately assessed since the number of sample groups and the number of samples within each group are large enough for an accurate comparison of within sample and between sample variance.

Rather than sampling 100 particles at a single spot on the central fall-line of the cones random selection of four sample stations, referred to as points within each zone was made. Then 25 particles were randomly chosen for measurement at each point.

Thus, the sampled population of the cone can be considered at three different levels:-

1) 1,000 individual particles
2) 40 sample stations or point means (25 particles at each point)
3) 10 strata or zone means (100 particles in each section)

Due to the large volume of data a complete statistical analysis could only be done for four of the talus cones. A summary analysis of the data collected for the other six talus cones was also carried out, however.

b) Measured characteristics

Size, shape, lithology, lichen cover and lichen sizes were measured for all particles. The inclination of the slope at the sample station and the distance of the latter from the top of the slope were also measured.

i) Particle size

The 'a', 'b' and 'c' axes of particles were measured according to the intercept method described by Krumbein (1941, p. 65-66) and the 'b' axis used to represent particle size in the subsequent statistical analysis. In Krumbein's technique the 'a' axis is the largest possible axis through the particle, the 'b' axis is the longest axis in the maximum projection plane perpendicular to the 'a' axis, the 'c' axis is then the longest axis which is mutually perpendicular to the 'a' and 'b' axes.

The particle axes were measured to the nearest 1 cm. The considerable error in the correct selection of axes due to irregularity of particle shapes and the large size of most of the particles did not justify more refined measurement.

Measurement of particle size and other attributes on talus particles is greatly complicated by the wide particle size range. The technique of triaxial measurement applied to debris in the cobble or boulder range of sizes is not applicable to the finer fraction of debris on the slope surface and an arbitrary lower limit to the size of particles measured triaxially had to be established. This limit is 1 cm for the 'b' axis.

If a particle finer than this was randomly selected at a sample station, a record was made, but particle characteristics were not measured. After sampling 25 coarse particles the number of fines selected but not measured is then known. From this the percentage of fines on the talus slopes could be calculated. A grab sample of fines was collected for mechanical analysis from every sample station on which a fine particle was randomly selected. In this way the effect of the fine fraction of debris could be assessed along with the coarse fraction.

ii) Shape of particles

Wadell (in Krumbein, 1941, p. 71) derived an index of sphericity which may be defined by the following equation

$$\text{Sphericity } \Psi = \sqrt[3]{\frac{\text{volume of particle}}{\text{volume of the circumscribed sphere}}}$$

where the volume of the particle is expressed in terms of a sphere having the same volume.

If the particle is nearly spherical, then Ψ closely approaches the maximum limit of 1 (Fig. 6.2a). If the volume of the particle becomes very small relative to the volume of the circumscribing sphere, then Ψ closely approaches the minimum limit of 0 (Fig. 6.2b).

(a) (b)

FIG. 6.2

Operationally sphericity was calculated by Krumbein (1941) on the assumption that particles approximate triaxial ellipsoids. He calculated particle volume as $\frac{\pi}{6}abc$, where a, b and c are the previously discussed particle axes. When this value is inserted into Wadell's equation the following expression for sphericity is obtained.

$$\Psi = \sqrt[3]{\frac{bc}{a^2}}$$

iii) Lithology

Of the four cones for which detailed analysis of the sampled data was made, cones 6830 and 6831 are located in the igneous intrusive zone and consist entirely of syenitic and monzonitic debris, whereas cones 6812 and 6824 are located within the zone of metasedimentaries and consist predominantly of dolomite and orthoquartzite respectively.

iv) Lichen cover and sizes of Rhizocarpon geographicum spp

For all particles the extent of the lichen cover was assesed qualitatively in terms of absence, sparseness and abundance. The sizes in millimeters of the largest thalli of Rhizocarpon geographicum spp were measured. In this manner the relative disturbance of the talus could be assessed. This data is used in chapter 7 when avalanche influences on the talus slopes are discussed.

v) Angle of slope at sample stations

These were measured by Abney level over ten metre long sections of slope centred on each sample station and aligned towards the apex of the slope.

vi) Distance downslope

The distance downslope in percentage terms was measured for each sample station as part of the locational procedure in the sampling.

c) Data analysis

The analysis of the field data involved several steps which are now described.

i) Test of normality and required transformations

Moment measures were used in the analysis and so the data must be reasonably normally distributed. The third and fourth moments of the distribution i.e. the skewness and kurtosis gave a measure of the departure of the distribution from a normal 'bell shaped' curve. If the distribution departed too far from a normal curve successive transformations were applied to reduce skewness and kurtosis to values acceptable for normal distributions, using methods described by Snedecor (1956, p. 201-203).

Particle size represented by the 'b' axis was not normally distributed but responded for all sample zones to a logarithmic transformation. In this case $\log_{10}$ was used although the data could also have been subjected to the ϕ transformation described by Krumbein (1936). Particle sphericity only met the requirements for normality when a transformation to sphericity squared was applied. Figure 6.3 illustrates the effects of transformation of 'b' axis and sphericity on the frequency histograms of a single sample zone.

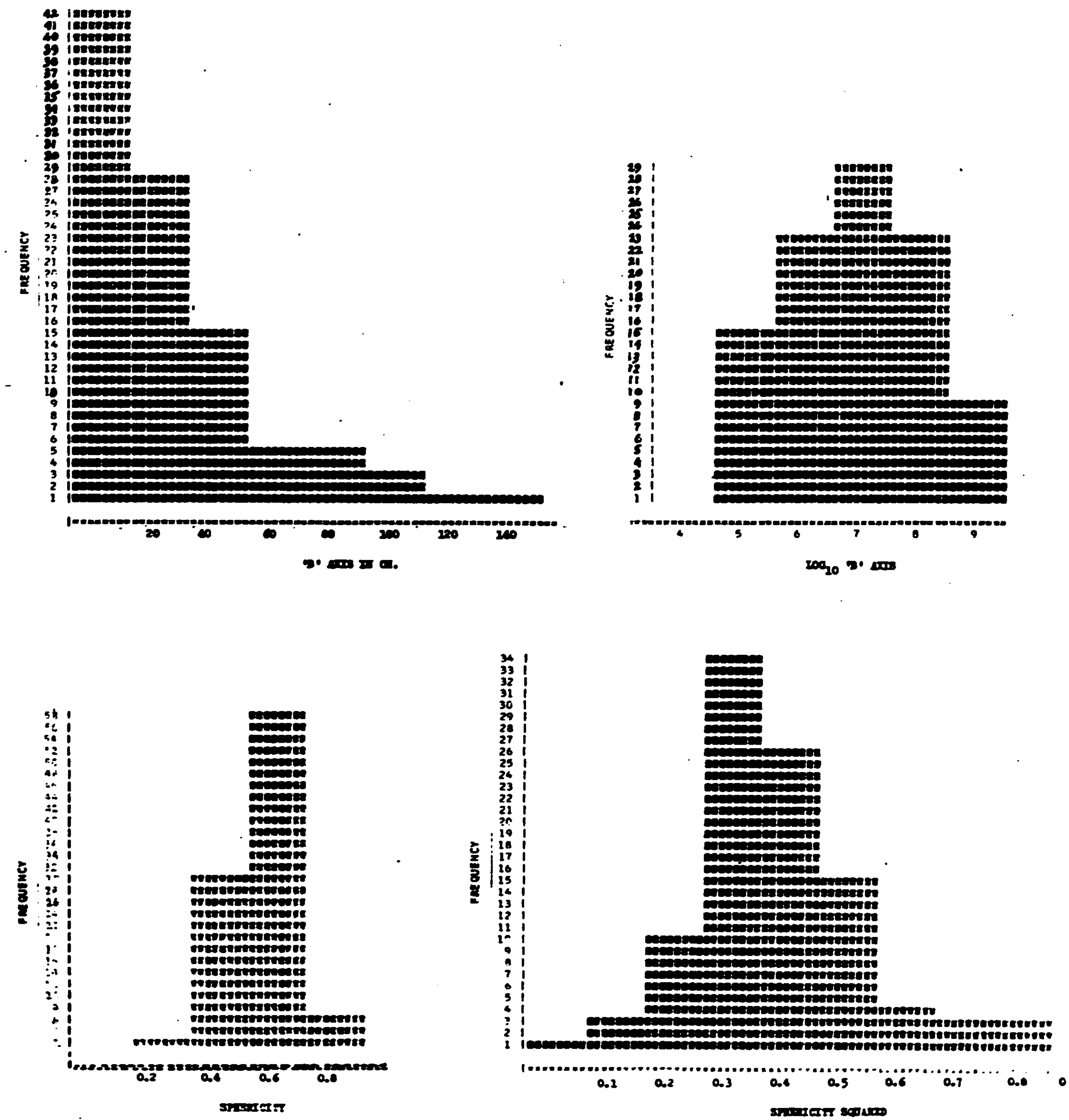

FIG. 6.3 EFFECT OF PARTICLE SIZE AND SHAPE TRANSFORMATION UPON FREQUENCY DISTRIBUTIONS FOR ONE SAMPLE ZONE

The other variables considered in the statistical analysis, slope angles at sample points and percentage distance of each sample point from the apex of the cones, were not subjected to this normality test, since there is only one value for each point and only four values for each zone. It must be assumed that if a sufficient number of readings of slope angle were taken within a section, distribution would be reasonably normal.

ii) Analysis of variance

Simple one way analysis of variance was carried out on the 'b' axis, and sphericity, both transformed and untransformed, for each of the four talus cones. The data for this variance analysis was grouped successively by points (25 particles to each point) and by zones (100 particles to a zone). In all cases the estimate of variance between groups is greater than the estimate of variance within groups, although the calculated F statistic is reduced for the transformed data. The analysis of variance suggests that there is considerable variation between values at different points and sections on the slopes which cannot simply be explained by variation within the sample groups.

iii) Test of bias resulting from exclusion of fine particles

The magnitude of this problem depends fundamentally on whether the fines form a significant percentage of the talus cone surface, and to a lesser extent on whether they are largely composed of gravel, sand, silt or clay fractions.

The low percentage of the talus surface covered by fines was noted in chapter 2 (see Table 2.1). The cumulative frequency distributions prepared from mechanical analyses of the grab samples of fines and presented in Figures 2.1 and 2.2 indicate that less than 50% of the fines are below the size of gravel and less than 5% are in the silt-clay size range.

Despite the low percentage of fines on the talus slopes and the fact that they fall mostly within the coarse sand or gravel range, it was considered advisable to compute corrected means for the 'b' axis for all points and sections where fines were recorded.

The mean 'b' axis of the fines was readily calculated from the mechanical analysis data. For the fines sampled on the slopes in the igneous intrusives it is 3.5 mm and for those sampled on the slopes in the metasedimentary zone it is 7 mm.

A number of coarse particle measurements of the 'b' axis were replaced by the newly calculated mean 'b' axis of the fines. The number removed depended on the percentage of fines at the point and were of course the last few coarse particle measurements made.

New sample means and standard deviations for the 'b' axis were then calculated and normalisation and analysis of variance tests carried out on the new data. Inclusion of the fine fraction on the surface of the talus cones was found to make a negligible difference to the mean and standard deviations of the 'b' axis (Table 6.1).

TABLE 6.1

EFFECT OF INCLUSION OF FINES ON MEAN DEBRIS SIZE

	1,000 particles with 'b' axis > 1 cm		1,000 particles including those with 'b' axis < 1 cm	
	Mean	S. Dev.	Mean	S. Dev.
Cone 6812	107	93	105	94
Cone 6824	106	78	106	79
Cone 6830	198	225	193	227

Since the required transformations for normalising the distributions and results of the analysis of variance also remain unchanged, the original data was restored and the analysis continued without further consideration of the relatively unimportant fine gravel and sand fractions on the cone surface.

c) Statistical evidence for fall sorting from simple correlation and regression model.

Simple correlation of particle size represented successively by the 'b' axis and $\log_{10}$ 'b' axis against distance downslope was conducted for 1,000 individual particles on cones 6812, 6824, 6830 and 6831. The values for the correlation coefficients (r) and the percentages of variance in particle size explained by distance downslope (r^2 x 100) are given in Table 6.2

TABLE 6.2

CORRELATION OF 'b' AXIS & LOG 'b' AXIS AGAINST DISTANCE DOWNSLOPE

	'b' axis		log 'b' axis	
	r	r^2 x 100	r	r^2 x 100
Cone 6812	0.50	25	0.51	26
Cone 6824	0.47	22	0.47	22
Cone 6830	0.45	20	0.47	22
Cone 6831	0.41	17	0.61	37

A highly significant level of association (i.e. with 99% confidence was found between the 'b' axis of particles and distance downslope using a Student's t test (Fisher, in Snedecor, 1956, p. 173-174), both for transformed and untransformed values of the particle 'b' axis. The correlation coefficients and percentages of explained variance increase only slightly from about 0.45 and 20%, to 0.50 to 25% when particle size is logarithmically transformed.

These results indicate that fall sorting occurs on the four talus cones. Table 6.3 illustrates the actual size ranges for debris in different zones.

TABLE 6.3

PARTICLE SIZE VARIATIONS ON TALUS CONES (in cms)

Zone	Cone 6812		Cone 6824		Cone 6830		Cone 6831	
	Mean	S.dev.	Mean	S.dev.	Mean	S.dev.	Mean	S.dev.
1	22.7	(14.6)	19.1	(10.9)	53.2	(30.2)	65.4	(62.6)
2	16.0	(8.6)	18.5	(9.3)	32.9	(29.1)	51.5	(38.0)
3	15.6	(7.7)	11.0	(6.4)	23.3	(30.8)	45.9	(79.7)
4	9.8	(5.9)	8.7	(3.7)	15.1	(11.4)	45.6	(53.4)
5	7.0	(4.6)	10.1	(6.1)	12.7	(11.3)	20.4	(12.9)
6	8.6	(8.2)	8.8	(5.4)	12.0	(9.4)	14.5	(12.6)
7	7.5	(5.8)	8.4	(4.3)	15.5	(8.9)	14.9	(29.3)
8	6.7	(5.9)	6.9	(6.0)	11.6	(11.5)	11.4	(9.6)
9	6.6	(4.6)	6.0	(3.6)	13.0	(10.4)	10.2	(8.7)
10	6.2	(5.4)	8.4	(6.1)	8.8	(5.1)	11.5	(8.5)

The logarithmic relationships between particle size and distance downslope are illustrated in Figures 6.4a), b), c) and d) for the four talus cones. For diagram clarity the data had to be grouped into forty sample means for each cone.

In order to determine whether a significant relationship between particle size and distance downslope holds generally for all talus cones for which field data was collected, the 'b' axis and $\log_{10}$ 'b' axis means were calculated for all ten sections on the ten talus cones for which sample data was available, and were then correlated with the distance downslope. The correlation coefficients are 0.46 and 0.56 respectively. These values are highly significant and indicate fall sorting for all sampled talus cones, although not so accurately as the values given in Table 6.2. This is because the former result from the correlation of summary measures from several populations.

e) Influence of other variables

Although the simple correlation and regression model indicates that fall sorting occurs on the talus slopes, it cannot in itself indicate whether particle size is the dominant influence in the distance moved downslope by falling particles. The following additional influences were noted, either from the theoretical rock-fall model or from observations of rock-fall on the slopes.

1) Particle shape
2) Slope angle variations over the surface of the talus cones
3) Angle of rock wall above the talus cones

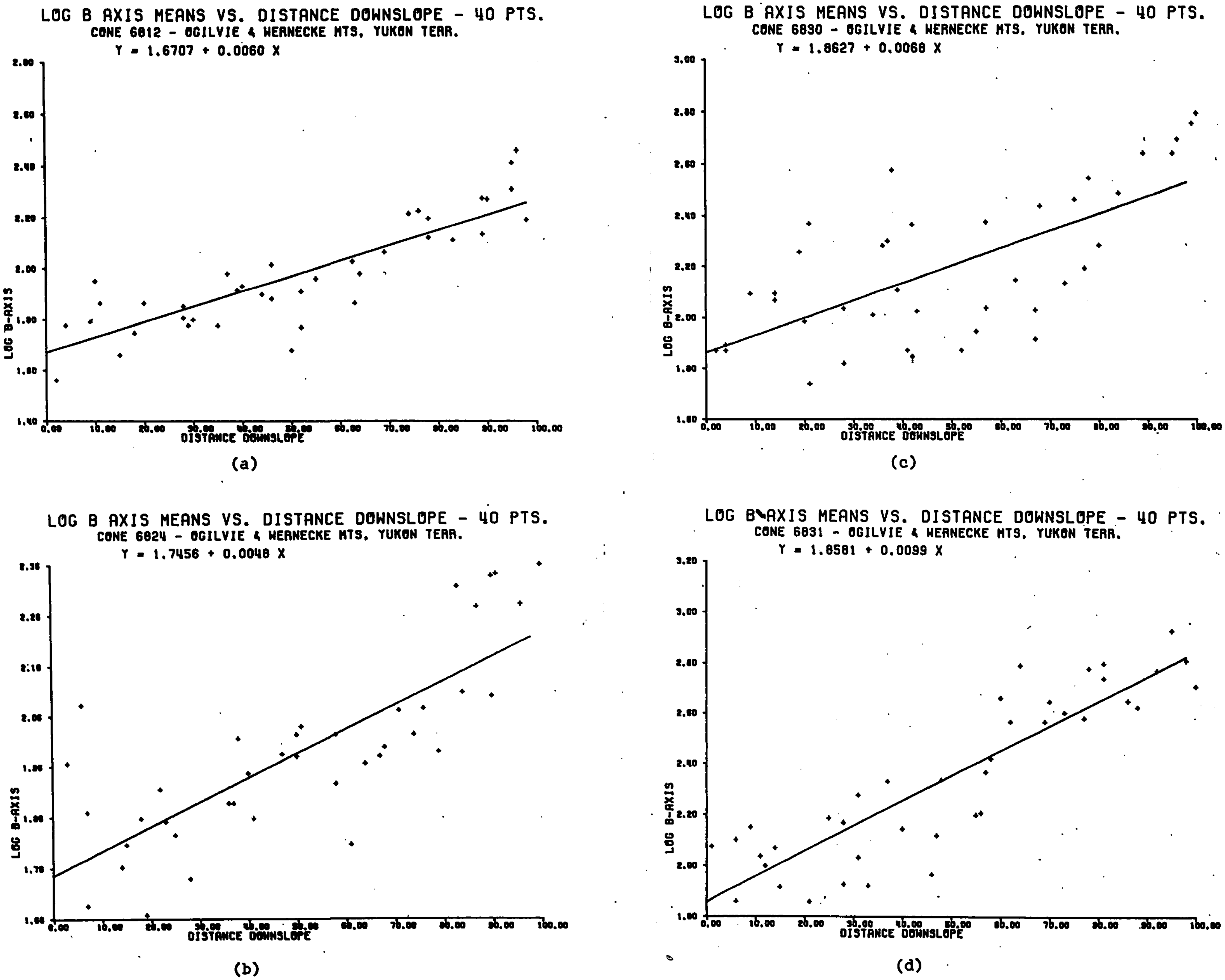

FIG. 6.4 RELATIONSHIPS BETWEEN PARTICLE SIZE AND DISTANCE DOWNSLOPE FOR FOUR TALUS CONES

4) Distance of rock-fall
5) Frequency of occurrence of rock-falls in different size ranges.
6) Coefficient of restitution e for bounding particles
7) Coefficient of kinetic friction λ for sliding particles
8) Momentum transfer upon impact
9) Other processes.

Particle shape and slope angle variations on the talus cone surfaces were measured along with particle size in the sampling procedure and can be statistically related to distance downslope, in the present study. The effects of the rock wall angle, the distance of rock-fall and the frequency of occurrence of rock-falls in different size groups are then assessed qualitatively from the limited evidence available in talus environments. The coefficient of restitution e and the coefficient of kinetic friction λ may be considered constant and therefore unimportant in variation of particle velocity and distance travelled on an individual talus slope. Momentum transfer is of unknown significance in moving debris downslope through impact. Other processes may have an influence in removal of debris downslope but consideration of their importance is withheld until chapter 7.

i) <u>Effect of inclusion of particle shape and slope angle variations in fall sorting model</u>

A stepwise correlation and regression model was used for all data from cones 6812, 6824, 6830 and 6831, in order to compute the effects of each of the variables of particle size, particle shape and slope angle as they interact to produce the downslope variation. This model then becomes a superior statistical explanation of the relationship between particle size and distance downslope to that previously proposed by a simple two variable correlation and regression model.

Table 6.4 lists correlation coefficients and the degree to which the independent variables of particle size, particle shape and talus slope angle influence the distance moved downslope by particles.

TABLE 6.4

STEPWISE CORRELATION RELATING PARTICLE SIZE, SHAPE AND SLOPE ANGLE TO DISTANCE DOWNSLOPE.

		Data non normalised			Data normalised		
Cone No.	Dependent variable	Indep. variables added	r	$r^2(100)$	Indep. variables added	r	$r^2(100)$
6812	distance downslope	slope ang. 'b' axis sphericity	0.85[1] 0.86 0.87	73 74 75	slope ang. log 'b' axis sphericity[2]	0.85[1] 0.87 0.87	73 76 76
6824	"	slope ang. 'b' axis sphericity	0.85[1] 0.86 0.86	73 74 74	slope ang. log 'b' axis sphericity[2]	0.85[1] 0.87 0.87	73 75 75
6830	"	slope ang. 'b' axis sphericity	0.65[1] 0.69 0.69	42 47 47	slope ang. log 'b' axis sphericity[2]	0.65[1] 0.69 0.69	42 48 48
6831	"	slope ang. 'b' axis sphericity	0.68[1] 0.71 0.71	47 50 50	slope ang. log 'b' axis sphericity[2]	0.68[1] 0.75 0.75	47 56 56

1 r is an inverse coefficient of correlation between slope angle and distance downslope.

Slope angle shows a high negative correlation with distance downslope, and is an important determinant of the downslope component of gravitational acceleration of a particle. For this reason it would be only too easy to assume simplistically that the downslope change in slope angle is the factor of greatest importance in the pattern of debris distribution on the slope. But it was shown in the theoretical model that the downslope acceleration due to gravity does not affect large particles any differently from small particles for all types of motion and so slope angle variations are not the cause of fall sorting. Furthermore fall sorting was observed on artificial slopes which are rectilinear or even slightly convex in profile. Indeed, the pattern of debris distribution, itself, is partly responsible for the slope angle variations that exist. This will be elaborated fully when talus form is discussed.

Since slope angle is not a factor causing fall sorting it is now excluded from the regression model since it obscures a true assessment of the fall sorting relationship. The results of the new stepwise correlation model are presented in Table 6.5.

$\log_{10}$ 'b' axis variations account for 23%-37% of the variation in distance downslope according to the revised model, but particle sphericity hardly increases the percentage explanation at all.

TABLE 6.5

STEPWISE CORRELATION RELATING PARTICLE SIZE AND SPHERICITY TO DISTANCE DOWNSLOPE.

		Data non normalised			Data normalised		
Cone No.	Dependent variable	Indep. variables added	r	$r^2(100)$	Indep. variables added	r	$r^2(100)$
6812	distance downslope	'b' axis sphericity	0.50 0.52	25 27	log 'b'axis sphericity^2	0.57 0.57	33 33
6824	"	'b' axis sphericity	0.47 0.47	22 22	log 'b'axis sphericity^2	0.51 0.51	26 26
6830	"	'b' axis sphericity	0.45 0.46	21 21	log 'b'axis sphericity^2	0.48 0.48	23 23
6831	"	'b' axis sphericity	0.41 0.41	16 17	log 'b'axis sphericity^2	0.61 0.61	37 37

A simple correlation and regression model for the four cones revealed that sphericity increases in a downslope direction on cones 6812 and 6824 but shows no significant trend on cones 6830 and 6831 (Fig. 6.5a) b) c) d). Sphericity indices on cones 6812, 6824 6830 and 6831 tend to cover a relatively limited part of the possible range between 0 and 1 (Table 6.6) and this may partly account for the relative unimportance of this variable.

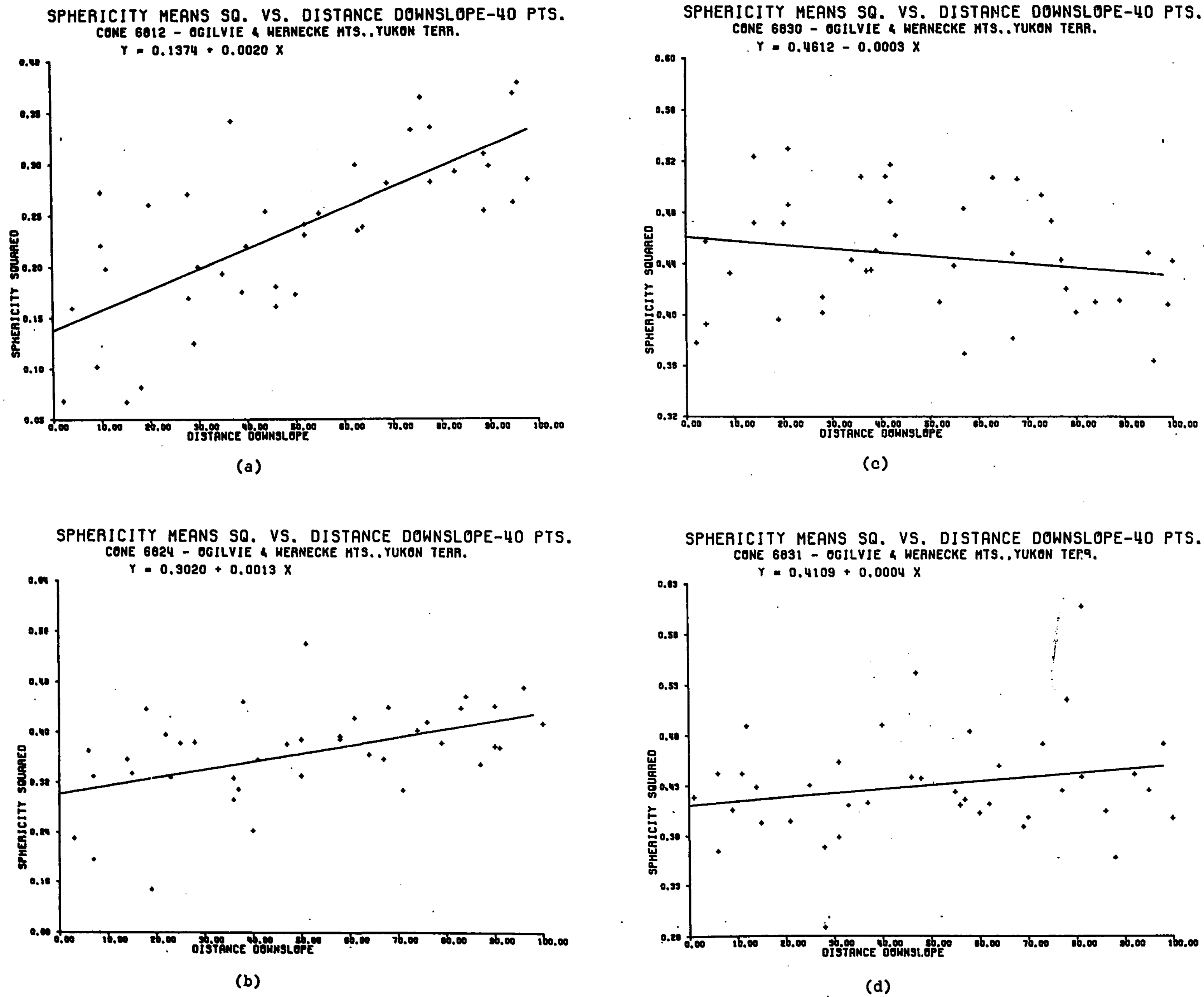

FIG. 6.5 RELATIONSHIPS BETWEEN PARTICLE SHAPE AND DISTANCE DOWNSLOPE FOR FOUR TALUS CONES

TABLE 6.6

RANGE OF SPHERICITY MEANS FOR ALL SAMPLE ZONES ON CONES 6812, 6824, 6830 AND 6831.

	Range of means of zonal groups of 100 particles.
Cone 6812	0.37 - 0.57
Cone 6824	0.53 - 0.65
Cone 6830	0.64 - 0.70
Cone 6831	0.61 - 0.69

The fact that particle size and shape are far from perfectly correlated with distance downslope indicates that they only partially influence the distance moved downslope by particles. The other influences which reduce the degree of correlation are measurement and sampling errors, and the other variables listed on p. 122. The careful sampling procedure suggests that these other variables are of greatest importance.

ii) Mean angle of rock wall

The velocity attained by a falling particle when it arrives at the talus cone is directly related to the rock wall angle. Therefore, all else being equal, particles falling from the steep walls in the igneous intrusives possess higher velocities than particles falling from the more gently graded metasedimentary gullies and walls, and might be expected to travel further and have their motion arrested at lower slope angles than in the case of the metasediments. Measurements of talus cone angles on the two rock types do not indicate a lesser slope angle for the talus below the steep rock walls in the Tombstone intrusion, than for the talus in the metasedimentary zone. Therefore this is a factor of minor importance in the distance travelled by rock falling particles on the basal slopes. Where talus slopes are poorly developed, surface roughness has less of a retardational effect and this accounts for low angle talus aprons below some steep syenite walls.

iii) Distance of rock-fall

If retreat is parallel, as suggested for at least several rock walls above talus slopes (Rapp, 1960b, in Bird 1967), distance of fall should be a statistically random factor, whose only effect would be to reduce the degree to which all the other variables explain the distance moved downslope by particles. In the short term rock-fall may be concentrated at a few points which result in bias of particle velocity upon arrival at the apex of a talus cone. Obviously, if a large number of particles of all sizes fall from only a few metres above the talus cone none of them may have acquired the necessary velocity to travel far over the talus surface. Even large particles may come to rest high on the talus slopes, especially if they have not developed bounding or rolling motion.

iv) Frequency of occurrence of rock-falls in different size ranges

When rock-falls were observed on the rock walls in the Ogilvie and Wernecke Mountains, shattering of large falling particles upon one or more of their impacts with bedrock was noted. It occurred more readily in the closely bedded and jointed metasediments than in the massively jointed igneous intrusives, and had the effect of rapidly reducing the size of the falling particles. An inverse logarithmic relationship between the volume of rock-fall debris on the lower slopes and the size of the individual particles is therefore predicted.

Evidence for the validity of this prediction was found on the talus slopes. The foregoing statistical assessment of the fall sorting pattern on ten talus slopes clearly indicated that the increase of particle size downslope is exponential rather than linear. This suggests that, in the recent past, rock-falls in the smaller size ranges may have been more frequent than rock-falls in the larger size ranges. But in calculating proportions of recently derived debris of various sizes on the cone surfaces allowance must be made for the larger area of the sample zones near the base of the talus cones (see Fig. 6.1). This undoubtedly raises the proportion of debris in the coarse size ranges but Figure 6.6 shows that, even when this factor is allowed for, there is still a pronounced logarithmic decrease in percentage of area covered as particle size increases.

Figure 6.6 was constructed in the following manner. Each sample zone on a cone surface was assigned its correct percentage of the

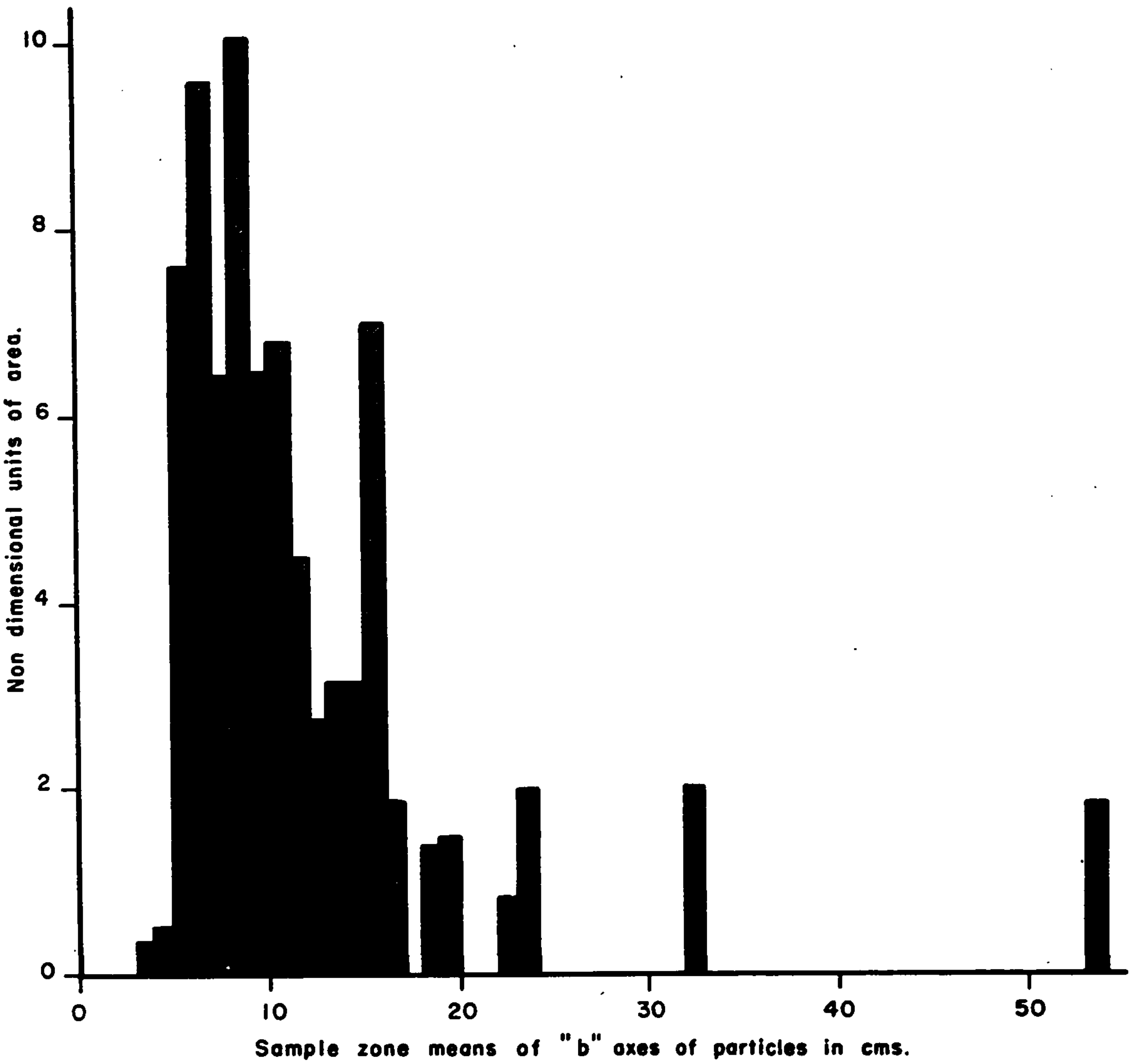

FIG. 6.6 SIZE FREQUENCY DISTRIBUTION FOR DEBRIS ON CONES 6805, 6806, 6810, 6811, 6812, 6824, 6825 and 6830

total cone area. These percentages were then plotted against the mean size of the 'b' axis of particles for each zone. The resultant histograms for eight cones were then superimposed to give a composite histogram (i.e. Fig. 6.6).

3. TALUS FORM

a) Field measurements

Apart from the measurements of slope angle at 40 sample stations on ten talus cones, slope angles and fall-line profiles of twenty-one other talus slopes were obtained. Thus eight slopes in the igneous intrusive zone and twenty-three slopes in the metasedimentary zone were were measured.

Mean slope angles and the angles of the steepest 30 m (100 ft) intervals were then determined for all talus cones. The degree of concavity or convexity of the profile down the central fall-line of seventeen talus cones were determined using indices derived by Stock (1968). His method for assessing talus profiles not only expresses the overall form but it also takes account of minor deviations from this form.

An exaggerated hypothetical example will illustrate the steps in Stock's method. Profile indices will be derived for the talus cone whose hypothetical profile is illustrated in Figure 6.7.

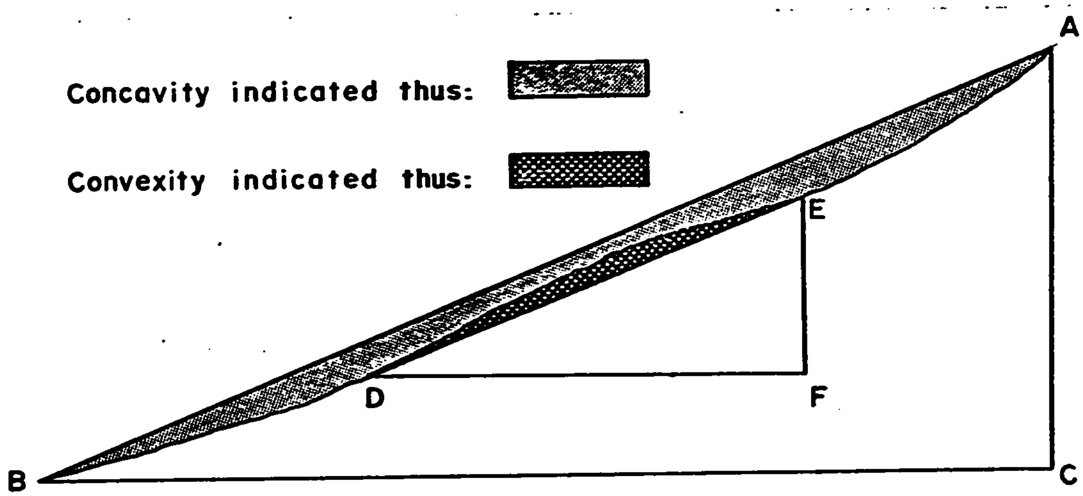

FIG. 6.7

AB is the straight line from the top to the base of the talus cone. The slope profile does not intersect this line. Therefore the slope is generally concave and the degree of overall concavity is calculated by measuring the area between the curve and the straight line AB. To remove the varying effect of slope length on total concavity this area is divided by the area of the right angled triangle ABC, whose hypotenuse AB subtends the major concavity. The minor convex element is then defined, its area measured and divided by the area of triangle DEF, whose hypotenuse DE subtends the convexity. The values for the convex and concave elements are then summed and if the total deviation from perfect uniformity (i.e. from a value of 0) is less than .03 (an arbitrary figure) the slopes are defined as uniform or rectilinear. If the total departure exceeds .03, then the ratio of the sum of all the values for the convexities to that for the major concavity determines how the slope is defined (Table 6.7).

TABLE 6.7

CLASSIFICATION OF NON-UNIFORM SLOPE PROFILES

Description of profile	Ratio of areas of convex to concave segments (corrected for length of slope)
Concave	$>$ 0.125
Concave, minor convexity	0.1250 - 0.750
Concavity and convexity equal	0.750 - 1.250
Convex, minor concavity	1.250 - 8.750
Convex	$<$ 8.750

If the slope curve had crossed the line AB in Figure 6.7, the total convexities and concavities would have been examined for each major slope segment in turn and then summed for the whole slope. This would have given indices for total deviation from rectilinearity and the nature of this deviation would have been determined from convexity concavity ratios as before.

b) Analysis of the data

The overall mean slope angle for thirty-one talus cones in the two field areas is 27.0°. Individual values vary from 23.1° to 32.1°. When plotted on a histogram (Fig. 6.8a), the distribution is found to be bimodal. When the mean slope angles were divided into twenty-three observed on metasediments and eight observed on igneous intrusives, the two distributions become unimodel (Fig. 6.8b) and c), although that for the metasedimentary cones is positively skewed. The bimodality of the distribution in Figure 6.8 a) appears at first sight to be caused by the inclusion of mean angles from two groups of talus slopes developed in different lithologies. The histograms in Figure 6.8 prompted the testing of the hypothesis that talus slope angles below the igneous intrusives are steeper than those below the metasediments. A chi-square test was preferred to a Student's t test since one of the groups of data was not normally distributed.

The results indicated that there is a 0.2-0.3 probability that the observed differences between the groups can occur by chance. Therefore it is not possible to make the inference that the mean angles of talus slopes developed in metasediments differ from those of talus slopes in the intrusives.

Andrews (1961) has indicated from studies in northern England that considerable variation in angle below the angle of repose may occur on individual slopes. Therefore perhaps it would be more revealing if the steepest segments of the talus cone profiles were

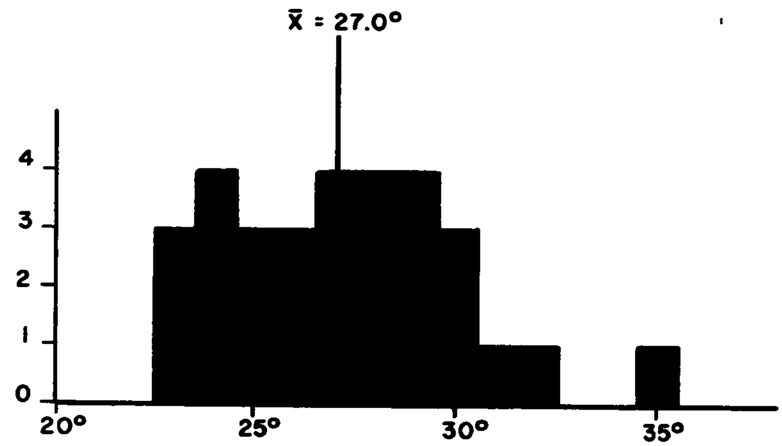

(a) All slopes.

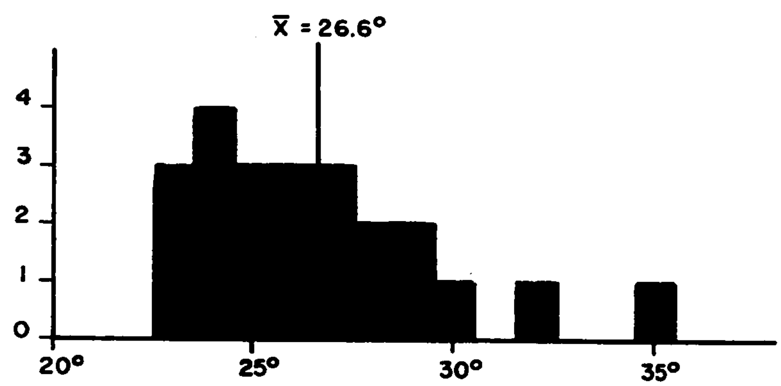

(b) Slopes in metasedimentary zone.

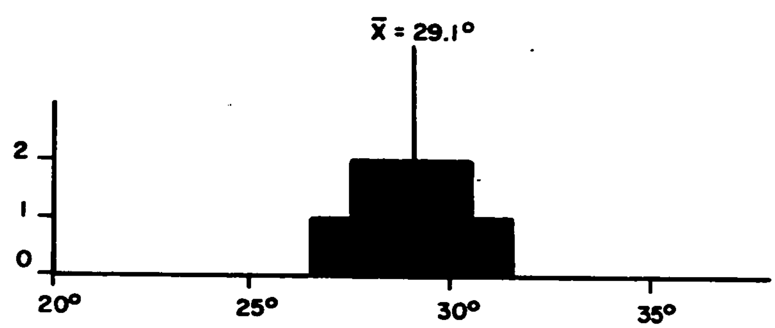

(c) Slopes in igneous intrusive zone.

FIG. 6.8 FREQUENCY DISTRIBUTIONS OF MEAN ANGLES OF TALUS SLOPES analysed instead of the mean slope angles. This is especially important, because the small amount of very large rocks, accumulated postglacially at the base, may have prevented the whole talus accumulation from achieving an angle entirely independent of the underlying bedrock profile.

The overall mean for the angles of the steepest segments of all thirty-one cones is 32.0^{o}. Individual values vary from 27^{o} to 38^{o}. The frequency distribution for the steepest segments is plotted in Figure 6.9 a). The data is very irregularly distributed and even when the metasedimentary and igneous intrusive groups are considered separately (Fig. 6.9 b) and c), the distributions do not become any more regular. A chi-square test indicates that there is a 0.3 to 0.5 probability that the steepest angles on the igneous intrusive talus slopes differ from those on the metasedimentary talus slopes by chance. Therefore the statistical evidence provides no proof of a significant difference in angles of talus cones in the two lithologies.

Because the mean slope angle of the laboratory built debris slopes increased as they grew in size until a certain limiting angle was reached, it was thought that differences in the angles of the talus slopes might be due to different degrees of debris build-up at the base of the slopes. But correlation of the length of the talus slopes along the fall-line with mean slope angles and the angles of the steepest segments revealed that no significant relationship exists between the length of the talus slopes (which expresses their size) and their steepness.

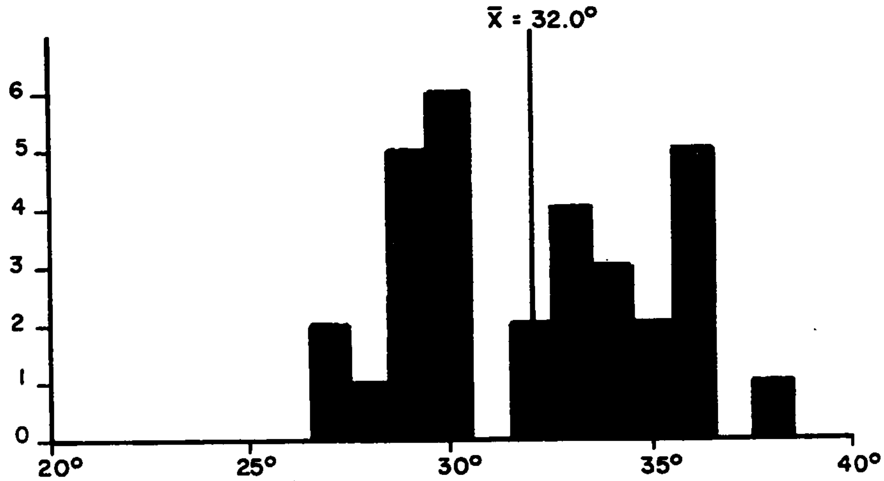

(a) All slopes.

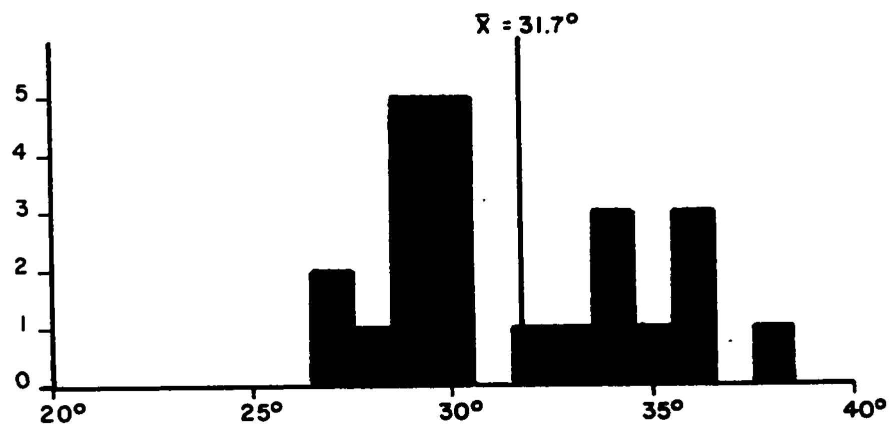

(b) Slopes in metasedimentary zone.

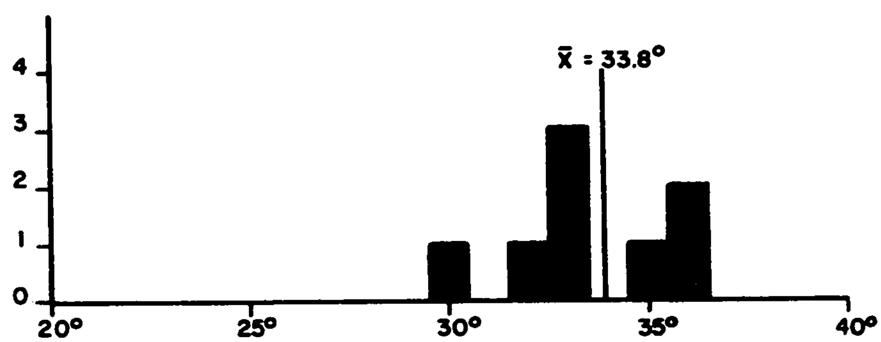

(c) Slopes in igneous intrusive zone.

FIG. 6.9 FREQUENCY DISTRIBUTIONS OF ANGLES OF STEEPEST SECTIONS ON TALUS SLOPES

The results of the analysis of talus cone profiles are presented in Table 6.8. The values for total deviation from uniformity (rectilinearity), the ratio of convexity to concavity, and appropriate verbal descriptions are given.

TABLE 6.8

FORM OF FALL LINE PROFILES OF TALUS CONES

Talus cone no.	Total deviation from uniformity	Convex./concav. ratio	Description of slope profile
6801	0.060	< 0.1250	concave
6804	0.131	"	"
6805[1]	0.061	"	"
6806	0.062	"	"
6807	0.035	"	"
6808[1]	0.037	"	"
6813	0.024	-	uniform
6814	0.000	-	"
6815	0.029	-	"
6816	0.057	< 0.1250	concave
6821	0.120	"	"
6822	0.063	"	"
6825[1]	0.050	"	"
6830	0.085	"	"
6836	0.103	"	"
6837	0.135	"	"
6838	0.101	"	"

1 The forms of these talus cones along with seven others not included in Table 5.7 are illustrated graphically in Figure 6.10.

Figure 6.10 shows a composite profile of the ten talus cones whose surficial debris was analysed statistically. They have been scale adjusted to be of equal lengths enabling a visual impression of the general nature of the slope profiles to be obtained.

Table 6.7 indicates that most of the talus cones in the field areas are concave in long profile, with no prominent convexities and that the remainder are uniform. Figure 6.10 indicates that the concavity of most of the cones is more strongly pronounced near the base than along the rest of the slope.

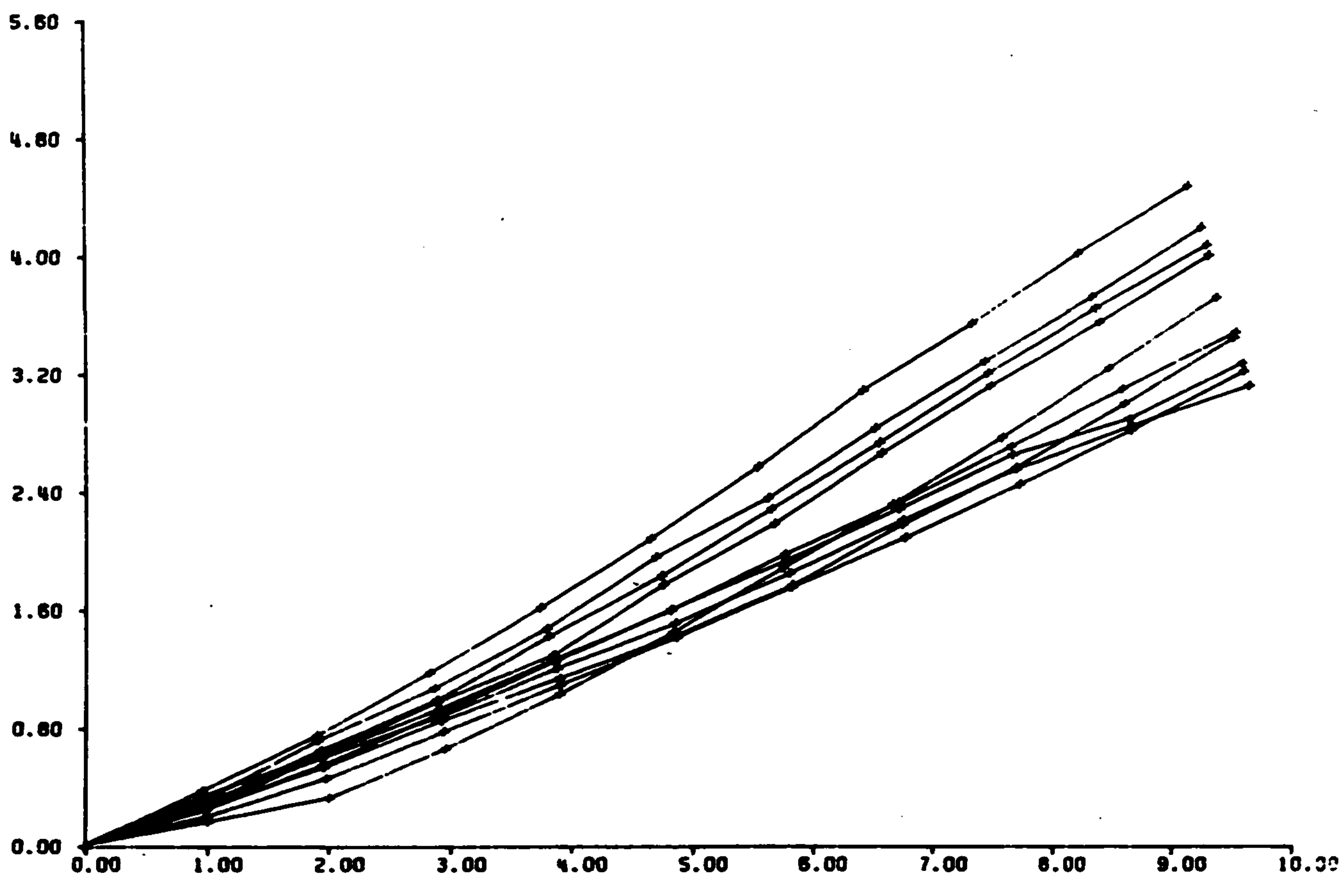

FIG. 6.10 LONG PROFILES ON TEN TALUS CONES

4. CONCLUSIONS ON THE IMPORTANCE OF THE ROCK-FALL PROCESS ON THE TALUS SLOPES.

It is appropriate at this stage to compare patterns of debris distribution and angles of slope for the theoretical and artificial rock-fall models with those observed on the talus slopes of the field areas. Differences between the models and the real world situation can then be attributed either to fundamentally different conditions controlling the rock-falls, or else to the operation of additional processes in the rock wall, talus slope environment.

The theoretical analysis of rock-fall suggested that the larger particles could be expected to travel further down the talus slopes than the smaller particles due mainly to slope roughness, which is induced at an early stage in talus build-up. This fall sorting pattern was substantiated in the laboratory model, on mine dump slopes and on the talus cones in the field areas. It is evident that rock-falls are a very important agency in the transfer of weathered debris to the lower slopes. The relatively large percentage of unexplained variance in the correlations between particle size and distance downslope suggests that several variables other than particle size, and processes other than rock-fall influence both the artificial slopes and the talus slopes.

The mean angles and the angles of the steepest segments of the talus slopes (Figs. 6.8 and 6.9), were compared with the slope angles for the mine dump slopes and the laboratory models, using χ^2 tests. The mean angles of the talus slopes, and the angles of their steepest segments, were found to be lower than the angles of the artificial slopes with less than .001 probability that the differences occur by chance. If all talus slopes are compared with all artificial slopes the average differences in mean angle and angle of steepest segment are 8° and 3°, respectively.

It was initially thought that this difference might have resulted from a contrast in the conditions controlling rock-fall on the talus slopes and on the artificial slopes. The much higher velocities possessed by particles arriving at the talus cone apices, as a result of the greater distance of fall, might have resulted in slopes achieving stability at lower angles than in the case of the artificial debris piles, where particles were dropped over the crest of the slopes with only slight initial velocity. If this is valid reasoning, then the particles falling down the steep igneous intrusive walls should accumulate as talus at lower angles than those falling down the more gently graded metasedimentary walls, since the downslope component of gravitational acceleration is less in the latter case. No significant difference between the talus slope angles below the two lithological groups was found, however. Therefore other reasons have to be sought to explain the reduction in talus slope angles as compared with the artificial slopes. Processes other than rock-fall which are operative on the talus slopes might be responsible agents. This possibility is considered in chapter 7 when all processes other than rock-fall are discussed.

Profiles of artificial slopes built of debris of mixed sizes were found to be rectilinear or slightly convex. The talus slopes are generally slightly concave throughout most of their length, and have a pronounced basal concavity.

The conspicuous basal concavity on the talus slopes may be explained in the following manner. The high initial velocity of falling particles tends to encourage the movement of large particles from high on the rock walls all the way downslope to the very low angle basal section of the concave bedrock slope where after a sufficient length of time a fringe of very large boulders accumulates. Smaller debris usually comes to rest above this basal fringe due to the initial effect of bedrock slope roughness and the subsequent effect of debris slope roughness. Only the very large boulders can travel all the way to the basal zone. These boulders do not comprise a large proportion of the total talus volume, due in part to their tendency to shatter as they fall. Furthermore, accumulation of debris has not proceeded for long enough during the relatively short postglacial period for large boulders to build up the basal fringe into a foot-slope entirely independent of the underlying low angle bedrock slope.

Therefore the basal debris slope still exhibits the low angle of the latter, and this results in a marked concavity by comparison with the rest of the debris slope. It is predicted that, as rockfall continues to build up the debris slope, the basal concavity will tend to be replaced by a wholly rectilinear slope, assuming of course that other processes do not complicate the model. The slight concavity of the upper parts of the talus slopes cannot be similarly explained and its relationship to other processes is examined in the next chapter.

CHAPTER 7

EROSIONAL MODIFICATION OF TALUS SLOPES

Geomorphic processes other than rock-fall that might influence the talus forms through redistribution of the surficial debris are:

1. Spring snow avalanches
2. Torrent avalanches
3. Ephemeral stream flow
4. Slow mass movement of debris, i.e. debris shift

1. SPRING SNOW AVALANCHES

Avalanches have been cited as important agents of debris redistribution on coarse debris slopes in New Zealand (Caine, 1969) and in Scandinavia (Rapp, 1959). Rapp in fact differentiated coarse debris slopes below rock walls into talus slopes or avalanche boulder tongues on the basis of whether rock-falls or avalanches are the dominant processes. Characteristics of these avalanche boulder tongues are their concavity, their relatively low angle as compared with talus cones, and debris tails below prominent boulders on the slopes. Debris tails suggested to Rapp (1959) that small areas of these slopes were protected from avalanche erosion by large boulders lying immediately upslope. They have also been noted by Gardner (1968) on slopes in the southern Canadian Rockies. Luckman (1971, p. 96) has noted the presence of avalanche derived debris superimposed on the surfaces of large boulders as the snow and ice in the avalanche deposits melted.

Caine (1969) developed a model which suggested that avalanches play an important role in the build-up of markedly concave debris slopes in a mountain environment. According to the model, avalanches redistribute debris from the tops to the lower parts of the talus slopes. Since the avalanches prevent the talus slopes from attaining steep angles, most of the rock-fall derived debris tends to accumulate near the apices of the talus cones to await later removal downslope by avalanches. Thus the slope angles never have an opportunity to build up to the angle of repose of debris slopes built by rockfall alone.

An exponential increase in the quantity of recently accreted debris towards the base of the slope was observed by Gardner (1968) for several talus slopes in the Lake Louise area and by Caine (1969), for talus slopes in New Zealand. Field evidence of this nature tends to support Caine's model of redistribution of debris by avalanches.

The evidence from the talus slopes in the Ogilvie and Wernecke Mountains, on the other hand, does not favour the redistribution of debris by avalanches from the top to the base of the slope. Avalanches have contributed to the build-up and modification of the talus slopes, but in a more limited way.

Many of the characteristic indications of avalanche activity found at the base of talus slopes in other mountain areas, e.g. debris tails, precariously perched boulders and fine debris on the top surface of large boulders, are conspicuously rare or absent in the basal zones of the forty talus cones examined in the Ogilvie and Wernecke Mountains.

The well developed lichen cover on the debris of the lowest one third to one fifth of ten sampled cones indicates that many of the boulders in the basal parts of the talus slopes must be very infrequently turned over or buried by freshly accreted debris(Fig. 7.1a).

The degree of lichen cover is somewhat underestimated in Figure 7.1 a) because of the inclusion of data from three dolomite cones on which lichen growth is inhibited for chemical reasons, and from three cones which debouch onto rock glaciers. Figure 7.1 b) divides the data on lichen cover into that observed on the seven normal cones (A) and that observed on the three cones ending in rock glaciers (B). The percentage of boulders covered with lichens in the basal third of group A averages between 40% and 70%. The percentage of boulders with lichen cover in the basal third of group B averages between 0% and 8%. This suggests that the rock glaciers may remove debris from the basal zones of the three talus cones in group B before they acquire an abundant lichen cover.

In order to assess the probable minimum recurrence period for such disturbance in the basal parts of the slopes, the sizes of the thalli of the largest five <u>Rhizocarpon geographicum spp</u> at each of 40 sample stations on the talus cones were averaged. Figure 7.2

(a)

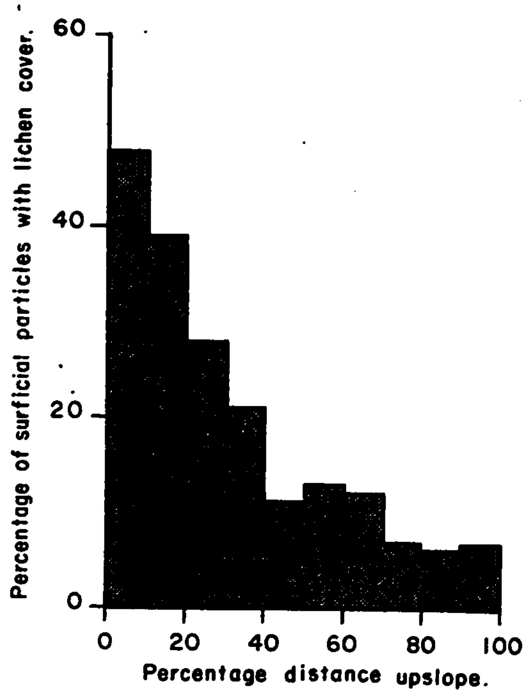

(b)

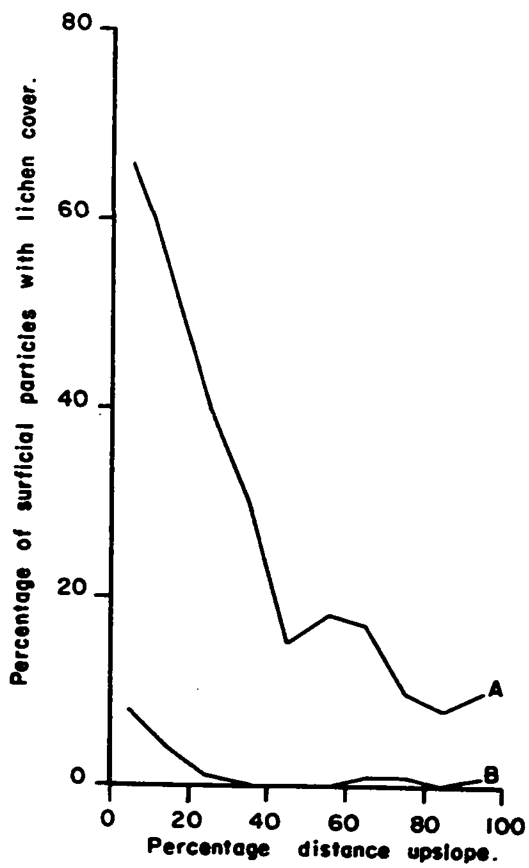

FIG. 7.1 PERCENTAGE LICHEN COVER ON TEN TALUS CONES PLOTTED AGAINST DISTANCE UPSLOPE

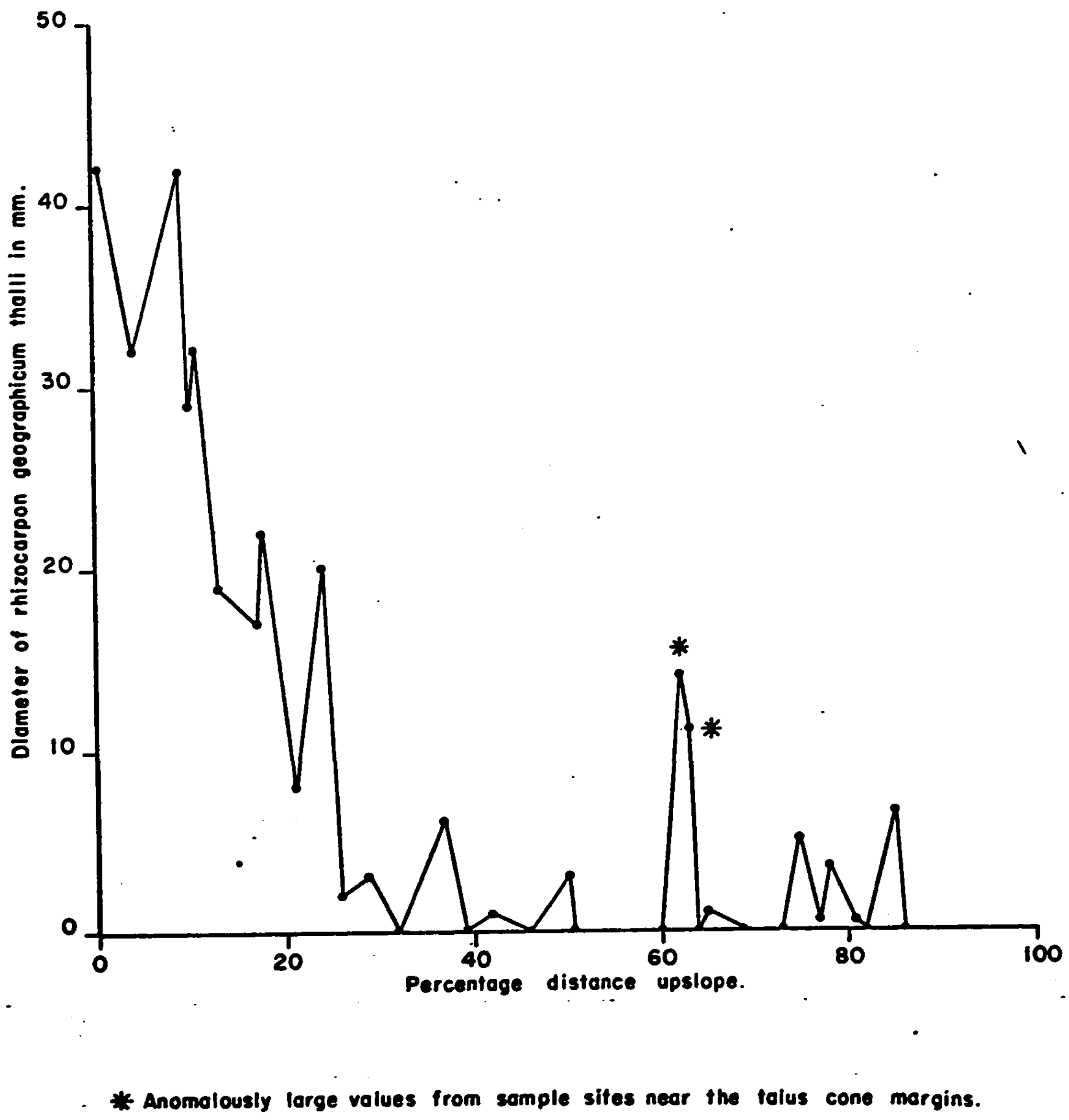

FIG. 7.2 MEANS OF LARGEST FIVE LICHENS OF *RHIZOCARPON GEOGRAPHICUM SPP* ON CONES 6824 PLOTTED AGAINST DISTANCE UPSLOPE

shows the plot of the mean of the largest five lichens at each of the sample stations against distance upslope for cone 6824.

The growth rate of 35 mm/100 yrs for Rhizocarpon geographicum spp, calculated in chapter 3 for the Klondike gold tailings, was then applied, as a maximum rate, to cones 6804, 6824 and 6825.

The minimum period since moderate disturbance of the debris on various parts of the talus slope was then computed. It varies from 63-85 years in the basal tenth of the talus cones to 15-25 years at one quarter of the distance up the talus cones.

The significant degree of fall sorting on four talus slopes examined in detail suggests that avalanches cannot be of sufficiently great importance in redistribution of debris to obliterate the pattern established as a result of rock-fall, since they tend to incorporate a mixture of coarse and fine particles in their passage downslope. Values for coefficients of correlation between particle size and distance downslope when the basal third of the talus cones is successively included and excluded are shown in Table 7.1. They reveal that fall sorting occurs in both cases. The correlation coefficients are reduced, however, when the data from the basal zone is excluded and this suggests that fall sorting is less well developed where avalanche redistribution is most frequent, i.e. in the upper two thirds of the talus cones.

TABLE 7.1

FALL SORTING ON LENGTH AND UPPER ZONE ONLY

	Correlation coefficients and level of significance, log 'b' axis and distance downslope for 40 sample station means.			
	whole cone		upper 7/10 of cone	
Cone 6812	0.85	(99)	0.55	99
Cone 6824	0.79	(99)	0.42	95
Cone 6830	0.68	99	0.25	not signif.
Cone 6831	0.89	99	0.70	99

Marked boulders near the base of five talus cones were accurately surveyed for movement in successive years. The lack of disturbance of these boulders indicated the probable negligible avalanche influence in the basal zone of these talus cones in the interval between the surveys.

All this indirect evidence is supported by direct observations of avalanches on the talus slopes in the Tombstone area in the spring of 1967 and in the Bear River area in the spring of 1968. Avalanches in the early spring occasionally extended to the base of the talus slopes but the surfaces of the talus slopes were still frozen and protected by a mantle of hard snow. In the late spring many avalanches occurred on partially snow free talus slopes but, with one exception, they were all observed to come to a halt in the upper two thirds of the talus cones.

Although avalanches are of slight significance in the basal sections, they are rather important in the upper two thirds of the talus slopes. Late spring avalanches are quite effective in picking up debris from the snow free talus surfaces (Plate 12). Displacement downslope of several of the marked boulders above the basal slopes of the talus by distances of 1 to 20 m (3-65 ft) over a two year period also suggests frequent redistribution of debris on the talus surfaces.

Lichens are sparse or non-existent on the rock surfaces in the upper two thirds of the talus slopes (Figure 7.1). This indicates frequent overturning of the boulders already on the surface, or else their frequent burial by debris arriving from higher on the talus slopes and from the rock wall. Rock-falls alone would not likely be able to prevent nearly all particles on the upper slopes from developing a lichen cover. It is probable that avalanches have been important in causing disturbance of all debris on the upper parts of the slope, except that very close to the lateral margins, at a recurrence interval of less than about five to fifteen years (assuming this to be a reasonable interval for colonisation by lichens, at least for foliose species).

Supportive evidence of the role of avalanches on the upper parts of the talus slopes is offered by the existence of large embedded boulders striated in a downslope direction by the repeated passage of debris laden avalanches, by the occurrence of lobate rims of very coarse debris on two of the talus slopes (Plate 22) and by some resemblances between a number of the talus slopes and the avalanche boulder tongues described by Rapp (1959).

The bull-dozed rims of coarse debris on the talus cones are rather rare indicators of avalanche erosion. The coarse debris was probably deposited initially by rock-fall, at the apices of talus slopes which are well below the angle of repose of falling particles. It then became available for incorporation in large late spring avalanches, and was probably bull-dozed downslope to form lobate rims in the terminal zone of these avalanches. On most of the slopes avalanches operate frequently but on a lesser scale. They prevent any really large build-up of rock-fall debris near the apices of the cones but they cannot erode the talus to any great depth, since the active layer on the latter is only a few centimetres thick during the period of avalanche activity.

A number of talus slopes in the metasedimentary zone resemble in some ways the avalanche boulder tongues of the 'road-bed' type (Rapp, 1959). They consist of embankments whose side slopes lie at angles of 30° - 36° and whose crestal slope lies at 25° - 30°. Figure 7.3 illustrates the form three dimensionally.

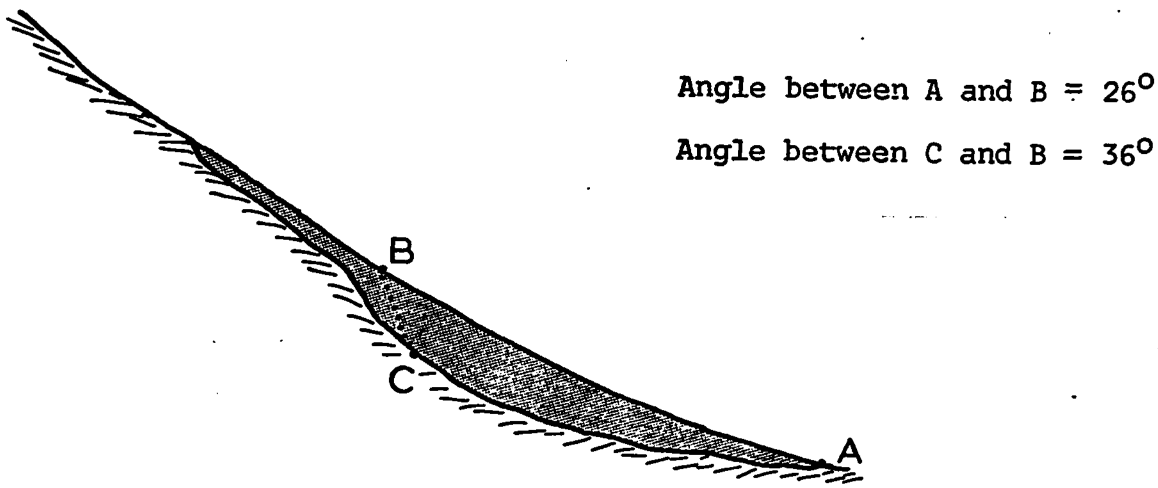

FIG. 7.3 SIDE VIEW OF CONE 6825

The side slope BC, which is developed by rock-fall from the crest of the talus slopes, is much steeper than the crestal slope AB, which is modified by frequent avalanche erosion.

The reduction in the angle of talus slopes and their overall concavity has been attributed by several writers to avalanche erosion (Rapp, 1959; Caine, 1969; Gardner, 1968; Luckman, 1971). In the Ogilvie and Wernecke Mountains the avalanches are probably of great importance in reducing talus angles in the upper part of the talus cones, but the pronounced basal concavities were explained in chapter 6 by factors other than the redistributive role of avalanches. A hypothetical model is presented in Figure 7.4 to illustrate the degree of probable avalanche modification of talus slopes. Avalanches

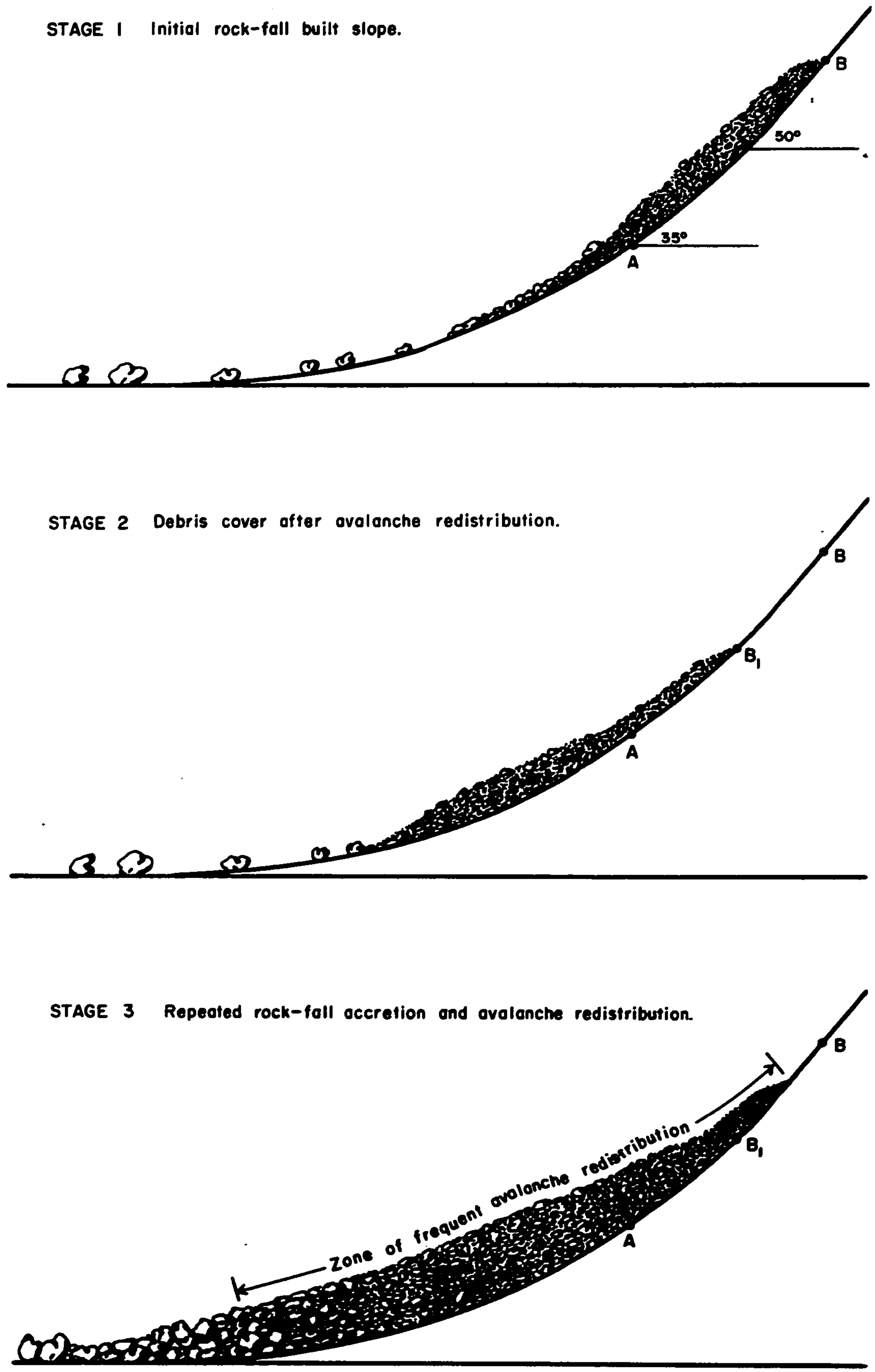

FIG. 7.4 HYPOTHETICAL MODEL OF EROSIONAL MODIFICATION OF TALUS SLOPES

and rock-falls are undoubtedly concurrent processes in the build-up of the talus slopes, but, for the sake of clarity, an initial debris slope is assumed to be built by rock-fall alone on a concave bedrock slope (stage 1 in Fig. 7.4). Avalanche redistribution is then assumed to modify the slope as shown in stage 2. The present stage of development of the talus slopes in the field areas is indicated in stage 3.

In stage 1 the small total quantity of large debris near the base of the slope means that the debris slope surface maintains the basal concavity of the bedrock slope for a long interval. Rock-fall build-up commences at A and proceeds both downslope and upslope from that point depending on the size of debris reaching the slope. Due to retardational effects of surface roughness, and the fact that most of the rock-fall volume is in the small boulder rather than the large boulder range, a greater quantity of debris tends to accumulate between A and B than elsewhere on the slope. Eventually this results in over-steepening of the debris slope which ought to result in small debris slides. Instead of readjustment by small debris slides, for which no evidence is visible, it is suggested that frequent redistribution of debris by avalanches and rock-fall impact prevents oversteepening of the slopes. In stage 2 the exaggerated effects of avalanche redistribution are indicated. The basal concavity is still evident and now an upper concave segment has developed, as a result of avalanche redistribution. Continuing rock-falls maintain the fall sorting pattern but avalanche disruption tends to reduce the correlation between distance upslope and particle size. In stage 3 the talus cone has built up to the point where the basal concavity inherited from the bedrock slope is restricted to a small fringe zone. Above this is a zone of frequent rock-fall accretion and avalanche redistribution where a slightly concave slopes is maintained at an angle of about 30°.

Spring snow avalanches occur much more frequently on slopes in the metasedimentary zone than on slopes in the zone of igneous intrusives. The main reason for this is that the steep, smooth walls of the Tombstone intrusion do not encourage the accumulation of great quantities of avalanche prone snow, and when the snow does avalanche it tends to fall in curtains rather than being channelled down the few chimneys and narrow gullies that exist above the talus slopes. Furthermore, by the time the talus slopes have become snow free and potentially susceptible to avalanche erosion, the snow on the steep rock walls lingers only in narrow hard beds in the chimneys and does not avalanche.

2. TORRENT AVALANCHES

Torrent avalanches consist of a mixture of snow, ice and meltwater which flow down rock wall gullies during the spring melt. Occasionally, late in the melt season, they flow onto snow free talus cones, and they may erode narrow channels near the apices of these cones. If they pick up large quantities of talus debris they continue in their progress downslope as debris flows. Eventually the debris is deposited in the form of frontal tongues and lateral levées.

In the field areas, the debris flows appear to have been of much greater significance on one moderately inclined slope, mantled with deeply frost weathered syenites and monzonites, on the north side of Tombstone valley, than on any of the forty talus slopes studied in detail. Only three of the latter display evidence of debris flows. A relatively large erosional channel, ending in a frontal tongue with several small distributary lobes, was observed on cone 6801. Small channels and levées were noted near the apices of cones 6826 and 6827.

Many talus cones, which are developed below rock walls of gentler gradient and lower elevation than those studied in detail, displayed channels and large terminal lobes. This evidence suggests that debris flows are of some importance below low angle rock walls in the field areas (e.g. Plate 6, Locality BL6). Furthermore, the partly vegetated surfaces of the talus cones below these low angle rock walls indicates that large avalanches and rock-falls are not of frequent occurrence on these slopes, and may have less geomorphic significance at the present day than the debris flows resultant from torrent avalanches.

3. EPHEMERAL STREAM FLOW

During the melt season every year, tiny streams run from patches of snow in the gullies onto the apices of the talus cones. These streams quickly disappear into the talus debris and their re-emergence at the base of the talus slopes can only rarely be traced.

Usually these streams flow for the first two or three weeks of summer only, and then they dry up as the snow patches in the gullies melt.

Streams do not play an important role in the transfer of talus debris downslope. The rounding and surface smoothness of the talus particles and stream gravels are in marked contrast. The talus particles are angular and rough surfaced, with few exceptions, whereas stream gravels tend to be somewhat rounded and smoothed as a result of impact and abrasive action associated with fluvial transport. There are no forms typical of regular fluvial erosion or deposition on the talus slopes. Also, in the rare instances where streams could be observed emerging from the base of talus slopes onto low angle protalus slopes, alluvial fans and cones were not present.

Whilst ephemeral run-off does not normally have a significant effect on the talus slopes, occasional violent summer storms may have resulted in a few of the debris flows, although the process responsible for most of them is probably torrent avalanches.

4. SLOW MASS MOVEMENT

Frontal bulges have been observed on several talus cones in the metasedimentaries of the Bear River valley. These bulges may be the initial stage in the development of protalus rock glaciers. They indicate some displacement of talus debris by processes of slow mass movement, variously referred to by Sharpe (1934) and Rapp (1960 b) as talus creep, by Gardner (1969) as talus shift, and in thesis as slow debris shift.

Slow debris shift on talus slopes in some arctic areas is very slight or non-existent (Rudberg, 1963; King, 1969). Nevertheless, its possible significance in the development of protalus rock glaciers in the field areas suggested that it should be evaluated quantitatively. Therefore, embedded and surficial boulders were marked and surveyed in 1967 on five talus cones contributing debris to rock glaciers, and on five talus cones without basal rock glacier development. Resurvey of all the marked boulders in 1968 and of those on one talus cone in 1969 indicated movement of some of the embedded and surficial boulders several centimetres downslope, but the maximum possible measurement error involved suggests that definite conclusions on the importance of processes resulting in slow mass movement must await resurvey after an interval of a few more years.

CHAPTER 8

THE DISTRIBUTION AND NATURE OF ROCK GLACIERS BELOW THE TALUS SLOPES.

1. INTRODUCTION

a) Classification of forms

Rock glaciers occur below many of the talus slopes in the southern Ogilvie and Wernecke Mountains. They appear to be the end products of coarse debris transport from the rock walls, by way of the talus slopes, to the valley floors. Vernon and Hughes (1966) have mapped the majority and sub-divided them on the basis of surficial characteristics, and on the basis of occasionally observed exposures of ice, into debris-covered glaciers and "true" rock glaciers. The former consist mainly of banded glacial ice veneered with 0.15-3 m (0.5-10 ft) of debris, whereas the latter are masses of debris, which contain ice interstitially or in the form of relatively minor lenses. The latter were grouped by Vernon and Hughes (1966, p. 17) into the three categories of tongue shaped, lobate and spatulate rock glaciers, according to a morphological classification first used by Wahrhaftig and Cox (1959).

Outcalt and Benedict (1965) sub-divided rock glaciers in the Colorado Front Range into cirque-floor rock glaciers and valley-wall rock glaciers. Analysis of air photographs indicated that the great majority of all rock glaciers in the Ogilvie and Wernecke Mountains can be classified as cirque-floor or valley-wall rock glaciers whether they are ice cored or debris cored. In plan view most of the cirque-floor and valley-wall rock glaciers conform to Wahraftig and Cox's tongue shaped rock glaciers and lobate rock glaciers, respectively. Spatulate rock glaciers were rarely observed in the Bear River and Tombstone field areas and are in any case a special form of either cirque-floor rock glaciers or valley-wall rock glaciers, caused by the lateral spreading of a rock glacier after passing over a bedrock bench.

This initial classification, based on morphology and topographic position, is preferable to one based on the presence or absence of an ice core, since the latter must usually be inferred indirectly. A minor number of the forms studied were difficult to categorise however. Some are multiple forms due to either the amalgamation of tongue shaped rock glaciers originating at the heads of cirques with lobate rock glaciers lining the lateral walls, or occasionally due to the overriding of older rock glaciers by younger ones (see Vernon and Hughes, 1966, Plate 1). Others are lobate forms which line the headwalls of a number of cirques and have been classified as valley-wall rock glaciers rather than cirque-floor rock glaciers since they consist of a series of bulges generally related to individual talus cones.

The following dimensional limits were observed during air photograph interpretation of the characteristics of twenty-eight rock glaciers in the Bear River field area. Eighteen valley-wall rock glaciers vary from 50 to 350 m (160-1,150 ft) in length, with a mean of 225 m (725 ft), and from 100 to 900 m (325-3,000 ft) in width, with a mean of 270 m (900 ft). Ten cirque-floor rock glaciers vary from 150 to 1,300 m (500-4,300 ft) in length with a mean of 650 m (2,100 ft), and from 75 to 300 m (250-1,000 ft) in width, with a mean of 200 m (650 ft).

b) The rock glaciers of the Ogilvie and Wernecke Mountains in a continental setting.

The presence of rock glaciers in the Western Cordillera of North America is clearly a response to climatic conditions (Thompson, 1962). Most rock glaciers occur in mountain areas which receive a moderate or small quantity of winter snowfall, insufficient to cause the development of large ice fields and glaciers. These mountain areas must also be sufficiently high, in latitude or altitude, for the moisture from the snowmelt and the summer precipitation to penetrate coarse debris accumulations and become permanently frozen, thereby inducing mass flow of the debris.

The following distribution was noted by Thompson (1962, p. 218):

> "In moutains facing the Pacific in North America, rock glaciers seem to be absent, except on the Alaska Peninsula near the northern limit of the prevailing west winds in winter, and perhaps near the southern limit of the dominant west wind in the Sierras. In the alpine zone of the interior Cordillera, from the Brooks Range to southern Colorado and including the less glaciated parts of the Wrangell and Alaska Ranges, which are sheltered by the Chugach, they are apparently numerous, except possibly in a zone of southern interior British Columbia and south-western Alberta which has heavy snowfall and many glaciers".

The Ogilvie and Wernecke Mountains, in the alpine zone of the interior Cordillera, are within Thompson's zone of numerous rock glaciers, and are characterised by only a few small ice glaciers.

Vernon and Hughes (1966, p. 17) have noted that rock glaciers are far more frequent in the Wernecke Mountains than in the Ogilvie Mountains. To test this statistically, the density of rock glaciers was calculated for an area of 1,000 km^2 (400 mi^2) in the Tombstone area and for an identical area in the Bear River area (Table 8.1).

TABLE 8.1

DENSITY OF DISTRIBUTION OF ROCK GLACIERS IN THE FIELD AREAS

	No. of rock glaciers in 1,000 km^2 area	Density per km^2	Mean elevation of area (m)
Tombstone	24	0.024	1,520
Bear River	187	0.187	1,455

Rock glaciers are evidently more abundant in the Bear River area than in the Tombstone area. Approximate mean elevations in the two areas, calculated from two groups of 100 randomly chosen spot elevations for each area, indicate that the increase in frequency of rock glaciers is not related to an increase in altitude. The Bear River area has, in fact, a lower mean elevation than the Tombstone area.

2. FIELD WORK

Field studies were designed to evaluate the regional distribution of the rock glaciers, the probable role of ice in their growth, their postglacial and present development, and their relationship to the talus cones and rock walls from which they were derived. The following programme was carried out in the two field areas.

a) Bear River area

Rock glaciers B1 - B28 are located in the valley of the Bear River South Fork and its western tributaries. Their fundamental type, dimensions, orientation, altitude, lithology and surficial characteristics were examined from air photographs, supplemented by detailed ground work on B1, B9, B14, B15, B18 and B20. Long term studies of motion were commenced on B14 and B18. Results are available for a two year period on B14. Detailed examination of permafrost levels and ice content was made on B20. Rock glaciers B29-B64 are located further to the south, in the basin of the southward flowing McClusky Creek. Their orientation was examined to correct for a possible northward bias in the orientation of the rock glaciers in the valley of the northerly flowing Bear River South Fork. Most of the rock glaciers studied in the Bear River valley are located in Plate 6.

b) Tombstone area

Rock glaciers T1 - T3 are cirque-floor rock glaciers in the syenite zone. Their surficial features were examined on the ground.

Long term studies of motion were commenced on T1 and some results are available for a two year period. Direct evidence concerning ice content was drawn from T2 and T3. T4 and T8 are valley-wall rock glaciers in metasediments whose surficial features were examined on the ground. Rock glaciers T1 - T4 are located in Map 3.

3. REGIONAL DISTRIBUTION OF ROCK GLACIERS

Some distinct relationships between lithology and rock glacier development have been noted in the Alaska Range, (Wahrhaftig and Cox, 1959, p. 415 ; Foster and Holmes, 1965). According to these authors rock glaciers in the Alaska Range consist mainly of coarse blocky fragments resulting from the weathering of granites, greenstone, prophyry, conglomerates and gabbro. They are rare in zones of argillites, slates, phyllites and schists whose weathering products are generally platy and of finer texture. Wahrahftig and Cox considered that the talus composed of the latter rock types moved downslope by solifluction but that in talus composed of the blocky weathering rocks the large voids encouraged the growth of considerable quantities of interstitial ice which caused the development of rock glaciers by semi-viscous flow.

Porter (1966) has noted a striking relationship between two cirque-floor rock glaciers in the Anaktuvuk district of the central Brooks Range, Alaska and the occurrence of brecciation along fault zones. Neighbouring cirques, alike in lithology, orientation, altitude, but without fault traces on the cirque headwalls, do not possess rock glaciers. It is implied that rapid erosion during the postglacial period has caused the accumulation of large quantities of debris in the valley floors which in due course become rock glaciers.

In order to determine if there is a significant structural and lithologic influence in their development, the distribution of rock glaciers in the Ogilvie and Wernecke Mountains was examined in some detail.

In the Bear River area, one valley wall rock glacier (B20) is much larger in proportion to the area of its source wall, than neighbouring valley wall rock glaciers (B21 and B22) with a similar elevation and aspect. It may reflect the influence of brecciation along a dolomite quartzite contact on the rock wall source area. Breccia is indeed a major constituent of the debris in the rock glaciers.

Other than this example, the valley wall and cirque-floor rock glaciers in the region have no obvious relationship to zones of structural weakness. Indeed even on bedrock of differing lithologies such as dolomites and quartzites (with minor slate) the rock glaciers occur with similar frequency. Neither debris characteristics, nor rates of supply from the rock walls differ much in these two rock types. They weather to form similar sized blocks on the talus slopes, and the postglacial erosion rates observed in chapter 2 for quartzite cones 6801, 6813, 6814 and 6816 and dolomite cones 6804 and 6808 are not sufficiently different to induce differential rock glacier development at the base of the talus cones.

In the Tombstone area, six cirque-floor rock glaciers were noted in the intrusives, but valley-wall rock glaciers are conspicuously absent due to the slow rate of postglacial erosion and the non-availability of large masses of pre-existing debris because of glacial erosion. Surficially, the three cirque-floor rock glaciers examined consist of relatively coarse blocks, whose long axis occasionally exceeds 10 m (33 ft) and averages about 0.5-1.5 m (1.5-5 ft). These blocks are separated by large voids. The majority of the cirques in the intrusion do not possess rock glaciers, however and it is probable that the cirque-floor rock glaciers which are present contain only a moderate volume of postglacially derived debris.

In the orthoquartzites of the Tombstone area cirque-floor rock glaciers and valley-wall rock glaciers occur but, for some unexplained reason, are relatively infrequent by comparison with those in a similar lithological zone in the Bear River area.

The slate and phyllite belt surrounding the quartzites is conspicuous for the total absence of rock glaciers. This accords well with extensive observations on the slates and phyllites of the Alaska Range, (Wahrhaftig and Cox, 1959).

Rock glaciers are very rare in the mountains to the north of the Tombstone area. On the Dawson map sheet, north and north west of the belt of orthoquartzites surrounding the intrusion, Vernon and Hughes (1966) have mapped only fourteen rock glaciers and debris covered glaciers. Cursory examination of the air photographs of the central Ogilvie Mountains and limited ground checking in the vicinity of the Dempster Highway between mile 78 and mile 102 failed to reveal any rock glaciers. This area is composed predominantly of limestones interbedded with shales, but local climate rather than lithology may account for the absence of rock glaciers, since the mountains to the north and west of the Tombstone area, on the Dawson and Ogilvie River map sheets, are of lower elevation. Their mountain summits rarely exceed 1,500-1,800 m (5,600-6,000 ft) as compared with 2,000-2,300 m (6,500-7,500 ft) for the Tombstone area.

Within the Tombstone-North Klondike area, certain rock glaciers appear to be related to fault zones or to zones where instability has resulted in rock slides. The valley-wall rock glaciers (T6 -T8 in Map 3) on the east side of the North Klondike valley at mile 30 are developed in close proximity to the North Fork thrust fault noted by Green and Roddick (1962) and Tempelman-Kluit (1970). The presently inactive rock glacier T5, at the North Klondike bridge at mile 42 has developed subsequent to a slide of quartzites along a failure plane in underlying phyllites. Rock glacier T4, in Landslide valley in the Tombstone area also developed subsequent to a large rock slide.

Thus, lithological reasons probably explain the general absence of rock glaciers below the fine weathering slates and phyllites surrounding the Tombstone area, and their presence only as cirque-floor rock glaciers below the slow weathering syenites of the intrusion itself. But the fact that many occur selectively within similar lithologies and the dimensional variations in rock glaciers, especially in the Bear River area, cannot be readily explained as yet. Detailed studies of the bedding and joint spacing and direction, minor shear zones and overall strength characteristics of the rock walls are definitely needed to solve these problems.

4. ROLE OF ICE IN ROCK GLACIER DEVELOPMENT

It is difficult and expensive to drill into rock glaciers, and so details of the internal structure and composition of only a few of these features have been studied so far, e.g. Brown (1925); Johnson (1969, pers. comm). In the present study indirect evidence such as orientation, topographic situation, shape, minor surface forms and hydrologic characteristics of rock glaciers were used to supplement the limited evidence on probable ice content offered by exposures.

Knowledge of the ice content is of great importance in establishing whether rock glaciers have originated as ice glaciers or through penetration of moisture into the interstices of the basal talus where it freezes and induces rock glacier development. The calculations of volumes of debris accumulated in rock glaciers and rates of rock-wall erosion represented by this debris, are also very dependent upon the ice content.

In the southern Ogilvie and Wernecke Mountains, Vernon and Hughes (1966) have observed exposures of ice in four cirque-floor rock glaciers. In one closely examined case they found 11 m (35 ft) of exposed ice. This ice contains parallel dirt bands, and is veneered by a few centimetres to more than 13 m (10 ft) of debris. In the present study large exposures of banded ice were noted in rock glaciers T2 and T3 in the Tombstone area. A large waterfall has been cut down to the ice level at the front of the latter.

Analysis of the orientation of sixty-four rock glaciers in the Wernecke Mountains from air photographs, and thirty-nine rock glaciers in the Tombstone area and surrounding mountain area from one of the surficial geology maps in Vernon and Hughes (1966), (see Map 3 in end pocket), indicates a strongly marked preference for northerly, northwesterly and northeasterly orientations. In the Tombstone area some possible bias exists since the structural dip is mainly towards the south. But no such bias exists in the data from the Wernecke Mountains which is plotted on a rose diagram in Figure 8.1.

Rock glaciers may therefore be associated with permafrost conditions, leading to increased interstitial ice content in the accumulated debris on north facing slopes. Alternatively they may be associated with the lingering of glaciers in north facing cirques since the last regional glaciation, or with their postglacial regeneration, these glaciers being subsequently buried with debris. Both of these climatic effects may be operative, the first being of greater importance in the case of the valley-wall rock glaciers and the second being of greater importance in the case of the cirque-floor rock glaciers. The lower altitudinal limit of approximately 1,400 m (4,500 ft) for presently active rock glaciers in the Ogilvie and

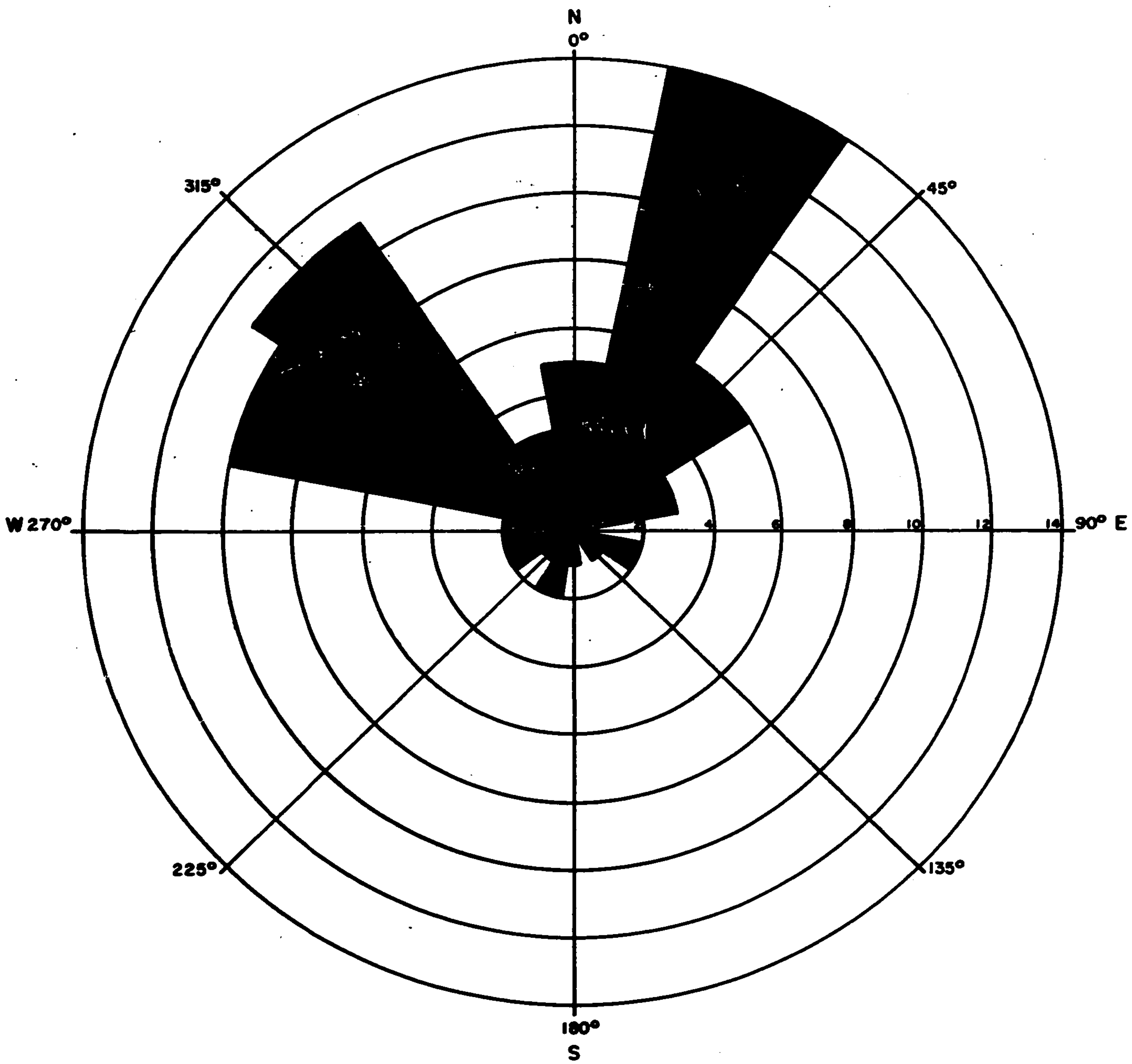

FIG. 8.1 ORIENTATION OF ROCK GLACIERS IN BEAR RIVER AND MCCLUSKY CREEK REGION, WERNECKE MOUNTAINS

Wernecke Mountains, lends support for the role of ice in rock glacier development.

If any of the cirque-floor rock glaciers are in reality ablation moraines on the surface of stagnant glaciers, then collapse pits, irregular assortments of fine and coarse debris and perched mounds of glacial debris isolated by downwasting of an ice surface (Plate 24) should occur over the surface. Furthermore concentrations of debris along the margins of the rock glaciers should reflect lateral moraines of the glacier surface. Wahrhaftig and Cox (1959) and Vernon and Hughes (1966) have described longitudinal furrows, meandering furrows, transverse ridges and occasional pits on cirque-floor rock glaciers. A large collapse pit on one rock glacier 16 km (10 mi) north east of the Bear River area was used by the latter authors to infer a 75% minimum ice content for the entire feature. Surficial phenomena such as these, were counted for the cirque-floor and valley-wall rock glaciers in the Bear River area and are summarised in Table 8.2. Ablation pits and mounds occur only infrequently and the tranverse and longitudinal ridges possess a certain rhythmic regularity which is not characteristic of ablation moraine ridges.

The following hypothesis is suggested for the cirque-floor rock glaciers which are ice cored. During slight moderation of glacial conditions, gullies and the upper parts of the zone of talus accumulation became uncovered for part of the summer and so debris reaching the ice surface by rock-falls and avalanches increased.

TABLE 8.2

SURFICIAL CHARACTERISTICS OF 28 ROCK GLACIERS

Characteristics	% of 10 cirque-floor rock glaciers with characteristics	% of 18 valley-wall rock glaciers with characteristics
Large snow beds at back of rock glaciers	100%	60%
Depression at back of rock glaciers	70%	45%
Collapse pits and average number on each rock glacier	90% (3.5)	85% (2.6)
Transverse ridges and average frequency in number/100 m	40% (5.2)	5% (2.6)
Longitudinal ridges and average width	80% (17 m)	70% (19 m)
Longitudinal ridges with origins in talus cones	60%	65%

As glacier flow continued the whole glacier eventually became debris covered. The debris cover was sufficiently thick to protect the underlying ice from the considerable differential melting which would have led to the production of collapse pits. Then aided by a permafrost regime the debris covered glacier was able to retain its ice core for a period of several hundreds, and perhaps several thousands of years.

Rock glacier (B15) is a good example of a rock glacier developed in this way (Plate 25). Along its margins are two ridges which are probably lateral moraines indicative of the maximum extent of the glacier. As climatic conditions moderated the glacier ablated slightly. The lateral moraines are only 8-15 m (25-50 ft) above the level of the rock glacier and so frontal recession was probably minimal. The rock wall at the back of the glacier started to feed debris onto the glacier at an increased rate and eventually, through continued glacier motion, the whole surface became debris covered. Small transverse ridges on the surface may be associated in some way with this glacial motion. At the present time, this rock glacier is vegetated, but cracks in the cover indicate some motion. No collapse features are apparent, and it is evident that the ice is very well protected from ablation by the vegetation and debris cover, and by the existence of a permafrost condition only 1-2 m (3-6 ft) below the surface, on a talus cone in the vicinity.

Whilst valley-wall rock glaciers generally have a northerly orientation there are more exceptions than in the case of cirque-floor glaciers. Surficial irregularities are less common than on cirque-floor rock glaciers. Nearly all the bulges in the fronts of the valley-wall rock glaciers occur in front of feeder talus cones suggesting that the supply of debris is of paramount importance to the form. When considered along with their topographic location on straight valley sides this evidence suggests that ice occurs as an interstitial component of the active valley-wall rock glaciers in the region, rather than as a massive core of glacier ice.

A rare opportunity to observe the internal characteristics of a well developed valley-wall rock glacier in the Bear River area (B20) was presented, when a violent rainstorm occurred on July 16th, 1969. Figure 8.2 is a sketch map showing the form and hydrologic characteristics of this rock glacier immediately after the rainstorm.

A springline was noted at point X, 9 m (29 ft) below the surface of the rock glacier and 17 m (55 ft) above the toe. A surface stream also emerged from the base of the rock glacier at point Y. The evidence suggests a permafrost level about 9 m (29 ft) below the rock glacier surface. Several depressions 1.5-3 m (5-10 ft) deep were noted on the rock glacier surface and the fact that none of these held water, even temporarily, is supportive evidence that ice was at a depth of greater than 3 m (10 ft) over the entire rock glacier. It also suggests that above the frozen zone the debris is of a calibre coarse enough to encourage rapid drainage. Within an hour after the storm, the rock glacier run-off carried by stream P returned to its normal flow.

A light snowfall, a few days later, gave an opportunity to confirm the existence of the springline. Plate 26 shows the front of the rock glacier when the snow had begun to melt. A very conspicuous and level snowline is noted 9 m (30 ft) below the rock glacier lip in the quartzites. It is terminated abruptly at the junction with the breccias. Below the snowline there is a completely snow free zone and then the snow mantle increases at the base. It is evident that the 9 m (20 ft) of debris above the springline retained its snow

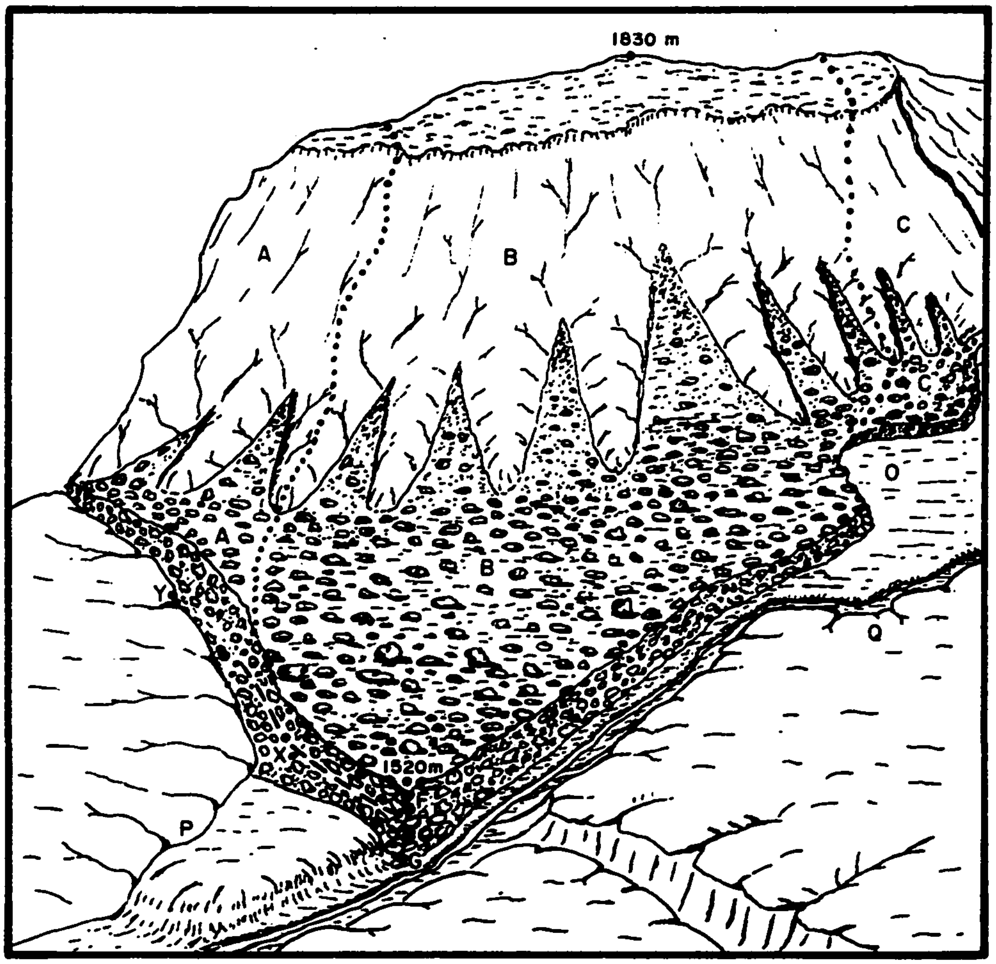

FIG. 8.2 ROCK GLACIER B20, WERNECKE MOUNTAINS

cover longer than the section below, because the latter suffered disturbance and melting, from the seepage of meltwater down the front below the springline. The increase in the snow mantle at the base is due to an accumulation of coarse boulders, through fall sorting at the front, which are not affected by the seepage of meltwater beneath them. The breccias do not have a clearly defined snowline, probably because, despite percolation of meltwater down the front, the surficial debris is coarser than in the case of the quartzites, and suffers less from disturbance due to seepage.

The topographic position of the rock glacier along a straight valley wall, the absence of collapse pits, meandering furrows and transverse ridges support the inference that the frozen zone of this rock glacier contains interstitial ice rather than an ice core.

In summary, a number of the cirque-floor rock glaciers are definitely ice cored whereas the valley-wall rock glaciers appear to contain only interstitial ice. Indeed, one valley-wall rock glacier B20 with a relatively high elevation of 1,600 m (5,200 ft) does not contain ice at all in the upper third of its thickness. One of the important indications that valley-wall rock glaciers have probably been characterised by interstitial ice during their development is that despite the very considerable altitudinal range of the features, from 1,200-1,900 m (4,000-6,000 ft), the lower ones do not show any more evidence of the expected ablation mounds and pits, associated with the melting out of an ice core, than do the higher ones. On the other hand differential melting of interstitial ice in rock glaciers at different altitudes need not result in great differences in their surficial appearance.

5. POSTGLACIAL DEVELOPMENT OF THE ROCK GLACIERS

1. Short term measurements

Paint marks on boulders on two cirque-floor rock glaciers and one valley-wall rock glacier were surveyed in 1967 with a Wild T2 theodolite, reading to one second. Theodolite stations were located, if possible, on bedrock or large stable boulders beside the rock glaciers. Several were necessarily located on moving points on the rock glaciers and their change in position has to be determined with respect to bedrock points. This change in position is then applied as a correction to the horizontal and vertical displacement of other moving points surveyed from the stations. A re-survey of the features was carried out in 1968. The horizontal and vertical scale of error varies from ± 2 cm for points surveyed from bedrock to ± 5 cm for points surveyed from theodolite stations on the moving points. Calculated movement for one year, however, was only of the order of a few centimetres. Therefore a second re-survey in 1969 was limited to one cirque-floor rock glacier (T1) and one valley-wall rock glacier (B14) and results presented from lines of points whose horizontal and vertical displacement error is known to be only ± 2 cm. These are transverse lines close to theodolite stations, located on large stable boulders off the edge of the rock glaciers.

Figure 8.3 a) represents the horizontal displacement of the points along the base of the front of rock glacier T1 in the Tombstone area over the period 1967-1968, 1968-1969 and 1967-1969. This is a cirque-floor rock glacier, about one mile long, which is advancing slowly into a small lake bounded at the far end by late or postglacial moraines. Maximum advances of 5.4 cm and 5.0 cm were observed for 1967-1968 and 1968-1969.

Figure 8.3 b) represents advances of embedded boulders at higher elevations in the front, varying between one third to two thirds of the depth from the surface to the base of the rock glacier. These varied from a minimum of 2.7 cm to a maximum of 14.3 cm for the two year period 1967-1969.

The mean advance along the basal line for the 1968-1969 period for seven values was 2.2 cm compared with 3.4 cm for six values on the higher line for the same period. This is an indication that the rate of movement decreases with depth as predicted by Wahrahftig and Cox (1959).

Movement values are small, but because there are no readings suggesting backward motion, and because the maximum possible error is ± 2 cm, it is suggested that they demonstrate movement exceeding the scale of errors involved.

A transverse profile of movement in the relatively steep (20°) middle section of rock glacier (B14) in the Bear River area is presented in Figure 8.4 for the periods 1967-1969, 1968-1969 and 1967-

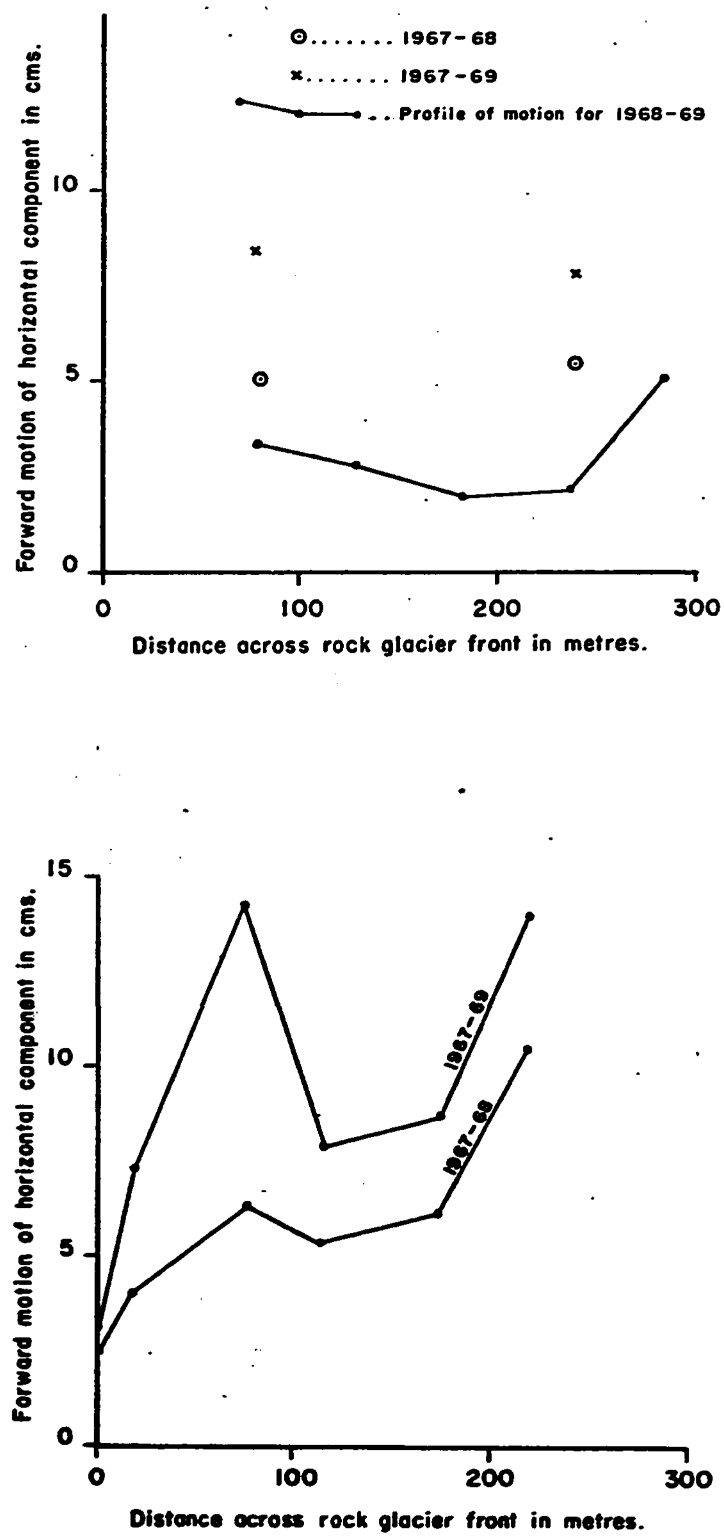

FIG. 8.3 RECENT RATES OF ADVANCE OF ROCK GLACIER T1, TOMBSTONE AREA

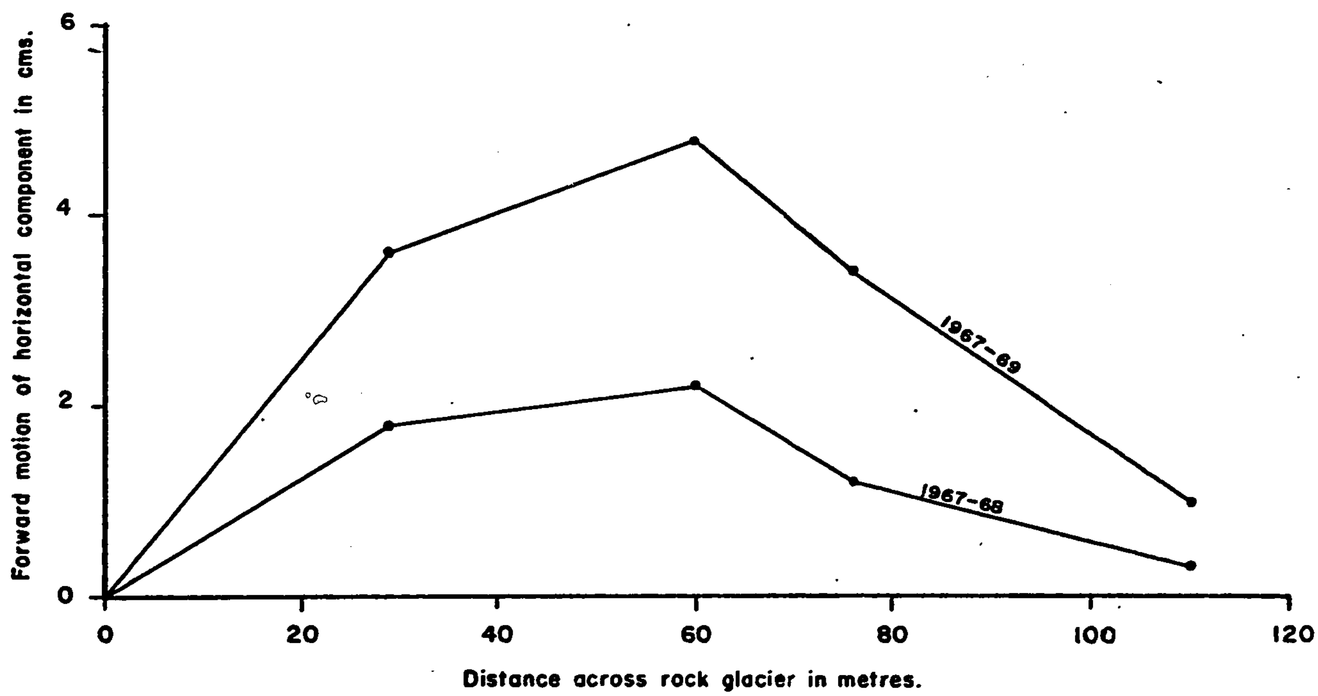

FIG. 8.4 TRANSVERSE PROFILES OF RECENT MOVEMENT ON ROCK GLACIER B14, BEAR RIVER AREA

1969. A maximum two year advance of 4.8 cm was noted. Reduction of rate of advance towards both edges due to frictional retardation is evident from the movement profiles.

Rock glacier B14 is a valley-wall rock glacier, but with its tongue shape it resembles a cirque-floor rock glacier. It descends from talus filled rock-wall gullies for 300 m (1,000 ft) at a moderately steep angle, varying from 15° to 20°, levels off briefly and then plunges down to the valley floor in a steep front about 90 m (300 ft) high. This long profile is related to lithological conditions in the vicinity. The rock wall above the transition from the talus zone to the gully zone consists mainly of quartzites (with a 15 m (50 ft) capping of dolomite). From the commencement of the rock glacier to its frontal zone, the bedrock consists of slates and phyllites whose relative erodibility has caused the enlargement and reduction of angle of a rock wall gully. The latter has since become occupied by a rock glacier supplied with debris from the quartzite zone above. Below the slate-phyllite zone, quartzite beds are repeated, and correspond with a steepening of the angle, which causes the rock glacier to tumble over an inferred bedrock ledge to the valley below. Plate 27 is a frontal view of the rock wall and the existence of similarly shaped rock glaciers can be noted at points A, B, C,D. In all cases the sharp transition from the top surface to the frontal surface corresponds with the transition from slate beds to underlying quartzite beds.

T1 and B14 were both considered to be among the most active rock glaciers of the Ogilvie and Wernecke Mountains. They do not possess collapse features, and their fronts sharply intersect their top surfaces. Rock glacier B14 is characterised by a sparse lichen cover, and by a sharp demarcation at its lateral margins, between rock glacier debris and locally derived felsenmeer. But their present rate of advance of only a few centimetres per year in a horizontal direction, (increased by a small proportion when converted to the component of forward movement in a direction parallel to the slope), suggests that most of the rock glaciers in the field areas may be very slow moving at present.

Indeed, the rates of recent movement have been so slow that analysis of their variations on different parts of the rock glacier surfaces will have to await resurvey after a time interval of at least five years.

ii) Long term measurements

A lichenometrical method was used to establish the maximum rates of surface movement of two rock glaciers over the last few hundred years. These rock glaciers are T1 in the Tombstone area and B18 in the Bear River area.

For the calculations, lichen growth rates were needed. The probable maximum and the absolute maximum growth rates for Rhizocarpon geographicum spp on the Klondike gold tailings were established as 35 mm and 41 mm per century. These were then extrapolated to the rock glacier sites with the proviso that true growth rates for the rock glacier environments are almost certainly lower. The diameters of the largest single lichen and those of the largest five lichens were measured on sample plots on the rock glaciers and minimum time intervals since the boulders had fresh non lichenous surfaces were thus established. If undisturbed growth of lichens took place as the boulders rode along on the rock glaciers, certain minimum periods were required for the movement of originally non lichenous debris from the zone of talus accretion to their present positions. By measuring the distances from the sample plots to the talus zone minimum rates of mass movement were calculated for each sample plot.

Apart from the problem of extrapolating lichen growth rates from the gold tailings to the rock glacier sites, there is the possibility of disturbance of the lichen growth by rock glacier motion. If disturbance by rock glacier motion destroys the lichens and subsequent regeneration takes place, then lichen thalli of a given size represent a longer period of development than suggested by the growth rate. This is a second important reason for using lichenometry on the rock glaciers only to establish a maximum rate of advance.

Results from rock glacier B18

Lichenometrical sampling across the surface of rock glacier B18 from the base of its feeder talus cones to its front revealed that the largest *Rhizocarpon geographicum spp* increase to a maximum size within 80 m (260 ft) of the talus base and thereafter remain large but irregularly variable towards the front (Fig. 8.5). Thus only the first 80 m (260 ft) can be feasibly used to determine possible rates of advance.

In Figure 8.5 a) the maximum lichen factor of 41 mm/century derived from the gold tailings is used in conjunction with the largest single lichen in each sample plot of 400 m^2 (4,200 ft^2) to compute rate 1. Rate 2 is computed by using the mean lichen factor of 35 mm/century in conjunction with the five largest lichens in each plot. The derived rates of 0.28 m/annum or 0.15 m/annum are probable maxima.

In order to check these calculations over a shorter and more recent period, rates 3 and 4 in Figure 8.6 were calculated by application of the maximum and mean lichen factors to the change in size of the largest thallus and the five largest thalli over the narrow strip 0-20 m (0-65 ft) from the talus base. These are 0.09 m/year and 0.33 m/year respectively and are also maxima.

It is therefore suggested that the maximum rate of advance for the last few decades for rock glacier B18 has been roughly similar to that for the last few hundred years, i.e. 10-30 cm/yr. This mass movement has been insufficient to cause much rupture of the surface material as indicated by observations of minimal disturbance of the component particles of large shattered blocks of dolomite on the rock glacier surface.

FIG. 8.5 LICHEN DIAMETER ON ROCK GLACIER B18 AND DISTANCE FROM TALUS SOURCES

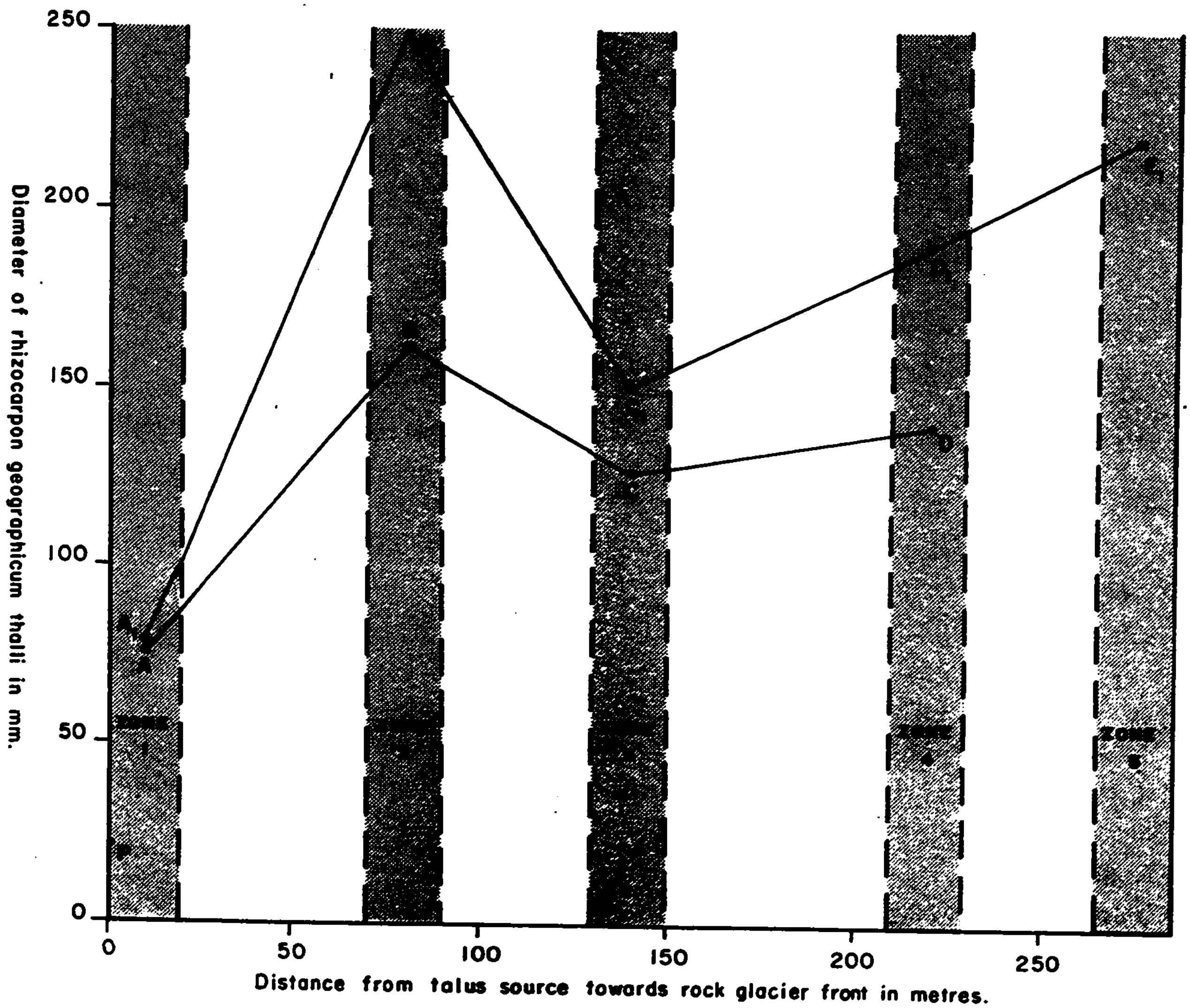

<u>Calculation of movement rate 1</u>

Increase in diam. of largest thallus of <u>Rhiz. geog. spp</u>, from A_1 to B_1	=	228 mm
Max. growth rate (rate 1 on gold tailings)	=	41 mm/century
∴ Min. time for 10 m advance from A_1 to B_1	=	550 yrs
∴ Movement rate 1 = 80/550	=	<u>0.14 m/yr</u>

<u>Calculation of movement rate 2</u>

Increase in diam. of mean of 5 largest thalli of <u>Rhiz. geog. spp</u>, from A to B	=	88 mm
Max. growth rate (rate 2 on gold tailings	=	35 mm/century
∴ Min. time for 10 m advance from A to B	=	250 yrs
∴ Movement rate 2 = 70/250	=	<u>0.28 m/yr</u>

FIG. 8.6 LICHEN DIAMETERS AND DISTANCE FROM NON-LICHENOUS TALUS SOURCE FOR ZONE 1 OF FIGURE 8.5

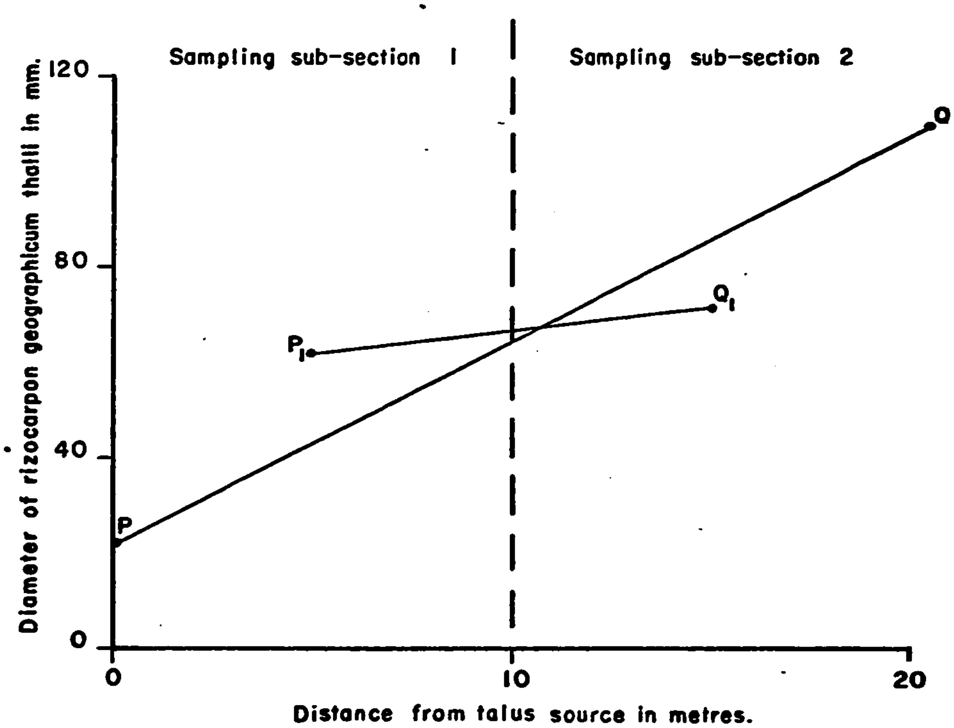

<u>Calculation of movement rate 3</u>

Increase in diam. of largest thallus of <u>Rhiz. geog. spp,</u> from P to Q	=	88 mm
Max. growth rate (rate 1 on gold tailings)	=	41 mm/century
.˙. Min. time for 10 m advance from P to Q	=	215 years
.˙. Max. rate of movement	=	0.09 m/yr

<u>Calculation of movement rate 4</u>

Increase in diam. of mean of 5 largest thalli of <u>Rhiz. geog. spp</u>, from P to Q	=	10 mm
Max. growth rate (rate 2 on gold tailings)	=	35 mm/century
.˙. Min. time for 10 m advance from P_1 to Q_1	=	30 years
.˙. Max. rate of movement	=	<u>0.33 m/yr</u>

The maximum rate of movement on rock glacier T1 in the Tombstone area was calculated for one sample plot as follows.

	Max. size of <u>Rhizocarpon geographicum spp</u> on boulders on rock glacier 150 m from source wall	= 170 mm
	Max. lichen growth rate	= 41 mm/100 yrs
∴	Min. age of boulders since incorporation into rock glacier as fresh rock-fall debris	= $\frac{170}{41}$ x 100 yrs
		= 400 yrs (app.)
and	Max. rate of advance of boulders from source wall	= 0.375 m/yr

This rate is two to three times the most rapid advance of a frontal boulder over the two year period 1967-1969.

iii) <u>Summary of results of movement studies</u>

The maximum rates of advance over the last few hundred years for two active rock glaciers in the field areas are 0.1-0.4 m/yr. The mean advance of the frontal zone of rock glacier T1 from 1967 to 1969 was 0.09 m and the mean advance of the middle zone of rock glacier B14 for the period 1967 to 1969 was 0.03 m. These rates of advance are much slower than the values of 0.48-0.72 m/yr quoted by Wahrhaftig and Cox (1959) for a rock glacier in the central Alaska Range, and the value of 2.0 m/yr quoted by Hughes (1966) for the Cantung rock glacier in south east Yukon. They are comparable, however, to values of .005 .007 and .010 m/yr quoted by White (1969) for three rock glaciers in the Colorado Front Range.

b) Age of the rock glaciers

During the last glaciation in the Bear River area, ice moved along most of the high tributary valleys containing valley-wall rock glaciers, as well as along the main Bear River valley. It must have removed or considerably deformed pre-existing rock glaciers. Well preserved striae on a bedrock rib crossing the head of one such valley in the Bear River area, (Plate 6, Locality BL2) testify to the passage of ice during the glaciation. Some of the rock glaciers near the upper surface of valley glaciers were probably only truncated, as a result of being submerged by only a thin ice cover. An example in the upper Bear River valley, has a steep front 18 m (60 ft) high and is only 50-100 m (160-325 ft) wide. The rocks in the front appear to be compacted as if they had previously been in the interior of a large deposit. It appears to be a form partially destroyed, rather than a form in the process of being built.

Advance of the valley-wall rock glaciers has taken place since truncation or removal by glacial ice. In several surfaces the rock glaciers have advanced to the centres of the valley floors and, in two cases, B18 and B20, right to the distal edge of the valley. The latter caused streams to be diverted from the valley centres to incised courses along the valley edge (Fig. 8.2 and Plate 28). The ice cored cirque-floor rock glaciers, are thought to be initially a product of the late stages of the last regional glaciation or subsequent re-advance within the cirque zone, with one or several phases of renewed activity in the debris covered state. The lichen cover on most of the rock glaciers of the cirque-floor and the valley-wall type suggests a minimum age of several hundreds of years for their development. A maximum long term rate of movement of 0.1-0.4 m per year for the last few hundred years was derived for two cirque-floor rock glaciers. This gives a maximum rate of movement for the rock glaciers for the period dating from the time of incorporation into the rock glaciers of boulders to the present time when they are 150 metres and 80 metres respectively from the source wall. To extrapolate this rate a further distance of several hundred metres to the present fronts and thereby assign a minimum age for the features is predicated on the intangible assumption that the rate of movement has remained constant throughout the entire period of development of the rock glaciers. Such an extrapolation through 300 m for rock glacier (T1) in the Tombstone area gives a suggested minimum age of 1,100-4,000 years B.P. For rock glacier B18 in the Bear River area the maximum long term rate of movement was calculated as 0.10 to 0.40 m/yr, and the distance from source wall to front is 320 m. Therefore B18 has a minimum calculated age of 800-3,000 years B.P.

The low rates of movement relative to some other areas in the Western Cordillera suggests that optimal conditions for rock glaciers development in the field areas may not exist at present. In one of the highest valley-wall rock glaciers permafrost is about 9 m (29 ft) below the surface. If interstitial ice content is indeed an important factor in the development of valley-wall rock glaciers they may be deficient in this respect at the present day.

6. ROCK GLACIERS AS INDICATORS OF ANOMALOUS RATES OF ROCK WALL EROSION.

The horizontally projected area of twenty-eight rock glaciers and their rock wall sources were measured from air photographs, and the ratios of rock wall to rock glacier area plotted on Figure 8.7. The equation of linear regression of the two variables suggests that the mean ratio of rock wall area to rock glacier area can be predicted as approximately 9:1. This mean ratio is much greater than that of 1.4:1 calculated by Wahrhaftig and Cox (1959) for forty rock glaciers by the same method, and suggests that the rock glaciers in the Ogilvie and Wernecke Mountains represent much lower erosion rates than those in the Alaska Range.

Despite the high ratio of the horizontally projected rock wall area to the rock glacier area in the Wernecke Mountains (and still higher ratio of actual rock wall area to rock glacier area), the valley-wall rock glaciers clearly represent more rapid postglacial rate of erosion than is represented by the talus cones.

Calculations in Appendix V reveal that an average of 4.1 m of rock were removed from the rock wall to form rock glacier B20. This represents a rate of erosion of 340 mm/1,000 yrs if averaged throughout the postglacial period. This rate is two times greater than the mean rate of erosion calculated for the most rapidly eroded rock wall above a talus cone and seven times higher than the median rate of erosion calculated for all ten rock walls above talus cones.

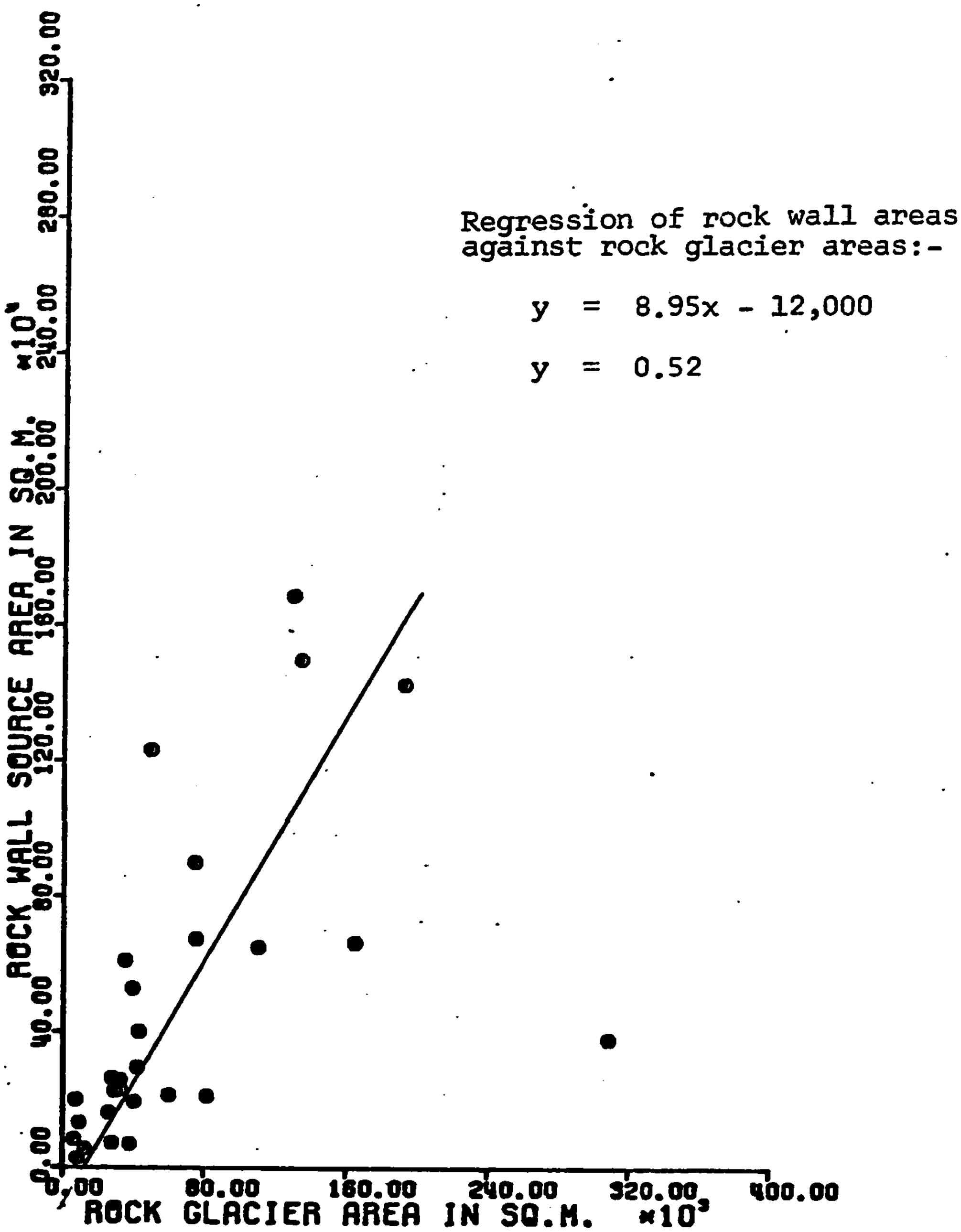

FIG. 8.7 ROCK GLACIER AREAS PLOTTED
AGAINST SOURCE WALL AREAS

CHAPTER 9

SUMMARY OF CONCLUSIONS

This thesis has examined the nature and rate of operation of the processes involved in the postglacial and present day transport of debris from mountain walls to valley floors in selected areas of the Ogilvie and Wernecke Mountains, central Yukon Territory. These areas were subjected to at least three episodes of glaciation, the later of which appears to have culminated 10,000 to 14,000 years B.P.

The processes have been considered as they acted on the rock walls, on the talus slopes and on protalus rock glaciers. These morphological zones proved to be an excellent unit for a study of debris transport, because they form a system that can be considered essentially closed within the relatively short postglacial period. It is reasonable to assume that valley glaciers removed most of the pre-existing debris from the lower slopes of the mountain walls, and that the present debris accumulations are derived postglacially from the steep upper slopes. At the other end of the system, comminution and removal of accumulated wastes has been found to be of insignificant importance during the postglacial interval. In effect, the postglacial products of rock wall erosion are the talus slopes and the rock glaciers at the foot of the rock walls.

The postglacial rate of removal of weathered bedrock from ten rock walls, was assessed in chapter 2 by measuring the quantities of debris accumulated in ten talus cones, and relating these values to the measured areas of the rock walls tributary to the talus cones. The median value for the mean thickness of rock removed from the rock walls during the postglacial period of 10,000 to 14,000 years lies between 0.636 and 0.510 m. The range of values is from a possible maximum of 3.88 m for the most rapidly eroded rock wall area to a possible minimum of 0.0651 m for the least rapidly eroded rock wall area. The median rate of erosion has been 43-53 mm/1,000 yrs. The largest possible range of values for the ten rock walls is from 388 mm/1,000 years to 5 mm/1,000 years.

In the igneous intrusives of the Tombstone area, the low ratio of talus height to rock wall height and the thin talus mantle indicate that the average rate of postglacial erosion on syenites and monzonites has been much less than in the metasediments of both the Tombstone and the Bear River areas. Quantitative studies tend to support this conclusion, although the fact that only two erosion rates were available from the igneous intrusives prevents it from being couched in mathematical probability terms. For two igneous intrusive rock walls a mean erosion rate of 19 mm/1,000 years was established. The corresponding mean rate for eight metasedimentary rock walls has been 73 mm/1,000 years.

An additional erosion rate of 313 mm/1,000 years was calculated in Appendix V for a rock wall, which has supplied sufficient debris to create a relatively large rock glacier in the postglacial period.

This rate is about seven times the median rate of erosion established above, but still represents only 3-4 m of bedrock removal during the postglacial period.

This is believed to be the largest and most detailed evidence on rock wall recession ever assembled from a mountain region. In view of the fact the mean rates of erosion agree to within an order of magnitude with those calculated by Rapp (1960a) for rock walls in limestones, cherts and sandstones in Spitsbergen, it can be firmly concluded that postglacial rock wall retreat in metasedimentary and in some sedimentary lithologies in the periglacial zone has not been nearly so rapid as used to be commonly believed.

The present effectiveness of processes transporting weathered debris from the rock walls to the talus slopes was studied directly by measuring debris accretion on the talus slopes over short time intervals, varying from one month to one year. The results of this work were presented in chapter 3.

Difficulties in comparing the rates of bedrock erosion represented by short term debris accretion on talus slopes with long term rates are noted. Still, there is some indication that the currently observed level of operation of geomorphic processes is insufficient to account for the postglacial talus accumulations. Medium and large scale erosional events, of more infrequent occurrence than those for which observations or measurements have been made in the field areas, may account for most of the postglacial transport of debris from the rock walls to the talus slopes.

The direct observations of individual processes of transport suggest that rock-falls and avalanches are the most significant processes of frequent occurrence. Small scale rock-falls associated both with the spring thaw and with summer rains occur quite frequently, and certainly form a considerable proportion of the annual debris accretion on the talus slopes. The only moderate to large scale rock-fall observed, during three summers' observations, took place on a large wall in the Tombstone intrusion (Plate 5, Locality TL5).

Spring snow avalanches are of much less significance to debris accretion. In the metasedimentary zone, where they occur on an almost annual basis, they are relatively debris free. They may have a significant role in removing some of the debris accumulated in the gully beds but certainly not on an annual basis. In the syenite zone, avalanching is of minor importance by comparison with rock-falls, the rock walls being too steep to permit the build-up of an avalanche prone snow cover.

Torrent avalanches, otherwise known as slush avalanches, have been of some significance in removing debris from moderately graded rock walls with many gullies. They have been especially effective in the removal of weathered bedrock from the north slope of the Tombstone valley, and in its deposition as colluvial debris tongues. But torrent avalanches have been of minor overall significance in adding debris to the talus slopes below the steeper rock walls of both the metasedimentary and igneous intrusive zones.

In chapters 4, 5, 6 and 7 the processes by which the talus slopes are erosionally modified received attention. Theoretical and artificial models of talus slopes were constructed and compared with the real talus slopes, in order to ascertain the probability that the latter were modified by processes other than rock-fall. The distribution of particle characteristics such as size, shape, lichen cover and lichen sizes, and of morphologic characteristics such as long profiles and gradients were used in this analysis.

Fall sorting on talus slopes has been documented in many alpine and arctic environments, and is a good indication of the importance of rock-fall on these slopes. The theoretical model of rock-fall developed in chapter 4 indicates that fall sorting on debris slopes is the natural result of rock-fall of mixed sizes from steep walls onto low angle basal bedrock slopes. For particle sizes and distance of fall similar to those encountered on rock walls and talus slopes the really significant factors in fall sorting are the original rock wall roughness and acquired roughness of the basal slopes as a debris mantle develops.

The artificial slopes at small and medium scales, and the talus slopes studied in the field areas displayed moderately well developed fall sorting. In a laboratory rock-fall model, fall sorting characterised the debris slope throughout build-up.

Other factors than particle size, e.g. particle shape, variation in distance of fall, shattering of particles, momentum transfer upon impact, have a significant influence in reducing the degree of fall sorting on the talus slopes.

Other processes than rock-fall have also been erosionally effective on the talus slopes and by redistributing debris on the slope may have affected the relationship between particle size and distance downslope. These processes include spring snow avalanches, torrent avalanches and slow debris shift.

The concavity of talus slopes in certain other high mountain zones has been attributed to the redistributive role of snow or torrent avalanches Gardner, (1968); Caine, (1969); Luckman (1971). Snow avalanches have undoubtedly redistributed debris on the upper parts of the talus surfaces in the Ogilvie and Wernecke Mountains, and have thereby reduced the overall talus slope angles. They have only slightly affected the basal areas of the talus slopes, however. A hypothetical model was presented in chapter 7, in order to illustrate the probable relative roles of rock-falls and avalanches in the development of the talus slopes. The marked basal concavity of the slopes is attributed to the pre-existing, concave bedrock slopes, and to the small number of boulders which remain large enough to reach the base of the talus slopes. Given a sufficiently long period of talus build-up before disturbance by glaciation, this basal concavity would be reduced and perhaps almost eliminated.

Debris flows resulting from torrent avalanches and/or violent rainstorms have caused erosional channels to be developed on the talus slopes, below relatively low angle, well dissected rock walls. These erosional channels are succeeded downslope by depositional forms, such as levées and tongues with distributary lobes. These forms are, however, only occasionally developed on the talus slopes below the high angle rock walls.

Slow mass movement of debris may have been of some importance on the talus slopes, particularly on those which feed onto rock glaciers. But conclusions on the present importance of slow debris shift on talus slopes must await the resurvey of marked boulders after a sufficient time interval has elapsed.

Most of the talus slopes are the end product of coarse debris transport down the steep mountain walls. In a number of instances, however, the talus has been transported relatively slowly as rock glaciers towards the valley centres. These rock glaciers may be classified after Outcalt and Benedict (1965) as cirque-floor rock glaciers and valley-wall rock glaciers. The selective occurrence of rock glaciers within apparently homogeneous lithologies and their variability in size were noted. Lithological reasons account for the absence of rock glaciers below the fine weathering shales and phyllites surrounding the Tombstone area, and their relative abundance in the blocky weathering quartzites and dolomites of the Bear River area. A few rock glaciers in the Tombstone-North Klondike area have developed from debris produced by rock slides along zones of structural and lithological weakness.

The reasons for the relative scarcity of rock glaciers in the orthoquartzites of the Tombstone area by comparison with the zone of quartzites and slates in the Bear River area are obscure, however. Furthermore it is not completely clear why a few of the cirques in the Tombstone intrusion have nurtured large cirque-floor rock glaciers when the rate of postglacial weathering of most of the syenite and monzonite rock walls is very slow.

The banded ice exposures observed at a few points in two of these rock glaciers may partially solve this problem, by indicating that the observed debris incorporated in these rock glaciers may merely veneer glacial ice bodies. Ice exposures suggesting an ice core were observed by Vernon and Hughes (1966) in three other cirque-floor rock glaciers in the Ogilvie and Wernecke Mountains. This direct evidence along with indirect morphologic evidence suggests that at least a moderate number of the cirque-floor rock glaciers are ice cored. By contrast, many of the valley-wall rock glaciers appear to contain ice only interstitially or in lenses.

Most of the valley-wall and cirque-floor rock glaciers in the field areas have originated subsequent to destruction or truncation by ice during the last regional glaciation. Lichenometric evidence for two of the active rock glaciers indicates that they did not originate in the last millenium.

Most of the rock glaciers in the field areas are advancing relatively slowly as compared with rock glaciers in certain other regions in western North America. The maximum rates of advance over the last few hundred years for two relatively active rock glaciers have been between 0.1 and 0.4 m/year. Advance of the front of one of these rock glaciers over the two year period, 1967-1969, is between 0.05 and 0.07 m/year, and of the middle zone of a third rock glacier, between 0.01 and 0.03 m/year.

In conclusion, a few comments on the practical potential of these studies may be made. Highways construction in mountainous regions has to cope with many problems due to the vigorous mass wasting that goes in these environments. The need for highway protection from rock-falls and avalanches is evident. Avalanche zones have been recognised and localised defences installed to protect highways, but rock-fall control appears to be at a less advanced stage, in some mountain regions at least.

The theoretical rock-falls model in this thesis is only an initial one and needs much elaboration, but it does point out many of the factors which govern the nature of rock-fall motion and the horizontal and vertical velocity components under various conditions. Nets for channelling rock-fall to the base of the slope by rolling or sliding motion, foot slope roughness, inclination and length, and rock-fall fences, can be designed to prevent falling rocks from reaching roads providing the dynamics of rock-fall are properly evaluated, using advanced theoretical models, suitably backed up by controlled experiments.

APPENDICES

APPENDIX I

DEFINITION OF TERMS FOR FORMS AND PROCESSES

1. LANDFORMS

Scarp slopes, slopes where the strata dip very steeply, or slopes steepened by cirque development, can be sub-divided into two major facets (Plate 1). These comprise an upper facet referred to as a rock wall and a second facet below this, referred to as a talus slope. In some cases a protalus rock glacier forms a third facet below the talus slope.

a) Rock walls

Rock walls in the field areas are usually at least three times as high as the talus slopes, and are inclined at mean angles between 35° and 90° according to the nature of the bedrock structure and lithology. In the syenites of the Tombstone area the average rock wall angles are 60° to 70° and several overhanging sections occur. In the metasediments the rock walls recline at angles of 35° to 45°.

The rock walls are dissected to varying degrees by gullies. When dissection is slight shallow grooves described as rock wall chutes (Markgren, 1964) are formed. These chutes are defined by Markgren (p.51) as, "usually narrow and shallow elongated gullies or scars often arranged in consequent series along the mountain walls". Chutes have also been identified and described by Matthes (1938) in the Sierra Nevada in California.

The gullies may deeply dissect the rock walls, however, and may have tortuous courses and interruptions due to rock steps. They may be joined by tributary gullies near the head of the rock wall giving a generally dendritic topographic pattern in plan view.

On rock walls consisting of strata of varying resistance many gullies consist of large amphitheatre shaped hollows alternating with narrow gorge sections. These have been described by Rapp (1960a, p. 4) as rock-fall funnels.

Markgren (p. 142) attributes some variations in gully form to structural control e.g. he notes the complete lack of chutes in places where the slopes parallel steeply dipping cleavage or bedding planes.

The rock walls in the Ogilvie and Wernecke Mountains are scarred with gullies both of the chute form and of the funnel form. Chutes tend to occur more frequently on the steep dip slopes of meta-sedimentary rock walls characterised by lithological homogeneity and on occasional slopes within the Tombstone intrusion where the jointing pattern has given relatively low angle slopes (i.e. between 30^{o} and 50^{o}), and where the lithology is also fairly homogenous over the whole area of the rock wall. The funnel form predominates on scarp slopes in the metasediments where thick dolomite and quartzite beds alternate with less resistant slates phyllites and thin bedded dolomites. Igneous intrusive walls whose slope angles exceed 50^{o} are not seamed with chutes, but isolated vertical or sub-vertical joints have been widened and deepened to form narrow gullies deeply inset in the rock wall. Most of these are better termed rock chimneys.

Despite the obvious topographic variety all gully forms will henceforth be known in this thesis as rock wall gullies. Differentiation is not very important in this study since the rock walls could not be examined in detail in this study.

b) Talus slopes

One of the earliest descriptions of talus slopes, known also as taluses, and as scree slopes, was that of Lyell, (in Glossary of Geology and Related Sciences, 1960, p. 291)

> "when fragments are broken off by the action of the weather from the face of a steep rock, as they accumulate at its foot they form a sloping heap, called a talus".

Not all colluvial debris slopes, whose component materials have been derived by processes of weathering and transportation from the rock wall zone above, may be described as talus slopes, however.

Rock slides may be the source of colluvial debris, but such instantaneous accumulations are clearly not included in Lyell's defination of talus. Furthermore, although there are rock slide deposits in the Ogilvie and Wernecke Mountains they are not associated with the high rock wall facets observed on scarp slopes and around cirque headwalls. They occur mainly on dip slopes below pronounced bedrock scars and are readily differentiated from the talus slopes described by many geomorphologists since Lyell. The rock slides of the region were not part of the study, and do not receive further attention in this thesis.

If water has been the chief agency of transport of the weathered debris down the gullies in the rock wall the resultant accumulation at the foot of the wall is known as an alluvial cone or an alluvial fan. Water transport by itself plays a minor role in the development of talus slopes, however, the chief agent of transport of the weathered debris being a gravitational force acting alone or in association with avalanches lubricated in varying degrees with water. The particular form of talus, known as a talus cone, sometimes resembles an alluvial cone at a distance, but the latter invariably has a lower slope angle and a more continuously concave profile. Its component rock particles are rounded or sub-rounded by contrast with the angular talus particles.

In arctic and alpine regions, where winter snow cover is significant, avalanches assume an important role along with rock-falls in the production of coarse debris accumulations. Some confusion is evident in the literature over the use of the term talus in such cases. In a study in northern Sweden, Rapp (1959, p. 47), has suggested that both talus cones and alluvial cones may be transformed by avalanche erosion into avalanche boulder tongues, and implies that the term talus cone should be used to refer to features produced and modified by rock-falls alone. But it is difficult to decide prima facie whether avalanche or rock-fall activity plays the major role in debris accretion on a particular colluvial debris form, or in the erosional modification of this form. Nearly all of the rock walls studied in the Ogilvie and Wernecke Mountains have gullies which contribute avalanches or small ice falls to the debris slopes.

Although debris forms may differ depending on the importance or otherwise of avalanches, the predominant process is not the only factor which creates the form of the debris slope. Through its effect on particle size and shape the lithology of the rock walls debris may influence the debris slope morphology. The bedrock profile beneath the debris cover may also affect the form of the latter. Therefore it is considered prudent and expedient to use the term talus in a broad sense in this thesis, to include all colluvial debris accumulations which have been derived directly from rock walls and which are neither fluvial nor rock slide deposits.

The talus slopes may be grouped into two categories in the field areas.

i) Talus cones are developed below gullies in the bedrock with their apex at the point where the gully debouches from the rock wall facet onto the basal slopes. In plan view they are irregularly triangular (Plates, 1, 13, 22).

Talus cones are the principal colluvial debris forms below the metasedimentary escarpments in both field areas. The metasediments are thinly bedded and well jointed and are therefore very fissile. The rock walls have therefore been subjected to considerable erosion and are seamed at frequent intervals by deeply incised gullies which form the source of the talus cones.

Talus cones are by contrast very infrequent in the igneous intrusives of the Tombstone area, where gully networks are infrequent and poorly developed. A few large talus cones do exist, however, below narrow, joint-controlled gullies and chimneys.

ii) Talus aprons or sheet taluses consist of thin veneers of coarse blocks spread over a narrow zone at the base of the rock walls. Talus aprons rather than talus cones characterise the basal slopes in the Tombstone intrusives (Plate 2).

c) Protalus rock glaciers

Rock glaciers have been recognised and described over a period of at least seventy years. They have been defined by Capps (1910) as "tongue-like bodies of angular boulders resembling a small glacier, generally occurring at high altitudes in rugged terrain".

The following two-fold classification of rock glaciers is considered relevant for the Bear River and Tombstone areas. It was proposed by Outcalt and Benedict (1965) in their description of rock glaciers in the Colorado Rocky Mountains.

i) Cirque-floor rock glaciers

Rock glaciers of this form result from the accumulation of talus on the basal parts of the mountain walls, and its subsequent movement over cirque floors. Ultimately they may occupy the entire cirque basin (Plates 18, 25 and 28). Cirque-floor rock glaciers occur at the heads of many of the valleys in the Bear River area and, to a lesser extent, in the Tombstone area.

Most of these rock glaciers are tongue-shaped in plan view and may correspond to the tongue-shaped rock glaciers described by Wahrhaftig and Cox (1959) in Alaska.

ii) Valley-wall rock glaciers

These rock glaciers are located below the side walls of valleys and around the headwalls of cirques, mainly in the Bear River area (Plate 3). Their form in plan view is usually lobate and thus they may be related to Wahrhaftig and Cox's lobate rock glaciers.

2) PROCESSES

The processes defined are those which transport weathered debris from rock walls to talus slopes or which modify these talus slopes.

a) Rock-fall

Sharpe (in Glossary of Geology and Related Sciences, 1960, p. 74) has given the following definition for rock-fall under the heading debris fall.

> "The relatively free falling of a newly detached segment of bedrock of any size from a cliff, steep slopes, cave or arch".

This definition in the writer's view is not complete, since relative free fall is a vague term. Rock-fall may occur both as free fall from a rock face and by bounding or rolling motion of a particle along a steeply inclined rock surface. It results in the immediate or delayed removal of newly weathered debris from the rock wall facet to the talus facet.

Dislodgement of a block from a gully wall may cause the block to bound into the gully bottom and then to change angle and bound and roll down the gully onto the talus slope below. It may also shatter or stop on sudden impact with a projecting surface in the gully, or it may even cause other weathered particles in the rock wall gullies to start moving, thus inducing secondary rock-falls.

Rapp (1959), in Spitsbergen, divided rock-falls into three categories - large boulder falls which comprise particles greater 2 m (6.5 ft) in diameter, small boulder falls and pebble falls. He concluded that there is a much greater frequency of pebble falls than boulder falls and that these pebble falls were of much greater quantitative significance throughout the period of build-up of the talus. In the Ogilvie and Wernecke Mountains the relative importance of large and small rock-falls may be dependent on the rock wall lithology, and so this classification of rock-falls by size is considered to be a good one.

b) Snow avalanches

The following description by Page, (1859, in the Glossary of Geology and Related Sciences, p. 81) is one of the earliest.

"Avalanches originate in the higher regions of mountains and begin to descend when the gravity of their mass becomes too great for the slope on which they rest or when fresh weather destroys its adhesion to the surface".

Since Page's description there have been several classification of avalanches (Allix, 1924; De Quervain, 1966; La Chapelle, in Fairbridge, 1968). From the point of view of geomorphic effects of snow avalanches in the field areas a fundamental distinction may be made between winter avalanches and spring avalanches. Winter avalanches tend to be associated with the creation of layers of instability known as depth hoar layers through constructive metamorphism in the lower layers of the snow pack. Age densification of overlying layers of snow, aided by wind action, results in the creation of extremely unstable conditions in the snowpack. Minor events such as a person skiing across the slope or bigger events such as a series of fresh snowfalls may then trigger large avalanches.

Winter avalanches have a minimal geomorphic influence in the field areas. When they occur the talus slopes and the debris mantle on the rock walls are frost congealed and also possess a protective covering of early winter snow which is hardened by the assumed presence of ice layers. Even when winter avalanches involve the sliding of the entire snow pack as in the case of ground avalanches (La Chapelle, in Fairbridge, 1968, p. 1021) they do not appear to erode much debris for the rock walls.

Spring avalanches result from the penetration of meltwater into the snow pack. The water reduces the snow strength and may provide a good lubricating layer for avalanche release (La Chapelle, in Fairbridge, 1969, p. 1024).

If the sliding layer is heavily lubricated by meltwater the avalanche may exhibit semi-viscous flow and descend like a cascade of water (Allix, 1924, p. 533). On a large scale and on relatively low angle slopes this type of wet warm avalanche is associated with the ponding of large quantities of meltwater behind ice barriers and has been described as a slushflow (Washburn and Goldthwait, 1958) or slush avalanche (Nobles, 1959). When these avalanches occur on steep slopes in individual gullies in the rock walls or on the talus slopes, they may be termed torrent avalanches (Rapp, 1960b, p. 138).

Some of the late spring avalanches in the Ogilvie and Wernecke Mountains have geomorphic significance. Frequently parts of the talus slopes are snow free while there is still sufficient snow on the rock wall slopes for avalanching to continue. Then the talus slopes undergo some avalanche modification for a week or two in the late spring (Plate 12). The late spring avalanches are also able to remove debris from parts of the rock wall zone which are no longer protected by basal layers of hard snow and ice and which are no longer frost congealed. If a snow avalanche contains a high but undefined proportion of debris it is known as a dirty avalanche (Rapp, 1960b, p. 127).

c) Fluvial processes

These are processes of abrasion of bedrock or loose debris, and transport of the latter by rainwash, rills and streams in the rock wall gullies and on the talus slopes.

d) Slow debris shift

This general term embraces the complex group of processes inducing slow gravitational mass movement from the rock wall gullies down the talus slopes and over the basal slopes.

The term talus creep has been widely used to characterise slow mass movements of relatively coarse debris on relatively steep slopes. Sharpe (1938, p. 30) defines talus creep as "the slow down-slope movement of a talus or scree, or of any of the material of a talus or scree". It is not usually possible to clearly separate the effects of rock-falls, avalanches and fluvial processes from other processes inducing slow mass movements in the rock wall gullies and on the talus slopes. Thus a variety of different processes may cause the slow transfer of debris downslope, e.g. slight dislodge-ment of particles by avalanches or by rock-fall impact, localised shallow debris slides and downslope transfer of debris due to freeze thaw processes in the presence of moisture and due to thermal changes. For this reason and for the reason that these processes operate in the rock wall gullies as well as on the talus slopes the less connotive term slow debris shift adapted from the term talus shift (Gardner, 1969) is preferred to the term talus creep.

No special term has been given for the slow mass movement on low angle basal slopes which leads to the development of protalus rock glaciers but its nature and importance may be examined under the heading of <u>rock glacier motion</u>.

APPENDIX II

CALCULATIONS OF TALUS VOLUMES AND ROCK WALL AREAS

1. CALCULATION OF NET VOLUME OF TALUS (VN)

For his calculations Rapp (1960a) assumed that the talus slope represented a geometrical cone bisected along its length. He then used topographic maps with the small contour interval of 20 m (65 ft) to measure the length of the talus slope and the basal arc which he considered as a semi-circle. The talus volume was then found by applying these measured values to a modification of the formula for the volume of a cone.

In the field areas being considered in the present study, the contour interval on the largest scale topographic maps is 155 m (500 ft). This is obviously totally inadequate to indicate either the length of the talus slope or the length and curvature of the basal arc. Furthermore all the talus slopes possess bulges and irregularities of areal outline to a considerable degree, and a bisected cone does not represent the true form of the talus slope.

Therefore it was considered more accurate to divide the talus cones along the length of the fall line into component cross sectional slices as in Figure II.1. The bulk volumes for the individual slices were than calculated and integrated to obtain the bulk volumes of the talus cones. The total porosities were then calculated and the net volumes of the talus cones derived.

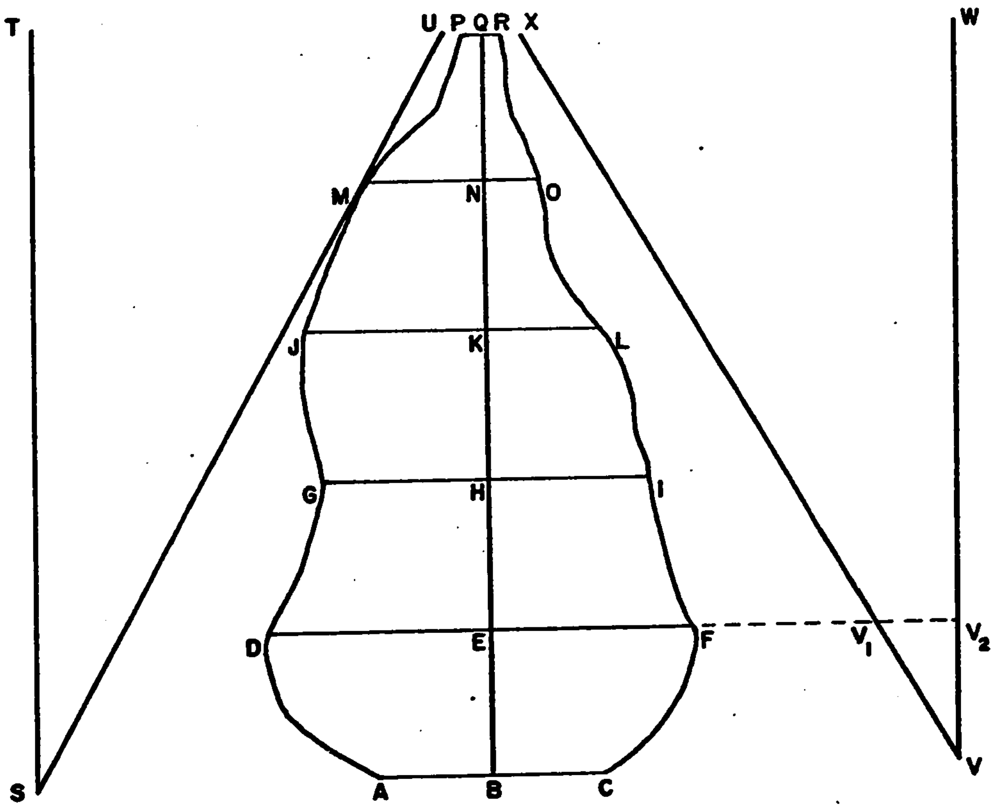

FIG. II.1

a) Calculation of bulk volume of talus cone slice

The bulk volume of each slices in Figure II.1 was derived by multiplying the surface area of the slice by its mean depth. Both of these variables had first to be calculated.

i) Calculation of area of top surface of slice

The fall line distance BQ along the length of the talus cone was measured initially by photogrammetry for all cones, and later by tape traverse for cones 6801, 6813, 6814, 6821, 6824, 6825 and 6830.

This length was divided into five sections and horizontal distances to both edges of the cones were measured from points B, E, H, K, N and Q on the fall line. The lengths AC, DF, GI, JL, MO and PR are then calculated as the sum of each pair of distances to the talus edge.

The area of each of the slices was then calculated using the formula for a trapezoid figure.

e.g. area ACFD $= \dfrac{BE\ (AC + DF)}{2}$

where BE, AC and DF are known.

The other areas DFIG, GILJ, JLOM, MORP are similarly calculated.

A slight error is introduced into the volume calculations however by measuring the lengths DF, GI, JL and MO along the curved cross sectional surface of the talus cone. In order to illustrate this the slice DFIG is constructed three dimensionally in Figure II.2.

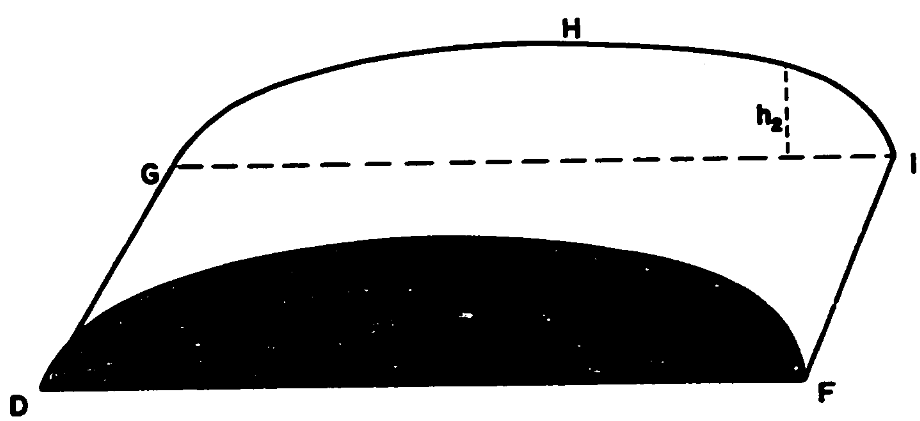

FIG. II.2

Strictly speaking the slice volume is the planar area DFIG multiplied by$(h_2 + h_1)/2$ and not the curvilinear area DEFIHG multiplied by $(h_2 + h_1)/2$.

The difference in the length of DEF and DF is so slight that DEF readily approximates the values of DF calculated independently. Table II.1 lists values for the curvilinear length and planar length for all cross sections, on cone 6801.

TABLE II.1

COMPARISON OF LENGTH OF CURVILINEAR AND PLANAR CROSS SECTIONS OF CONES 6801 (IN METRES)

Cross section	Planar length	Curvilinear length
AC	30	30
DF	152	153
GI	159	161
JL	115	117
MO	70	71
PR	48	48

The maximum error in the surface area of any cross sectional slice is that for GILJ. It is of the order of 1.5% which is considered negligible. Results from the other talus cones show even smaller errors.

ii) Calculation of mean depth of talus in a slice

Applying the assumption that the bedrock slope on either side of the talus cone may be extrapolated as a planar surface beneath the talus, angle traverses were made on adjacent bedrock on both sides of the talus cone. These were parallel or sub-parallel to a third traverse up the centre of the cone. Angles were read with an Abney level at intervals defined precisely using a tape.

All three traverses were begun and completed at precisely the same elevations, and are illustrated in plan view by BQ, VX and SU in Figure II.1. For each talus cone three profiles were constructed on graph paper starting from the same basal point, S, B and V all being at the same height. Figure II.3 is an illustration of the technique for cone 6801. The maximum depths from the talus surface at points B, E, H, K, N and Q along the centre line of the cone to the assumed bedrock surface beneath the talus cone, were obtained by dropping approximate perpendiculars to the means of the two bedrock profiles at each point.

Where the talus cone is fairly triangular in plan view as in Figure II.1, the bedrock profiles SU and VX have of necessity a greater length than the profile up the centre line of the cone BQ. This results in an erroneous graphical plot of the form shown in Figure II.4.

(1) Refers to talus cone surface profile.

(2) Refers to bedrock profile on South margin of talus cone.

(3) Refers to bedrock profile on North margin of talus cone.

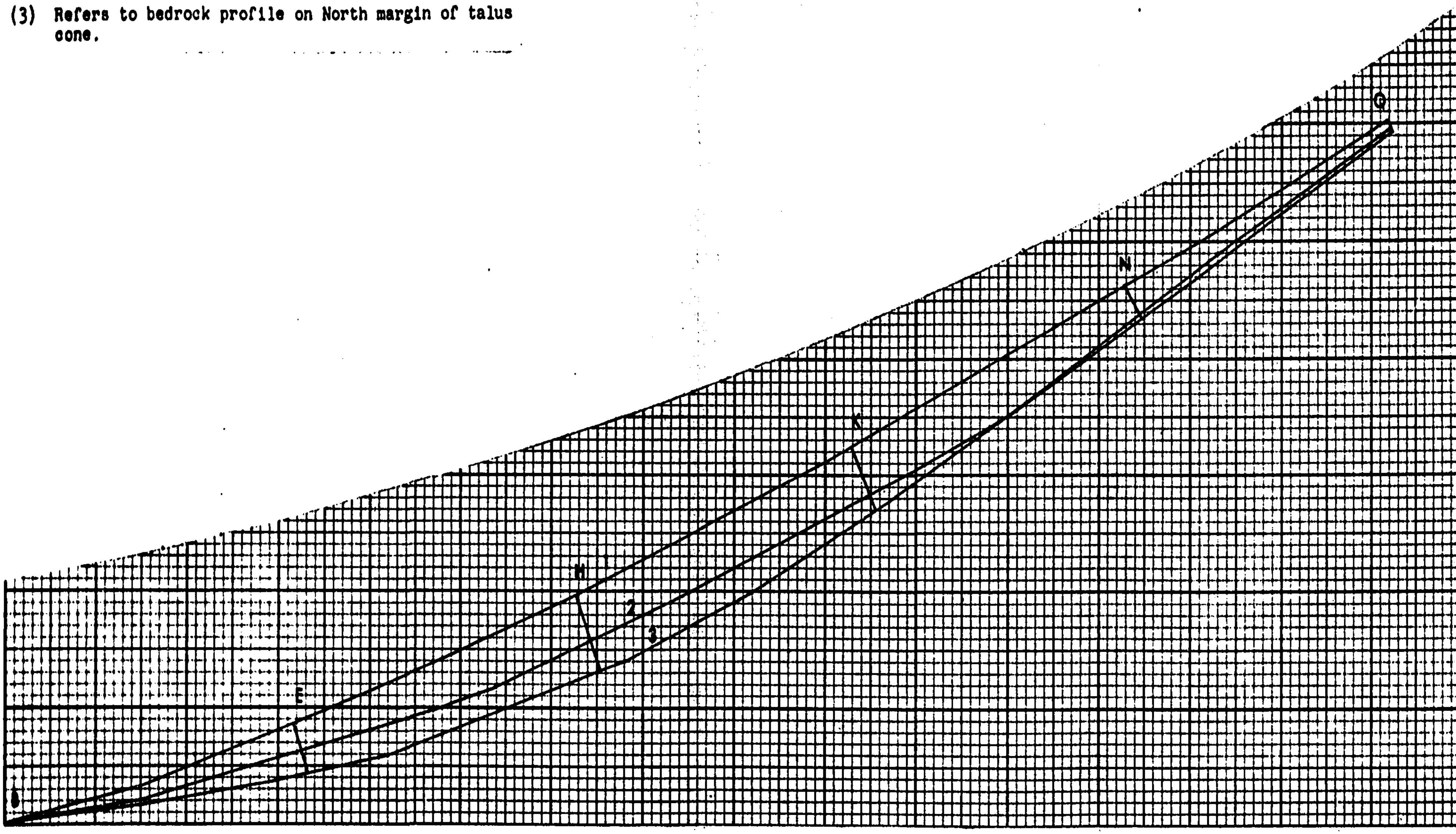

SCALE: 1" = 20m

Fig. II.3

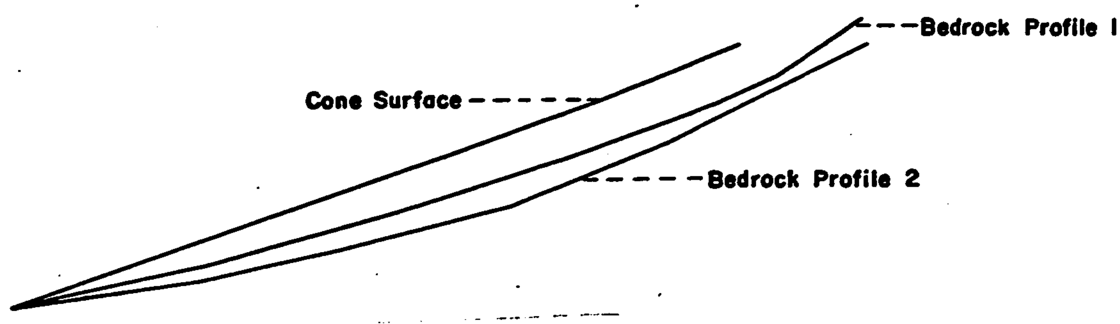

FIG. II.4

Theoretically these profile traverses must be exactly parallel as well as starting and finishing at the same elevations before one can prepare an accurate graphical plot as in Figure II.3. ST and VW in Figure II.1 represent such ideal profile traverses. A problem is introduced, however, because the further the top of the bedrock traverses are from the apex of the cones the more liable is the extrapolation of the bedrock surface beneath the cone to gross errors. Therefore before graphing the data, each interval VV_1 on the bedrock traverse for which an angle was read must be shortened to VV_2 so that the total length of this traverse is equal to that of the traverse along the centre line of the talus cone. This corrected value is achieved by use of the following formula.

$$VV_2 = VV_1 \left(\frac{BQ}{VX}\right)$$

The net effect is that the mean overall profile is shortened and steepened but the relative height of the top as compared with the base remains unchanged.

The corrected graphs of bedrock and talus profiles were similarly prepared for all talus cones. The maximum talus depths at one fifth intervals are read off the appropriate graph for each cone as in Figure II.3. The depths at B and Q are theoretically zero although a small closing error usually existed on the profile diagrams.

Using the maximum depths of the talus at E, H, K and N the mean depth was calculated for the horizontal cross sections of the talus cone at these points. The cross section at point E is illustrated in Figure II.5 in which the circle circumscribing points D, E and F on the talus cone is also drawn.

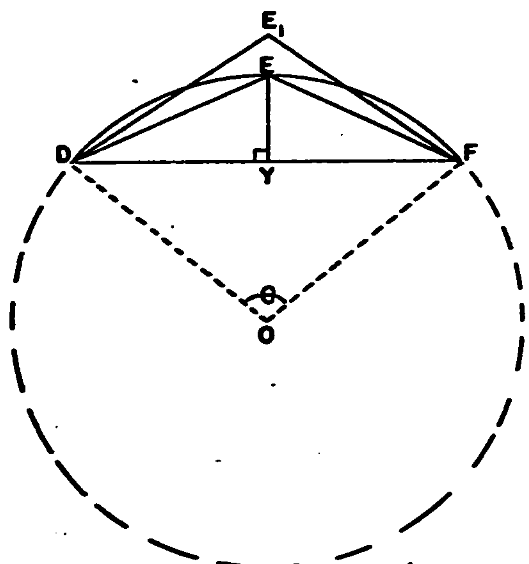

FIG. II.5

The length of the curved surfaces DE and EF is already known, and EY the maximum depth of talus has just been derived.

Because of the high radius of curvature of the circle circumscribing $\triangle$ DEF, chords DE and EF $\simeq$ arcs DE and EF.

The mean height of $\triangle$ DEF = EY/2 = ½ max. depth

But the true mean depth of the cross section DEF is greater on account of the additional areas enclosed by arc and chord DE and arc and chord EF.

To find the true mean depth of the circular cross section let the area of this cross section known as the segment DEF be equal to a slightly larger $\triangle\, DE_1F$ with the same base DF and a new slightly greater height E_1Y. Then the mean height of this triangle is the corrected mean depth for the circular cross section.

The mean height of $\triangle\, DE_1F = E_1Y/2$

From the formula for area of triangles

$$\text{area of } \triangle\, DEF = DF\,(EY/2)$$

$$\text{area of } \triangle\, DE_1F = DF\,(E_1Y/2)$$

$$\therefore \quad \frac{\text{area of } \triangle\, DE_1F}{\text{area of } \triangle\, DEF.} = (E_1Y/2)/(EY/2)$$

$$\therefore \quad E_1Y/2 = EY/2 \left(\frac{\text{area of } \triangle\, DE_1F}{\text{area of } \triangle\, DEF}\right)$$

$$\therefore \quad \text{corrected mean depth} = \text{mean height of } \triangle\, DEF \times \left(\frac{\text{area of } \triangle\, DE_1F}{\text{area of } \triangle\, DEF}\right)$$

$$= \tfrac{1}{2}\left(\begin{array}{l}\text{max. depth read}\\ \text{off Fig. II.3}\end{array}\right) \times \left(\frac{\text{area of segment DEF}}{\text{area of } \triangle\, DEF}\right)$$

$$\therefore \quad h_2 = (h_1/2) \times (K_1/K_2) \qquad \text{..... equation II.1}$$

where K_1 = area of segment DEF

K_2 = area of $\triangle$ DEF

h_1 = maximum depth of talus

h_2 = corrected mean depth of talus cross section

The area of the segment DEF (K_1) can be determined once the radius of curvature (R) of the circle circumscribed through D, E and F is obtained. R is calculated from the following equation (Ayres, 1954, p. 112)

$$R = EF/2\sin EDF$$

$$= (EF \times DE)/2EY \qquad \text{.... equation II.2}$$

EF, DE and EY are all known and R is obtained.

Now the area K_1 = area of sector DOF - area of $\triangle$ DOF

$$= R^2\theta/2 - R^2\sin\theta/2 \qquad \text{.... equation II.3}$$

where θ in radians is angle subtended by DOF (Ayres, 1954, p. 114)

$$\text{and} \quad \theta = \frac{\text{arc DEF}}{R} \simeq \frac{DE + EF}{R}$$

$$\therefore \quad K_1 = \frac{R^2}{2}\left[\left(\frac{DE + EF}{R}\right) - \sin\left(\frac{DE + EF}{R}\right)\right] \qquad \text{.... equation II.4}$$

DE, EF, R are all known and so K_1 is obtained.

$$\text{Area of } K_2 = DF(EY/2)$$
$$= (DY + YF)\ (EY/2)$$
$$= \left(\sqrt{DE^2 - EY^2} + \sqrt{EF^2 - EY^2}\right) \times (EY/2) \quad \text{... equation II.5}$$

EY, DE, EF are all known and so K_2 is obtained.

The values of K_1 and K_2 can now be fitted into equation II.1 and the mean depth h_2 of the circular cross section DEF of the talus at the point E obtained. The calculations of the mean depth of all the cone cross sections were then computed using equations II.1, II.2, II.3, II.4 and II.5.

The mean depth for each of the five horizontal cone slices was taken as the mean of adjacent cross sectional mean depths. For example, referring back to Figure II.1

$$\text{the mean depth of ACFD} = \left(\frac{0 + h^E{}_2}{2}\right)$$

where $h^E{}_2$ is the corrected mean depth of the cross section at E

$$\text{and the mean depth of DFIG} = \left(\frac{h^E{}_2 + h_2{}^H}{2}\right)$$

where $h_2{}^H$ is the corrected mean depth of the cross section at H

The mean depths of GILJ, JLOM and MORP were similarly calculated.

The bulk volume of each slice was then calculated by multiplying the newly derived figure for the mean depth of the cone slice by the already derived surface areas of the slices. The values for the five slices were then integrated and a total gross volume of debris in the cone was obtained.

b) Calculation of net volume of talus cones

This total bulk volume included void spaces and had to be corrected to the net volume of rock eroded from the rock wall zone. This necessitated knowledge of the porosity of the talus cones.

Graton and Fraser (1935, p. 805) used theoretical considerations to derive the porosities of assemblages of uniform spheres under various packing structures. But many factors in nature alter the hypothetical values. In the first place a deposit such as a talus cone, which is laid down or subsequently modified by several different processes, is made up of assemblages of different packing structures and may be characterised as a system of chance packing. For spherical particles the porosity of such a system lies between 47.64% for the least dense arrangement (cubic packing) and 25.95% for the most dense arrangement (rombohedral packing). Grain size is theoretically of no significance in itself but, because of greater adhesion of small particles and bridging effects, porosity increases as the size of the particles decreases. The shape of the grains is also undoubtedly of some importance, increasing roundness and sphericity tending to decrease the porosity under conditions of chance packing.

The varying sizes of the debris on the talus cones probably reduces the overall porosity of the latter, although this effect may be counteracted by the high angularity and low to moderate sphericity of the particles. In randomly packed assemblages comprising two grades of debris, the ratio of diameter of the smaller particles to that of the larger particles must be 0.158 for the smaller particles.

to enter the voids between the larger particles, and less than 0.433 for the smaller particles to occupy these voids without disturbing the packing arrangement between the larger particles. These ratios are known as the critical ratio of entrance and the critical ratio of occupation (Fraser, 1935, p. 919). Figure II.6 from Fraser (p. 924) shows the relationship between porosity and the percentage of large to small particles in a two component system for both critical ratios.

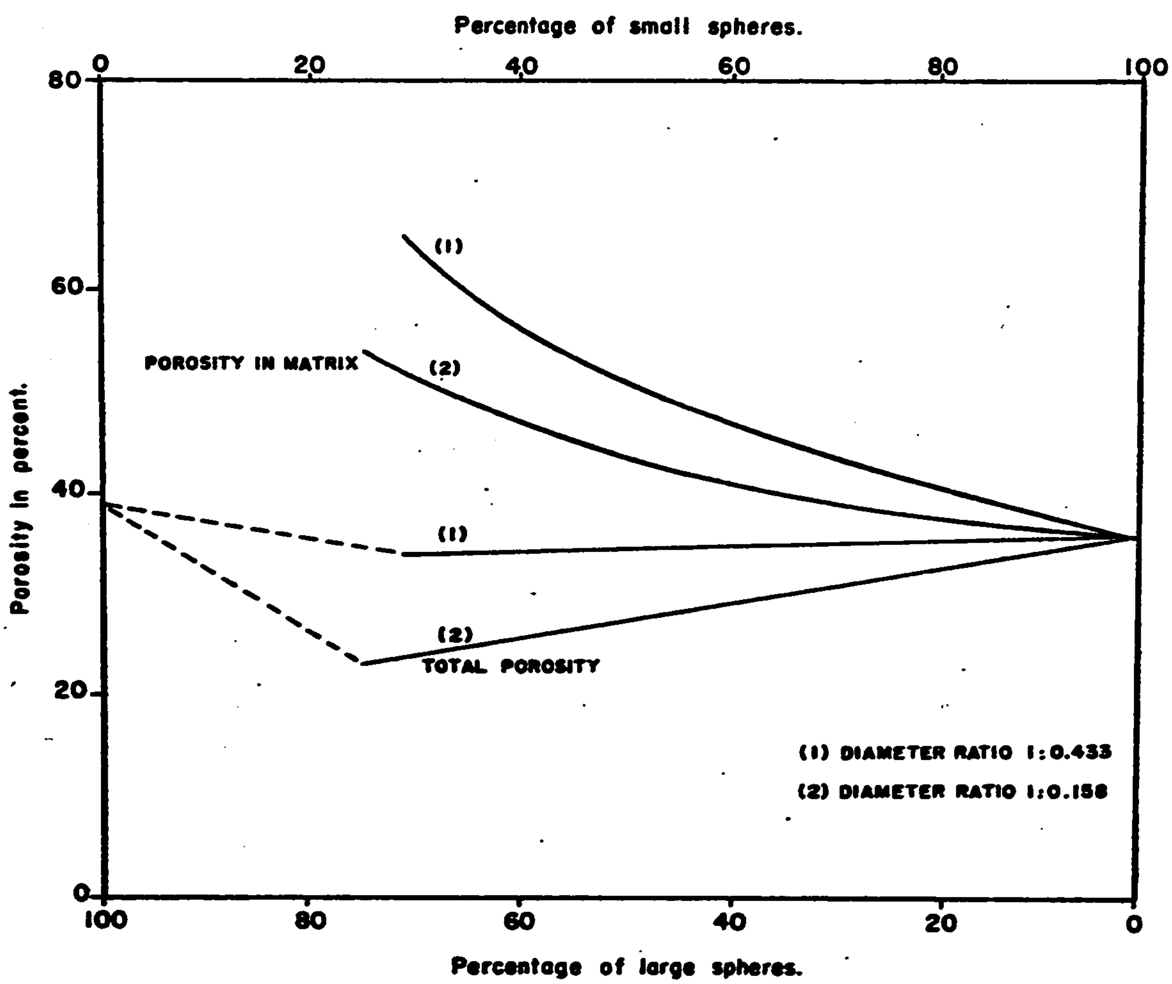

FIG. II.6

Obviously the talus consists of a much more complex assortment of particle sizes and at the moment there is no way to predict the porosity directly from knowledge of the size frequency distribution. Empirically, however, through the use of one, two and three component systems built in the laboratory, and through assessment of natural deposits Fraser suggests that a uniformly sized gravel may have porosities up to about 40% whereas a poorly sized gravel may have porosities as low as 20% (Fraser, p. 992). A mean value of 30% with error limits of $\pm$ 10% is considered acceptable for porosities of the talus cones for which estimates of the net volumes are required. Using this value the net volumes of the talus cones were then calculated as follows:

$$\text{Net volume (VN)} = \text{Bulk volume} \times 7/10$$

c) Errors in the calculation of net volumes of talus cones (VN)

Two major sources of error exist in the calculation of VN

i) error in mean depth of each horizontal slice

ii) error in porosity

i) Error in mean depth

This is a compound error based on the following assumptions and instrumental errors.

a) the assumption that the bedrock surface beneath the talus cone is a planar surface which can be extrapolated from bedrock on one side of the cone to bedrock on the other side;

b) the error in angle readings with the Abney level.

c) the assumption that the cross section of a talus cone approximates the arc of a circle.

Unfortunately the first type of error cannot be quantified but it probably causes a slight underestimate of the true volume of talus. Figure II.7 shows the probable bedrock form beneath the talus cone, i.e. a mostly planar surface with a narrow rock wall gully running from the apex to the base.

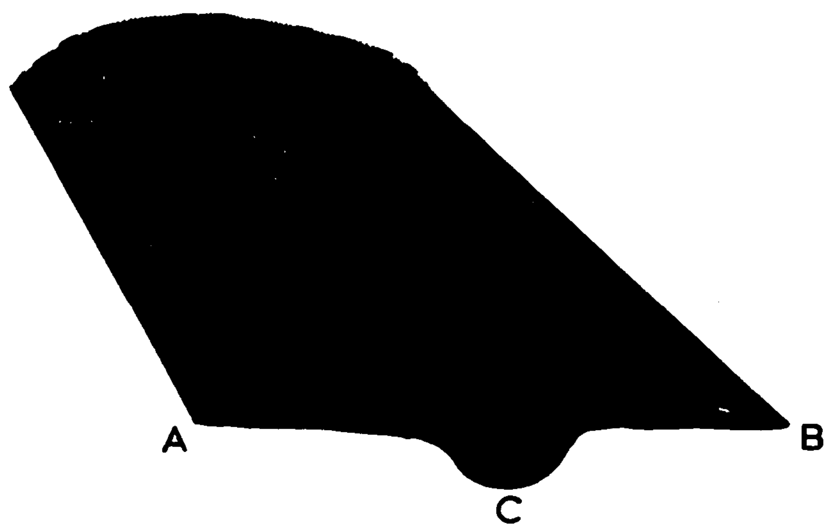

FIG. II.7

During successive deglaciations, prior to accumulation of large quantities of protective debris, ephemeral run-off in the rock wall gully had ample opportunity to erode a water course to the base of the slope.

The amount of error in net talus cone volumes resulting from error in angle measurements with the Abney level was calculated in detail for cone 6801 and then applied in percentage terms to the net volumes for all other cones.

A theodolite was fixed at the base of cone 6801, and precise readings of angles to points on the three Abney level traverses were made. Figure II.8 shows errors discovered when the heights at these points, obtained from theodolite and Abney level readings, are compared.

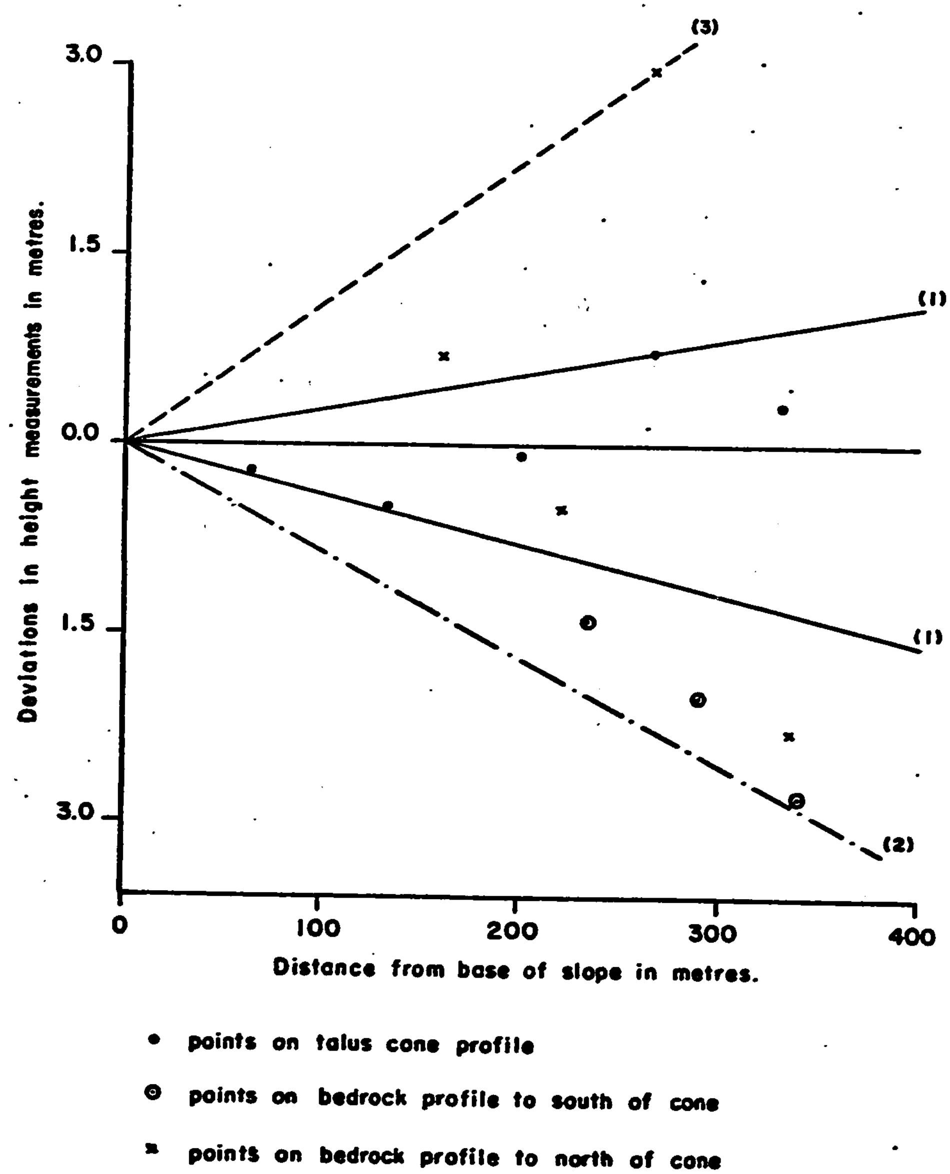

FIG. II.8

These figures permit the calculation of maximum error limits for the angles in each of the three profiles.

Error	band	(1)	for	talus profile				=	± 20'
"	"	(2)	"	bedrock	profile	to	south	=	± 30'
"	"	(3)	"	"	"	"	north	=	± 40'

The three profiles were then re-graphed in such a way as to obtain the absolute minimum and maximum depth values for the talus up the centre of the cone, based purely on the maximum possible angular errors. (Fig. II.9).

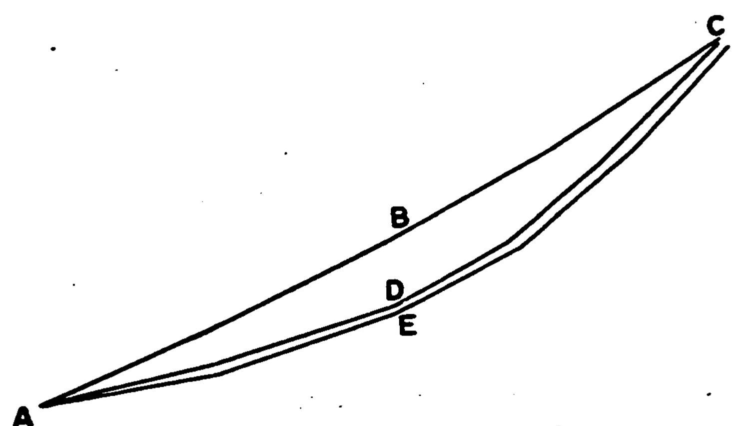

FIG. II.9

In section AB of the talus profile ABC, i.e. the lower half of the profile, the individual angles were all decreased by 20'. In the section BC they were all increased by 20'. In this way the over-all mean value for the angle of the slope, and correspondingly the position of C with respect to A does not change. The converse operation was done on the bedrock profiles ADC and AEC. The angles in sections AD and AE were increased by 30' and 40' respectively. Sections DC and EC were correspondingly decreased. Thus the terminals of the profilès are unchanged but the mean depth at all points between is diminished.

Table II.2 gives the mean, maximum and minimum values for depth of talus at five equal intervals along the centre line of cone 6801 and the possible error in depth at these points that results from angle measurement error. The percentage error in the mean depth of each horizontal slice of talus is then obtained by averaging the percentage error in the mean depth of each adjacent pair of cross sections.

TABLE II.2

POSSIBLE ERRORS IN DEPTH OF TALUS IN CONE 6801 DUE TO INSTRUMENTAL VARIATION (in m)

Point	Mean depth h_2	Max. value for h_2	Min. value for h_2	% pos. error in h_2
B	0	0	0	0
E	4.65	5.07	4.23	± 9%
H	8.65	10.75	6.29	± 19%
K	7.73	9.27	6.19	± 20%
N	4.25	4.81	3.69	± 13%
Q	0	0	0	0

Cone slice	% error in mean depth of cone slice
ACFD	± 4.5%
EFIG	± 14%
GILJ	± 19.5%
JLOM	± 16.5%
MORP	± 6%

Assumption of a perfectly spherical boundary for the horizontal cross sections of the talus cones is also likely to give an error in the mean talus depth. Figure II.10 a), b), c) and d) are representations of theoretical cross profiles. The profiles in Figures II.10a) and II.10b) give an increased mean depth as compared with the assumed profile in Figure II.10c), whereas the profile in Figure II.10d) gives a reduced mean depth. Profiles of the form shown in Figure II.10d) have not been noted on the talus slopes and it is therefore suggested that assumption of a circular cross section as in Figure II.10c) can only give an under estimate of the true value.

If Figure II.10a) represented the cross profile it would give an absolute maximum value for the mean height of the talus cross section which would correspond to the depth of talus along the central profile of the cone. A tendency towards this cross section is seen in some talus slopes which have been labelled avalanche boulder tongues by Rapp (1959). None of the cones for which calculations have been made in the central Yukon are of this extreme form. Therefore the intermediate profile in Figure II.10b) is postulated as giving the smallest radius of curvature likely to occur. A maximum value for the mean depth of each of the cross sections is then assumed to lie between the calculated mean depth (h_2) of the circular cross sections and the maximum height at the centre lines of the talus cones. These values are indicated in Table II.3 for cone 6801. The percentage errors for the mean depth of each cross section and each cone slice are also tabulated.

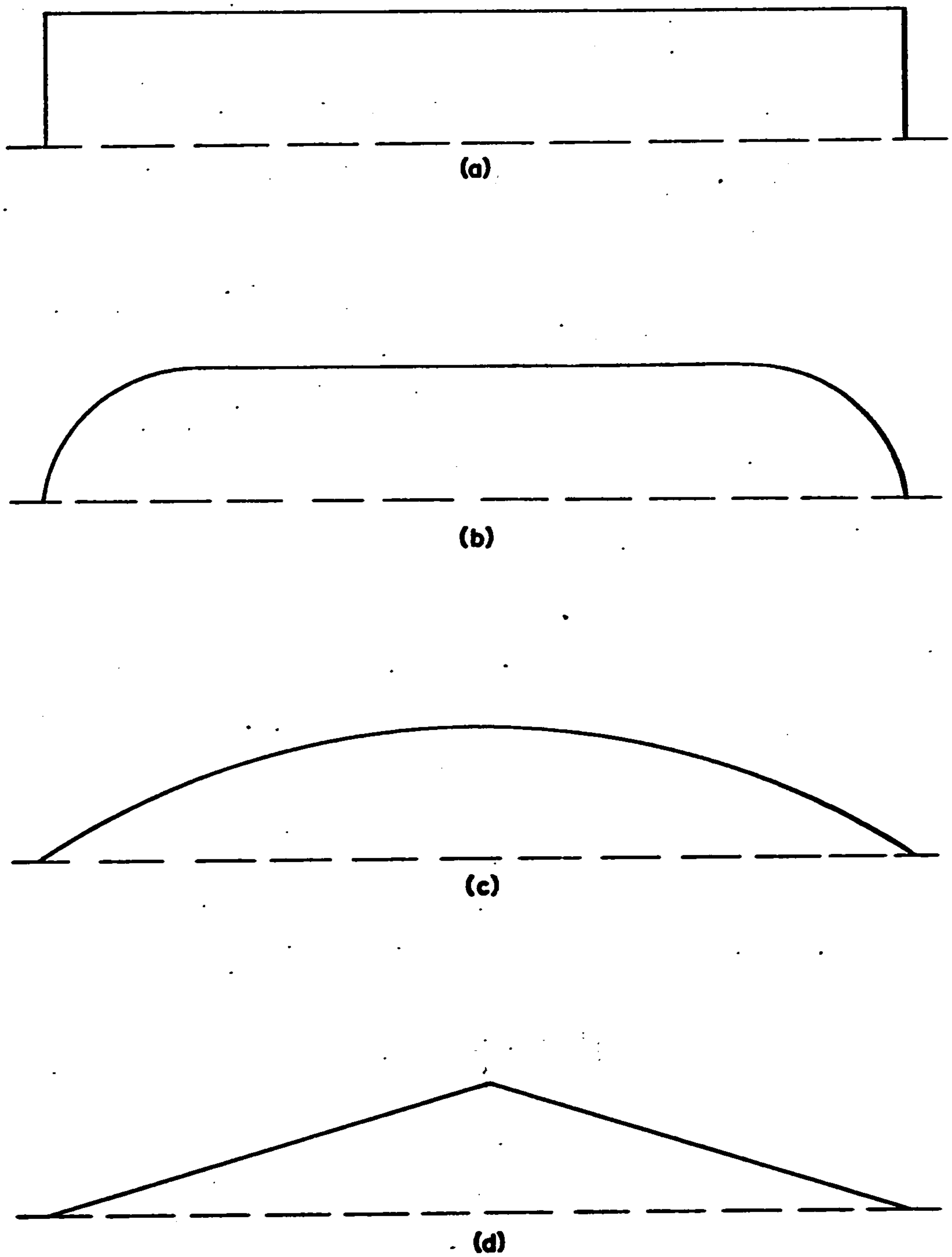

FIG. II.10 THEORETICAL CROSS PROFILES OF TALUS CONES

TABLE II.3

POSSIBLE ERRORS IN DEPTH OF TALUS DUE TO CROSS SECTIONAL SHAPE VARIATION (in m)

Cross Section	Mean depth h_2	Max. depth h_1	Max. poss. value for h_2	Max. poss. % error in h_2
ABC	0	0	0	0
DEF	4.65	6.88	5.77	+ 24%
GHI	8.52	11.72	10.12	+ 19%
JKL	7.73	11.10	9.42	+ 22%
MNO	4.25	6.40	5.33	+ 25%
PQR	0	0	0	0

Cone Slice	% poss. error in depth of cone slice
ACFD	+ 12%
DFIG	+ 21.5%
GILJ	+ 20.5%
JLOM	+ 23.5%
MORP	+ 12.5%

This possible error may now be added to the possible error quoted in Table II.2 for each cone slice to give accumulated possible errors for the mean depth of each talus slice (Table II.4).

TABLE II.4

ACCUMULATED POSSIBLE ERRORS IN DEPTHS FOR CONE 6801 (in m)

Talus slice	Mean depth	Max. poss. depth	Min. poss. depth	% poss. error
ACFD	2.3	2.7	2.2	+ 16.5% - 4.5%
DFIG	6.6	8.9	5.7	+ 35.5% - 14%
GILJ	8.1	11.4	6.6	+ 40% - 19.5%
JLOM	3.0	8.4	5.0	+ 40% - 16.5%
MORP	1.1	2.5	2.0	+ 19% - 6.5%

It is suggested that +40% and -20% of the mean value be taken as the maximum error limits for the depths of all slices and this is converted directly to +40% and -20% maximum possible error for the bulk volume of the cone 6801, the errors in the surficial areas of the slices being negligible. This percentage error is then applied to all other talus cones.

Error in porosity

The newly derived error in the bulk volumes of talus cones is increased in the calculation of net volumes due to variations in porosity from the assumed value of 30%. Possible variations of ± 10% of the bulk volume were indicated. This gives net volume of solids of 70% ± 10% of the bulk volume. Thus the possible percentage error in the calculated net volume due to porosity variation is ± 15% (± 10/70 of net volume).

If these possible errors in porosity are applied to the largest and smallest possible bulk volumes derived in the previous section, then maximum and minimum values are derived for the net volume of cone 6801.

For cone 6801 the results of these calculations are as follows:

net volume of solids = 142,000 cu.m +60% -31%

∴ max. volume of solids = 227,000 cu.m

and min. volume of solids = 97,980 cu.m

The mean, maximum and net volumes of the remainder of the cones were calculated using the error limits thus derived and the values are indicated in Table II.5.

TABLE II.5

MEAN, MAXIMUM AND MINIMUM NET VOLUMES OF TALUS CONES. (in cu.m)

Cone no.	Mean vol.	Maximum vol.	Minimum vol.
6801	142,000	227,000	98,000
6804	164,500	263,000	113,000
6808	101,000	161,500	69,700
6813	320,000	512,000	222,000
6814	14,350	23,000	9,900
6816	78,000	125,000	53,900
6821	135	155	115
6824	90,800	145,000	62,600
6825	4,810	7,700	3,320
6830	17,150	27,400	11,800

2. CALCULATION OF ROCK WALL SUPPLY AREA

Topographic maps of sufficient accuracy for determination of the area of the gully and buttress system above individual talus cones, were not available. Therefore photogrammetry and field traverse methods were used.

a) Photogrammetric method

Air photographs taken in 1951 at a height of 6,250 m (20,000 ft) and 10,700 m (35,000 ft) above sea level were available for the Bear River valley and Tombstone area respectively. The focal length of the camera in both cases was 15 cm (6 in). Average elevation of the base of the rock walls is 1,400 ± 150 m (4,500 ± 500 ft) in both areas. The average elevation of the top of the rock walls is 1,800 ± 150 m (6,000 ± 500 ft). The average elevation of the rock walls as a whole is therefore 1,600 ± 150 m (5,250 ± 500 ft). The mean horizontal scale of the rock walls in the air photographs can then be calculated from the following formula.

$$\text{Horiz. scale} = \frac{\text{focal length of camera (F)}}{\text{ht. of aircraft above terrain (H)}}$$

where F and H are in same length units

For the Bear River valley photographs the mean scale of the rock walls is calculated as 1:29,500 and the range of scale as 1:28,500 to 1:30,500. For the Tombstone area the mean scale of the rock walls 1:59,500 and the range of scale is 1:58,500 to 1:60,500.

The photographs were enlarged to twice these scales for both areas but it was evident that good photogrammetric measurements of rock wall area would only be obtainable from the Bear River valley. In the Tombstone area the scale of the photographs is too small and too much shadow is present for the rock wall areas to be outlined accurately. The mean scale of the enlarged photographs for the Bear River area becomes 1:14,750. The range of this mean is 1:14,250 to

1:15,250. For convenience, the mean scale is taken as 1:15,000 and the maximum horizontal scale error is included as ± 5%.

Stereopairs were then set up under a Delft scanning stereoscope, flight lines being chosen so that the rock wall areas of interest were fairly central on the photographs. This procedure minimises normal scale distortion which becomes very serious near the corners of the photographs.

The rock wall areas were clearly outlined and the area of the horizontal projection was measured. When divided by the cosine of the mean slope angle*, a crude measure of the actual rock wall area is obtained.

A major disadvantage of this preliminary method is that the rock wall has not only a general slope trend towards the valley but also minor trends towards the gully bottoms. Therefore the quality of a value based on a simple conversion of a horizontally projected area to the actual area, using only the mean angle of inclination towards the valley, is poor. Different parts of the rock wall lie on plane inclined at varying angles in a number of different directions.

This problem can only be resolved by recourse to a more sophisticated method, based on sub-division of the rock wall area into a

---

* Obtained by measurement of horizontal distance between apex of cone and peak of rock wall and by photogrammetric calculation of relative height between the two points.

group of simple geometrical forms and on calculation of sufficient parameters to solve equations for the area of each form. As a working example the rock wall area above cone 6801 is considered. Figure II.11 is a simplified diagram of the rock wall designed to illustrate the mode of analysis.

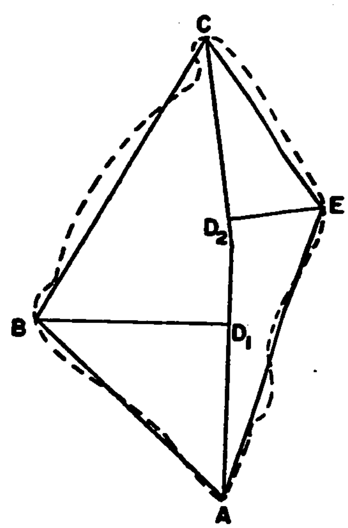

FIG. II.11

This area is considered fairly accurately as being composed of two triangles, ABC and ACE. In order to calculate the actual surface area, the base and height of the two triangles are required. To obtain these values along inclined surfaces, vertical and horizontal distances between the points must be calculated.

i) <u>Calculation of vertical distances between points</u>

A parallax bar was used in conjunction with the stereoscope to determine parallax differences between points at differing elevations. The basic formula for relative height calculation from parallax differences between two points is given by Ray (1960, p. 53) as:

$$h = \frac{\Delta p \times H}{b} \qquad \text{.... formula 1}$$

where h = relative height of one point above the other point

H = height of airplane above mean terrain

b = photobase (average of distances between the centre and conjugate centre of each photograph of the stereopair).

Δp = parallax difference

b and Δp must be in the same units, either mm or in

h and H must be in the same units, either m or ft.

This formula is only valid for terrain which possesses low relief. A corrected formula is suggested by Ray for areas of high relief.

$$h = \Delta p \times \frac{H'}{ab + \Delta p} \qquad \text{.... formula 2}$$

where H' = height of airplane in feet above the lower of the two points between which the parallax difference was measured.

ab = photobase adjusted to the lower of the two points whose parallax difference has been measured; commonly determined by measuring the distance between the photograph centres and subtracting from it the distance between conjugate image points at the lower altitude. (units same as Δp).

Relative heights between points were therefore obtained for the triangles ABC and AEC in Figure II.11. The results using the corrected and uncorrected formulae are shown in columns 1 and 2 in Table II.6.

ii) Calculation of horizontal distance between points.

Distances on the photographs were measured with a ruler graduated to 0.5 mm. The results are indicated in column 3 in Table III.6.

The slope distance between points is then readily calculated as follows:

$$\text{Slope distance} = \sqrt{\text{horiz. distance}^2 + \text{vert. distance}^2}$$

The appropriate values for cone 6801 are given in column 4 in Table II.6.

TABLE II.6

PHOTOGRAMMETRIC DISTANCES ON ROCK WALL ABOVE CONE 6801 (in m)

	Vert. dist. (formula 1)	Vert. dist. (formula 2)	Horiz. dist.	Slope dist.
AC	420	433	915	1,012
D_1B	102	106	246	267
D_2E	135	140	100	172

The rock wall area is then calculated as the sum of $\triangle$ABC and $\triangle$AEC.

Area of $\triangle$ABC = $(D_1B \times AC)/2$ = 135,000 m^2

Area of $\triangle$AEC = $(D_2E \times AC)/2$ = 87,000 m^2

$\therefore$ Area of rock wall above cone 6801 = 222,000 m^2

The measurable errors in this value are the horizontal scale error, and measurement errors in horizontal and vertical distances between points.

i) <u>Horizontal scale error</u>

This has already been determined as ± 5%

ii) <u>Measurement errors in horizontal and vertical distance between points</u>

The maximum horizontal distance measurement error is 1 mm at each ruler mark. Thus a total linear error of 2 mm exists for each measured distance. At a scale of 1:15,000 this gives a possible error of 30 m (100 ft).

A vertical distance measurement error results from a maximum parallax variation of ± 5 mm (determined from five readings at each point). This gives maximum errors in height for AC, D_1B and D_2E of ± 30 m.

To calculate the maximum and minimum possible values of the rock walls area resulting from these errors the maximum and minimum values for all vertical and horizontal distances must be calculated.

Max. vert. distance = mean vert. distance + 30 m

Min. " " = " " " - 30 m

Max. horiz. distance = (mean horiz. distance + 25 m) x 1.05

Min. " " = (" " " - 25 m) x 0.95

(the factors 1.05 and 0.95 take account of the horizontal scale error)

The maximum and minimum possible rock wall areas are then determined in the same manner as the mean rock wall area.

Max. rock wall area = 289,000 m^2

Min. rock wall area = 162,000 m^2

These values differ by 67,000 m^2 from the mean value and correspond to a maximum possible deviation of 32% from the latter. This is rounded off to $\pm$ 30% for calculations of rock wall areas above cones 6804, 6808 and 6816 (Table II.7) and represents the calculated error resulting from the photogrammetric method.

b) Ground traverse method

In the summer of 1969 it was decided to check the photogrammetrically measured rock wall area above cone 6801 in Bear River valley by ground traverses with measuring tape and Abney level. In the Tombstone area ground traverses were used for two rock wall areas of metasedimentary composition and one rock wall area of diabase composition on account of photogrammetric problems resulting from scale and shadow. Calculations for the syenite rock wall above cone 6830 were also made on the ground but because of the steepness of the wall a special method had to be employed. The general method of calculation of rock wall areas with ground traverse information and the special method used for the rock wall above cone 6830 are discussed separately.

i) General method

The rock wall above cone 6801 is again used as the illustrative example. A foot traverse was carried out by two men with a tape and an Abney level, (Fig. II.12). Angles were measured between adjacent points on the traverse and the distances between these points obtained by integrating 30 m tape intervals. Height differences between points were calculated trigonometrically from angle and distance measurements. They were then checked against the photogrammetically determined height differences.

Figure II.12 is a polygonal diagram which was graphically constructed from the measurements of the ground distances between points and the angles between the legs of the traverse measured directly off the air photographs. An indication of the high quality of the field data is the very small closing error AA_1. The polygon encloses the actual area of the rock wall, not a horizontal projection of it. This area was then measured directly off the diagram.

	Area of polygon ABCD[1]	=	135,000 m^2
	Area of polygon A_1ECD[2]	=	59,000 m^2
∴	Rock wall area	=	194,000 m^2

1 Considered in Figure II.11 for photogrammetric method as approximately the $\triangle$ ABC.

2 Considered in Figure II.11 for photogrammetric method as approximately the $\triangle$ ACE.

Note small horizontal error of closure at A. The vertical error of closure was found to be only 4m., although such a low error is probably fortuitous.

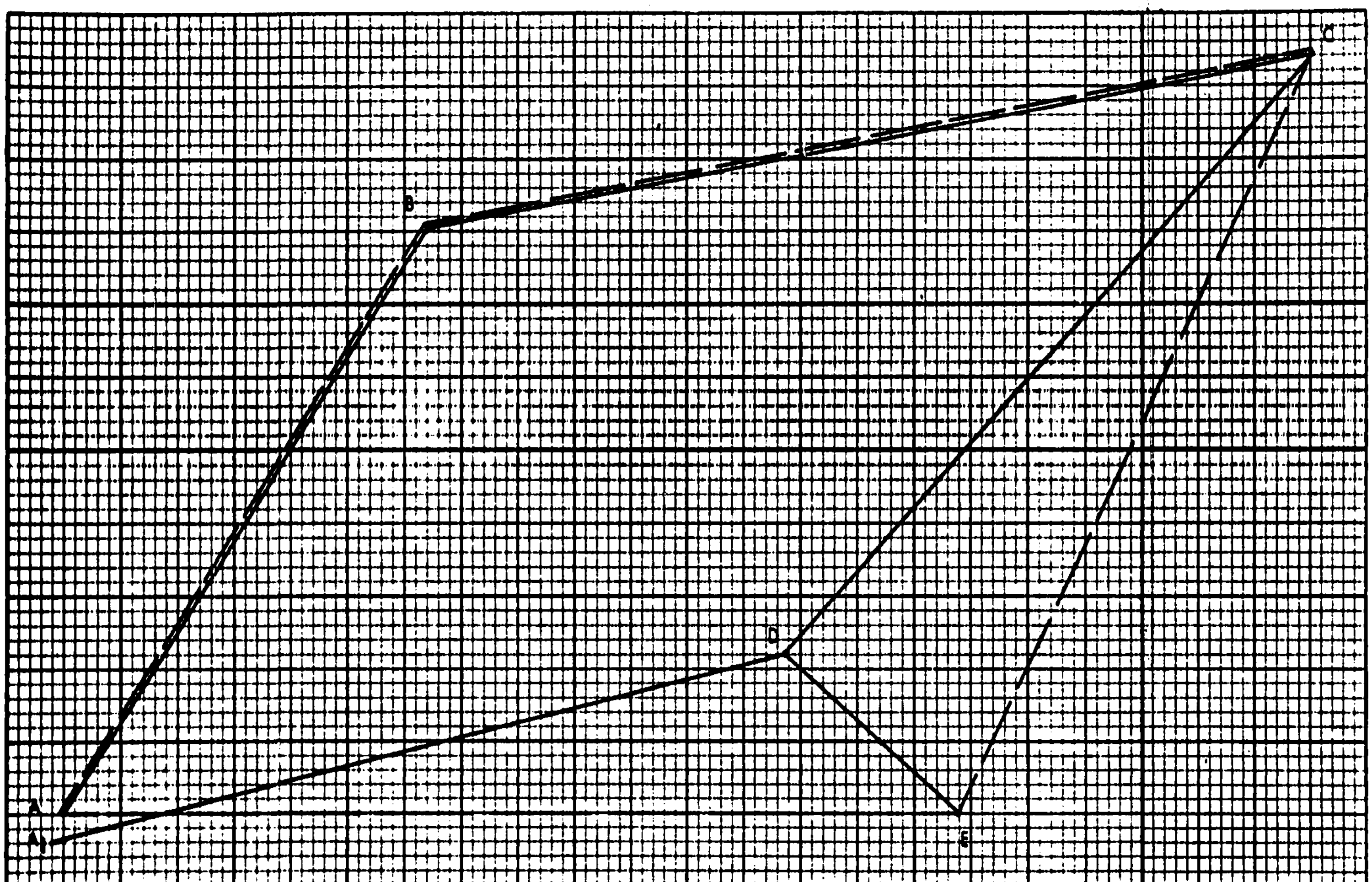

Horizontal Projection of Rockwall Traverse

(above cone 6801)

SCALE 1" = 76 m.

— — — Approximate boundary of rockwall area.

——— Actual traverse.

Fig. II.12

This value is 28,000 m^2 less than the mean area determined photogrammetically. This deviation is 13% of the latter value and is well within the scale of error for the photogrammetric method.

It is suggested that the values derived for all rock wall areas by this method are minimum values, as it was necessary to simplify the areas into triangles and rectangles which were in all cases slight under estimates of the true areas.

For all rock wall areas where ground traverses were used instead of photogrammetry the calculated values increased by 15% are taken as mean values for the rock wall area and the scale of error suggested for the method is $\pm$ 15%.*

ii) Special method of calculation of rock wall area above cone 6830

Plate 13 is a ground view of the rock wall area above cone 6830. It is composed approximately of two massive triangular walls, on either side of a narrow joint controlled gully.

* Although not precisely determined except in relation to the photogrammetrically determined values, the error in the case of the traverse method is for obvious reasons much less than in the case of the photogrammetric method.

The east wall may be considered in plan section (Fig. II.13).

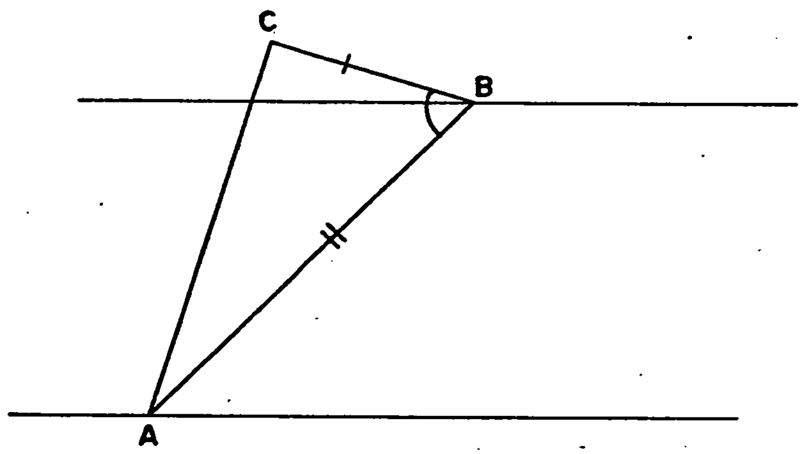

FIG. II.13

AB, along the inclined gully bottom, is readily calculated trigonometrically, the height difference between A and B having been obtained by aneroid barometer, and the slope angle from Abney level measurements. BC the distance along the rim of the cliff is similarly calculated. Angle ABC is obtained by summation of Abney angle readings from B to C and B to A.

Then, the area of ABC can be found from the following trigonometrical formula (Ayres, 1954, p. 109)

$$\text{Area of ABC} = (\text{BC} \times \text{AB} \times \sin \text{ABC})/2$$

Similarly the area of the west wall is found and the total wall area calculated.

For the rock walls above cones 6801, 6813, 6814, 6821, 6824, 6825 and 6830, the mean areas derived by the ground traverse method have been used in calculating erosion rates, because they are more accurate than photogrammetrically derived values. For the rock wall above cone 6801 the area was obtained using a special adaptation of the general ground traverse method. For the rock wall areas above cones 6804, 6808 and 6816 the values derived by photogrammetry have been used since ground traverses were not made. The mean, maximum and minimum values for all rock wall areas are indicated in Table II.7.

TABLE II.7

MEAN, MAXIMUM AND MINIMUM AREAS OF ROCK WALLS, ABOVE TEN TALUS CONES (in m^2)

Identification by associated cone	Mean area	Maximum area	Minimum area
6801	223,000	252,000	194,000
6804	190,800	248,000	141,000
6808	198,000	258,000	139,000
6813	155,000	195,000	134,000
6814	14,000	15,800	12,100
6816	288,000	375,000	202,000
6821	1,590	1,820	1,370
6824	73,000	82,000	63,000
6825	13,960	15,780	12,140
6830	48,000	54,000	42,000

3. CALCULATION OF RATES OF EROSION

The mean amount of erosion of the whole rock wall surface was then calculated by dividing the mean net volume of talus by the mean rock wall area. The maximum and minimum amounts of erosion are calculated using the following equations:

$$\text{Max. amount of erosion} = \frac{\text{max. net volume of talus}}{\text{min. rock wall area}}$$

$$\text{Min. amount of erosion} = \frac{\text{min. net volume of talus}}{\text{max. rock wall area}}$$

The mean maximum and minimum values for rock wall erosion are presented in Table 2.3 on p. 31.

The mean rock wall recession is then converted into the mean annual rate of erosion based on a 12,000 year time interval. The minimum and maximum amounts of rock wall recession are converted into the minimum and maximum rates of recession based on a possible 14,000 year and a possible 10,000 year time interval respectively. These rates of erosion expressed in mm/1,000 yrs are presented in Table 2.3.

APPENDIX III

EMPIRICAL EQUATIONS FOR AGGREGATE PARTICLE VOLUMES IN TERMS OF 'a', 'b' and 'c' AXES.

The volumes of a small number of sampled talus particles of dolomite, orthoquartzite and syenite lithology were calculated from the product of the density of the particles and their accurately measured weight. Rock densities for dolomites, quartzites and syenites range from 2.5 gm/cc to 2.9 gm/cc (Clark, 1966). The figure of 2.7 gm/cc approximates the density of all three rock types. Linear regression models were then derived relating the particle volumes to the product of the three axes as follows:

1) Syenite particles from cone 6830 (no. in sample = 73)

   Volume = 0.537 ('a' x 'b' x 'c') + 15.3

2) Orthoquartzite particles from cone 6824 (no. in sample = 100)

   Volume = 0.504 ('a' x 'b' x 'c') + 25.4

3) Dolomite particles from cone 6812 (no. in sample - 147)

   Volume = 0.602 ('a' x 'b' x 'c') + 6.9

In all cases the intercept constant is so small relative to the product 'a' x 'b' x 'c' that it may be neglected.

Limitations of these equations, when applied universally to debris volume calculations in the field areas, are that the samples are very small in relation to the total population of a talus cone and also that the 'a' axis of the particles used to derive the regression equations had to be limited to <15 cm for the sake of convenience in collecting and weighing the particles.

APPENDIX IV

MODEL TO ILLUSTRATE EFFECT OF SURFACE ROUGHNESS ON PARTICLES SLIDING AND ROLLING DOWNSLOPE

1. INTRODUCTION

The sliding or rolling of particles whose diameter is about the same as or smaller than the diameter of the debris already on the surface, and the sliding or rolling of a particle whose diameter is several times larger than the debris on the surface, is represented diagrammatically in Figure 4.5.

2. HYPOTHESIS 1

Hypothesis 1 states that on a slope assumed to be composed of frictionless debris, acceleration in the downslope direction is less for A than for B in Figure 4.5 due to the difference in the path traversed by the particle.

This is proved by considering a segment of any rough slope in isolation (Fig. IV.1).

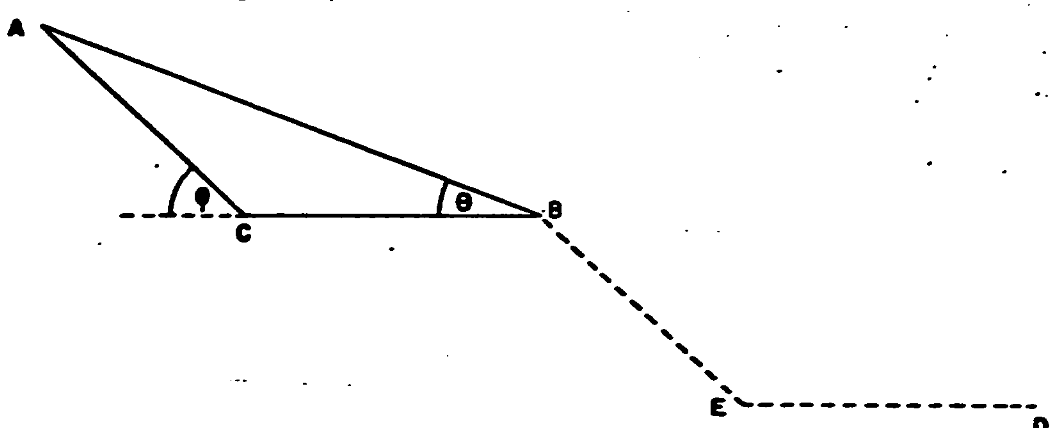

FIG. IV.1

AB and ACB can be regarded as small sections of the direct and indirect paths followed by particles in Figure 4.5. In order to find the velocity at B in the downslope direction after travel by either path, use is made of:

i) equation of motion:

$$v^2 = u^2 + 2\ gs \qquad \text{..... equation 1}$$

where v = final velocity of a particle in the direction of motion

u = initial velocity of a particle in the direction of motion

s = distance traversed

g = gravitational acceleration

ii) parallelogram of velocities, which resolves velocities into vector components.

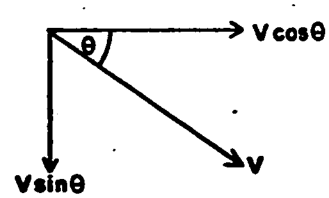

FIG. IV.2

In Figure IV.2 the horizontal and vertical components of velocity v are given as follows:

$$v_{horiz} = v\cos\theta \qquad \text{.... equation 2a}$$

$$v_{vert} = v\sin\theta \qquad \text{.... equation 2b}$$

Let it be assumed that in Figure IV.1 a particle starts to slide at A. Then the components of gravitational acceleration in the directions AB, AC and CB are, respectively, $g\sin\theta$, $g\sin\phi$ and 0.

i) For a particle starting from rest and moving by the direct route AB, velocity at B $= 0 + \sqrt{2AB\ g\sin\theta}$ (from equation 1)

$$= \sqrt{64.4 \times AB \sin\theta} \qquad \text{... equation 3}$$

ii) For a particle moving by indirect route ACB the velocity at B is calculated in two steps.

Velocity at C $= \sqrt{2\ ACg\sin\phi}$ (from equation 2)

But acceleration in direction CB $= 0$

$\therefore$ using eqns 1 & 2 velocity at B $= \sqrt{2\ ACg\sin\phi\cos^2\phi}$ .... equation 4

By giving sample values to AB and angles θ and ϕ, the final velocities at B for particles travelling by paths AB and ACB can be calculated

Let $\theta = 40^\circ$, $\phi = 60^\circ$, AB = 10 feet

$\therefore$ By elementary trigonometry

$$AC = \frac{10 \sin 40^\circ}{\sin 60^\circ} = 7.42 \text{ feet}$$

and

$$CB = \frac{10 \sin 20^\circ}{\sin 60^\circ} = 3.95 \text{ feet}$$

i) Path AB

Velocity at B for particle taking direct route AB

$$= \sqrt{64.4 \times \sin 40^\circ \times 10} \qquad \text{(from equation 3)}$$

$$= \underline{20.35 \text{ ft/sec}}.$$

This is now the initial velocity of the particle in a downslope direction for the next slope segment BD.

ii) Path ACB

Velocity at B for particle taking indirect route ACB

$$= \sqrt{2 \times 10\sin 40^{\circ} \times 32.2 \times \cos^{2} 60^{\circ}} \quad \text{(from equation 4)}$$

$$= \underline{11.74 \text{ ft/sec}}$$

The component of this velocity which can now act in a downslope direction as the particle continues down the next slope section

$$= 11.74 \cos 60^{\circ} \quad \text{(from equation 2a)}$$

$$= \underline{5.87 \text{ ft/sec}}$$

Thus the effective velocity at B for a particle taking the path ACB is only about one quarter of that for a particle taking the direct path AB and so the hypothesis is proved.

The same reasoning can be applied in the case of rolling motion except that the component of velocity in the downslope direction for a rolling solid sphere is 5/7 $g\sin\theta$ instead of $g\sin\theta$ (Mendenhall, Eve, Keys and Sutton, 1956, p. 84).

3. HYPOTHESIS 2

Hypothesis 2 suggests that if frictional retardation is now introduced into the model the downslope velocity at B will also be less for a particle starting from rest at A and travelling by path ACB.

Let the angles of static and kinetic friction have values less than the gradient of AB, e.g. 38° and 30° respectively so that a particle can be set in motion on the surface. Let λ represent the angle of kinetic friction.

In order to find the velocity at B after a particle has followed path AB or ACB the resultant of the downslope component of the gravitational acceleration due to gravity and the retardation due to friction must be calculated.

i) Path AB

Resultant acceleration in direction AB

$= g(\sin\theta - \tan\lambda\cos\theta)$ (see Fig. 4.4 and p. 87)

$= g(\sin 40^{\circ} - \tan 30^{\circ} \cos 40^{\circ})$

$= 6.45 \text{ ft/sec}^2$

$\therefore$ Velocity at B $= \sqrt{2 \times 6.45 \times AB}$ (from equation 1)

$= \underline{11.36 \text{ ft/sec}}$

ii) Path ACB

<u>Section AC</u>

Resultant acceleration in direction AC

$= g(\sin\phi - \tan\lambda\cos\phi)$

$= 32.2 (\sin 60^{\circ} - \tan 30^{\circ} \cos 60^{\circ})$

$= 18.56 \text{ ft/sec}^2$

$\therefore$ Velocity at C $= \sqrt{2 \times 18.56 \times AC}$ (from equation 1)

$= \sqrt{2 \times 18.56 \times 7.42}$

$= 16.6 \text{ ft/sec}$

Section CB

The component of velocity of the particle in the horizontal direction CB

$$= 16.6 \cos 60^\circ \qquad \text{(from equation 2a)}$$

$$= 8.3 \text{ ft/sec}$$

Gravitational acceleration in this direction is zero but retardation due to friction $= \tan 30^\circ$

$\therefore$ Velocity at B in horizontal direction CB (from equation 1)

$$= \sqrt{(8.3)^2 - 2 \tan 30^\circ \times CB}$$

$$= 8.21 \text{ ft/sec}$$

The component of this velocity in the new downslope direction BE

$$= 8.21 \cos 60^\circ \qquad \text{(from equation 2a)}$$

$$= \underline{4.11 \text{ ft/sec}}$$

Thus the downslope velocity at B for a particle taking the indirect route ACB is about one third of that at B for a particle taking the direct route AB and hypothesis 2 is proven. The same hypothesis is also true for a rolling particle although frictional retardation is much less than for a sliding particle.

In conclusion, rolling or sliding particles travelling by the indirect path ACB have a lower net acceleration downslope than particles travelling by the direct path AB with or without frictional retardation. Table IV.1 summarises the results of the given example.

TABLE IV.1

VARIATION IN VELOCITIES WHICH PARTICLES ATTAIN BY TRAVELLING BY DIRECT AND INDIRECT PATHS ON A SLOPE

	Velocity at B after direct path AB followed ft/sec	Velocity at B after indirect path ACB followed ft/sec
Smooth surface (frictionless)	20.35	5.87
Rough surface (inducing friction)	11.36	4.11

APPENDIX V

AMOUNT AND RATE OF ROCK WALL EROSION ABOVE ROCK GLACIER B20

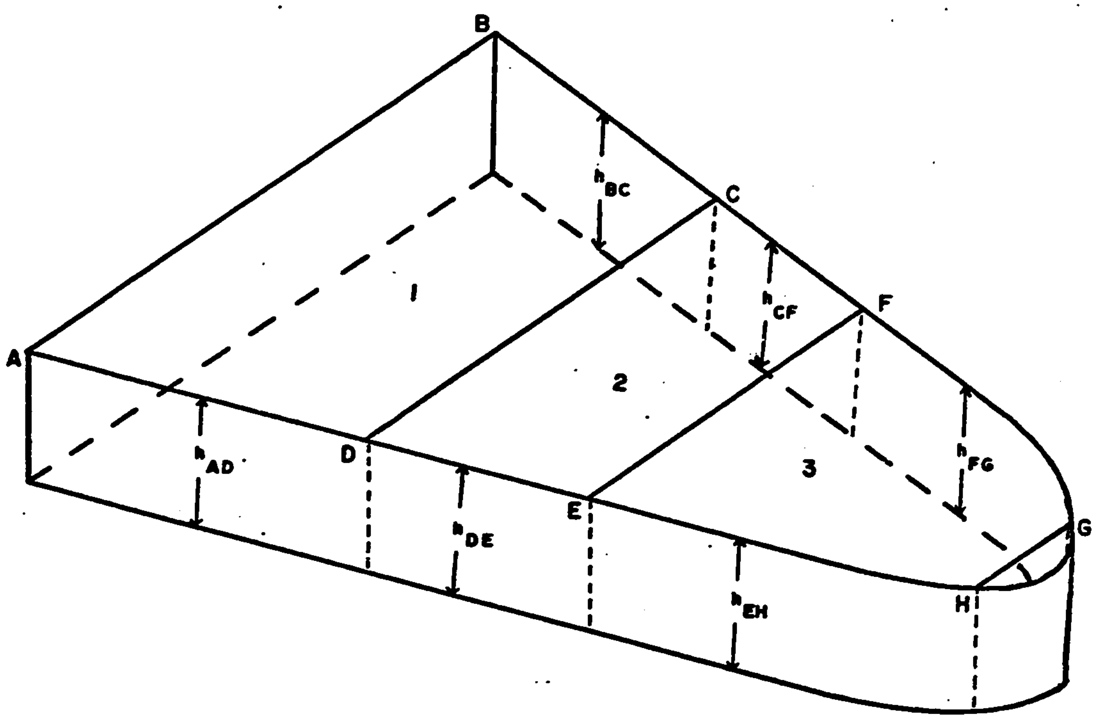

FIG. V.1

1. VOLUME OF DEBRIS IN ROCK GLACIER

The rock glacier is represented diagrammatically in Figure V.1.

$$\text{Bulk vol. of section 1} = \text{trapezoid area ABCD} \times \left(\frac{h_{AD} + h_{BC}}{2}\right)$$

$$= 29{,}600 \left(\frac{12 + 13.6}{2}\right) \text{cu.m}$$

$$= 379{,}000 \text{ cu.m}$$

Bulk vol. of section 2 $= \text{area DCFE} \times \left(\frac{h_{DE} + h_{CF}}{2}\right)$

$$= 16{,}900 \left(\frac{26.5 + 11}{2}\right) \text{cu.m}$$

$$= 318{,}000 \text{ cu.m}$$

Bulk vol. of section 3 $= \text{area EFGH} \times \left(\frac{h_{EH} + h_{FG}}{2}\right)$

$$= 10{,}100 \left(\frac{22 + 12}{2}\right) \text{cu.m}$$

$$= 172{,}000 \text{ cu.m}$$

Total bulk vol. of rock glacier B20 = 869,000 cu.m

Total net vol. of rock glacier B20 (assuming 30% porosity) = <u>608,300 cu.m</u>

2. ROCK WALL AREA

Horiz. rock wall area = 869,000 cu.m

Rock wall angle = 35° (approximately)

$\therefore$ Actual wall area $= \text{secant } 35^\circ \times 132{,}800 \text{ m}^2$

$$= 1.22 \times 132{,}800 \text{ m}^2$$

$$= \underline{162{,}000 \text{ m}^2}$$

3. AMOUNT AND RATE OF POSTGLACIAL ROCK WALL RECESSION

Amount of erosion $= \frac{608{,}300}{162{,}000}$ m

$= \underline{3.75 \text{ m}}$

Rate of erosion over postglacial period (i.e. 12,000 yrs approx.) $= \frac{3.75 \times 10^6}{12{,}000}$ mm/1,000 yr

$= \underline{313 \text{ mm/1,000 yr}}$

PLATES

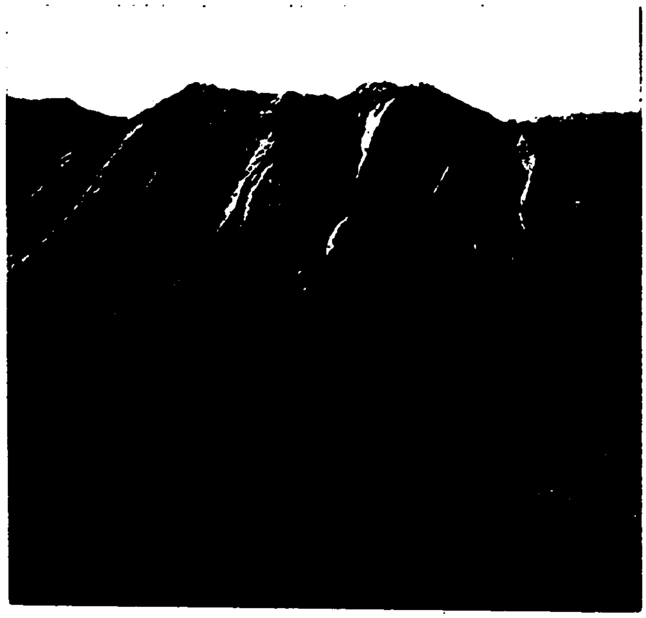

Plate 1 Rock wall gullies and talus cones in meta-sediments, north of Bear River airstrip. GSC 156927.

Plate 2 Talus aprons beneath syenite rock wall at Talus Lake, Tombstone Valley. Looking south west. GSC 156998.

Plate 1 Rock wall gullies and talus cones in meta-sediments, north of Bear River airstrip. GSC 156927.

Plate 2 Talus aprons beneath syenite rock wall at Talus Lake, Tombstone Valley. Looking south-west. GSC [illegible] 699H.

Plate 3 Valley-wall rock glacier B20 two miles west of Bear River, South Fork. Note the even crested ridges in the background. Looking east. GSC 156911.

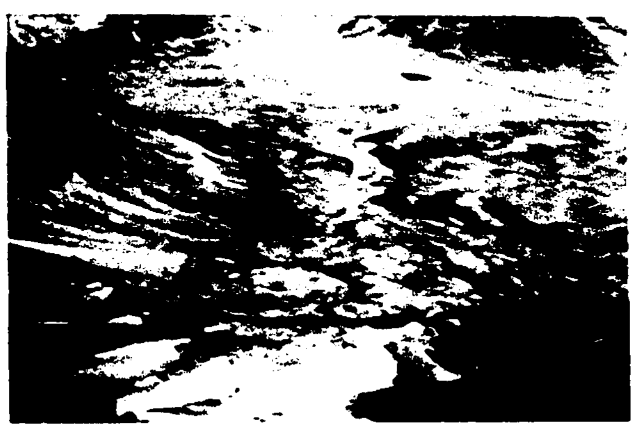

Plate 4 Protalus ramparts below the south wall of Mt. Frank Ray, Tombstone Valley.

Plate 3 Valley-wall rock glacier B20 two miles west of Bear River, South Fork. Note the even crested ridges in the background. Looking east. GSC 156911.

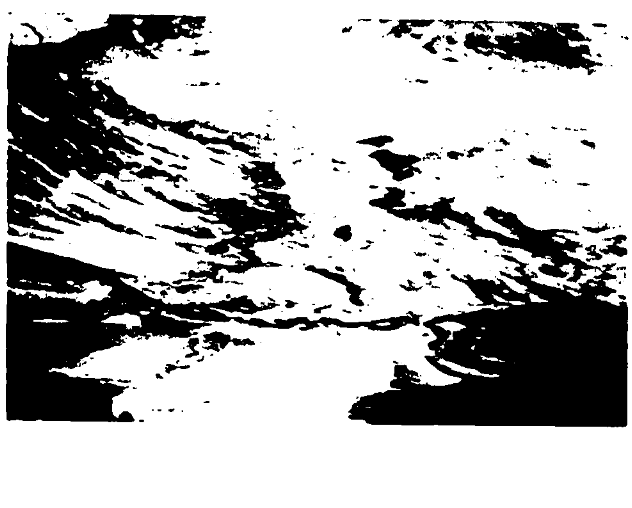

Plate 4 Protalus ramparts below the south wall of Mt. Frank Ray, Tombstone Valley.

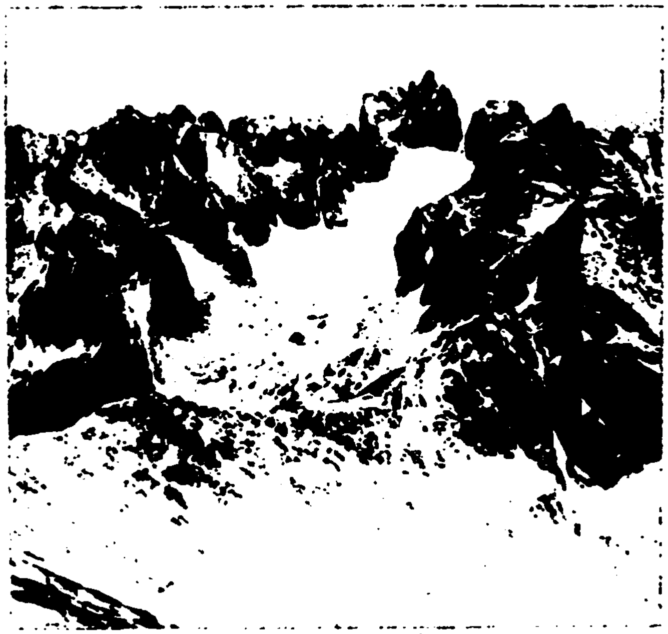

Plate 7 View westward across Tombstone syenitic intrusion. Note the narrow jagged arêtes.

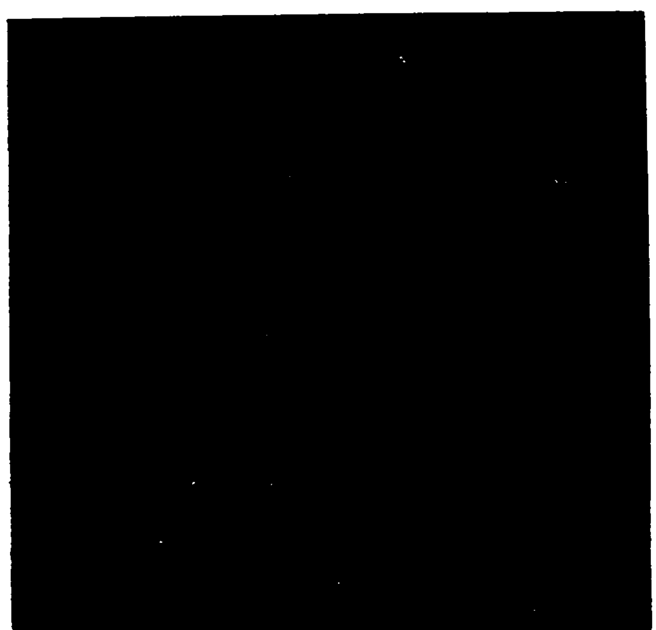

Plate 8 Contact zone between metasediments on left and igneous intrusives on right near the head of the North Klondike Valley, Tombstone region. Photograph taken in Mid-May 1967, looking south east. GSC 6-2-67.

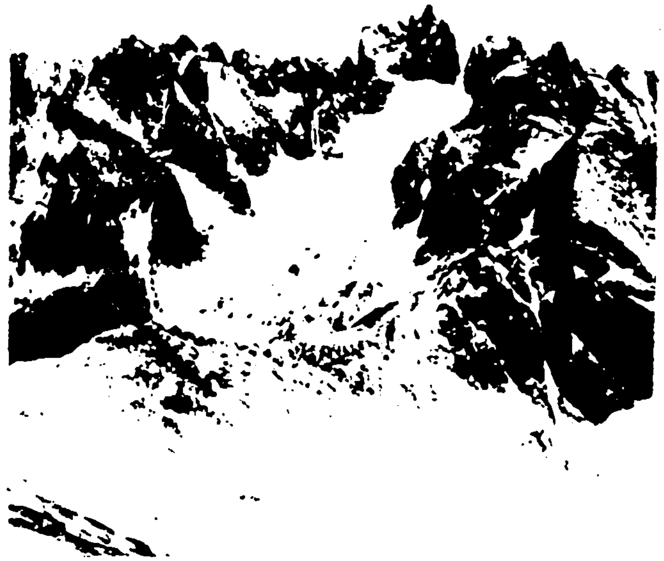

Plate 7 View westward across Tombstone syenitic intrusion. Note the narrow jagged arêtes.

Plate 8 Contact zone between metasediments on left and igneous intrusives on right near the head of the North Klondike Valley, Tombstone region. Photograph taken in Mid-May 196[illegible], looking south east. ([illegible] 6-[illegible]).

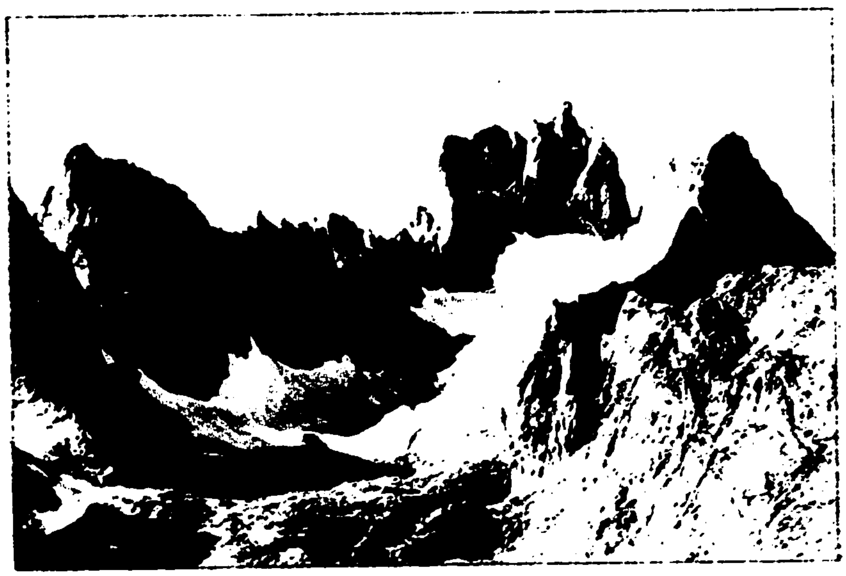

Plate 10 Small cirque glacier below east wall of Mt. Monolith, Tombstone region.

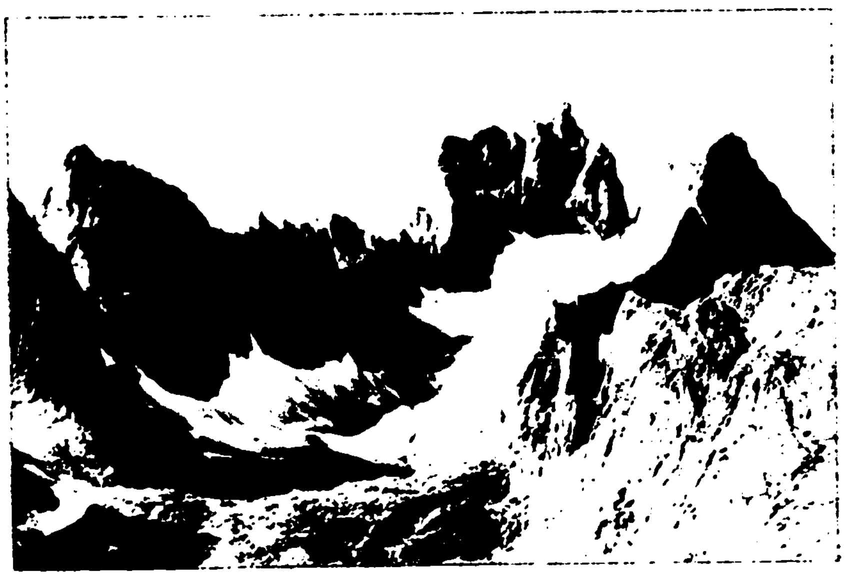

Plate 10 Small cirque glacier below east wall of
Mt. Monolith, Tombstone region.

Plate 11 Debris free avalanche on north facing slate and quartzite wall, Landslide Valley, Tombstone region. The avalanche occurred at the end of May 1967. G[illegible]C 9-7-67.

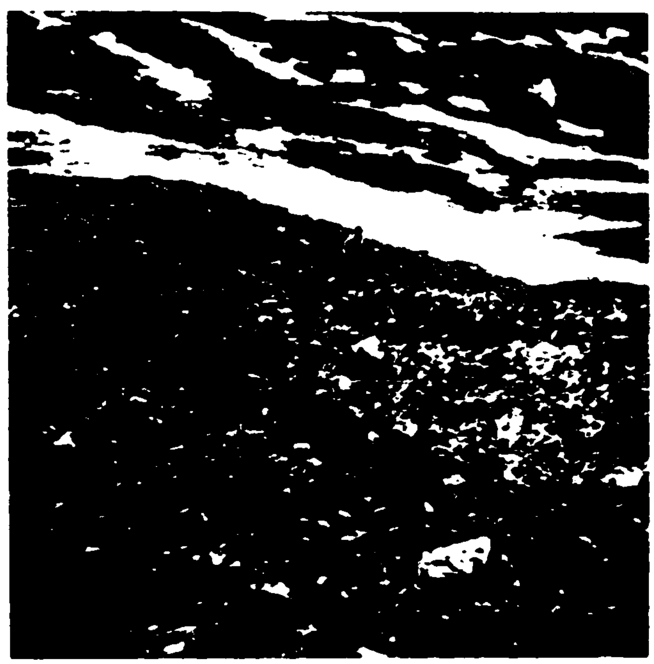

Plate 12 Debris laden avalanche on talus cone below north facing wall of Landslide Valley. Avalanche occurred in mid-June 1967. G[illegible]C 16-7-67.

Plate 11 Debris free avalanche on north facing slate and quartzite wall, Landslide Valley, Tombstone region. The avalanche occurred at the end of [illegible] 1967. [illegible] 9-7-67.

Plate [illegible] Debris laden avalanche on talus cone below north fac[illegible] wall of Landslide Valley. Avalanche [illegible]curred in mid-June 1967. [illegible]

Plate 13 Net for debris collection on talus cone 6830 above Talus Lake, Tombstone Valley. North facing rock wall is composed of syenite. GSC 157051.

Plate 14 Close-up of debris deposited on the net placed on metasedimentary cone 6620, Bear River Valley. GSC 157026.

Plate 13 Net for debris collection on talus cone 6630 above Talus Lake, Tombstone Valley. North facing rock wall is composed of syenite. GSC 157051.

Plate 14 Close-up of debris deposited on the net placed on metasedimentary cone 6620, Bear River Valley. GSC 1570[illegible]6.

Plate 15 Syenite rock wall south west of Divide Lake, Tombstone region. The debris from recent large rockfalls was measured along the base of this wall. GSC 1-5-67.

Plate 16 Slope in weathered syenites on the north side of Tombstone Valley exhibiting recent erosion in the form of large vertical gashes. GSC 157056.

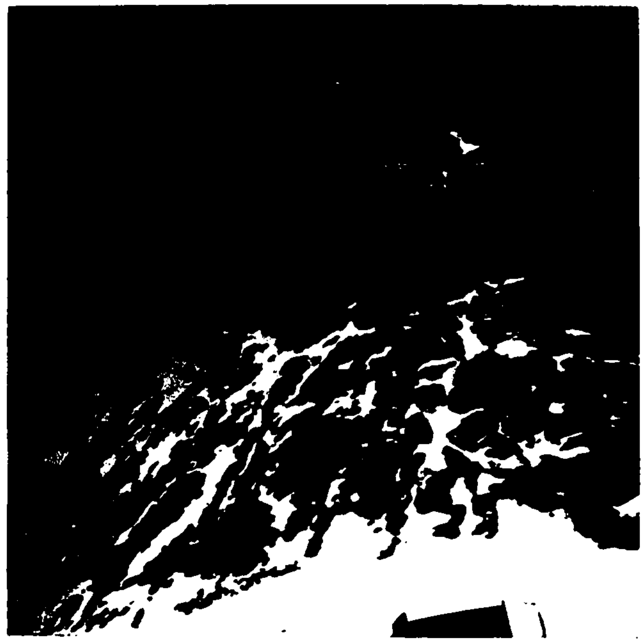

Plate 15 Syenite rock wall south west of Divide Lake, Tombstone region. The debris from recent large rockfalls was measured along the base of this wall. GSC 1-5-67.

Plate 16 Slope in weathered syenites on the north side of Tombstone Valley exhibiting recent erosion in the form of large vertical gashes. [illegible] 157056.

Plate 17 Tongue of a recent debris flow on the north slope of Tombstone Valley. GSC 13-1-67.

Plate 18 Molybdenite Rock Glacier (T1), Tombstone Valley. A localised area of house-sized syenite boulders indicates an unusually large rockfall in historical times. Photograph taken in mid-May 1967, looking east. GSC 4-8-67.

Plate 17 Tongue of a recent debris flow on the north slope of Tombstone Valley. GCC 13-1-67.

Plate 18 Molybdenite Rock Glacier (T1), Tombstone Valley. A localised area of house-sized syenite boulders indicates an unusually large rockfall in historical times. Photograph taken in mid-May 1967, looking east. GCC 4-6-67.

Plate 19 Fall sorting on syenite talus cone 6631, Tombstone region. Note the blocky angular nature of the debris. View southward. GSC 156978.

Plate 20 Fall sorting on slate and quartzite talus cone 6829, Landslide Valley, Tombstone region. Note the platy and angular nature of the debris. GSC 18-9-67.

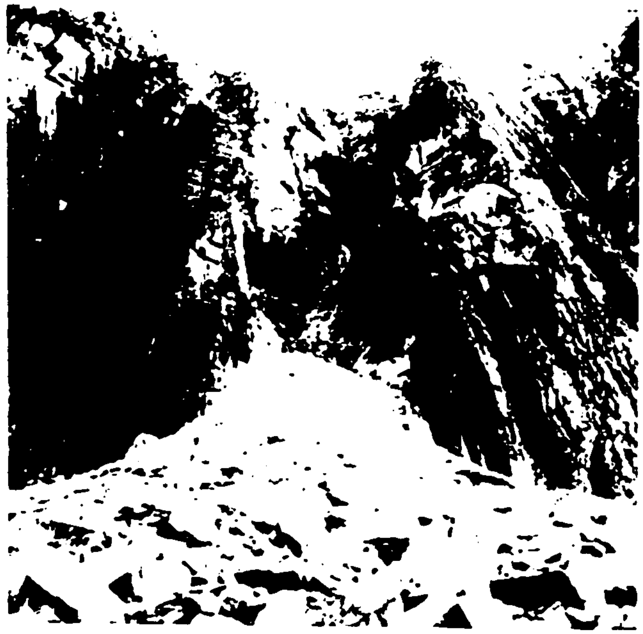

Plate 19 Fall sorting on syenite talus cone 6b31, Tombstone region. Note the blocky angular nature of the debris. View southward. GSC 156976.

Plate 20 Fall sorting on slate and quartzite talus cone 6b29, Landslide Valley, Tombstone region. Note the platy and angular nature of the debris. GSC 18-9-67.

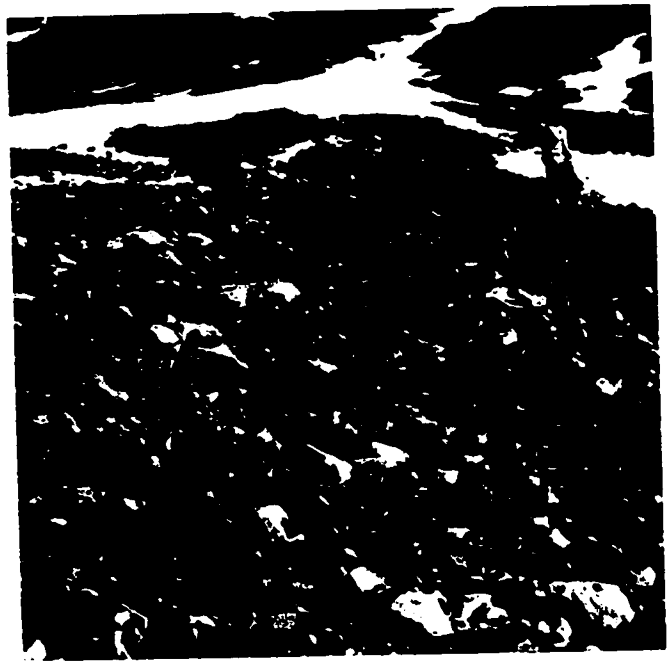

Plate 21 Apex of talus cone 6824, North Klondike Valley, Tombstone region. Note the variability in debris size within a narrow vertical zone. The main rock type is quartzite. GSC 14-1-67.

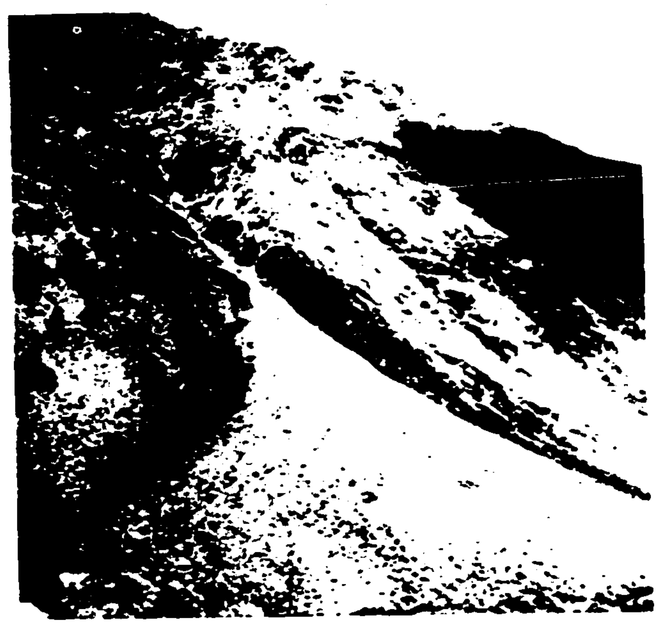

Plate 22 Lobate zone of fine debris fringed by coarse debris on southward facing dolomite talus cone. View from rock glacier 31E, Bear River Valley. GSC 156904.

Plate 1 Apex of talus cone 6+ 4, North Klondike Valley, Tombstone region. Note the variability in debris size within a narrow vertical zone. The main rock type is quartzite. [illegible] 14-1-67.

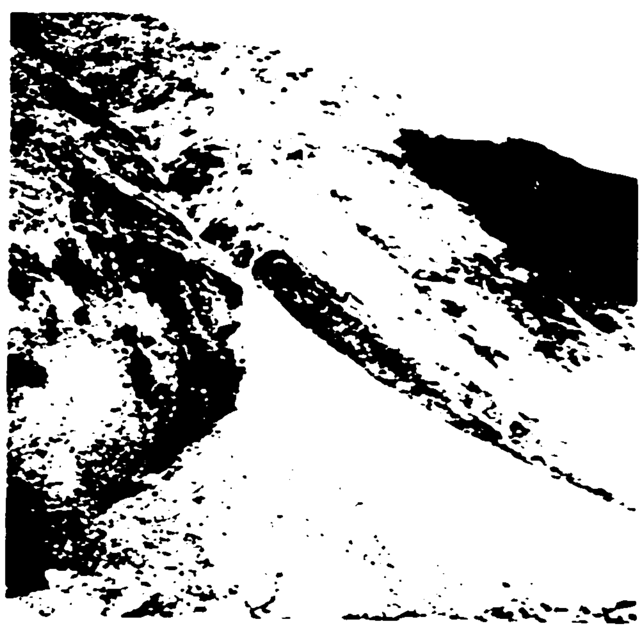

Plate [illegible] Lobate zone of fine debris fringed by coarse debris on southward facing dolomite talus cone. View from rock glacier [illegible], [illegible] River Valley. [illegible] 1,6?24.

Plate 23 Talus Lake Rock Glacier (T2), Tombstone Valley. In reality this is a debris-veneered glacier. The stratification is characteristic of glacier ice. GSC 156985.

Plate 24 Ablation debris perched on boulders on Talus Lake Rock Glacier. GSC 156987.

Plate 23 Talus Lake Rock Glacier (T2), Tombstone Valley. In reality this is a debris-veneered glacier. The stratification is characteristic of glacier ice. GSC 156985.

Plate 24 Ablation debris perched on boulders on Talus Lake Rock Glacier. GSC 156987.

Plate 25 Airstrip Rock Glacier, Bear River Valley. This is a cirque-floor rock glacier. Note the transverse ridges on the surface, and the probable lateral moraine beyond the far edge. GSC 156967.

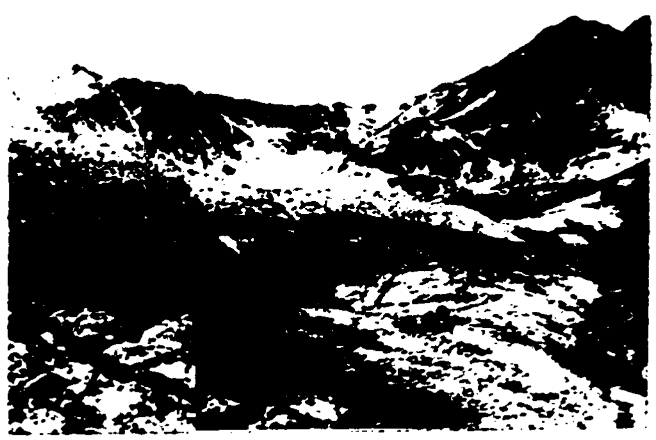

Plate 26 Snowline corresponding with springline on the front of rock glacier B20. Rock glacier in plan view is shown in plate 3. GSC 157011, 157012.

Plate 25 Airstrip Rock Glacier, Bear River Valley. This is a cirque-floor rock glacier. Note the transverse ridges on the surface, and the probable lateral moraine beyond the far edge. GSC 156967.

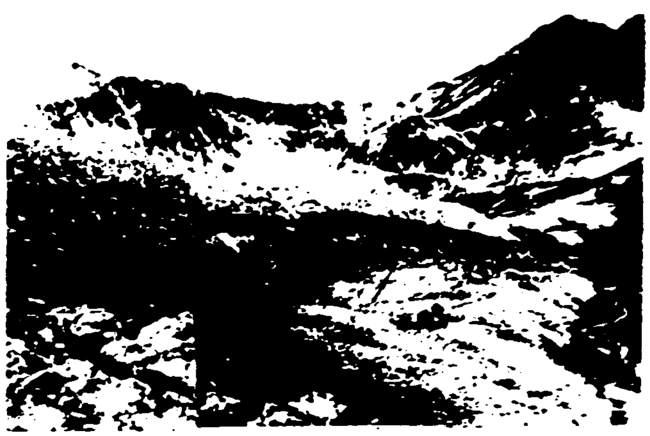

Plate 26 Snowline corresponding with springline on the front of rock glacier B2C. Rock glacier in plan view is shown in plate 3. GSC 157011, 157012.

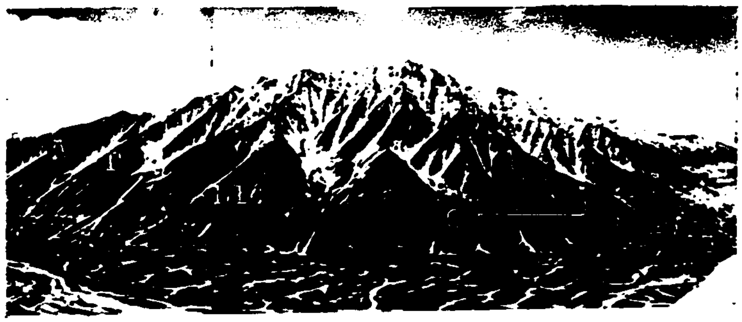

Plate 27 Rock glacier B14 on eastern side of Bear River Valley, South Fork. Note the distribution at A, B, C and D of other rock glaciers along the valley wall. GSC 156895, 156896, 156897.

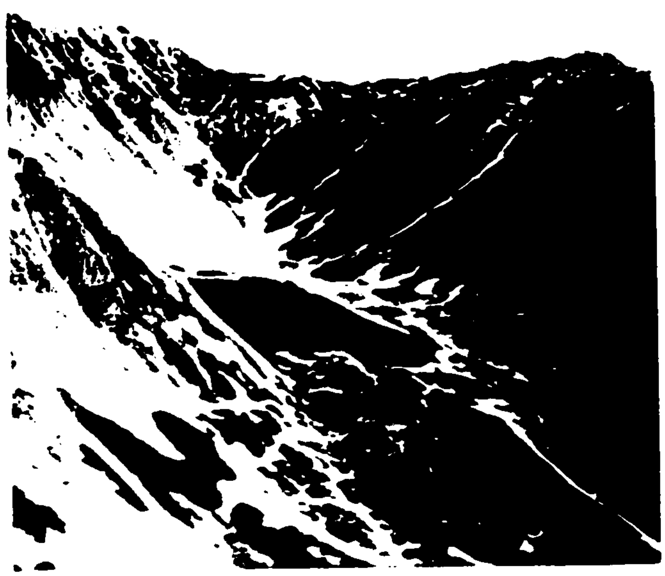

Plate 28 Stream diversion due to north westerly advance of cirque-floor rock glacier B18, Bear River Valley. GSC 156891.

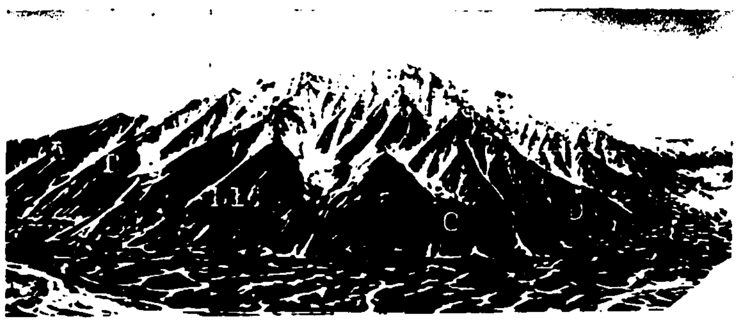

Plate 27 Rock glacier B14 on eastern side of Bear River Valley, South Fork. Note the distribution at A, B, C and D of other rock glaciers along the valley wall. GSC 156695, 156696, 156897.

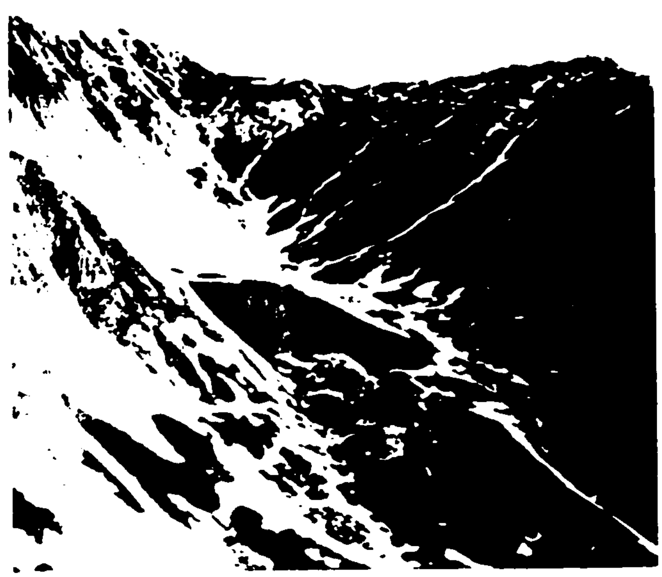

Plate 28 Stream diversion due to north westerly advance of cirque-floor rock glacier B16, Bear River Valley. GSC 156691.

REFERENCES

REFERENCES

ALLIX, A., 1924, Avalanches: Geog. Review, v. 14 p. 519-560.

ANDREWS, J.T., 1961, The development of scree slopes in the English Lake District and central Quebec-Labrador: Cahiers de Géog. de Québec, no. 10, p. 219-230.

______; 1969, Lichenometry to evaluate changes in glacial mass budgets: As illustrated from north central Baffin Island, N.W.T.: Arctic and Alpine Research, v. 1, p. 181-194.

______, and WEBBER, P.J., 1964, A lichenometrical study of the northwestern margin of the Barnes Ice Cap: A geomorphological technique: Geog. Bull. (Ottawa) no. 22, p. 80-104.

AYRES, F., 1954, Theory and problems of plane and spherical trigonometry, Schaum Co., New York

BEHRE, C.H. Jr., 1933, Talus behavior above timber in the Rocky Mountains; Jour. Geology, v. 41, p. 622-635.

BENEDICT, J.B., 1967, Recent glacial history of an alpine area in the Colorado Front Range, U.S.A., 1. Establishing a lichen-growth curve: Jour. Glaciol. v. 6, p. 817-832.

BESCHEL, R.E., 1958, Lichenometrical studies in West Greeland: Arctic, v. 11, 254 p.

______; 1961, Dating rock surfaces by lichen growth and its application to glaciology and physiography (lichenometry): Geology of the Arctic, v. 2, G.O. Raasch (ed) Univ. of Toronto Press, p. 1044-1062.

______; 1965, Epipetric succession and lichen growth rates in the eastern Nearctic: 7th Congress of Internat. Assoc. of Quaternary Research, Boulder, Colorado, Abstracts of General Sessions, p. 25-26.

BIRD, J.B., 1967, The physiography of Arctic Canada: Johns Hopkins Press, 336 p.

BOSTOCK, H.S., 1948, Physiography of the Canadian Cordillera, with special reference to the area north of the fifty-fifth parallel: Geol. Survey of Canada, Mem. 247, 106 p.

BROWN, R.J.E., 1970, Permafrost in Canada: Univ. of Toronto Press, 234 p.

BROWN, W.H., 1925, A probable fossil glacier: Jour. Geology, v. 33, p. 464-466.

CAINE, T.N., 1969, A model for alpine talus slope development by slush avalanching: Jour. Geology, v. 77, p. 92-101.

CAMSELL, C., 1905, Report on the Peel River and tributaries. Geol. Survey of Canada, 16th Ann. Report New Series., Publ. 200, p. 30-44.

CAPPS, S.R., 1910, Rock glaciers in Alaska: Jour. Geology, v. 18, p. 359-375.

CLARK, S.P. Jr., (ed) 1966, Handbook of Physical Constants: Geol. Soc. of America, Mem. 97.

COCHRAN, W.G., 1963, Sampling techniques: Wiley & Sons, N.Y. 413 p.

CORBEL, J., 1959, Vitesse de l'érosion: Zeit. fur Geomorph., v. 3, p. 1-28.

CROMPTON, P., 1968, Scree development of Baffin Island. B.A. Research Paper: Univ. of Toronto, 80 p.

DUCKWORTH, P.D., 1969, A laboratory method for determining the mass angle of repose of loose materials. B.A. Research paper: Univ. of Toronto.

DYCK, W. and FYLES, J.G., 1963, GSC Radiocarbon dates I and II: Geol. Survey of Canada, Paper 63-21.

______; and LOWDON, J.A., FYLES, J.G. and BLAKE, W. Jr., 1966, GSC Radiocarbon Dates V: Geol. Survey of Canada, Paper 66-48.

FAIRBRIDGE, R.W., (ed) 1968, Encyclopaedia of geomorphology, 966 p.

FLINT, R.F., 1967, Glacial and pleistocene geology: Wiley & Sons, N.Y., 553 p.

FOSTER, H.L., and HOLMES, G.W., 1965, A large transitional rock glacier in the Johnston River area, Alaska Range: U.S. Geol. Survey Prof. Paper 525-B, p. 112-116.

FRASER , H.J., 1935, Experimental study of the porosity and permeability of clastic sediments: Jour. Geology, v. 43, p. 910-1010.

FREISE, F.W., 1933, Beobachtungen über Erosion an Urwaldsgebirgsflüssen des brasilian Staates Rio de Janeiro: Zeit für Geomorph. v. 7, p. 2-3.

GARDNER, J., 1968, Debris slope forms and processes in Lake Louise district: a high mountain area. Unpubl. Ph.D. thesis, McGill Univ.

______; 1969, Observations of surficial talus movement: Zeit. für Geomorph. v. 13, p. 317-323.

______; 1970, Geomorphic significance of avalanches in the Lake Louise area, Alberta, Canada: Arctic and Alpine Research, v. 2, p. 135-144.

GOLDTHWAIT, R.P., 1966, Soil development, ecological succession in a deglaciated area of Muir Inlet, south east Alaska: 1 Glacial history. Inst. of Polar Studies, Ohio State Univ., Report no. 20, p. 1-17.

GRATON, L.C. and FRASER, H.J., 1935, Systematic packing of spheres - with particular relation to porosity and permeability: Jour. Geology, v. 43, p. 785-909.

GRAY, J.T., 1970, Mass wasting studies in the Ogilvie and Wernecke Mountains, central Yukon Territory: Geol. Survey of Canada, Paper 70-1A, p. 192-195.

GREEN, L.H., and RODDICK, J.A., 1962, Dawson, Larsen Creek and Nash Creek map areas, Yukon Territory: Geol. Survey of Canada, Paper 62-7.

HAURWITZ, C. and AUSTIN, A., 1944, Climatology: McGraw-Hill Inc. 410 p.

HUGHES, O.L., 1966, Logan Mountains, Y.T.: Measurements on a rock glacier: Ice, no. 20, p. 5.

JOCHIMSEN, M., 1966, Ist die Grösse des Flectenthallus Wirklichein brauchbarer Masstab zur Datierung von glazial morphologischen Relikten: Geografiska Ann., v. 48A(3), p. 157-164.

JUDSON, S., and RITTER, D.F., 1964, Rates of regional denudation in the United States. Jour. Geophys. Research, v. 69, p. 3395-3401.

KING, L.C., 1956, Research on slopes in South Africa. Premier Rapport, Commission pour l'étude des versants, Amsterdam: Internat. Geog. Union.

KING, R.H., 1969, Periglaciation on Devon Island, N.W.T.: Unpubl. Ph.D. thesis, Univ. of Saskatchewan.

KRUMBEIN, W.C., 1936, Application of logarithmic moments to size frequency distribution of sediments: Jour. Sed. Petrology, v. 6, p. 35-47.

LEBLANC, F., 1842, Observations sur le maximum d'inclination des talus dans les montagnes: Soc. Geol. de France, Bull. ser.1, v. 14, p. 85-88.

LANGBEIN, W.B. and SCHUMM, S.A., 1958, Yield of sediment in relation to mean annual precipitation: Am. Geophys. Union Trans., v. 39, p. 1076-1084.

LONEY, S.L., 1906, The elements of status and dynamics: Part 2 Dynamics, Cambridge Univ. Press.

______; 1960, Dynamics of a particle: Cambridge Univ. Press. 384 p.

LOWDON, J.A., and BLAKE, W. Jr., 1968, Geol. of Canada, Radiocarbon Dates VII in Radiocarbon, v. 10.

LUCKMAN, B.H., 1971, The role of snow avalanches in the evolution of alpine talus slopes: Pub. no. 3, Inst. of British Geographers, p. 93-110.

MARKGREN, L., 1964, Chute slopes in northern Fennoscandia: Lund Studies in Geography, Series A, no. 28.

MATTHES, F.E., 1938, Avalanche sculpture in the Sierra Nevada of California. Internat. Assoc. of Sci. Hydrol., Bull. 23, p. 631-637, Riga.

MELTON, M.A., 1965, Debris-covered hillslopes of the southern Arizona Desert - consideration of their stability and sediment contribution: Jour. Geology, no. 73, p. 715-729.

MENDENHALL, C.G., EVE, A.S., KEYS, D.A. and SUTTON, R.M., 1956, College physics: Heath & Co., Boston, 660 p.

NOBLES, L.H., 1966, Slush avalanches in north Greenland and the classification of rapid mass movements: Internat. Assoc. Sci. Hydrol. Publ. 69, p. 267-272.

NORRIS, P.W., and LEGGE, W.S., 1941, Mechanics via the calculus. Longman's Green & Co., 340 p.

OUTCALT, S.I. and BENEDICT, J.B., 1965, Photo-interpretation of two types of rock glacier in the Colorado Front Range: U.S.A. Jour. of Glaciol., v. 5, p. 849-856.

PEARCE, A.J., 1970, Postglacial rates of some denudation processes, Mt. St. Hilaire, Quebec: Unpubl. M.Sc. thesis, Dept. of Geological Sciences, McGill Univ., 61 p.

PORTER, S.C., 1966, Pleistocene geology of Anaktuvuk Pass, Central Brooks Range, Alaska: Tech. Papers of Arctic Institute of North America, no. 18.

PRANDTL, L., and TIETJENS, D.G., 1934, Applied hydro and aeromechanics: Dover Publications, N.Y., 311 p.

QUERVAIN, M.R. de, 1966, On avalanche classification: Internat. Assoc. Sci. Hydrol. v. 69, p. 410-418.

RAMPTON, V., 1969, Pleistocene geology of the Snag-Klutlan area south-western Yukon Terr. Canada. Unpubl. Ph.D. thesis, Univ. of Minnesota, 193 p.

RAPP, A., 1959, Avalanche boulder tongues in Lappland: Geografiska Ann.v.41, p. 34-48.

______; 1960a, Talus slopes and mountain walls at Tempelfjorden, Spitsbergen: Norsk Geol. Tiddsk. no. 119, p. 1-96.

______; 1960b, Recent developments of mountain slopes in Karkevagge and surroundings, northern Scandinavia: Geografiska Ann. v. 42, p. 71-200.

RAY, R.G., 1960, Aerial photographs in geologic interpretation and mapping: U.S. Geol. Survey Prof. Paper 373, 230 p.

REGER, R.D., 1968, Recent history of Gulkana and College Glaciers, central Alaska Range, Alaska: Jour. Geology, v. 76, p. 2-16.

RICKER, K., 1968, Quaternary geology in southern Ogilvie Ranges, Yukon Terr.: Unpubl. M.Sc. thesis, Dept. of Geology, Univ. of B.C. 211 p.

RUDBERG, S., 1963, Morphological processes and slope development in Axel Heiberg Island, N.W.T. Canada: Nach. Akad, Wis. Gottingen, Kl 2, no. 14, p. 218-228.

SHARPE, C.F.S., 1938, Landslides and related phenomena: Pageant Inc. New York, 137 p.

SNEDECOR, G., 1956, Statistical methods: Iowa State Univ. Press, 534 p.

STOCK, R., 1969, Morphology and development of talus slopes at Ekalugad Fjord, Baffin Island, N.W.T: Unpubl. B.A. thesis, Univ. of Western Ontario.

STORK, A., 1963, Plant immigration in front of retreating glaciers, with examples from the Kebnekajse area, northern Sweden: Geografiska Ann. v. 45, p. 1-22.

TEMPELMAN-KLUIT, D.J., 1970, Stratigraphy and structure of the "Keno Hill Quartzite" in Tombstone River - Upper Klondike River map areas, Yukon Terr. Geol. Survey of Canada Bull. 180.

THOMPSON, W.F., 1962, Preliminary notes on the nature and distribution of rock glaciers relative to true glaciers and other effects of the climate on the ground in North America: Ass. Internat. Hydrologie Sci., Comm. des Neiges et Glaces, p. 212-219.

TIMOSHENKO, S. and YOUNG, D.M., 1948, Advanced dynamics: McGraw-Hill, New York, 400 p.

VAN BURKALOW, A., 1945, Angle of repose and angle of sliding friction: an experimental study: Geol. Soc. America Bull. v. 56, p. 669-708.

VERNON, P. and HUGHES, A.L., 1966, Surficial geology, Dawson, Larsen Creek and Nash Creek map areas, Yukon Terr: Geol. Survey of Canada Bull. 136, 23 p.

WAHRHAFTIG, C. and COX, A., 1959, Rock glaciers in the Alaska Range. Geol. Soc. America Bull. v. 70, p. 383-436.

WASHBURN, A.L., and GOLDTHWAIT, R.P., 1958, Slush flows: Geol. Soc. America Bull. v. 69, p. 1657-1658.

WENTWORTH, C.K., 1922, A scale of grade and class terms for clastic sediments: Jour. Geology, v. 30, p. 377-392.

WOLMAN, M.G. and MILLER, J.P., 1960, Magnitude and frequency of forces in geomorphic processes: Jour. Geology, v. 68, p. 54-74.

WHITE, S.E., 1969, Rock glacier studies in the Colorado Front Range, 1961-1968: Arctic and Alpine Research, v. 3, p. 43-64.

YOUNG, A., 1956, Scree profiles in west Norway: in Premier Rapport, Comm. pour l'Etude des Versants, Amsterdam: Internat. Geog. Union.

12

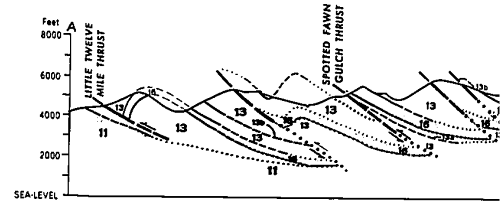

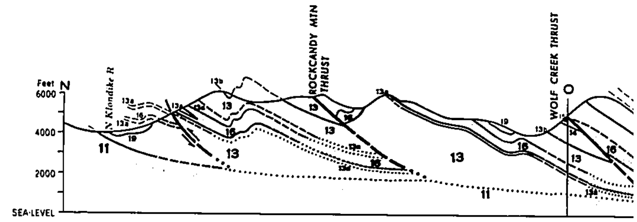

LEGEND

CENOZOIC

QUATERNARY

19	Drift

MESOZOIC

CRETACEOUS

MIDDLE CRETACEOUS (?)

18 — *Amphibole pyroxene syenite, pyroxene amphibole monzonite, hornblende quartz monzonite; medium-to coarse-grained, commonly porphyritic (orthoclase), with trachytoid texture: medium-grained biotite quartz monzonite and biotite quartz diorite near margins: minor granite: related porphyritic biotite latite and pyroxene trachyte dykes; 18a, pseudoleucite tinguaite*

17 — *Medium-grained porphyritic (hornblende) diorite*

LOWER CRETACEOUS (?)

16 — *Brown weathering, dark green diabase, tholeiitic diabase and medium-grained gabbro; sheared and altered equivalents*

Buff to brown weathering, thinly laminated and crosslaminated lime-cemented quartz siltstone with interbedded greyish brown shale; detrital muscovite ubiquitous

14 — *Pale green and bright red phyllitic siliceous slate with minor pale green argillaceous chert*

13 — *'KENO HILL QUARTZITE': resistant, thick-bedded, massive, light, medium and dark grey, fine-grained orthoquartzite with lesser interbedded black slate. Includes undifferentiated 13a and 13b. 13a, black slate and phyllitic with lesser greenish spotted slate; minor brownish quartz siltstone; 13b, buff weathering, brownish, thick-bedded, fine-grained, sandy limestone with minor interbedded brownish slate*

JURASSIC

Black, graphitic slate and phyllitic slate with minor interbedded brown siltstone; brownish green argillite at base; ironstone concretions plentiful in lower part

JURASSIC (?)

11 — *'LOWER SCHIST': black, graphitic slate and phyllitic slate with lesser interbedded chert-pebble conglomerate and immature feldspathic subgreywacke in lower part; minor pale green siliceous phyllite at top*

TRIASSIC

UPPER TRIASSIC (?)

10 — *Dark grey to black shaly and platy, fetid micritic limestone, locally contains pelecypod fragments and small chert pebbles*

LOWER, MIDDLE AND UPPER TRIASSIC

9 — *Dark grey, impure fossiliferous, platy micritic limestone (upper part) and thin-bedded, greywacke-like siltstone and shale (lower part)*

PALEOZOIC

PERMIAN

UPPER PERMIAN

TAHKANDIT FORMATION: grey and white, crystalline skeletal limestone rusty to light grey weathering, partially silicified and dolomitized; chert-pebble conglomerate at base, interbedded black chert in middle part

ORDOVICIAN AND SILURIAN

7 — *ROAD RIVER FORMATION: grey, black and pale green, thick-bedded chert with interbedded black slate (lower part), greenish grey argillite and siliceous argillite with minor interbedded black crystalline limestone (upper part)*

CAMBRIAN (?)

6 — *Brownish weathering, thin-bedded siltstone with minor interbedded greenish shale and chert*

CAMBRIAN (?) - SILURIAN (?)

5 — *Greenish grey weathering, massive, altered, amygdaloidal augite basalt with lesser lapilli tuff and volcanic breccia; calcite-filled vesicles and fractures; minor interbedded shale and grey crystalline limestone*

PROTEROZOIC AND/OR CAMBRIAN

CAMBRIAN (?)

c — *Massive to thin-bedded, deep maroon and light green slate and argillite; minor chert, limestone and quartz-pebble conglomerate*

Buff and yellowish weathering, submature, medium sand sized, lime-cemented feldspathic orthoquartzite; minor interbedded siltstone and shale; ... bottom part

Massive dark grey and blue-grey, partially recrystallized

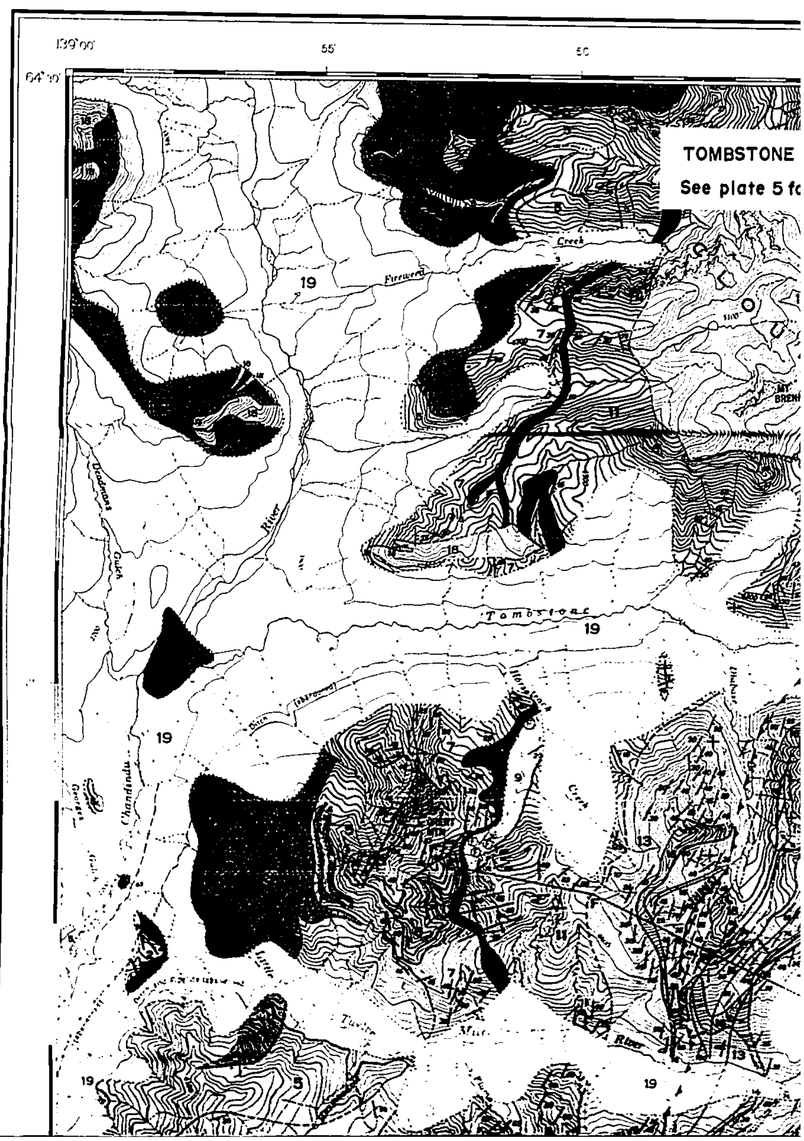

GEOLOGICAL SURVEY OF CANADA
DEPARTMENT OF ENERGY, MINES AND RESOURCES

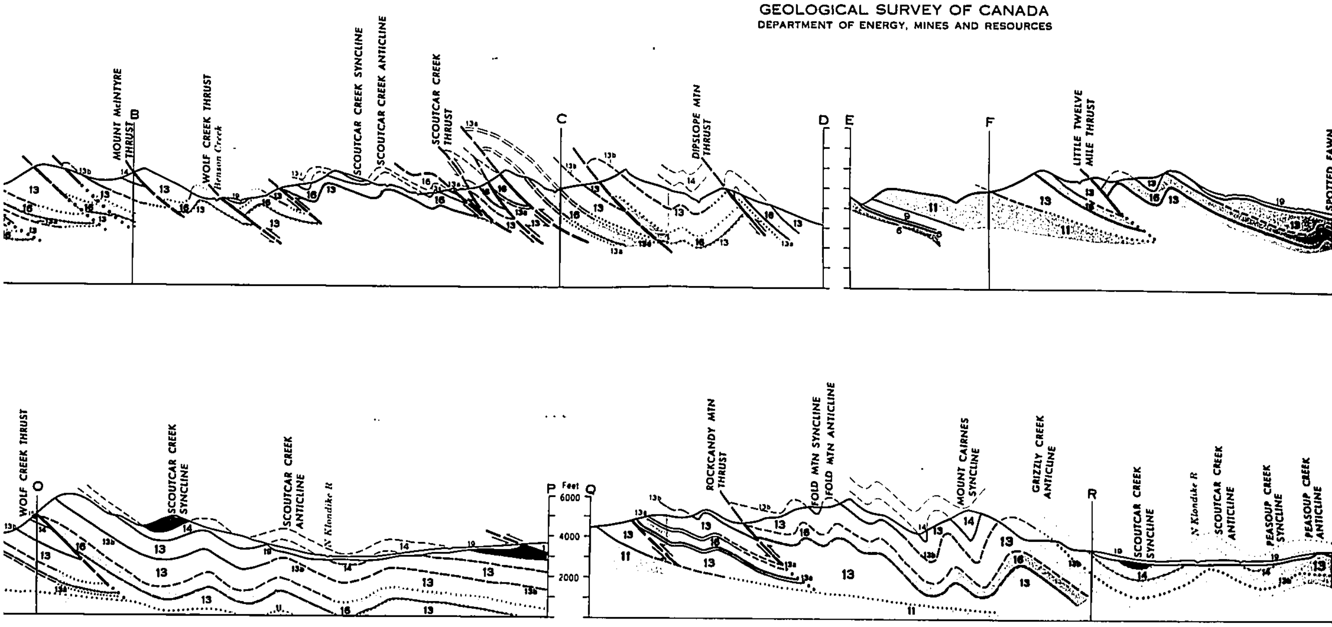

Diagrammatic cross-sections along lines A-D, E-M, N-P, Q-S, T-V

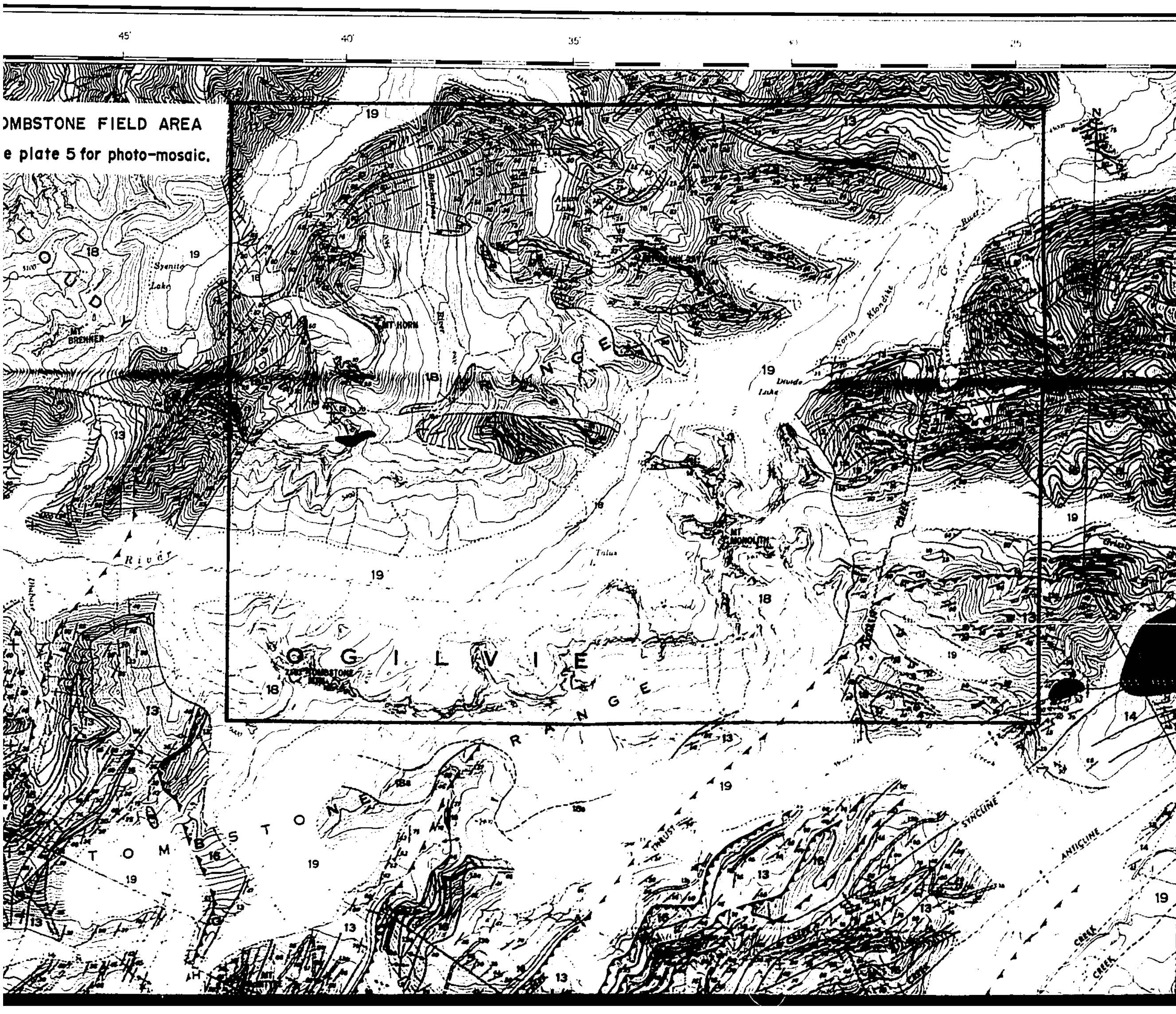

GEOLOGICAL SURVEY OF CANADA
DEPARTMENT OF ENERGY, MINES AND RESOURCES

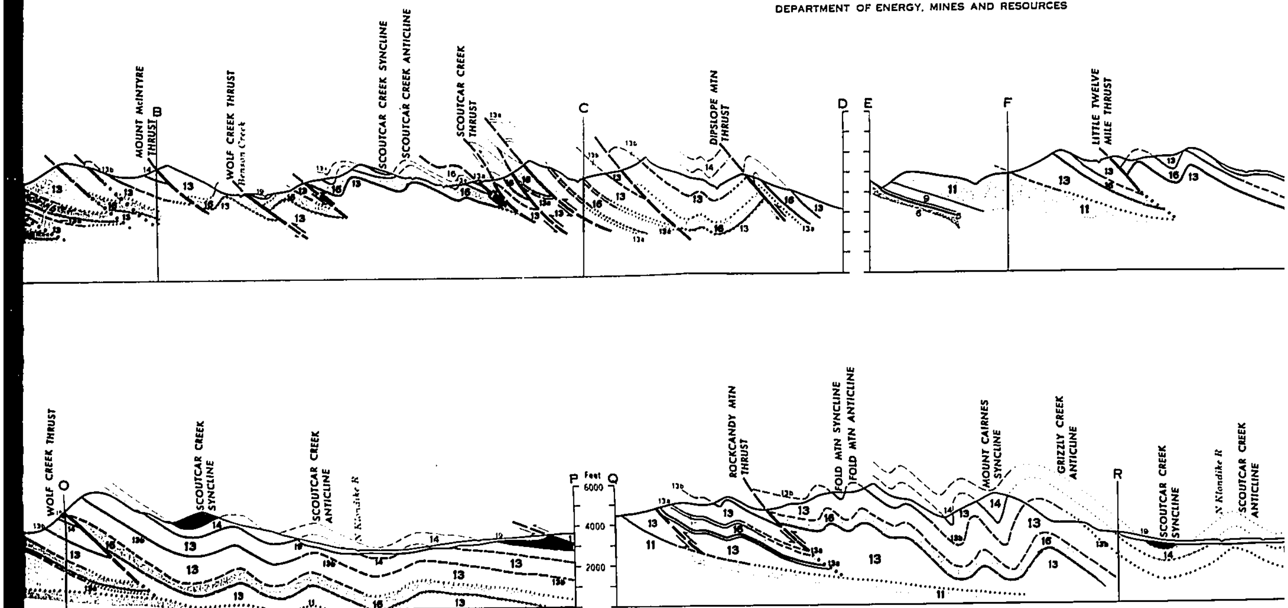

Diagrammatic cross-sections along lines A-D, E-M, N-P, Q-S, T-V

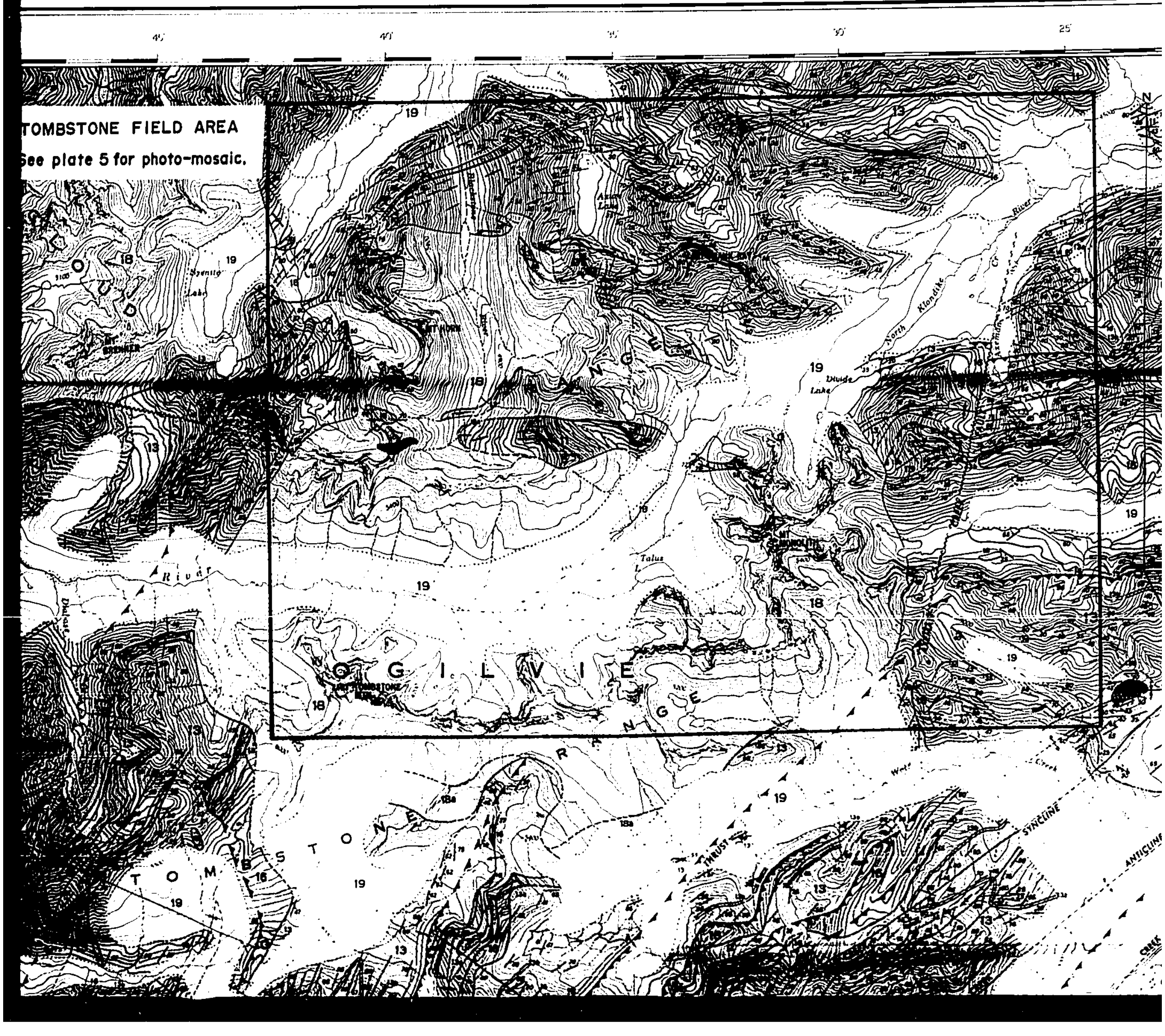

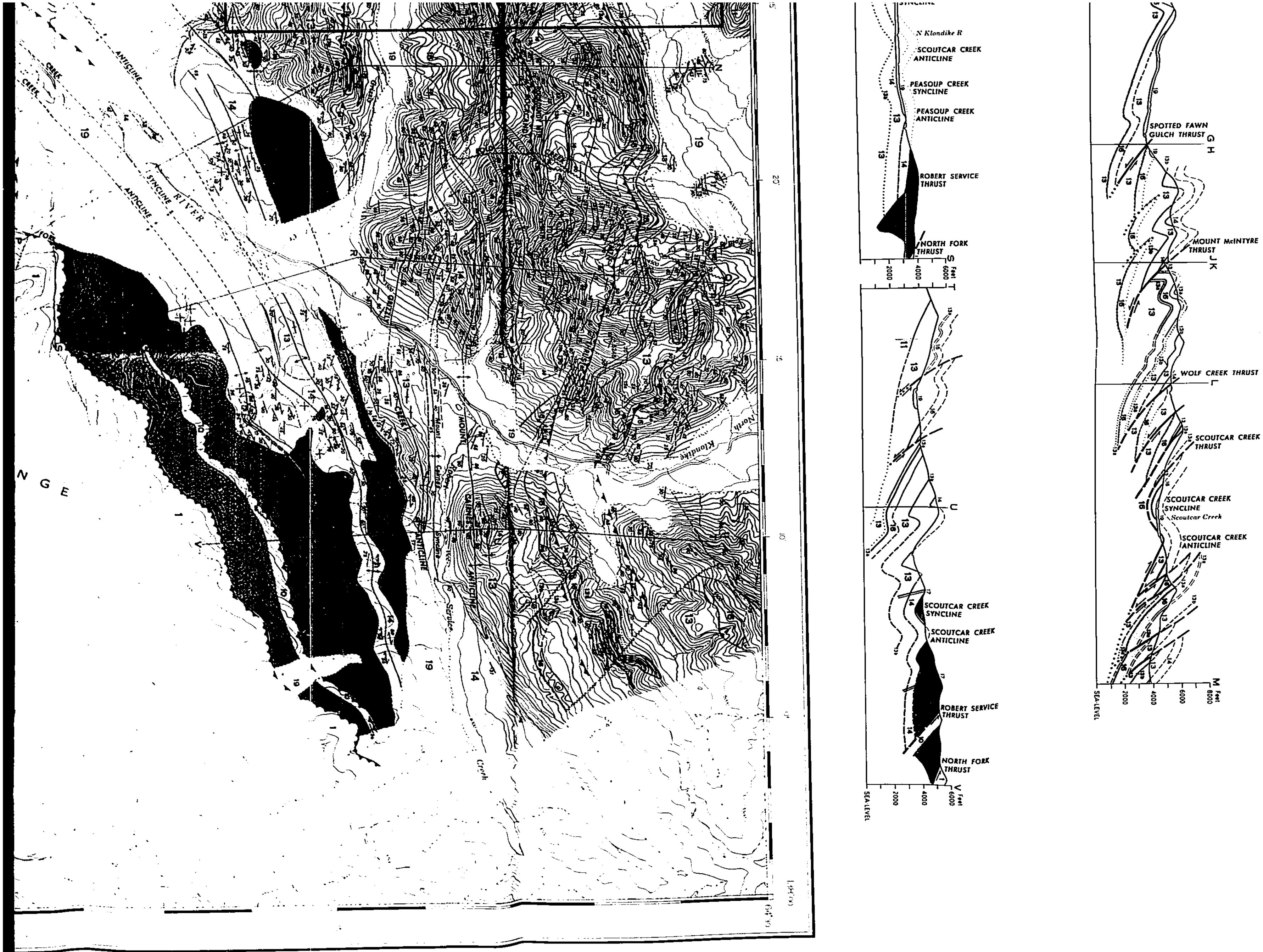
N Klondike R
SCOUTCAR CREEK ANTICLINE
PEASOUP CREEK SYNCLINE
PEASOUP CREEK ANTICLINE
ROBERT SERVICE THRUST
NORTH FORK THRUST
SCOUTCAR CREEK SYNCLINE
SCOUTCAR CREEK ANTICLINE
ROBERT SERVICE THRUST
NORTH FORK THRUST
SPOTTED FAWN GULCH THRUST
MOUNT McINTYRE THRUST
WOLF CREEK THRUST
SCOUTCAR CREEK THRUST
SCOUTCAR CREEK SYNCLINE
Scoutcar Creek
SCOUTCAR CREEK ANTICLINE
Feet
6000
4000
2000
SEA-LEVEL
8000

27.

pale green siliceous phyllite at top

TRIASSIC

UPPER TRIASSIC (?)

10 — *Dark grey to black shaly and platy, fetid micritic limestone; locally contains pelecypod fragments and small chert pebbles*

LOWER, MIDDLE AND UPPER TRIASSIC

9 — *Dark grey, impure fossiliferous, platy micritic limestone (upper part) and thin-bedded, greywacke-like siltstone and shale (lower part)*

PALEOZOIC

PERMIAN

UPPER PERMIAN

TAHKANDIT FORMATION grey and white, crystalline skeletal limestone rusty to light grey weathering, partially silicified and dolomitized chert-pebble conglomerate at base; interbedded black chert in middle part

ORDOVICIAN AND SILURIAN

7 — *ROAD RIVER FORMATION grey, black and pale green, thick-bedded chert with interbedded black slate (lower part), greenish grey argillite and siliceous argillite with minor interbedded black crystalline limestone (upper part)*

CAMBRIAN (?)

6 — *Brownish weathering, thin-bedded siltstone with minor interbedded greenish shale and chert*

CAMBRIAN (?) - SILURIAN (?)

5 — *Greenish grey weathering, massive, altered, amygdaloidal augite basalt with lesser lapilli tuff and volcanic breccia; calcite filled vesicles and fractures, minor interbedded shale and grey crystalline limestone*

PROTEROZOIC AND/OR CAMBRIAN

CAMBRIAN (?)

4 — *Massive to thin-bedded, deep maroon and light green slate and argillite, minor chert, limestone and quartz-pebble conglomerate*

Buff and yellowish weathering, submature, medium sand sized, lime-cemented feldspathic orthoquartzite; minor interbedded siltstone and shale oncolites in bottom part

2 — *Massive dark grey and blue-grey, partially recrystallized, silicified and dolomitized, oncolitic micritic limestone*

PROTEROZOIC

PROTEROZOIC (?)

1 — *Mature, feldspathic subgreywacke-pebble conglomerate with lesser olive green slate, maroon and green slate and dark grey limestone*

Geological boundary (defined, approximate, assumed)

Bedding, tops known (horizontal, inclined, vertical)

Bedding, tops unknown (inclined)

Cleavage (inclined, vertical)

Fault (defined, approximate, assumed)

Thrust fault (teeth in direction of dip, defined, approximate, assumed)

Anticline (defined, approximate inferred under drift)

Syncline (defined, inferred under drift)

Fossil locality

Geology by D.J. Tempelman-Kluit 1964, 1965

To accompany GSC Bulletin 180, by D.J. Tempelman-Kluit

Geological cartography by the Geological Survey of Canada, 1969

Road, all weather

Cart track

Intermittent lake and stream

Power transmission line

Horizontal control point

Marsh

Sand

Contours (interval 100 feet)

Height in feet above mean sea-level

Base map compiled and drawn by the Surveys and Mapping Branch 1961 1965

Approximate magnetic declination 1968 33 ... East decreasing 3... annually

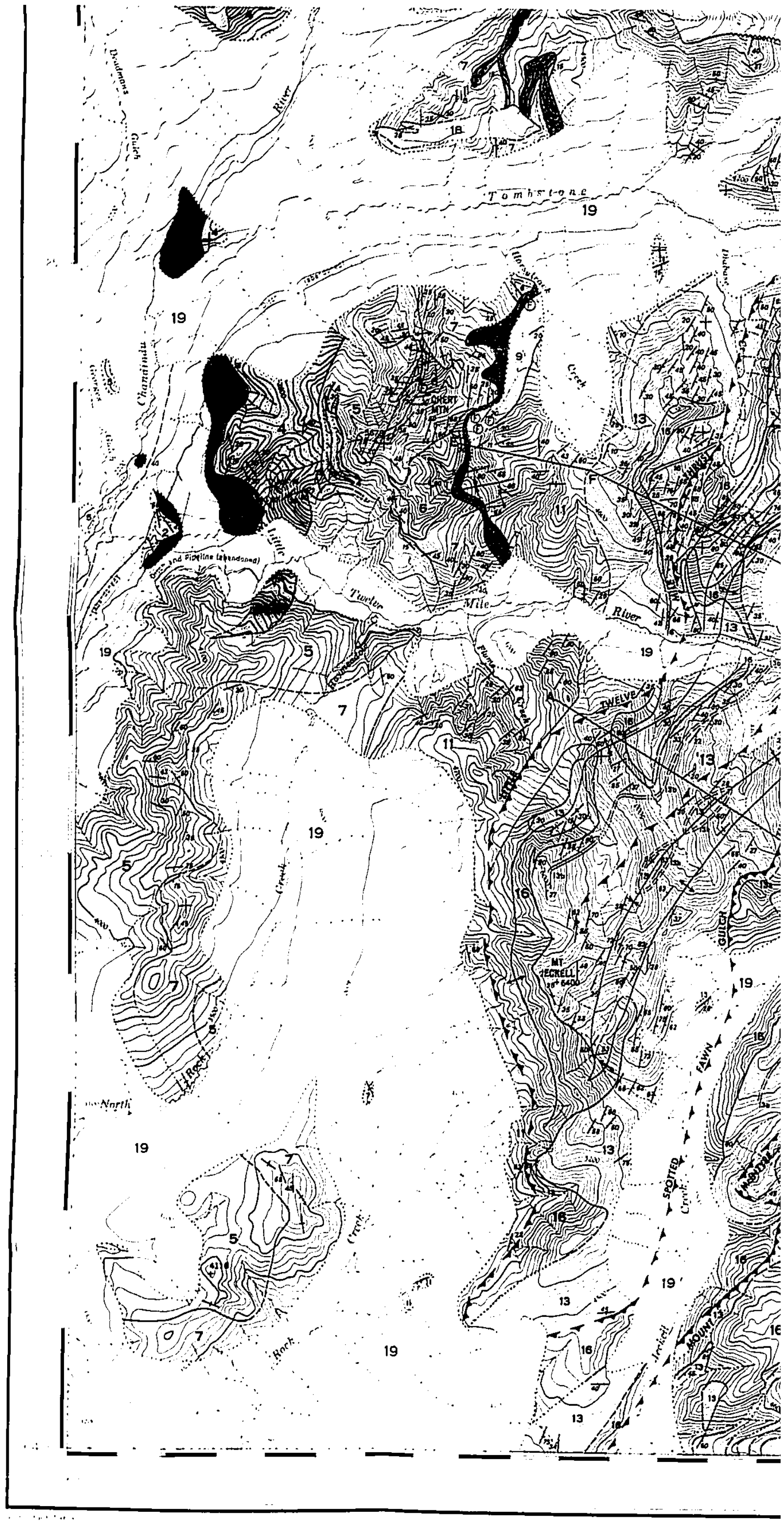

3 of

MAP 1248A

GEOLOGY

TOMBSTONE RIVER - UPPER KLONDIKE RIVER

YUKON TERRITORY

Scale 1:63,360

(1 inch to 1 mile)

Miles 0 1 2 3 Miles

Metres 0 1000 2000 3000 4000 5000 Metres

MAP 1248A

GEOLOGY

TOMBSTONE RIVER - UPPER KLONDIKE RIVER

YUKON TERRITORY

Scale 1:63,360

(1 inch to 1 mile)

Miles 1 0 1 2 3 Miles

Metres 1000 0 1000 2000 3000 4000 5000 Metres

MAP I

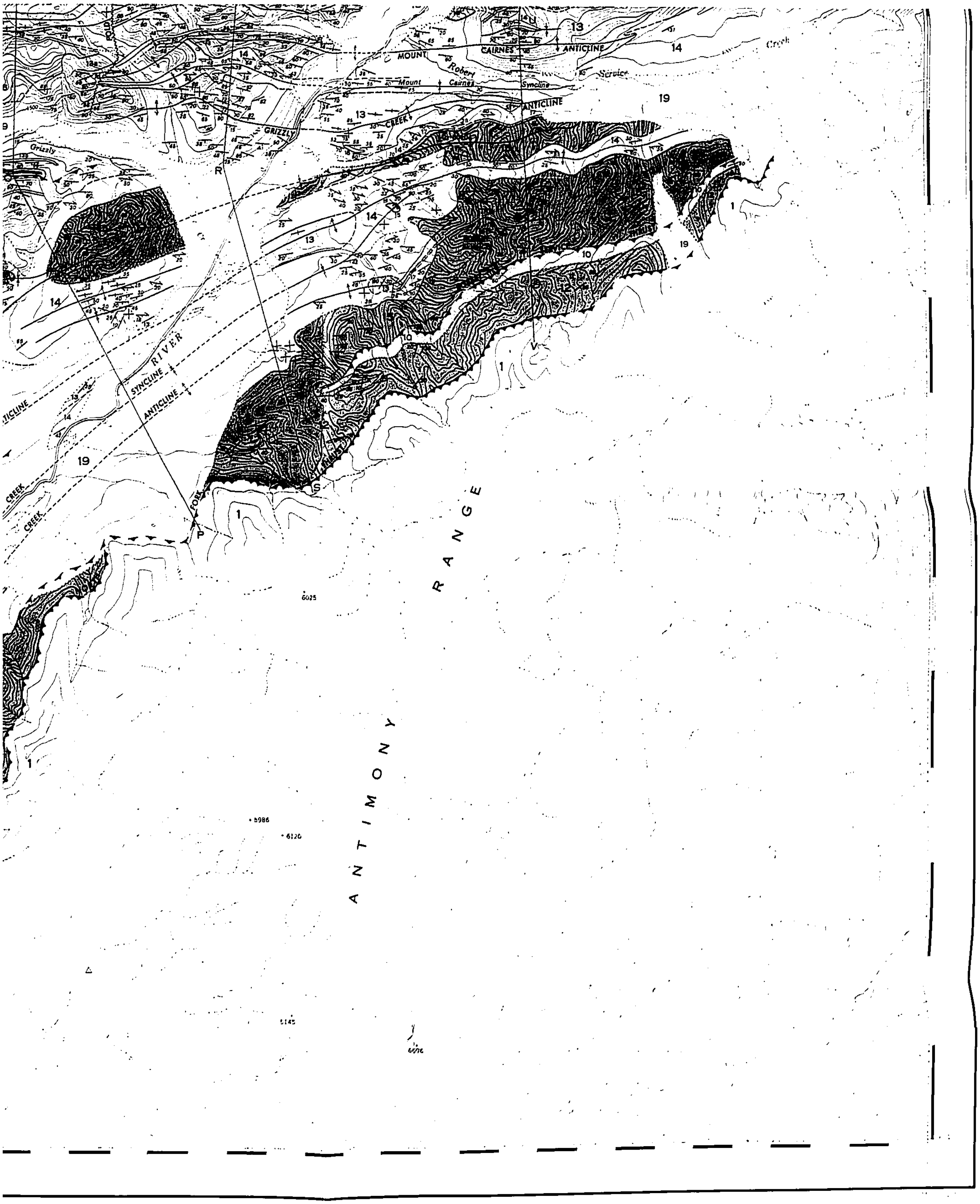

R

MAP I

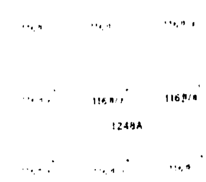

4 of 4

TOMBSTONE RIVER - UPPER KLONDIKE
YUKON TERRITORY

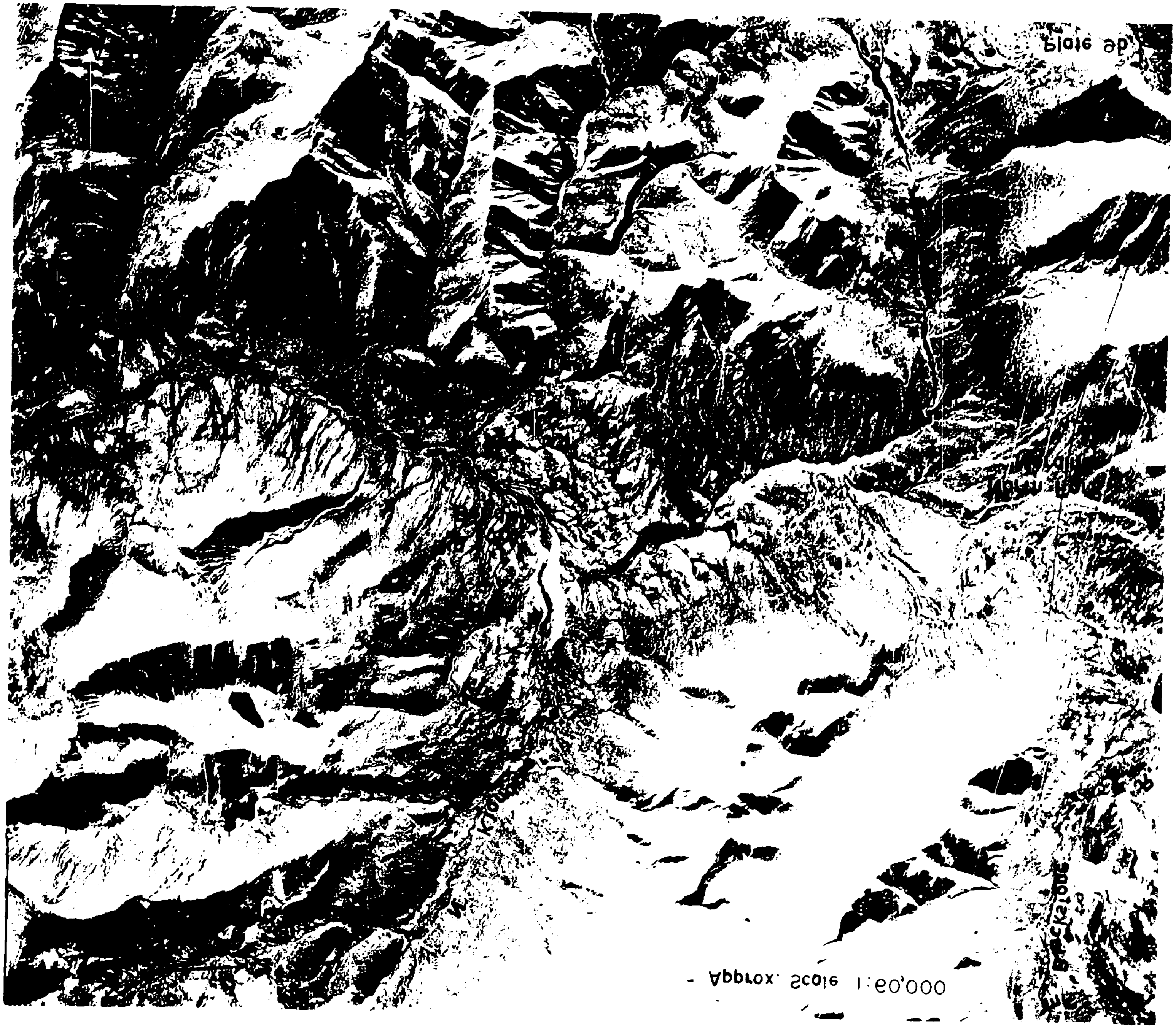
Plate 9b
Approx. Scale 1:60,000
Blackstone
North Fork